Development of New Strategies for Peptide Based Drug Design against Alzheimer's Disease

A Dissertation Submitted to the
Indian Institute of Technology Guwahati
As Partial Fulfillment for the Degree of
Doctor of Philosophy in Chemistry

Submitted by

Ashim Paul

Roll No 10612244

Department of Chemistry

Indian Institute of Technology Guwahati

Guwahati, Assam-781039

India

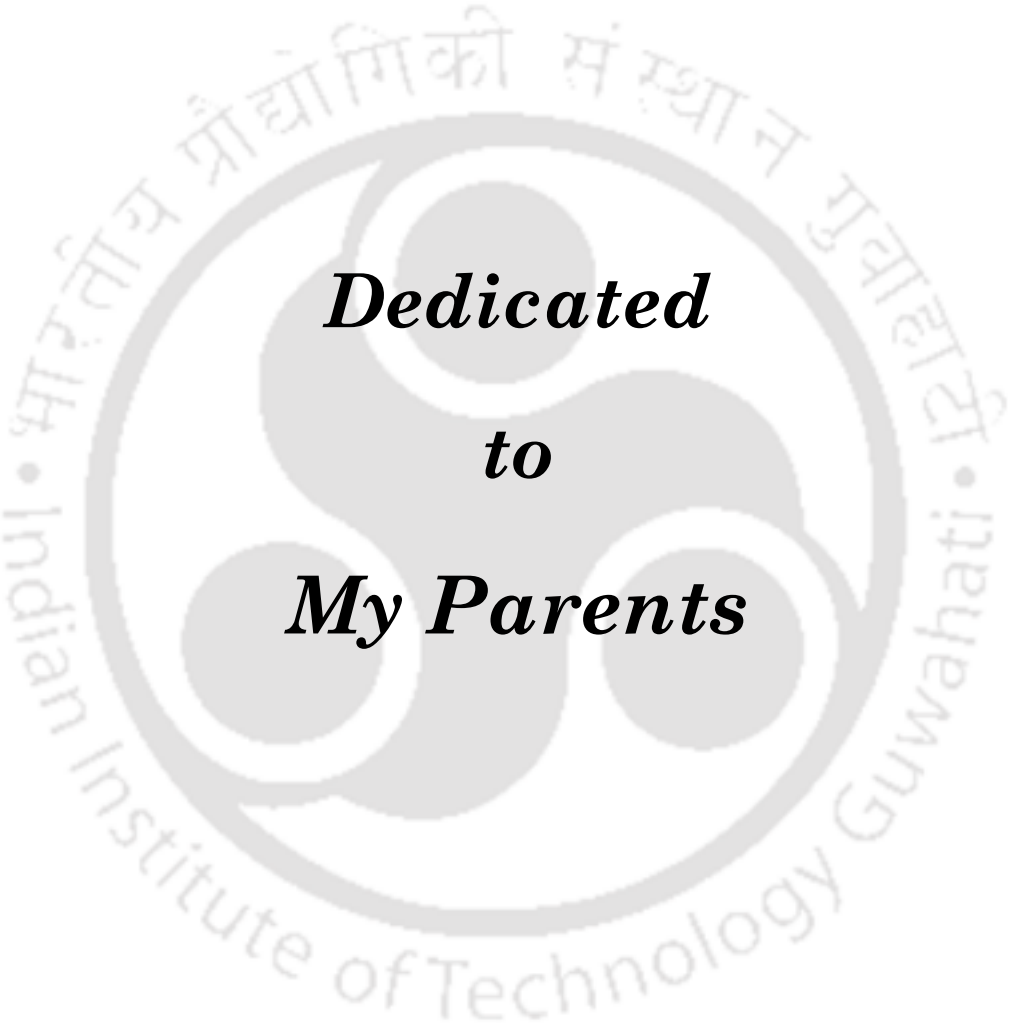

Dedicated

to

My Parents

Indian Institute of Technology Guwahati

Department of Chemistry

STATEMENT

I do hereby declare that the matter embodied in this thesis is the result of investigations carried out by me in the Department of Chemistry, Indian Institute of Technology Guwahati, India, under the supervision of Dr. Bhubaneswar Mandal.

In keeping with the general practice of reporting scientific observations, due acknowledgements have been made wherever the work described is based on the findings of other investigators.

18th April 2016

Ashim Paul

Indian Institute of Technology Guwahati

Certificate

Indian Institute of Technology Guwahati

Department of Chemistry

CERTIFICATE

This is to certify that **Mr. Ashim Paul** has been working under my supervision since December 2010 as a regular registered Ph. D. student. I am forwarding his thesis entitled "**Development of New Strategies for Peptide Based Drug Design against Alzheimer's Disease**" for being submitted for the Ph. D. (Science) degree from this institute. I certify that he has fulfilled all the requirements according to the rules of this institute regarding the investigations embodied in his thesis and this work has not been submitted elsewhere for a degree.

18th April 2016

Dr. Bhubaneswar Mandal

Thesis Supervisor

Department of Chemistry

Indian Institute of Technology Guwahati

Synopsis

The thesis entitled, "Development of New Strategies for Peptide Based Drug Design against Alzheimer's Disease", is divided into six main chapters along with the experimental section and future directions. The abstracts of the main chapters are described below,

Chapter 1: Introduction

The *in-vivo* aggregation of protein to form cytotoxic oligomers and amyloid fibrils causes cell damage and the pathogenesis of several human degenerative diseases including Alzheimer's disease (AD), Parkinson's disease (PD), and type-2 diabetes mellitus (T2DM). AD, a progressive neurodegenerative disorder which has no cure yet, is the foremost cause of dementia in elderly people. The growing evidences suggest that AD is developed by the deposition of amyloid plaques in the neuronal cells, which in turn is caused by the accumulation of Amyloid β peptide (Aβ, a 39-42 residue polypeptide). Aβ exists in random coil state in native form which undergoes misfolding and aggregates to β-sheet rich amyloid fibrils, characterized by cross-β structure. Therefore, a promising approach to inhibit the amyloid formation is to disrupt the formation of β-sheet at the early stages. In the past two decades, various strategies including small organic molecules, antibodies, and β-sheet breaker peptides have been developed to modulate or disaggregate the self-assembly of Aβ, none of them yet found suitable for therapeutic application. Since peptides are accepted as highly selective efficient and relatively safe, they are competent candidates for drug design against AD and other amyloid diseases. Also, for drug design against AD and other amyloid associated diseases, understanding the exact mechanism is desired. Therefore, in this thesis we have demonstrated a mechanistic pathway of early onset of amyloid formation and discussed various new strategies of peptide based drug design against AD based on early stage intervention of fibril formation.

Chapter 2: Early onset of amyloid formation by Alzheimer's amyloid β derived switch-peptide: A mechanistic pathway

Although it is largely agreed that Aβ, generated from the amyloid precursor protein (APP) after proteolytic cleavage by *β*- and *γ*- secretase, exists in random coil conformation natively which undergoes misfolding and aggregates to form amyloid plaques, the exact mechanism of amyloid formation and neurotoxicity remains unclear. The aggregation of Aβ peptide to form amyloid plaques is believed to be the main cause of AD, but the early events of amyloid formation is unknown that are very important for the elucidation of the mechanism of amyloid formation as well as for drug design. In this chapter we have described the early events of amyloid formation of a properly designed amyloidogenic switch-peptide (functional mimic of Aβ) as revealed by our investigations. To elucidate the early events of amyloid formation we have used ultra-violet (UV), circular dichroism (CD) and Raman spectroscopy as experimental techniques. The experimental results support that during conformational transformation of the amyloidogenic peptide, the rate of aromatic side chain interaction was faster than the conformational transition, *i.e.*, the side chains interact prior to the β-sheet formation and fibrillization process (Figure 1). Similarly, during disaggregation process, the β-breaker peptide first interacts with the amyloidogenic peptide through aromatic side chain, followed by disruption.

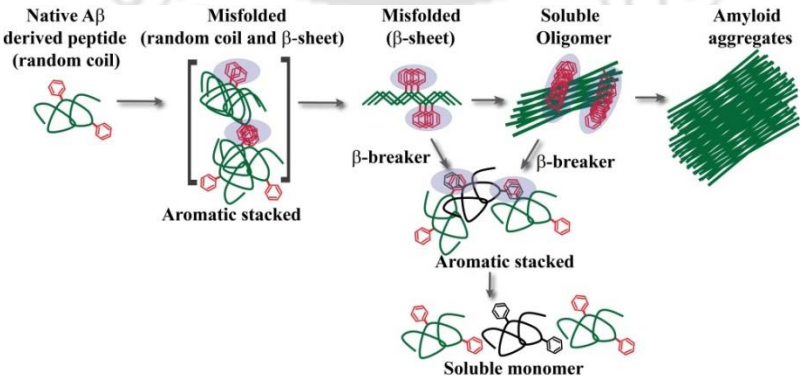

Figure 1: Hypothesis on early events of amyloid formation via aromatic side chain interaction.

Chapter 3: Introduction of β-sheet breaker hybrid peptide and its application for the inhibition of aggregation of model aggregating peptide

Since, the amyloid plaques are rich in β-sheet structure, a strategy which destroys the β-sheet structure would be an important strategy for amyloid disruption. In this chapter, we have introduced a new class of β-sheet breaker peptides (BSBps), comprised of the recognition motif of the amyloidogenic peptide and an anthranilic acid (Ant) as the β-breaker element, for inhibition and reversion of amyloid formation. Since, Ant is a non-coded β-amino acid, structurally rigid, and stable towards proteolytic degradation, we acquired it as a β-breaker element and incorporated in a BSBp, collectively called as β-sheet breaker hybrid peptide (BSBHp), and demonstrated its efficiency to inhibit as well as reverse the self-aggregation of the $A\beta_{1-40}$ peptide. Since, directly dealing with $A\beta_{1-40}$ would be difficult as well as expensive, we first tested the anti-amyloidogenic activity of BSBHp on a model aggregating switch-peptide before checking the effect on the aggregation of $A\beta_{1-40}$ peptide. Since, switch-peptide exists in random coil conformation initially and at physiological condition (pH 7.4 and 37° C) it aggregates to form amyloid similar to $A\beta_{1-40}$ peptide, we acquired it as a model amyloidogenic peptide. In this chapter we have demonstrated the anti-amyloidogenic activity of BSBHp on the aggregation of the model amylodogenic switch-peptide using various biophysical tools (Figure 2).

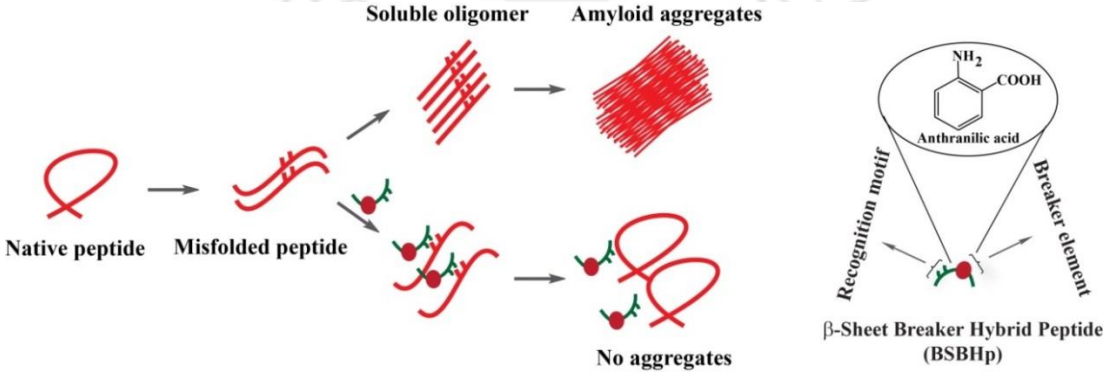

Figure 2: Hypothesis for the inhibition of amyloid formation by a β-sheet breaker hybrid peptide (BSBHp).

Chapter 4: Disruption of Amyloid-β peptide (Aβ) aggregates into non-toxic species by β-sheet breaker hybrid peptide

In this chapter, we have described our findings on the inhibition of formation and the disruption of $A\beta_{1-40}$ aggregates *in vitro* by a properly designed BSBHp using various biophysical tools. For this purpose we have designed and synthesized a BSBHp, Ac-LXFFD (X = Anthranilic acid, Ant), comprised of Ant that act as a breaker element and -F-F- part having sequence homology with $A\beta_{19-20}$ (-F-F) useful for proper recognition. We also synthesized a control breaker peptide (Ac-LPFFD) for comparison of efficacy. Our results (ThT, TEM, CD, *etc.*) suggest that the BSBHp significantly disrupted the preformed amyloid of Aβ. Since, soluble smaller Aβ oligomers are more toxic than the mature fibrils due to their cell membrane rupture potential, we also have performed *in vitro* toxicity studies of disrupted Aβ aggregates using dye loaded large unilamellar vesicles (LUVs) leakage assay and found that the disrupted Aβ aggregates were non-toxic. We also tested the efficacy of BSBHp for the disruption of amyloid present in cerebrospinal fluid (CSF) of the diseased brain and observed that BSBHp significantly disrupted the amyloid present in human-CSF. Results indicated that this novel class of BSBHp successfully disrupted the Aβ amyloid into non-toxic species *in vitro* (Figure 3).

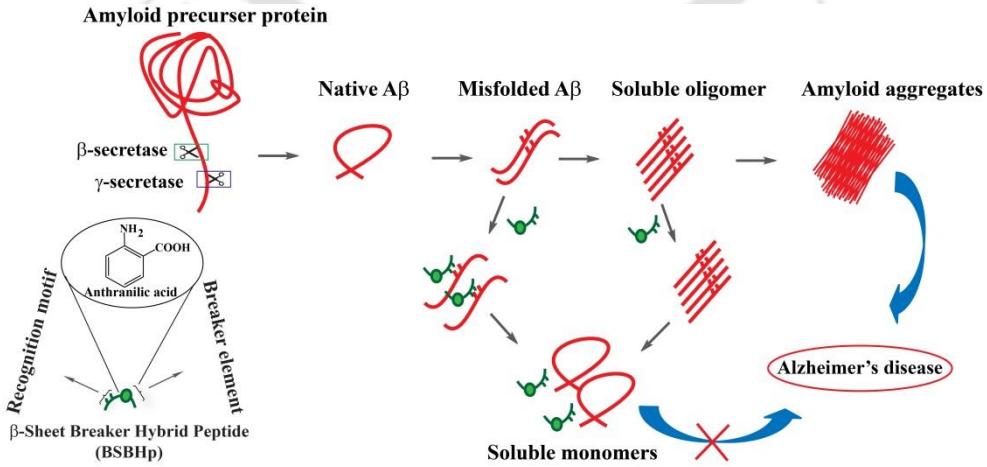

Figure 3: Hypothesis on disruption of Aβ aggregates into non-toxic species by a BSBHp.

Chapter 5: Disruption of Amyloid-β (Aβ) aggregates into non-toxic species by β-breaker di-peptide containing Pro-Drug peptide

In this chapter, we have introduced another new class of β-breaker peptides, called as Pro-Drug peptide (PDp), for the disruption of Aβ aggregates. We designed the PDp in a way that initially it adopts β-sheet structure and can align well with the β-sheet rich aggregated Aβ effectively resulting in eventual insertion into the amyloid due to reversibility of the aggregation process and disrupt the aggregates by *in situ* generation of breaker unit (kink). The PDp allows to generate a kink *in situ* in its backbone through aspartimide formation that forces to change its conformation from β-sheet to random coil and does not fit in the planer β-sheet assembly of the amyloid, and finally disaggregate them (Figure 4). Our results suggest that the PDp effectively disrupt the Aβ aggregates into non-toxic species at physiological condition (37 °C and pH 7.4) using various biophysical tools. We also demonstrated the efficacy of PDp for the disruption of amyloid present in human cerebrospinal fluid (CSF) of the diseased brain and we observed that PDp significantly disrupted the amyloid present in human-CSF. We performed a comparative study for the disruption of Aβ aggregates by the preinstalled breaker element containing peptide vs PDp and observed that the PDp was more efficient than the pre-installed breaker peptide.

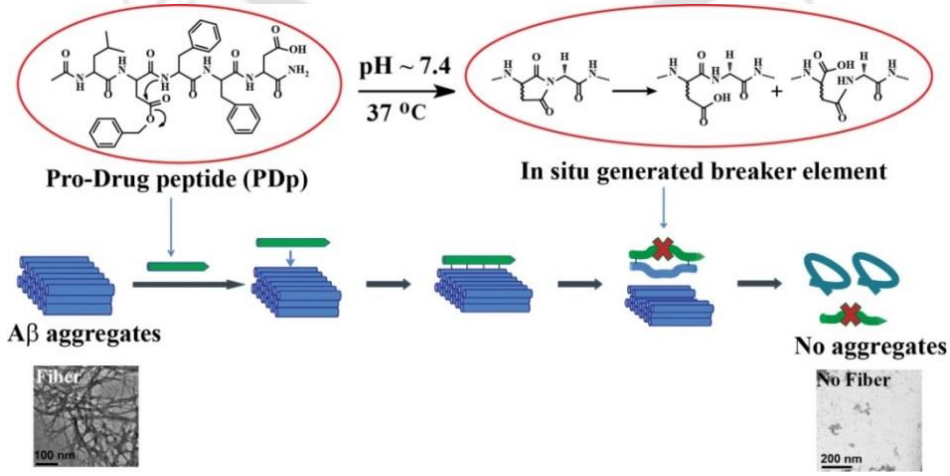

Figure 4: Hypothesis of Pro-Drug peptide (PDp) and its action for the disruption of Aβ aggregates.

Chapter 6: Disruption of Amyloid-β (Aβ) aggregates into non-toxic species by a synthetic zipper peptide

In this chapter, we have introduced a peptide based lead molecule, synthetic zipper peptide, keeping the sequence homology with Aβ peptide and investigated its efficacy for the inhibition of formation and the disruption of Aβ aggregates *in vitro*. We have designed the zipper peptide in a way that it will recognize and bind with Aβ, followed by zipping action and inhibit further aggregation by H-bond elimination using N-methylation at alternate residue of the peptide sequence technique (Figure 5). We performed FRET (fluorescence resonance energy transfer) study to determine the structural motif of the zipper peptide and found that both ends of the peptide were close to each other. Possibly, its hair pin like structure helped to encapsulate the Aβ unit from the amyloid assembly and disaggregated the amyloid by H-bond elimination for the presence of N-methylation. We have demonstrated that the zipper peptide effectively disrupt the Aβ aggregates into non-toxic species at physiological condition (37 °C and pH 7.4) *in vitro*. Zipper peptide also significantly disrupted the amyloid present in human cerebrospinal fluid (CSF) of diseased brain *in vitro*.

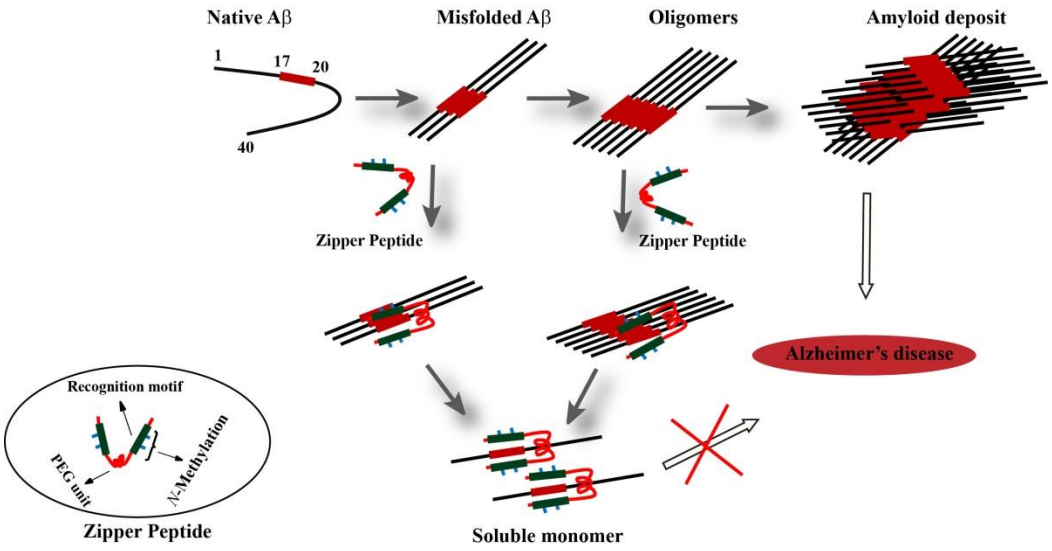

Figure 5: Hypothesis of the inhibitory activity of zipper peptide on aggregated Aβ peptide.

In conclusion, we have presented a mechanistic route for the early events of amyloid formation, which explains the importance of aromatic side chain interaction during the initiation of aggregation process, in this thesis. We also have demonstrated three different strategies of peptide based molecule design that showed significant efficiency for the disruption of Alzheimer's amyloid *in vitro*. These strategies can be extended to the drug design against Alzheimer's disease and other amyloid associated diseases as well.

Table of contents

Chapter 2. Early onset of amyloid formation by Alzheimer's Amyloid β derived switch-peptide: A mechanistic pathway

Chapter 3: Introduction of β-sheet breaker hybrid peptide and its application for the inhibition of aggregation of model aggregating peptide

Chapter 6: Disruption of Amyloid-β (Aβ) aggregates into non-toxic species by synthetic zipper peptide

Acknowledgements

At the outset, with a deepest sense of gratitude, I would like to express my sincere thanks to my supervisor, Dr. Bhubaneswar Mandal, for his invaluable guidance, encouragement, inspiration and moral support which helped me to enhance my knowledge and have inspired me to take right decisions at crucial moments. I am also thankful to him for giving me freedom to pursue my own interests in his lab and I find myself privileged to have worked under his kind guidance.

I would like to acknowledge my doctoral committee members, Prof. Anil Kumar Saikia, Dr. Sandip Paul, Dr. Lal Mohan Kundu and Dr. Debapratim Das for their valuable suggestions and advice. My special thanks to Dr. Debapratim Das for providing me facility of lyophylizer, Dr. Sandip Paul for the theoretical studies, Dr. Debasis Manna for providing some important chemicals at crucial time and Dr. Amal Kumar Mondal (faculty member of School of Life Sciences, JNU, New Delhi) for biological studies. Also I would like to thank all the faculty members of the department of chemistry for their consistent encouragement.

I would like to thank UGC New Delhi for financial support and IIT Guwahati for all the facilities that were made available to me. I am thankful to Dr. Babulal Das, Mr. Aniruddha Gogoi (for HRMS and LC-MS) of Department of Chemistry, Dr. Mohitosh Dey (for CD analysis) of Department of Bioscience & Bioengeneering, Mr. Chandan Borgohain & Mr. Keshu Singh of Central Instruments Facility (for RAMAN, TRPL and LC-MS) and all the non-teaching staff of Department of Chemistry for their help during my Ph.D. tenure. I also would like to thank SAIF NEHU, Shillong, for TEM analysis.

I must thank my former and present labmates Dr. N. K. Chaitanya, Dr. Nani Babu Palakurthy, Dr. Thalluri Kishore, Dr. Abhijit Saha, Dharm Dev, Tanmay, Srinivasa, Jyoti, Nibedita, Sourav, Rajat, Tapasi and Sujan for the constant cooperation, support and creating the humourous and pleasant environment in the laboratory. My special thanks to Dr. Palashuddin & Shilaj for TEM analysis, Sahnawaz for lyophilization, Subhashis & Saugata for fluorescence studies, Dr. Renjit & Bhanita for theoretical studies. I also would

like to thank all of my Ph.D. batchmates (Dec, 2010) specially Abhijit, Arindam, Anupal, Ganesh, Tridip, Sengoden and Murugovel for the wonderful time we had for the past five years. Also my sincere thanks to my seniors, friends and other research scholars @IITG specially Dr. Renjith, Dr. Kiran, Dr. Srimanta, Dr. Rajesh, Dr. Rajen, Dr. Subhojit, Dr. Chirantan, Dr. Aswini, Dr. Dipankar, Dr. Julfikar, Dr. Prithiviraj, Dr. Sukhamay, Dr. Prasanta, Dr. Arghya, Sayan, Barun, Ashim, Santosh, Anindya, Manoj, Suman, Sameer, Hemanta, Soumen, Soumya, Manish, Debasis, Uday, Prasenjit. I also thank my friends at IIT Guwahati with whom I spent time and shared many joyfull moments during festivals and picnics.

I extend my sincere thanks to all the teachers, who always encourage and help me, since my childhood, specially Mr. Nirmal sir, Mr. Molla sir, Dr. Parimal sir for their teaching, invaluable motivation, suggestions and advice for academic as well as for progress of life. I also would like to thank my school and college friends, Tarun, Saif, Pallab, Kaushik, Papiya, Nabamita, Sourav, Debu, Rishi, Sandip, Abhay, Malay, Ashwani and other close friends for their constant unfailing support, encouragement, and all the help they extended from time to time whenever required.

Most importantly, I am thankful to my Father, Mother, Brother, Sister-in-law and my little nephew Debojit, for their endless moral support and motivation especially at difficult times. My Ph.D endeavors would not have been completed without their blessings. They are the main soul and inspiration for each and every step that I achieve in my life. I express my sincere gratitude to them. I would like to thank all others who are associated with my work directly or indirectly at IIT Guwahati for their help.

Ashim Paul

Abbreviations

Aβ	**A**myloid **b**eta
Abs	**Abs**orbance
Ac_2O	**Ac**etic anhydride
AD	**A**lzheimer's **d**isease
Adi	**Adi**pic acid
AICD	**A**myloid precursor protein **i**nter**c**ellular **d**omain
Ant	**Ant**hranilic acid
APP	**A**myloid **p**recursor **p**rotein
AU	**A**rbitrary **u**nit
BBDP	**β**-**b**reaker **di****p**eptide
Boc	*tert*-**b**utyl**o**xy**c**arbonyl
BOP	**B**enzotriazol-1-yl**o**xy tris(dimethylamino) **p**hosphonium hexafluorophosphate
BSBHp	**β**-**s**heet **b**reaker **h**ybrid **p**eptide
Bzl	**B**en**z**y**l**
CD	**C**ircular **d**ichroism
CF	5(6)-**C**arboxy**f**luorescein
CR	**C**ongo **r**ed
CSF	**C**erebro**s**pinal **f**luid
DBU	1,8-**D**iaza**b**icyclo[5.4.0]**u**ndec-7-ene
DCM	**D**i**c**hloro**m**ethane
DIAD	**D**i**i**sopropyl **a**zo**d**icarboxylate
DIPEA	**D**i**i**so**p**ropyl**e**thyl **a**mine

DMF	N, N **d**i**m**ethyl **f**ormamide
DMPC	1,2-**D**i**m**yristoyl-sn-glycero-3-**p**hospho**c**holine
DPPC	1,2-**D**i**p**almitoyl-*sn*-glycero-3-**p**hospho**c**holine
ESI MS	**E**lectro**s**pray **i**onization **m**ass **s**pectrometry
Et_2O	Di**et**hyl ether
FE-SEM	**F**ield **E**mission **S**canning **E**lectron **M**icroscopy
Fmoc	9-**F**luorenyl**m**eth**o**xy**c**arbonyl
FTIR	**F**ourier **t**ransformation **i**nfra **r**ed spectroscopy
GM1	**M**onosialotetrahexosyl**g**anglioside
HEPES	*N*-2-**h**ydroxy**e**thyl **p**iperazine-*N*-2-**e**thane **s**ulphonic acid
HFIP	1,1,1,3,3,3-**h**exa**f**luoro-**2**-**p**ropanol
HOBt	1-**h**ydr**o**xy **b**enzo**t**riazole
HPLC	**H**igh **p**ressure **l**iquid **c**hromatography
KBr	Potassium **br**omide
LC-MS	**L**iquid **c**hromatography **m**ass **s**pectrometry
mL	**m**illi **l**iter
mM	**m**illi **m**ol
nm	**N**ano**m**etre
µM	**m**icro **m**ol
MW	**M**olecular **w**eight
NMI	***N***-**m**ethyl **i**midazole
NMP	***N***-**m**ethyl **p**yrolidine
NMR	**N**uclear **m**agnetic **r**esonance
O-NBS-Cl	***O****thro*-**n**itro**b**enzene **s**ulfonyl **c**h**l**oride
PEG	**P**oly**e**thylene **g**lycol

PBS	**P**hosphate **b**uffer **s**olution
PDp	**P**ro-**D**rug **p**eptide
PPh_3	Tri**ph**enyl **p**hosphine
PyBOP	**B**enzotriazole-1-yl-**o**xy-tris-**py**rolidine-**p**hosphonium hexafluorophosphate
RP	**R**everse **p**hase
SPPS	**S**olid **p**hase **p**eptide **s**ynthesis
Suc	**Suc**cinic acid
tBu	***t**ert*-**bu**tyl
TEM	**T**ransmission **e**lectron **m**icroscopy
TFA	**T**ri**f**luoroacetic **a**cid
TFE	**T**ri**f**luoro**e**thanol
THF	**T**etra**h**ydro**f**uran
ThT	**Th**ioflavin **T**
TRPL	**T**ime **r**eseolve **p**hoto **l**uminicence
Trt	**Tri**t**t**yl
UPLC	**U**ltra **p**ressure **l**iquid **c**hromatography
UV	**U**ltra**v**iolet

Amino Acids:

Ala	A	Alanine
Arg	R	Arganine
Asn	N	Asparagine
Asp	D	Aspartic acid
Cys	C	Cysteine
Gln	Q	Glutamine
Glu	E	Glutamic acid
Gly	G	Glycine
His	H	Histidine
Ile	I	Isoleucine
Leu	L	Leucine
Lys	K	Lysine
Met	M	Methionine
Phe	F	Phenylalanine
Pro	P	Proline
Pyl	O	Pyrrolysine
Sec	U	Selenocysteine
Ser	S	Serine
Thr	T	Threonine
Trp	W	Tryptophan
Tyr	Y	Tyrosine
Val	V	Valine

Chapter 1: Introduction and Objectives

1.1. Introduction:

This thesis describes the mechanism of amyloid formation in Alzheimer's disease (AD) focusing mainly at the early stages and the development of new strategies for peptide based drug design against AD. It is always important to know the background and fundamentals related with the problem before going into the solution. Therefore, in this introductory chapter, a brief discussion on proteins, peptides, their secondary structures, features related to self association, and a brief account on AD is provided.

1.2. Proteins and peptides:

Proteins are the most important class of biomolecules in the living system, constituting more than half the dry weight of a cell. Almost 20,500 protein-encoding genes have been found in the human genome and proteins encoded by them are responsible for almost all biological functions in living systems including cell-cell communication, immune protection, metabolic action, and muscle movement.[1-3] Proteins are made up of amino acids linked together by peptide bonds with an amino group of one amino acid and a carboxyl group of the other amino acid. Each amino acid contains an R (side chain) group at its α-carbon (Figure 1.1).[2] The diversity of protein functionality is directly related to the combinatorial possibilities of the 22 coded amino acids. Proteins can be distinguished based on the number of amino acids

present within the sequence. The long chain of amino acids is generally known as polypeptide. When a polypeptide contains 50 or less amino acids they are usually considered as peptide or oligo-peptide.

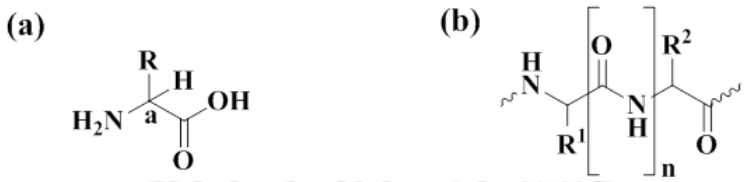

Figure 1.1: General structure of an amino acid (a) and general formula of a peptide bond (b) in a protein sequence.

1.3. Proteins structure:

Most of the protein molecules adopt a specific three dimensional (3D) structure in order to fulfill their various biological functions in the living system. The structure of proteins is described in four different structural levels, primary, secondary, tertiary and quaternary (Figure 1.2).[4,5] The amino acid sequence of long chain of polypeptide is known as the primary structure of protein. The short range three dimensional structure of protein is stabilized through hydrogen bonding (*H*-bonding) between NH and CO of the amide moieties of the protein backbone that results in the formation of secondary structures. The secondary structures of the polypeptide chains are further arranged in space to produce next level of protein structures that is known as the tertiary structure. Further many tertiary domains of a protein or many protein molecules stabilize to more complex functional machineries that are known as the quaternary structure. The secondary structures including α-helix, β-sheet and β-turn are very important for building the structure, stability and functionality of a protein.

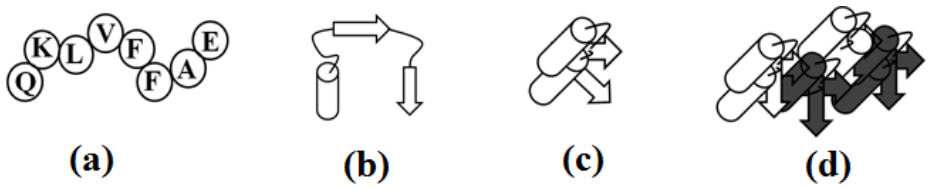

Figure 1.2: (a) Primary, (b) Secondary, (c) tertiary and (d) quaternary structure of protein.

α-helix:

It is a coiled structure of protein, stabilized by intra-molecular *H*-bonds between the NH and CO groups of the main chain (Figure 1.3). In an α-helix, the CO group n^{th} amino acid forms a *H*-bond with the NH group of the $(n+4)^{th}$ amino acid in the sequence. Thus, in α-helix, all the main-chain CO and NH groups are *H*-bonded except amino acids near the end. There are 3.6 amino acid residues present per turn of an α-helix and the distance between two amino acid residues along the helix axis is 1.5 Å.[2]

Figure 1.3: Structure of α-helix.

β-sheet:

When the polypeptide chains (strands) are found fully extended, stabilized through inter strand *H*-bonds and forms a sheet like structure, it is called a β-sheet (Figure 1.4).[2] The distance between adjacent amino acids along a β strand is ~ 3.5 Å. Adjacent β strands in a β-sheet can run either in opposite directions (antiparallel β-sheet) or in the same direction

(parallel β-sheet). Association of higher levels of β-sheets form protein aggregates and insoluble fibrils, which are responsible for many human diseases, including Alzheimer's disease (AD) and Parkinson's disease (PD).[6,7]

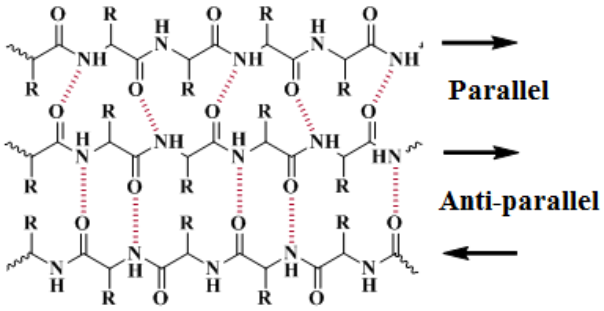

Figure 1.4: Structure of an anti-parallel and parallel β-sheet.

β-turn:

When in a polypeptide chain the CO group of the n^{th} residue is *H*-bonded to the NH group of the $(n+3)^{th}$ residue, the polypeptide chain runs in a reverse direction, and forms a bent or turn like structure, it is called β-turn or reverse turn (Figure 1.5). The two residues inside the turn do not participate in any kind of interactions.[2]

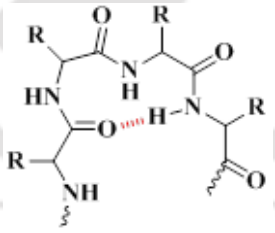

Figure 1.5: Structure of β-turn.

Among these secondary structures of protein β-sheet conformations are mostly found to aggregate to form amyloid and cause several neurodegenerative diseases.[6] Unlike β-sheet, α-helix are not commonly found in self-aggregating peptides, but in few cases, α-helix also

found to form amyloid by self-aggregation.[8] Hence the β-sheet conformation is very important for protein misfolding and aggregation leading to amyloid formation.

1.4. Protein folding and misfolding:

The process, by which a protein molecule attains a stable three dimensional structure to perform a function in the living system, is called protein folding. Although the mechanism of protein folding is very complex and remains unclear till date, it is believed that the driving force for protein folding is to be the lowest possible energy state which is governed by the interactions within the molecules as well as between the molecule and the surrounding solvent.[9] The role of amino acid sequence is very important for protein structure or folding and it depends on some factors, including the hydrophobic effect, hydrogen bonds, electrostatic interaction and van der Waals interaction.[2] The secondary structure of proteins is another important factor for folding process, α-helix is stabilized by hydrogen bonding between CO and NH groups within the same polypeptide chain whereas in β-sheet, the hydrogen bonding is between next neighboring strand. The folded proteins which are functionally active also called native state of the proteins (Figure 1.6).

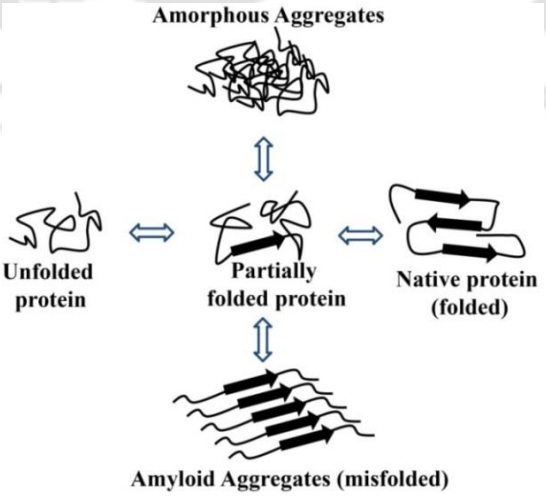

Figure 1.6: Protein folding and misfolding.

Proteins usually exist in native form, as they are thermodynamically and kinetically stable. If protein molecules were not to fold into some three dimensional conformation, it would not function. Thus, folding is important in living system to sustain life. Sometimes, protein cannot fold into desired three dimensional conformations, rather it remains partially folded or wrongly folded; it is called protein misfolding (Figure 1.6). The conformational disordering resulted from the misfolding of the secondary structure of the protein causes various human diseases, including AD and PD.[6] Although, the exact cause of protein misfolding is not known, it is believed that some factors, including pH, ionic strength, genetics and mutations are involved during the process of misfolding.[11,12]

1.5. Amyloids:

Many proteins and peptides undergo transitions from their native secondary structures into ordered β-sheet conformations that accumulate together and get deposited in the biological system as insoluble materials (Figure 1.6). These insoluble protein aggregates are known as amyloids.[13] Although, the morphology can differ, all amyloid fibrils were observed as highly ordered cross-β structure, long filaments, having a diameter of 3-10 nm and of indefinite length, characterized by a specific X-ray diffraction pattern and TEM (Figure 1.7).[14-18] The cross-β structure is the common structural motif of amyloid fibrils where the proteins are arranged in β-sheets perpendicular to the fibril axis.

It is generally agreed from the growing evidences that amyloid fibril formation is a nucleation dependent process.[19,20] The process of amyloid formation follows sigmoidal profile where three phases are noticed, (a) nucleation phase (b) growth phase and (c) saturation phase (Figure 1.7).[20] In the nucleation phase (also known as lag phase), protein

monomers are arranged and come closer to form the nuclei, *i.e.* the early pre-fibrillar oligomers, which later is elongated with the other monomers in the growth phase and further forms mature fibrils in the saturation phase. In this phase, the free monomers and the monomers incorporated into fibrils remain in equilibrium, *i.e.* the rate of monomer elongation is equal to the rate of monomer dissociation.[21,22]

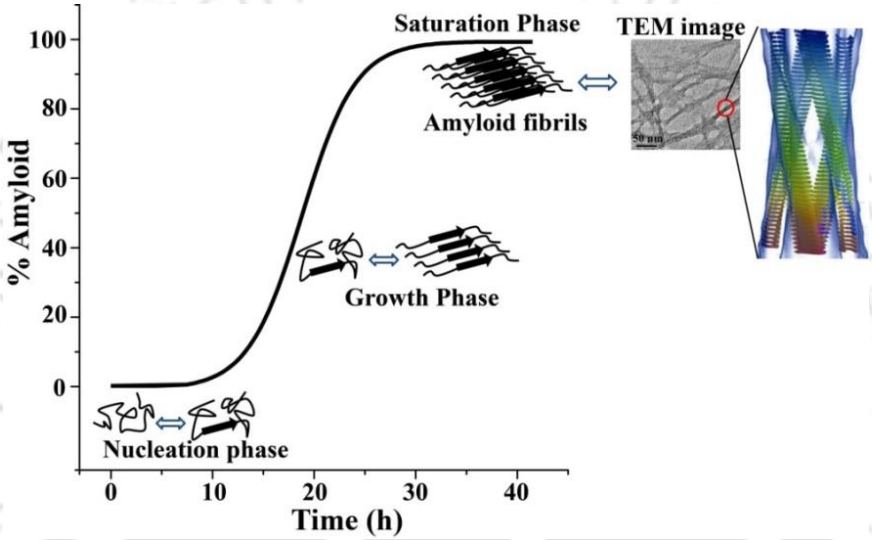

Figure 1.7: The process of amyloid formation is characterized by a slow nucleation phase, followed by growth phase and finally a saturation phase.

The kinetics of amyloid formation is generally monitored by fluorescence technique using dye molecule. A commonly used dye is thioflavin T (ThT).[23] Amyloid fibrils are toxic to the biological system and are responsible for numerous human diseases, known as "amyloidoses", and this includes AD, PD, Huntington's disease, type-2 diabetes *etc*. There are more than 30 proteins or peptides known to form amyloid. Some amyloid forming proteins or peptides are shown in the Table 1.1.[24-25]

Diseases	Protein/peptide involved	No of residues
Alzheimer's disease	Amyloid β	40 or 42
Parkinson's disease	α-Synuclein	140
Diabetes type-2	Amylin	37
Huntington's disease	Huntingtin with poly Q expansion	3144
Creutzfeldt-Jacob disease	Prion protein	253
Sickle cell anemia	Hemoglobin	141 or 146
Spinocerebellar ataxias	Ataxins with polyQ expansion	816
Medullary carcinoma of the thyroid	Calcitonin	32
Cataract	γ-Crystallins	Variable

Table 1.1: List of some protein misfolding diseases and the proteins involved in those.[25]

1.6. Alzheimer's disease:

Alzheimer's disease (AD) is a progressive neurodegenerative disorder and most common form of dementia, characterized by a decline in memory, language, problem-solving and other cognitive skills of the elderly population that eventually leads to death.[26,27] With an increase in the aging population, the worldwide prevalence of AD has increased remarkably and is expected to continue to do so. In 2015, 46.8 million people worldwide are suffering from AD and it is expected to be increased to 131.5 million by 2050.[28-30] Current statistics also suggest that in every 67 seconds someone in America develops AD and the rate is projected to more than double by 2050, to one every 33 seconds.[28] The pathology which

would later be identified as Alzheimer's disease was first identified by German neurologist, Dr. Alois Alzheimer (the disease named after him). In 1907, Dr. Alois Alzheimer presented the findings about the death of a 51-year-old female patient that showed severe cognitive disorders pertaining to memory, language, and social interactions.[31] From the post-mortem autopsy of the atrophied brain, he observed two major neuropathological hallmarks of AD. The twisted fiber-bands inside the nerve cells, called as the neurofibrillary tangles (NFTs), and some dense fibrillar deposits at the extracellular spaces, called as senile plaques (SPs) (Figure 1.8).

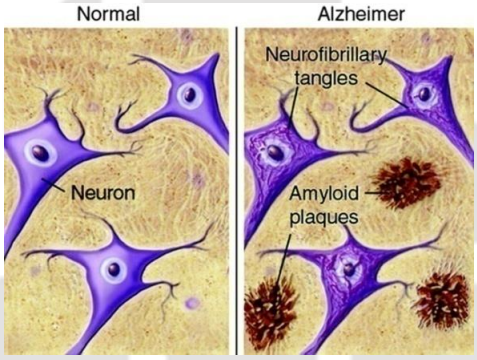

Figure 1.8: Comparison between a healthy neuron and diseased neuron comprising amyloid plaques and neurofibrillary tangles. (Courtesy: http://pakmed.net/academic/age/alz/alz030.htm)

1.6.1. Symptoms of AD:

The first symptom of AD is often short-term memory loss. As the disease progresses, disorientation, aphasia and a general decline in cognitive functions follows. Although, there are diverse tests and observations available for the diagnosis, a definite AD clinical diagnosis is only possible by a histopathological analysis of the brain to confirm the existence of the above mentioned neuropathological lesions.[32] Some common symptoms for AD are shown below:

- Short term memory loss
- Problems with language and communications
- Problems with thinking and recognition
- Disorientation and confusion
- Poor judgment

1.6.2. Risk factors for AD:

Numerous factors influence the risk of AD. There are mainly two types of AD existing, familial AD (FAD) which is highly dependent on family history, appears before the age of 65 and other one, late onset AD, sporadic AD (SAD) which is not dependent on the past history of the family, can be developed by the mutations in amyloid precursor protein (APP), Pinresenilin 1 or Presenilin 2 and other factors. Here, some common risk factors are listed below:[33-35]

- Advancing age
- Family history of Alzheimer's disease
- Certain bacterial infections
- Vascular risk factors (diabetes, atherosclerosis, high blood pressure, high cholesterol *etc.*)
- Central obesity (i.e., high waist-to-hip ratio)

1.6.3. Cause of Alzheimer's disease:

There are numerous factors responsible for the pathogensis of AD, including oxidative stress, inflammation, mitochondrial dysfunction, and accumulation of toxic protein aggregates in and around neurons.[36-38] Growing evidences suggest that age-related issues such as

decreasing hormone levels and vascular dysfunction are also responsible for the progression of AD.[35] The evidences from the research of the last three decades revealed that pathological hallmarks of AD are the formation of SPs (accumulation of misfolded amyloid-β (Aβ) peptides), NFTs (accumulation of hyper-phosphorylated tau proteins) and the metal ion dyshomeostasis (Cu^{2+}, Zn^{2+}, Fe^{3+} & Al^{3+}) in the brain (Figure 1.9).[32,39]

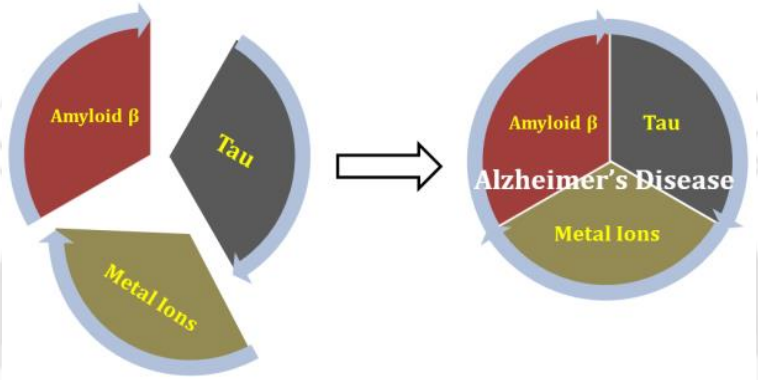

Figure 1.9: Major hallmarks of Alzheimer's disease.

Senile Plaques

The major cause of Alzheimer's disease is the senile plaques (SPs), which are comprised of "clumps" of the protein fragment Aβ. SPs accumulate and cause cellular damage in key areas of the brain, especially in the hippocampus, which is involved in various memory navigation.[40] Aggregation of Aβ contributed to oxidative damage, neurotoxicity, inflammation and neuronal cell death. The plaque formation also encourages the formation of neurofibrillary tangles (NFTs) and risks of AD.[41]

Neurofibrillary Tangles

Neurons contain a cyto-skeleton comprised of microtubules and complementary specialized proteins called tau. In AD, microtubules disintegrate and tau proteins come out of the skeleton and "clump" together to form aggregates called neurofibrillary tangles or NFTs.[41,42] NFTs function in a similar manner as the SPs do in the brain which lead to cellular dysfunction and death.

Metal ion dyshomeostasis

Metal ions including, Cu^{2+}, Zn^{2+}, Al^{3+} and Fe^{3+} are the major metal ions that contribute to the pathogenesis of AD.[43] Increased concentration of these metal ions in brain causes rapid aggregation of Aβ peptide to form soluble oligomers which is responsible for the generation of reactive oxygen species (ROS) and causes synaptic dysfunction, finally leading to the death of the neuronal cell.[39,43]

1.7. Amyloid β (Aβ) peptide:

Whether SPs or NFTs or metal ions dyshomeostasis are the major factor for Alzheimer's disease is unclear and this remains a debated topic within the scientific community. Since, this thesis is centered on the amyloid formation (Aβ aggregation) and its disruption using various strategies, it is important to know the details about Aβ.

A histopathological analysis of AD affected brain sample revealed that formation of senile plaques in the neuronal cells is the main culprit of the disease. The senile plaques found in AD affected brain are comprised of Amyloid β (Aβ) peptide, a 39- to 43- residue-long

polypeptide, generated from amyloid precursor protein (APP). APP is a type-I transmembrane protein, made up of 695-770 amino acid residues where the *N*-terminal end is exposed to the extracellular space and the C-terminal end remains in the membrane.[44] There are three main isoforms of APP found in the brain, APP_{695}, APP_{751} and APP_{770}, where APP_{695} is the predominant form expressed in neurons, but the exact function of APP is still unclear.[45] The cleavage of APP is performed by proteases (α-, β-, and γ-secretases) in two distinct pathways, and can be divided into a non-amyloidogenic and an amyloidogenic pathway (Figure 1.10). In non-amyloidogenic pathway, APP is cleaved extracellularly by α-secretase at residue 83 from the C-terminus and generates a soluble N-terminal fragment αAPP and a C-terminal fragment which remains in the membrane. Later, the C-terminal fragment is cleaved by γ-sectretase, yielding extracellular peptide p3 (partial fragment of Aβ peptide) and intracellular AICD.[44,46] The cleaved extracellular fragment, p3 peptide, do not form fibrils and thus the process is referred as non-amyloidogenic pathway.

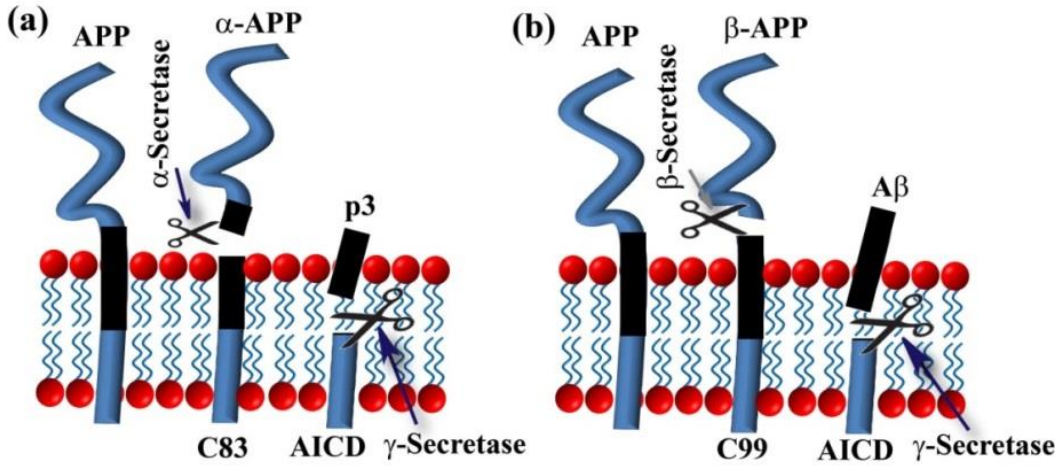

Figure 1.10: APP processing follows two distinct pathways, (a) the non-amyloidogenic pathway (APP cleaved by α- and γ-secretases) and (b) the amyloidogenic pathway (APP cleaved by β- and γ-secretases).[30]

In amyloidogenic pathway, APP first cleaved by β-secretase (BACE1) at position 99 from the C-terminus, releasing soluble βAPP and the membrane-associated C-terminal fragment. Subsequent cleavage by γ-secretase produces intracellular AICD and an extracellular fragment, a 39 to 43 residue long amyloid beta (Aβ) peptide.[44,46] $A\beta_{1-40}$ (40 residue long Aβ variant) and $A\beta_{1-42}$ (42 residue long Aβ variant) are the two common fragments observed in this process where $A\beta_{1-40}$ is 10 % predominant product than $A\beta_{1-42}$.[44] The primary sequence Aβ is shown below,

H_2N-D[1]AEFRRHDSGYEVHHQK**LVFFA**EDVGSNK**GAIIGLMVGGVV**[40]**IA**[42]-COOH

The Aβ peptide generated from APP has a hydrophilic N-terminal (1 to 16 residues) and a hydrophobic C-terminal (16 to variable lengths). NMR studies revealed that like other amyloids, Aβ aggregates form cross-β structure as evident from X-ray and TEM analysis.[16,17] From the structural elucidation, it is noticed that in the fibrillar assembly, the first 10 residues of $A\beta_{1-40}$ are structurally disordered, whereas residues 12–24 and 30–40 adopt β-strand conformations that form parallel β-sheets through intermolecular hydrogen bonding and residues 25–29 contain a bend of the peptide backbone that brings the two β-sheets in contact through side chain interactions.[17,47] Although, the secondary structure of monomeric $A\beta_{1-40}$ and $A\beta_{1-42}$ is very similar, their aggregation propensity is different, this is due to the C-terminal end of $A\beta_{1-42}$ that is more rigid and hydrophobic, for which $A\beta_{1-42}$ is more amyloidogenic and neurotoxic than $A\beta_{1-40}$.

Growing evidences suggest that Aβ peptide exists as random coil conformation in its native form, but in diseased condition it is found as β-sheet rich fibrillar aggregates (Figure 1.7). Although, the exact mechanism of Aβ fibril formation is unclear till date, it is well accepted

by the scientific community that native Aβ peptide first misfolded through some unknown pathway and adopts β-sheet structure which initially aggregate to form soluble oligomers, further aggregation yields fibrillar aggregates and deposition (Figure 1.11).[48, 49] The central hydrophobic region of Aβ ($A\beta_{17-21}$, LVFFA), also known as "core hydrophobic" region, is known to be more crucial for the amyloid formation than the C-terminus hydrophobic region, probably due to the presence of aromatic amino acids.[50-52]

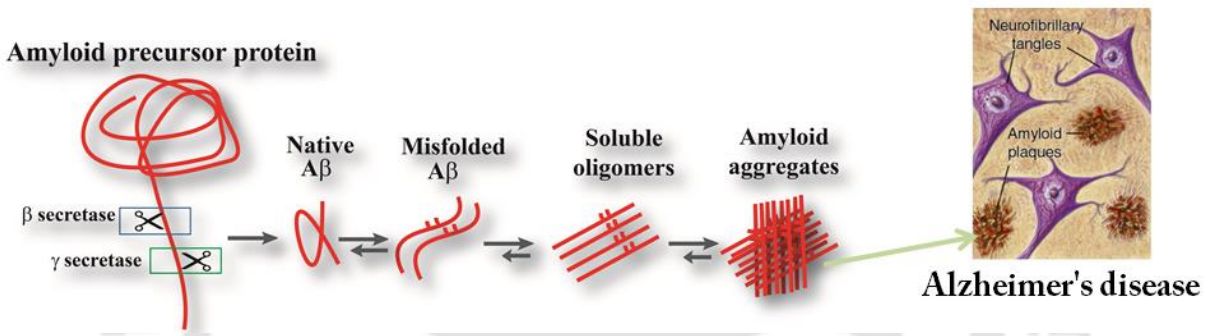

Figure 1.11: Molecular mechanism of amyloid plaques formation in Alzheimer's disease.

Even though the amyloid fibrils are found in the senile plaques, the soluble oligomers are accepted as more toxic to the neuronal cells because they are responsible for neuronal cell death by membrane disruption through pore formation. Consequently, it affects the brain by synapse loss, altered mitochondrial metabolism, DNA damage and inflammatory processes.[37, 53-55] It has been found that aggregation of Aβ in the brain promotes generation of reactive oxygen species (ROS) and also disrupts the intracellular Ca^{2+} homeostasis which causes neuronal cell death in AD brain.[56,57] Therefore, the aggregation Aβ to form oligomer and mature fibrils is the major culprit for AD and blocking the aggregation to cure AD is still a challenging task to the scientific community.

1.8. Existing therapeutics against AD:

For curing any disease and drug therapy, the diagnosis is very important and should be done as soon as possible. One way of diagnose AD is to detect and identify biomarkers for AD. In AD, the primary source of potential biomarkers are the cerebrospinal fluid (CSF)[58], blood (serum and plasma)[59], and brain imaging techniques, including magnetic resonance imaging (MRI), positron emission tomography imaging (PET), and single-photon emission computed tomography (SPECT).[40,58-60] There is no therapy available for AD, although some commercial drugs (Donepezil, Galantamine, Memantine, Rivastigmine and Tacrine) are available for temporary relief.[61-64] All these drugs are used to reduce the disease symptoms and temporary relief, but they are inefficient to cure AD completely, rather most of them have diverse side effects. Although, there is no cure for AD, extensive researches are going on for developing proper therapeutics against AD and the current strategies[63,64] for drug development against AD are divided into various categories, some of them are described below.

1.8.1. Modulation of Aβ production:

The most direct way of targeting AD pathogenesis would be the reduction of $A\beta_{1-40}$ and $A\beta_{1-42}$ production from APP. The target can be accomplished by inhibiting the activity of β- and γ-secretases or enhancing the activity of α-secretase.[65]

β- and γ-secretase inhibitors:

Since, Aβ is generated through amyloidogenic pathway in APP processing by β- and γ-secretases, blocking the activities of these proteases would be an excellent target for AD pathogenesis. Several β- and γ-secretase inhibitors have been developed as potential

therapeutics for AD.[65-67] A group of non-steroidal anti-inflammatory drugs (NSAIDs), including ibuprofen, indomethacin, and sulindac sulfide were identified as γ-secretase inhibitors.[65]

α-secretase activator:

Improving α-secretase activity and shifting APP processing towards non-amyloidogenic pathway results in decreased full length Aβ production, reducing probability of AD.[68,69] The development of α-secretase activators or α-secretase mimetics have been found greater interest in current research and has been regarded as a valuable approach in AD drug development.[68]

1.8.2. Modulation of Aβ aggregation:

In brain, the neuronal cells constitutively generate small amounts of the various Aβ isoforms. The monomeric Aβ, particularly $A\beta_{1-40}$ and $A\beta_{1-42}$ forms oligomeric aggregates which are thought to initiate AD.[32] Earlier it was assumed that the aggregated large fibrils of Aβ, a major constitute of the mature neuritic amyloid plaques, would exert toxic properties, but presently it is believed that the small soluble oligomeric assemblies of Aβ are more toxic than the mature fibrils and can directly induce synaptic dysfunction.[46, 55] In the diseased condition it is believed that the monomers of Aβ peptide converts from a nontoxic random coil or α-helical conformation to a toxic β-sheet conformation that is responsible for the initiation of Aβ aggregation. The strategies which can (i) prevent the Aβ aggregation, (ii) block the β-sheet formation, (iii) disrupt and re-dissolve the Aβ aggregates to non-toxic monomers, and (iv) destabilize Aβ oligomers are considered as modulators of Aβ aggregation.[65] The most effective modulation approaches are described below.

Peptide based approach:

Since, AD is believed to be a peptide aggregation disease, the peptide based modulators are accepted as one of the most interesting and effective therapeutic approaches against AD. A short peptide unit (LVFF) in Aβ sequence which was accepted as the central hydrophobic region of Aβ and assumed as recognition motif of peptide based drug design against AD.[50] Later, various peptide based molecules containing the recognition motif and the breaker elements, including proline,[70] N-methylation,[71] poly-lysine,[72] *etc*., are observed as promising approaches for drug design against AD.[73,74] These peptide based molecular approaches were also found efficient with other protein aggregation diseases including PD and type-2 diabetes.[75] The advantages of these approaches are that peptides are accepted as highly selective, efficient, and relatively safe.[76]

Small molecule based approach:

Use of small organic molecules as potent therapeutic approach towards drug design is another promising strategy against AD.[74,75] Although, the mechanistic action of these small molecules is unclear, it is believed that they break the Aβ aggregation through antioxidant properties or hydrophobic interaction or chelating the metal ions (Cu^{2+}, Zn^{2+} or Fe^{3+}) that are involved in Aβ aggregation.[77,78] Numerous small molecules, including curcumin, resveratrol, rifampicin, methylene blue, epigallocatechin-3-gallate (EGCG) and scyllo-inositol are known to act as anti-Alzheimer's agent for their antioxidant and aggregation inhibition capability.[74,75,79]

Metal ions homeostasis approach:

The metal ions (Cu^{2+}, Zn^{2+} Fe^{3+} or Al^{3+}) homeostasis plays an important role in the brain functionality and their dyshomeostasis contribute largely to the pathogenesis of AD. The therapeutic use of metal chelating compounds against AD has found large interest for the past few decades. 8-hydroxyquinoline (8-HQ), and its derivatives clioquinol (CQ), PBT2 and other molecule like 6-chlorotacrine have been recently established as anti-AD agents for their selective metal chelating ability and subsequent inhibition of amyloid formation.[74,80]

Antibody based approach:

Antibody based approach or Aβ immunotherapy was found as another potential therapeutic strategy against the AD.[81] For the past few years, more than ten immunotherapeutic agents have entered clinical trials and three are currently in Phase III trials, including elan's bapineuzumab (humanized 3D6), lilly's solanezumab (humanized 266) and Baxter's intravenous immunoglobulin G (IVIG).[82] Although, the mechanism of antibody based therapy is not clear but recent evidences suggest that a monoclonal antibody recognizing the central region of Aβ very efficiently sequestered Aβ in the senile plaques.[83]

1.8.3. Modulation of Tau and tangle formation:

Intraneuronal tangles containing hyperphosphorylated tau are another cause of AD.[42] Tau and tangle pathology are not only responsible for AD, but these are linked also to other human disorders, including Pick's disease, progressive supranuclear palsy, corticobasal degeneration and motor neuron diseases.[84] Therefore, finding of specific modulator of tau and tangles against AD is difficult. A rigorous research over last three decades resulted numerous compounds that inhibit the tau aggregation and methylthioninium chloride (methylene blue) observed to be the best among all till date.[85]

1.9. Biophysical tools used to monitor amyloid formation and modulation:

a) Ultraviolet (UV) absorption

UV absorbance is a useful technique to determine the structure and study the structural changes of a protein, because chromophores display shifted spectra upon changing the polarity of the medium.[86] For example, wavelength of maximum absorbance (λ_{max}) and molar extinction coefficient (ε) increases if chromophores are shifted to a less polar environment.[87] Proteins are known to absorb mostly at 240-310 nm for the presence of the aromatic side chain of Trp, Tyr and Phe. The peptide bond absorbs strongly below 230 nm due to $n\rightarrow\pi^*$ and $\pi\rightarrow\pi^*$ electronic transitions, whereas aromatic residues absorb in the near-UV region between 250 and 290 nm due to $\pi\rightarrow\pi^*$ electronic transitions.[87] We have used UV studies for probing side chain aromatic interactions of relevant peptides.

b) Circular dichroism (CD)

CD is one of the most routine techniques used for examination of the secondary structures of protein/peptide in a solution. The theory involved in the CD is the differential absorption of the right handed and left handed circularly polarized light. The resulting component shows elliptical polarization and is reported in terms of ellipticity (θ) in degrees ($\Delta\mathbf{A} = \mathbf{A_L}\text{-}\mathbf{A_R}$). As discussed earlier, the peptide bond absorbs strongly below 230 nm due to $n\rightarrow\pi^*$ and $\pi\rightarrow\pi^*$ electronic transitions, whereas aromatic residues absorb in the near-UV region between 250 and 290 nm due to $\pi\rightarrow\pi^*$ electronic transitions. The different types of secondary structures (helix, sheet or turn) are usually characterized by CD spectra in far UV region. In order to obtain the reliable data, exact protein concentration must be known and CD instrument should be properly calibrated.[88]

c) Fourier Transformation Infra-Red spectroscopy (FTIR)

FTIR is another technique to determine the secondary structure of a protein or a peptide. Generally, the asymmetric stretching frequencies of amide I band and N-H band of the peptide are measured by FTIR. Amide I band (1600 to 1700 cm^{-1}) and N-H band (3200 to 3500 cm^{-1}) are known to represent the secondary structure of peptide. For our investigation, sample was examined before and after fibril formation. FTIR has also been used to suggest the presence of either parallel or anti parallel β-sheet in a particular peptide.[23]

d) Raman Spectroscopy

Raman spectroscopy is a technique to characterize the change in vibrational band due to conformational change of a protein or peptide.[89] The aromatic side chain of a peptide is very sensitive to Raman spectroscopy and show distinct characteristic vibrational band for Phe, Trp or Tyr.[89] In aqueous solution, the amide I band of the peptide are obscured by the bending vibration modes of H_2O in FTIR spectroscopy but such interference is lesser in Raman spectroscopy.[90] Therefore, in aqueous medium the change of amide I band due to conformational change can be monitored by Raman spectroscopy.

e) Thioflavin T fluorescence

Thioflavin T (ThT) is a benzothiazole moiety containing fluorescent dye which is extensively used for quantitative analysis of amyloid fibrils *in vitro* or *in vivo*. Normally, the excitation and emission maxima of ThT dye is at 350 and 440 nm respectively, upon binding to amyloid fibrils the excitation and emission maxima shifts to higher wavelength at 435 to 490 nm respectively.[91] The fluorescence intensity of an aggregated peptide solution is directly proportional to the amount of fibrils present in the solution. Although the mechanism of ThT

activity is not clear but it is accepted that the enhancement of fluorescence indicate the increment of fibrils in the solution, on the other hand, decrement of intensity indicates inhibition of fibrillar assembly.[91,92]

f) Transmission electron microcopy (TEM)

TEM is mostly used as a qualitative technique to visualize amyloid fibrils present in any aggregated peptide assembly. In this technique a beam of electron from tungsten filament usually passes through the thin film of sample, interacts with the sample, and produces a high resolution image. TEM is commonly used for morphological observation of any sample. The thin film of sample (peptide solution) was prepared over carbon coated copper grid and stained with a negative staining agent (uranyl acetate) for better resolution of the image when viewed under optimum condition at 200 kV.[23,93]

g) Congo red birefringence

Amyloid fibrils are known to bind with Congo red dye and show characteristic green-gold birefringence when viewed under optical microscope using cross polarized light.[23,94] This technique is extensively used for monitoring amyloid fibril formation, where only mature fibrils and amyloid show birefringence, but other intermediates like oligomers or proto-fibrils do not give such birefringence.

h) Field emission scanning electron microscopy (FE-SEM)

FESEM is another microscopic technique similar to TEM, which is commonly used for visualization of a sample's surface topology. In FESEM, a high energy electron beam from an electron gun of field-emission cathode is exposed over the sample surface and capture

images by the in-built camera.[95] For our investigation the non-conducting samples, peptide or lipid samples, are placed over glass plate and coated with gold before analysis.

i) Large unilamellar vesicles (LUV) leakage assay

LUV is an artificial vesicle and commonly used to mimic the cell. Dye (carboxy fluorescein) loaded LUV leakage assay is extensively used for the *in vitro* toxicity analysis.[96] Since, the oligomers are known to be more toxic than the mature fibrils or monomers due to their ability of pore formation in the cell membrane, the oligomers cause more leakage from the LUV than the other forms of the peptide.[55,96] The leakage of dye is monitored by fluorescence.

j) Förster resonance energy transfer (FRET) study

Förster resonance energy transfer (FRET) is an important technique to determine the structural orientation of the biomolecules including proteins and nucleic acids.[97] FRET study is also useful to determine the mode of binding between two molecules. For FRET observation, some criteria must be fulfilled. For example,

(a) *the emission spectrum of a fluorophore (donor) overlaps with the absorption spectrum of another molecule (acceptor)*

(b) *the energy transfer from the donor to the acceptor expected to occur and consequently there will be a decrease in fluorescence of the donor (both intensity and lifetime), whereas the fluorescence of the acceptor is expected to be increased.*[97]

The fluorescence can be measured by fluorometer whereas the lifetime can be measured by the time-resolved photoluminescence (TRPL) spectrometer.

1.10. Objective of the thesis:

For the past few decades, extensive research have been carried out for the drug development against AD, still there is no cure. There are numerous strategies available against AD, more research have to be done to get the proper drug or therapy against AD. Since the exact role of APP is unclear, the modulation of Aβ production appears to be a topic of debate. Similarly, the research on targeting tau or tangles is also observed, but it is also a topic of debate. On the other hand, Aβ aggregates are the major cause of AD. Modulation of Aβ aggregation is a broadly accepted approach among all. Again, the small molecule based and metal chelating approaches are also found very effective, but most of them lack protein selectivity as well as ability to cross blood brain barrier (BBB). Thus, peptide based approach is mostly accepted as effective as well as safe approach among all, because peptides are very selective and less toxic.

Therefore, our main objective is to develop a suitable peptide based drug against AD and other protein aggregation diseases. To design a competent drug against these diseases, it is always important to understand the mechanism of amyloid aggregation, specially the initiation process.

In this thesis, the discussion is mainly centered on AD. Therefore, in this thesis we have demonstrated a mechanistic pathway of early onset of amyloid formation and discussed different strategies of peptide based drug design against AD. In this thesis, we performed experiments with $A\beta_{1-40}$ and its related sequences. Direct working with $A\beta_{1-40}$ is difficult and troublesome at the initial stage of optimization. Therefore, we started our experiments with model aggregating peptides which are known as functional mimic of Aβ peptide, later we moved to the native Aβ system. The objectives of the thesis are:

1. To elucidate the mechanistic pathway of amyloid formation, mainly the early onset of aggregation, using various biophysical techniques, including UV, CD, and Raman spectroscopy.
2. To introduce a new β-sheet breaker peptide, anthranilic acid containing β-sheet breaker hybrid peptide (BSBHp) and apply its anti-amyloidogenic activity upon model aggregating peptide using various biophysical tools, including ThT, FTIR, and TEM.
3. To apply the anti-amyloidogenic activity of BSBHp upon the Aβ aggregates using various biophysical tools, including ThT, FTIR, and TEM.
4. To develop a novel class of pro-drug peptide (PDp) against AD.
5. To develop another class of novel zipper peptide, containing *N*-methylated amino acids and PEG unit for the capturing of Aβ aggregates.

Chapter 2: Early onset of amyloid formation by Alzheimer's Amyloid β derived switch-peptide: A mechanistic pathway

2.1. Background:

The exact mechanism of amyloid formation and neurotoxicity in Alzheimer's disease is unclear. However, several models, namely, templated assembly (TA), monomer-directed conversion (MDC), nucleated polymerization (NP) and nucleated conformational conversion (NCC), exist which explain the plausible mechanism of aggregation and fibril formation.[98,99] All these mechanisms share some common information directing to the cascade hypothesis of amyloid formation (Figure 2.1).[20,32,100]

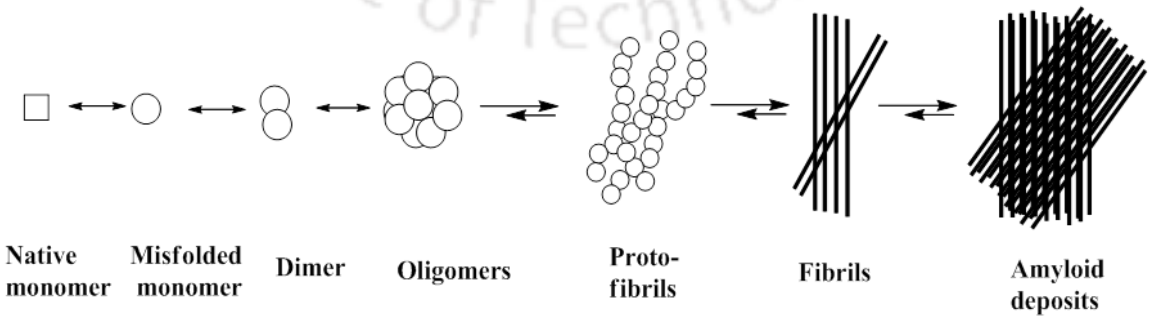

Figure 2.1: Plausible mechanism of amyloid formation in Alzheimer's disease: a cascade hypothesis.

Although, these models and mechanisms are quite informative, the exact mechanism particularly the early events of amyloid formation are not well-understood. In this regard, the amino acid sequence of a peptide is very important, more precisely, the role of side chain is important for recognition followed by self-aggregation to form amyloid. Most of the diseased proteins (amyloid) contain amino acids with aromatic side chains (Table 2.1) and the central role of stacking interactions in the self-assembly processes is not clearly understood, as there is no method for probing the initiation of aggregation.[101-103] In this chapter, we described the results of our investigations on the importance of aromatic amino acids at the early stage of aggregation using a properly designed amyloidogenic switch-peptide[104,105] as a functional mimic of Aβ peptide.

Parent peptide	Diseases	Amyloidogenic sequence (aromatic residues are highlighted)
Amyloid-β	Alzheimer's disease	KLV**FF**AE
Amylin	Diabetes type-2	N**F**GAIL
Calcitonin	Thyroid carcinoma	D**F**NK**F**
Lactadherin	Aortic medial amyloid	N**F**GSVQ**F**V
Gelsolin	Finnish hereditary amyloidosis	S**F**NNGDCC**F**ILD
Serum amyloid A	Chronic inflammation amyloidosis	S**FF**S**F**LGEA**F**D
PrP	Creutzfeldt-Jakob disease	PHGGG**W**GQ

Table 2.1: Amyloid forming short peptide sequence that contain aromatic residues.[102]

2.2. Proposed hypothesis:

Although the detailed mechanism of amyloid formation is unclear, it is mostly agreed that the early stage of amyloid formation is the adoption of a β-sheet conformation from an unstructured conformation.[32,100] Hence, the formation and stabilization of β-sheets have significant importance in understanding the aggregation process. The driving force and facts behind the process of transition from unstructured to β-sheet conformation is not understood yet, *i.e.* the early events of amyloid formation are not clear. In this chapter we have discussed the facts and events at the early stage of amyloid formation of an amyloidogenic peptide using UV, CD and Raman spectroscopic techniques. Since most of the diseased proteins contain one or more aromatic amino acids in their backbone, the importance of aromatic amino acids have been always considered as a matter of interest but no clear evidence has been observed.[101-103] We propose a hypothesis that at the early stage of aggregation, the aromatic side chains interacts prior to β-sheet formation during the conformational transformation of an aromatic side chain containing amyloidogenic peptide (Figure 2.2).

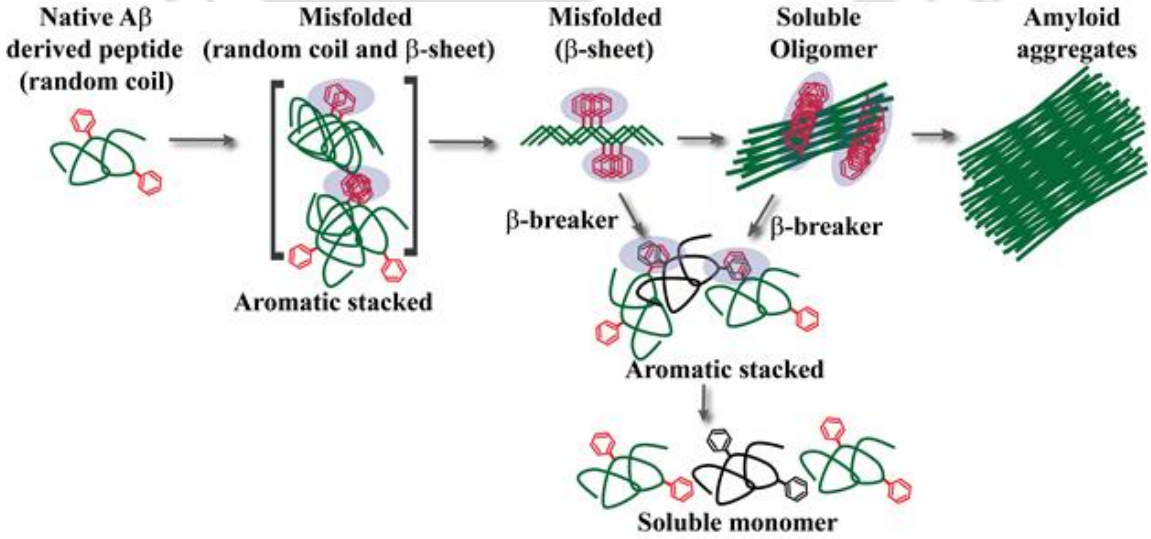

Figure 2.2: Hypothesis on the early events of amyloid formation via aromatic side chain interaction.

Also, if aromatic amino acid containing β-breaker peptides are added to the amyloid aggregates, it first interacts with the amyloidogenic peptide through aromatic side chain before the disaggregation process starts.

2.3. Design of peptides:

For the investigation on the early events of amyloid formation, we need a molecular mimic of Aβ peptide which aggregates *in vitro* in a similar way to that of the Aβ peptide and for that reason we have chosen a switch-peptide as amyloidogenic peptide. A switch-peptide is an iso-peptide which has an ability to transform its structure from one conformation (random coil) to another (β-sheet) depending on the pH and temperature. They exhibit similar aggregation property to that of the Aβ peptide and therefore widely known as the functional mimic of the Aβ peptide.[104] Mutter and co-workers reported -$(Ser\text{-}Leu)_n$- based peptide which forms amyloid like fibrils rich in β sheet architecture at physiological condition (pH ~7.4 and 37 °C). They incorporated an iso-peptide bond inside the sequence using the side chain of a specific serine residue and named them as "switch-peptides", where iso-peptide bond connected serine acts as a switch unit (Scheme 2.1).[104] Presence of the iso-peptidic bond forbids attaining β sheet conformation at the initial stage. As soon as the peptide reaches normal peptide backbone at physiological condition via *O* to *N* acyl migration, it forms β-sheet which finally converts to fibril and amyloid.

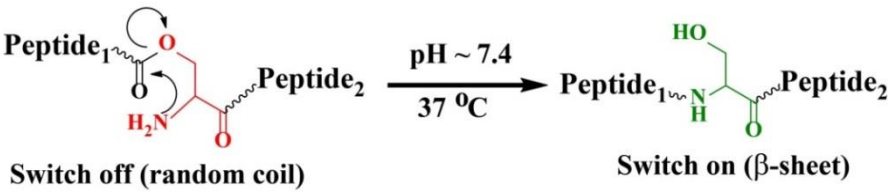

Scheme 2.1: Switch-peptide with a serine switch: *O* to *N* acyl migration takes place to get native peptide backbone from iso-peptide form.

To prove our hypothesis, we have used two model aggregating peptides (functional mimic of Aβ) based on the concept of switch-peptide as described above and two β-breaker peptides[50,70] (Table 2.2). We have designed the switch-peptides (**2A** and **2B**) based on -(Ser-Leu)$_n$- model, where peptide **2A** does not contain any aromatic ring in the side chain (for simplification of analysis) but **2B** contain two phenyl rings in the side chain (adapted from Aβ partial sequence). Two known β-breaker peptides (**2C** and **2D**) were used; both having partial homology to the peptide **2B** and contain aromatic amino acids.

Peptide No.	Peptide Sequence	Function
2A	Ac-SLSL-**(H$^+$)S**-LSLSLG-NH_2	Aggregating peptide
2B	Ac-SLSLHQKLVFF-**(H$^+$)S**-EDVSLG-NH_2	Aggregating peptide
2C	Ac-LPFFD-NH_2	β-sheet breaker
2D	Ac-LVFFD-NH_2	β-sheet breaker

Table 2.2: Sequences of designed peptides for the present study.

2.4. Synthesis and characterization of the designed peptides:

All the designed peptides were synthesized by solid phase peptide synthesis (SPPS) technique using standard Fmoc/^{t}Bu protection strategy on Rink amide MBHA resin following reported protocols.[106-108] Each amino acid coupling was performed using 2 equivalents of Fmoc amino acid and BOP (2.5 equivalents) in the presence of DIPEA (5 equivalents). Each coupling step was monitored by Kaiser's test and micro cleavage test. In case of incomplete coupling, the cycle was repeated and capping was done using acetic

anhydride and *N*-methyl imidazole (2 equivalents) for 30 minutes in two cycles. Fmoc group deprotection was achieved by 20% piperidine in DMF for 21 minutes (7 min x 3 times). After *N*-terminal Fmoc removal, peptide was washed with DMF and DCM (Scheme 2.2). Peptide was cleaved from the resin using the cocktail solution TFA/DCM/H_2O (9/0.5/0.5) for nearly 3 hours and precipitated using cold diethyl ether to obtain white solid crude peptide. The crude peptide was purified using C_{18} μ-Bondapak semi preparative reverse phase HPLC column using solvent A (H_2O with 0.1% TFA) and solvent B (CH_3CN with 0.1% TFA). For the separation, a linear gradient was used for a total runtime of 20 min. Initially 5% acetonitrile was running which linearly increased to 100% till 18 min and remaining 2 min was used for washing at 100 % acetonitrile till 20 min. Dual wavelength was selected at 214 nm and 254 nm. After HPLC, the acetonitrile was evaporated and the aqueous peptide solution was frozen using liquid nitrogen before lyophilization. After lyophilization the white solid powder of pure peptide was obtained (the detail of yield has been described in the experimental section, chapter 7).

A representative example of the synthetic protocol (peptide **2B)** has been depicted in Scheme 2.2. All the designed peptides were synthesized in a similar fashion. The purity of the peptide was determined by analytical HPLC and the peptide was characterized by mass spectrometry. The characterization data for all the designed peptides used for the mechanism investigation have been shown below.

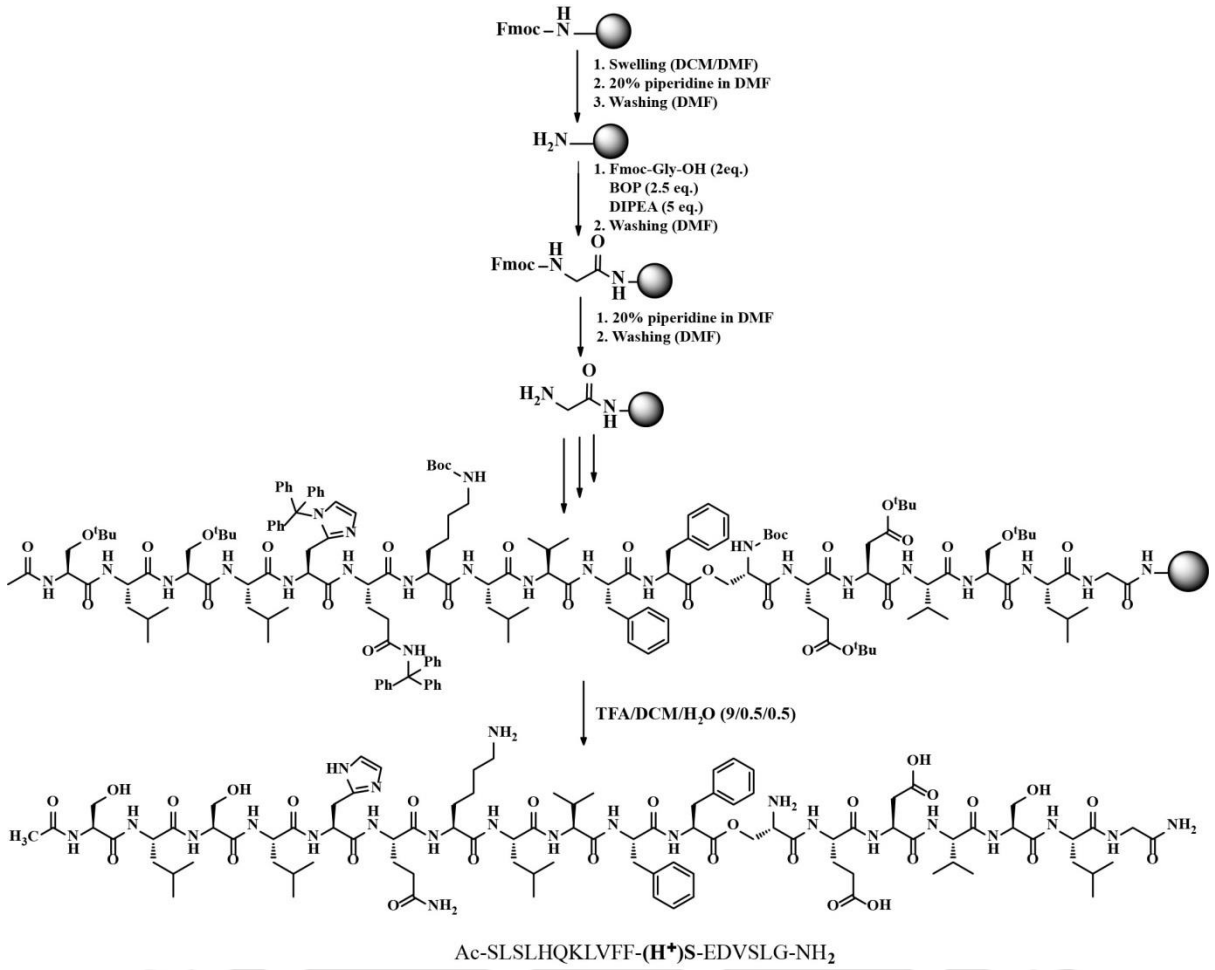

Scheme 2.2: Synthetic scheme of peptide **2B** using Fmoc/^{t}Bu protection based SPPS.

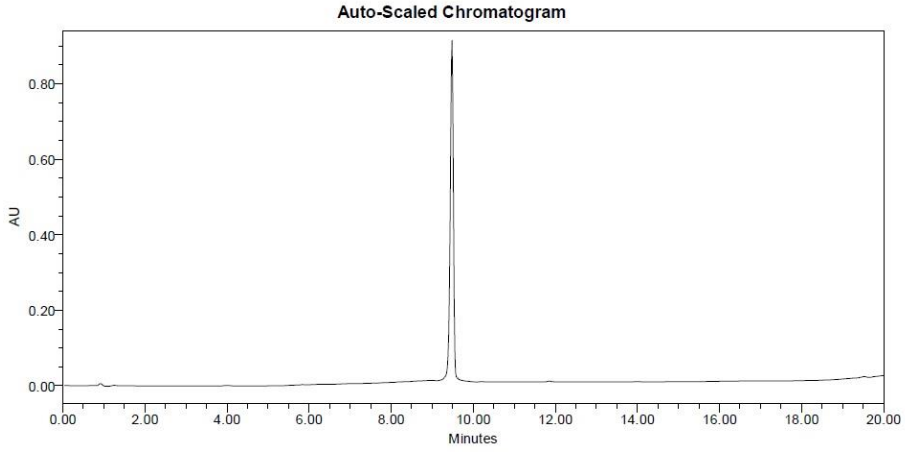

Figure 2.3: HPLC profile of the purified peptide **2A**.

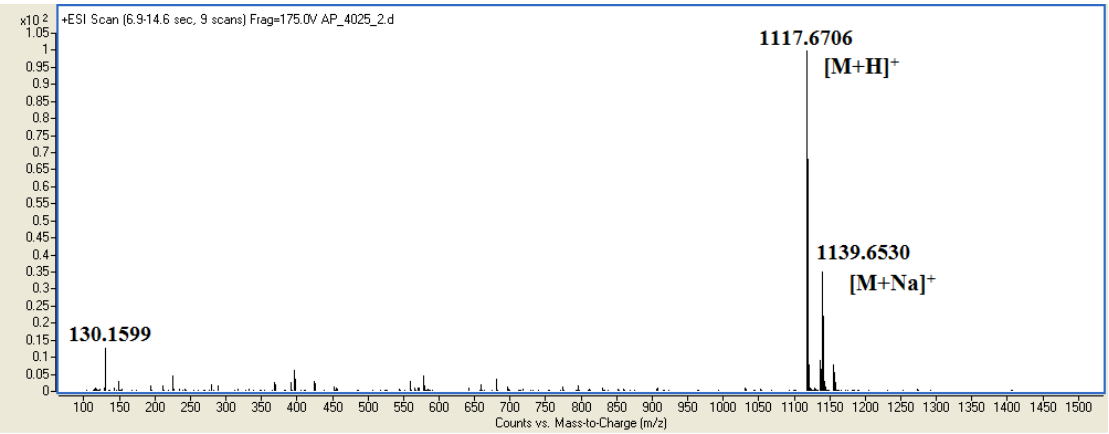

Figure 2.4: Mass spectrum of peptide **2A**, Calculated mass for $C_{49}H_{89}N_{12}O_{17}$ is 1117.64 $[M+H]^+$, observed 1117.67 $[M+H]^+$ and calculated mass for $C_{49}H_{88}N_{12}O_{17}Na$ is 1139.63 $[M+Na]^+$, observed 1139.63 $[M+Na]^+$.

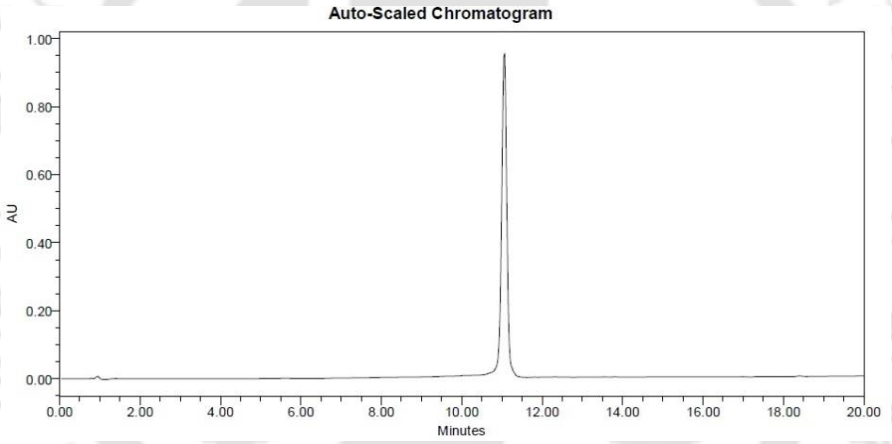

Figure 2.5: HPLC profile of the purified peptide **2B**.

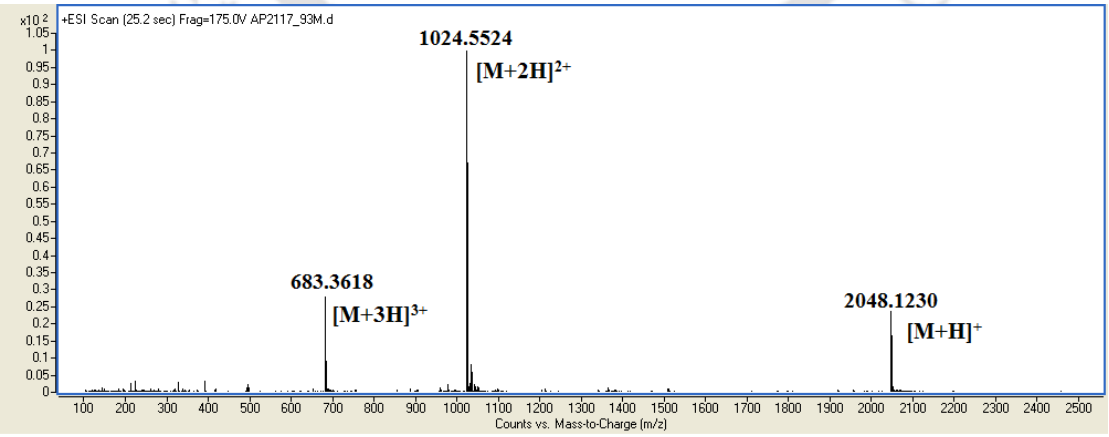

Figure 2.6: Mass spectrum of peptide **2B**, Calculated mass for $C_{94}H_{148}N_{23}O_{28}$ is 2048.09 $[M+H]^+$, observed 2048.12 $[M+H]^+$, 1024.55 $[M+2H]^{2+}$ and 683.36 $[M+3H]^{3+}$.

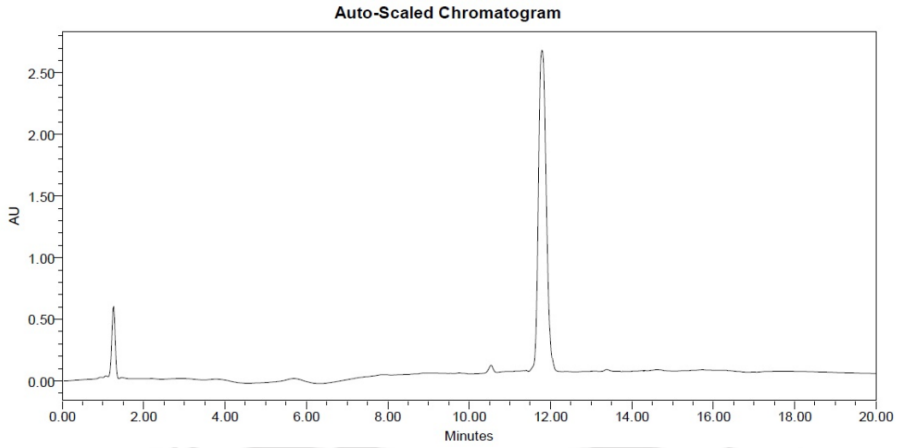

Figure 2.7: HPLC profile of the purified peptide **2C**.

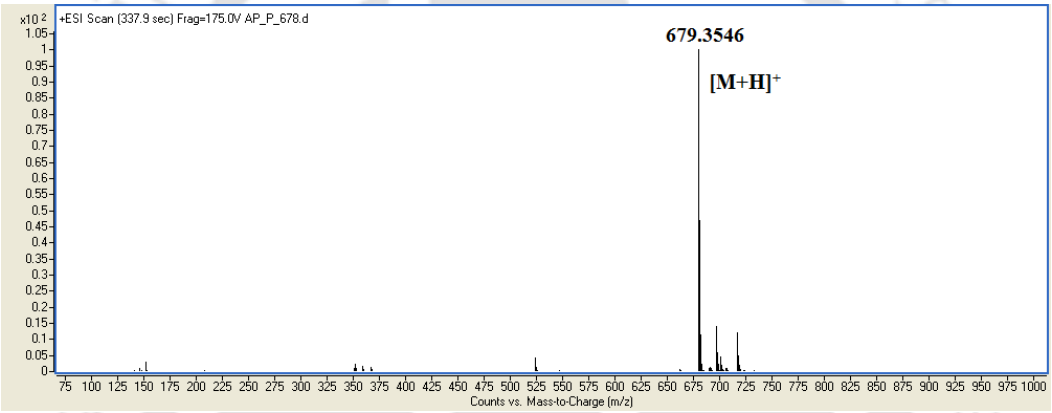

Figure 2.8: Mass spectrum of peptide **2C**, Calculated mass for $C_{35}H_{47}N_6O_8$ is 679.34 $[M+H]^+$, observed 679.35 $[M+H]^+$.

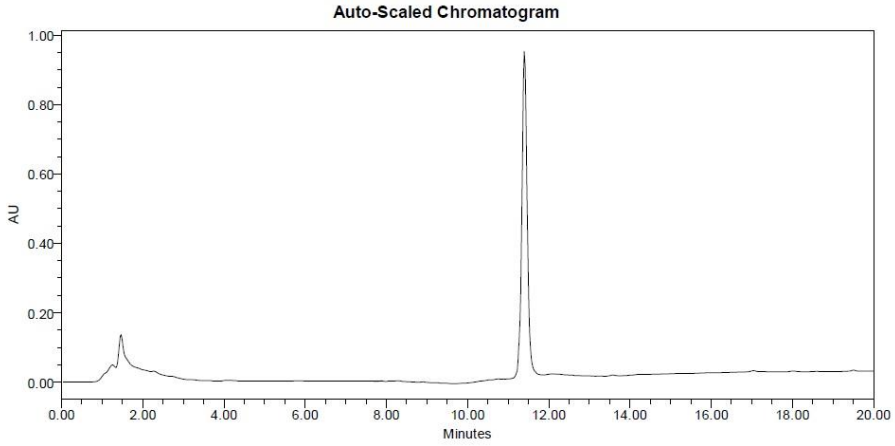

Figure 2.9: HPLC profile of the purified peptide **2D**.

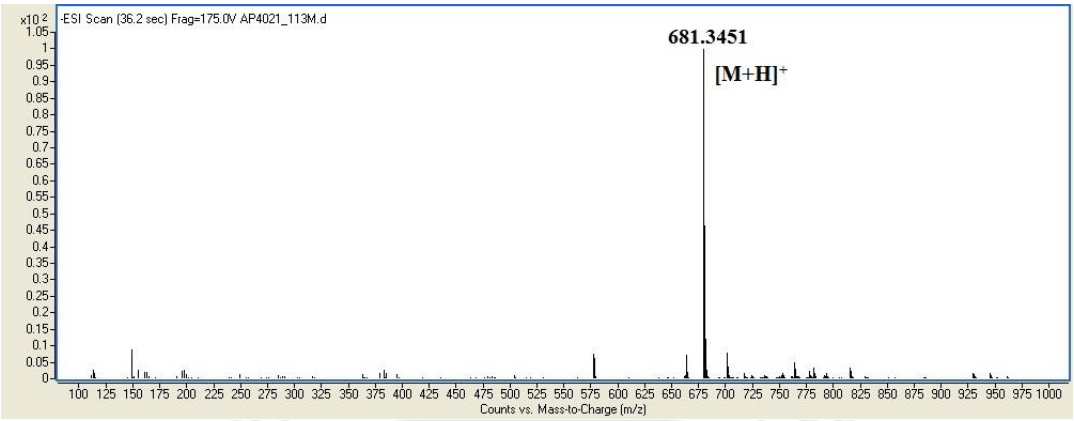

Figure 2.10: Mass spectrum of peptide **2D**, Calculated mass for $C_{35}H_{49}N_6O_8$ is 681.36 $[M+H]^+$, observed 681.34 $[M+H]^+$.

2.5. Amyloidogenicity of the switch-peptides:

We already discussed that the switch-peptides were amyloidogenic at physiological condition and were broadly known as functional mimic of Aβ. However, The amyloidogenicity of the synthesized switch-peptides were verified by various biophysical techniques. We have synthesized peptide **2B**, keeping the sequence homology (partial) with Aβ peptide and the amyloidogenicity was monitored by TEM and Congo red stained birefringence studies under cross polarized light. Prior to the study of amyloidogenicity the kinetics *O* to *N* acyl migration and the conformation of the switch-peptide **2B** was monitored.

2.5.1. Kinetics of *O* to *N* acyl migration of peptide 2B:

The switch-peptide converts its iso-peptide form to native peptide form at physiological condition (pH 7.4 and 37 °C) and the kinetics of *O* to *N* acyl transfer was monitored by LC-MS (Scheme 2.3). A stock solution of ~0.5 mM was prepared in phosphate buffer solution (PBS, 50 mM, pH 7.4) and incubated at 37 °C on water bath. At different time intervals 200

µL of sample was taken out from the stock solution in LC-MS vials, quenched with 1N HCl (final pH ~1.0) and injected in LC-MS. At the end all the text files were collected and plotted using MS-excel (Figure 2.11). Initially 5% acetonitrile in water solution was eluted for 2 minutes and then 5 to 100% acetonitrile for 6 minutes (linear gradient) in a total run time of 8 minutes was used. A dual detector of 214 nm and 254 nm wavelength was used.

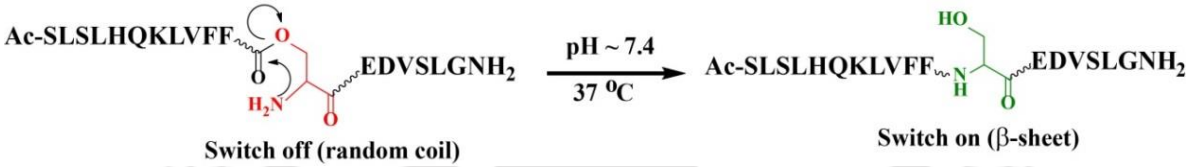

Scheme 2.3: pH triggered O to N acyl migration of peptide **2B**.

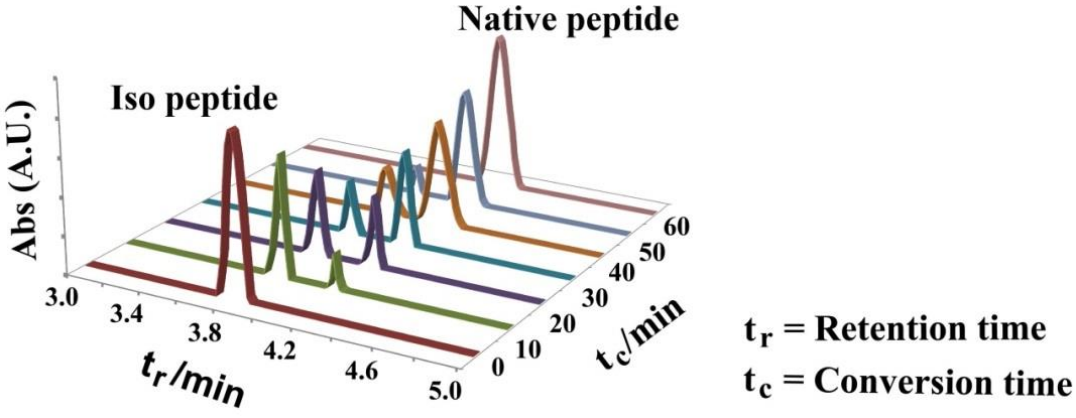

Figure 2.11: The kinetics of *O* to *N* acyl migration of the peptide **2B** at pH 7.4 and 37 °C.

At zero time, one major peak was observed at retention time (t_r) 3.8 min., corresponding to the pure peptide **2B**. Since the pH of the solution was basic, the protonated form of the peptide got converted to the free amine due to which *O* to *N* acyl migration started and a new peak was noticed at t_r 4.2 min., having the same mass value (Figure 2.12). The first peak was

assigned to the peptide in iso form (switch off state) which slowly converted to the native form (switch on state) in pH 7.4. Finally the peak at t_r 3.8 min. disappeared and the peak at t_r 4.2 min remained constant.

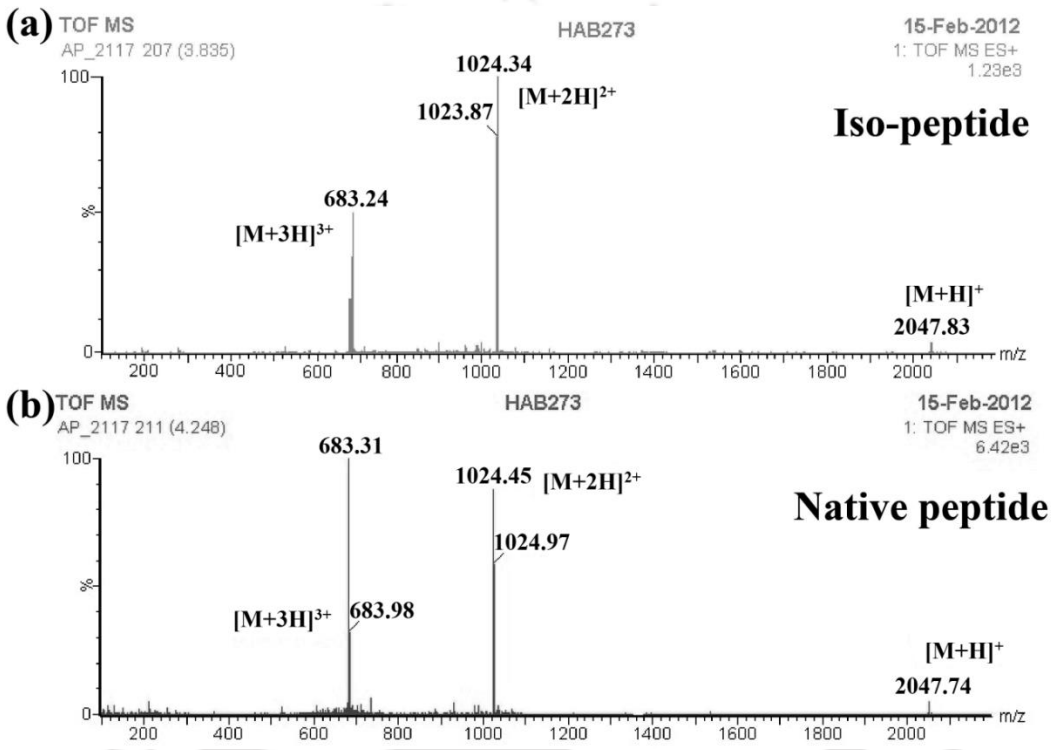

Figure 2.12: ESI-MS spectra of the peptide **2B** in, (a) iso form and (b) native form.

2.5.2. Monitoring conformational transition of peptide 2B by CD and FTIR studies:

In LC-MS study, we observed two different peaks having same molecular mass for the two different form of the peptide (Figure 2.11). It is known that switch-peptide form amyloid *in vitro* at physiological condition (pH 7.4 and 37 °C) and since the amyloids are rich in β-sheet conformation, it was essential to check the β-sheet forming ability of the switch-peptide. To get the exact conformation of the iso-peptide, we dissolved the peptide in sodium acetate

buffer (50 mM, pH 4.0) and for the native peptide we dissolved the peptide in PBS (50 mM, pH 7.4) as mentioned earlier. The conformation of the peptide at different pH was monitored using CD and FTIR studies (Figure 2.13).

For the conformational analysis of iso-peptide, the pure peptide was dissolved in sodium acetate buffer and immediately performed CD and FTIR studies. We observed a negative band at ~200 nm in CD (black, Figure 2.13a) and a strong band at 1648 cm^{-1} in FTIR (black, Figure 2.13b) studies; this corresponds to the random coil conformation of the peptide.[23,88] Again, to check the conformation of the native peptide, we dissolved the pure peptide in PBS and incubated the solution at 37 °C for 1 h to make sure the complete conversion of the iso-peptide to native peptide. Then the conformational analyses were performed using CD and FTIR studies. We observed a positive band at ~197 nm, with a negative band at ~214 nm in CD (red, Figure 2.13a) and a strong band at 1633 cm^{-1} in FTIR (red, Figure 2.13b) studies; this corresponds to the β-sheet conformation of the peptide.

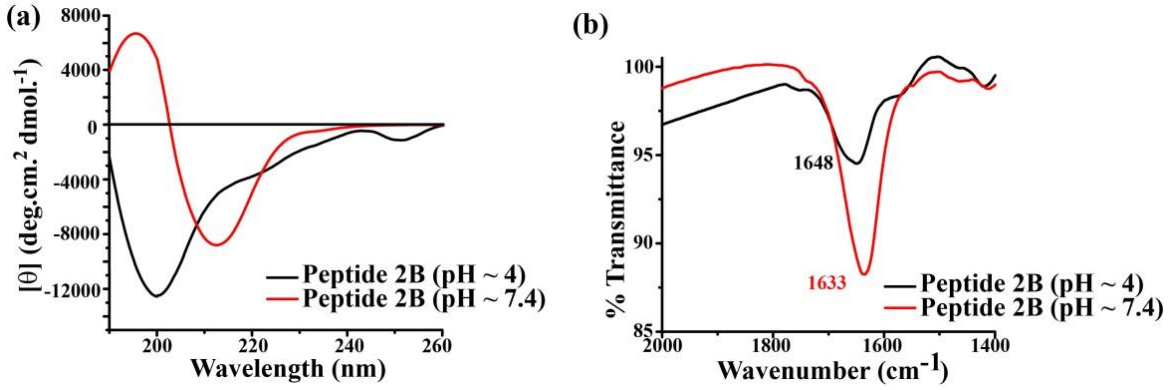

Figure 2.13: (a) CD and (b) FTIR spectra of peptide **2B** at pH 4.0 (black) & pH 7.4 (red).

2.5.3. Monitoring of amyloidogenicity of the peptide 2B by Thioflavin T fluorescence assay:

We have already observed that the peptide **2B** showed β-sheet conformation at pH 7.4 and 37 °C by CD and FTIR studies. Next, we wanted to examine the rate of fibril formation using thioflavin T (ThT) fluorescence at the same condition. ThT fluorescence assay provides quantitative information on fibril formation.[23] To check the amyloid forming ability of the peptide, we prepared a stock peptide solution ~0.5 mM in PBS (50 mM, pH 7.4) and incubated at 37 °C on water bath. At different time intervals, 40 μL of peptide sample was mixed with 200 μL of ThT solution (50 μM), total volume was made up to 400 μL with PBS (50 mM, pH 7.4) and fluorescence was measured (λ_{ex} = 440 nm, λ_{em} = 485 nm and band width 3 nm). We observed a significant increment of fluorescence intensity with time for the peptide solution (Figure 2.14). This confirms that the peptide **2B** aggregates to form fibrils at physiological condition (pH 7.4 and 37 °C).

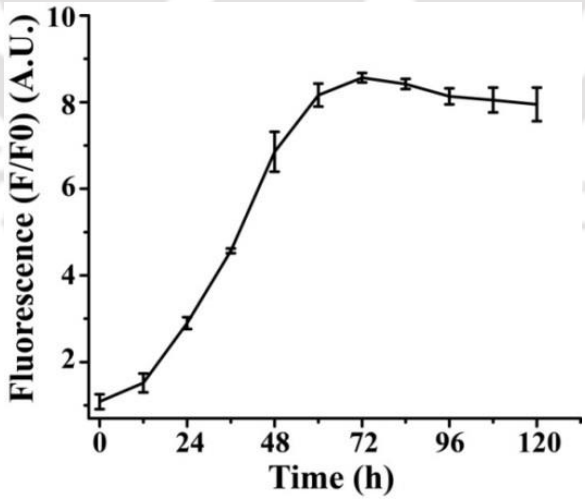

Figure 2.14: Time dependent Thioflavin T assay of peptide **2B** (0.5 mM) in PBS pH 7.4 (50 mM) at 37 °C.

2.5.4. Monitoring of amyloidogenicity of the peptide 2B by TEM and Congo red birefringence studies:

We already confirmed the amyloidogenic nature of the switch-peptide at physiological pH using Thioflavin T assay. We further confirmed the amyloidogenicity of **2B** using TEM and Congo red stained birefringence under cross polarized light. TEM provides direct evidence for the presence and absence of fibrils in a solution.[23] Sample was prepared in a similar way as described for Thioflavin T. The peptide solution was incubated for 5 days at 37 °C and 10 µL of the peptide sample from the stock solution was added over a carbon coated copper grid, followed by addition of 10 µL of 2% uranyl acetate over it. The droplet was allowed to stand for 2 min and excess solution was removed carefully by blotting paper. Grid was allowed to dry in open air and examined at 200 kV under TEM. We observed a clear fibrillar assembly of the peptide in TEM (Figure 2.15a), indicating the amyloidogenic nature of the peptide.

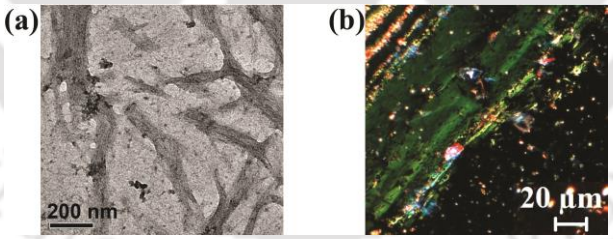

Figure 2.15: (a) TEM and (b) Congo red stained birefringence images of peptide **2B**. The images were taken after 5 days of incubation in PBS of pH 7.4 at 37 °C.

Appearance of green gold birefringence of a peptide sample when stained with Congo red solution under cross polarized light is another characteristic evidence of amyloidogenic nature of a peptide.[23] From the stock solution, 20 µL of sample was placed over a glass slide

and dried in air. Then 20 µL of saturated Congo red solution (in 80% aqueous ethanol) was added over it and allowed to dry in air. The dried spot was analyzed under optical microscope using cross polarized light. We observed clear appearance of green gold birefringence (Figure 2.14b), indicating the amyloidogenic nature of the peptide.

2.6. Investigations of the early events of amyloid formation:

After proper bio-physical characterization of the switch-peptides and being sure of the fact that they form fibril and amyloid aggregate as Aβ peptide does, we went for further investigations on the early events of amyloid formation using ultra-violet (UV), circular dichroism (CD) and Raman spectroscopic techniques. Peptide **2A** was chosen for the simplification of the system with no aromatic side chain but peptide **2B** contains two phenylalanine residues.

2.6.1. Monitoring conformational transition of peptide 2A using UV and CD:

The UV spectra of peptide **2A** recorded at the initial time (t = 0) and after completion of the conformational transition (t = 50 min) exhibited a distinct change, due to conformational transition of the peptide as confirmed by a parallel CD studies (Figure 2.16). Here, t = 0 refers to the time of triggering the acyl migration by changing the pH to 7.4 for switch-peptide **2A**. We noticed a significant change in the UV absorption spectra of peptide **2A** recorded at t = 0 and at t = 50 min (Figure 2.16a), which is essentially due to the conformational change of the peptide as no other change in the experimental conditions was allowed. During the time of observation, the peptide was converted from random coil to β-sheet conformation that was verified by parallel CD measurements. In CD curve, at t = 0 we

observed a negative band at ~197 nm which was a characteristic band for random coil conformation. Again at 50 min, we observed a positive band at ~199 nm and a negative band at ~217 nm, which were characteristic bands for a β-sheet conformation (Figure 2.16b). Importantly, UV spectra obtained from poly-L-lysine[109] due to random coil to β-sheet transition by Rosenheck and Doty resembled to our results (Figure 2.16a). The π→π* transition (centered at 200 nm)[88,110] was influenced significantly by random coil to β-sheet transition of peptide **2A** due to the decrease in polarity of the environment of the amide bond.[87] However, the change in absorbance at 220 nm, which arises due to n→π* transitions was also notable.

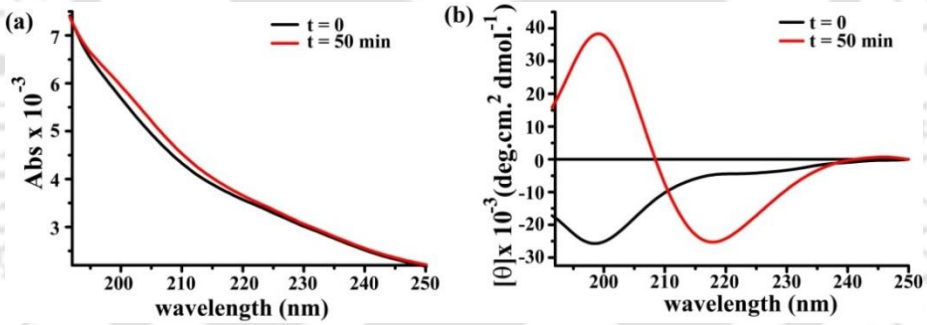

Figure 2.16: Change in (a) UV spectra and (b) CD spectra, due to conformational transition of switch-peptide **2A** (50 μM in PBS pH 7.4) occurred in 50 min.

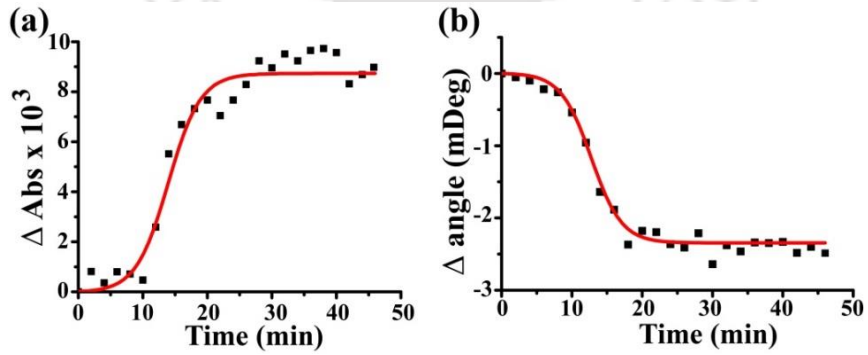

Figure 2.17: Time course measurement of the random coil to β-sheet transition of peptide **2A**, monitored by (a) UV absorbance (sigmoid fit, $R^2 = 0.98$) and (b) CD (sigmoid fit, $R^2 = 0.99$) (c = 20 μM, PBS pH 7.4, at 220 nm).

In the present study, the kinetics of the random coil to β-sheet transition of the switch-peptides due to acyl migration upon changing the pH was in the center of interest. The time dependent changes in both UV and CD spectra at 220 nm generated sigmoid curves due to conformational transitions of peptide **2A** (Figure 2.17). The half-life ($t_{1/2}$) values of the transitions were obtained by fitting the experimental curves with Boltzmann equation. The $t_{1/2}$ value (13.95 ± 0.6 min) obtained by UV was in accordance with that obtained by CD measurement (12.76 ± 0.3 min).

2.6.2. Monitoring of conformational transition of peptide 2B using UV and CD:

We observed similar change in the UV (Figure 2.18) and CD (Figure 2.13a) spectra upon conformational (random coil to β-sheet) transition for the other switch-peptide **2B**, keeping the experimental condition same. Therefore, the change in the UV and CD absorption was accepted as a characteristic feature of the conformational change of the switch-peptide. Due to high symmetry, Phe has a smaller extinction coefficient compared to Trp or Tyr.[87] Nevertheless, the appearance of two positive bands at 265 and 285 nm in CD analysis due to aggregation was known for amylin peptide.[111] The reason was the conformational restrictions of the aromatic rings of Phe15, Phe23 and Tyr37 of amylin associated with aromatic interactions that was related to β-sheet stacking. For the present investigation we have used the switch-peptide **2B** which neither contained Trp nor Tyr but Phe. Therefore, the change in UV spectra for peptide **2B** at two different wavelengths 220 nm and 257 nm was due to the conformational change and due to aromatic stacking respectively.

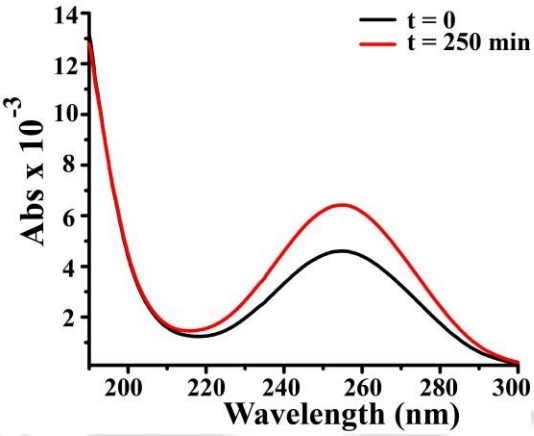

Figure 2.18: Change in UV spectra due to conformational transition of switch-peptide **2B**.

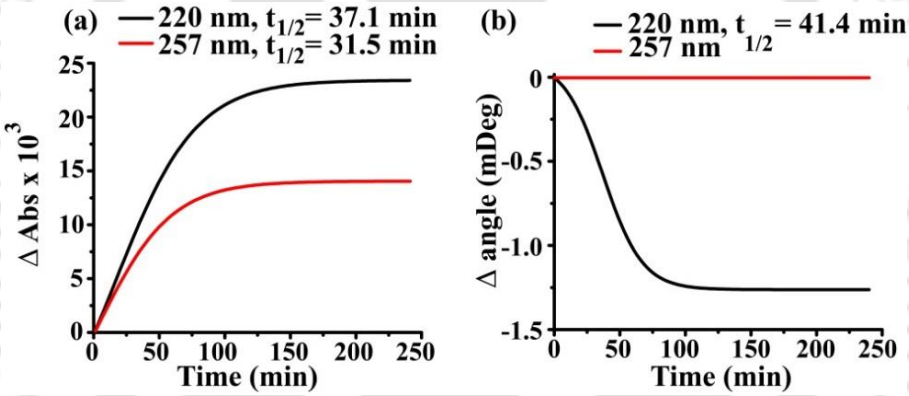

Figure 2.19: Normalized sigmoid fit of the change in (a) absorbance and (b) ellipticity, at 220 nm & 257 nm of peptide **2B** (20 μM in PBS pH 7.4).

The time dependent kinetics for the change in UV absorption at 220 and 257 nm of peptide **2B** were compared with CD signals at 220 nm (Figure 2.19) to monitor the effect of the onset of β-sheet structure on the environmental alteration of the aromatic side chain of Phe. The UV and CD at 220 nm indicated particularly the onset of β-sheets. Again, the absorbance due to the amide bond was negligible compared to π→π* transition of aromatic side chains at near UV region. The significant change in UV at 257 nm was expected to be influenced by

the environmental alteration of the aromatic side chain of Phe residues resulting from conformational transitions. Therefore, absorbance at 257 nm was preferred for investigation on the environmental change of Phe.

The $t_{1/2}$ of random coil to β-sheet transition of peptide **2B** (20 μM) at 220 nm was found to be 37.1 ± 0.4 min, due to the change in absorbance (black, Figure 2.19a), whereas the $t_{1/2}$ obtained by monitoring the ellipticity at 220 nm was found to be 41.4 ± 0.6 min (black, Figure 2.19b). The results again support the inference that kinetics of random coil to β-sheet transition of the switch-peptides can be measured by monitoring the UV absorption at 220 nm. Again, $t_{1/2}$ of the change in absorbance at 257 nm was observed to be 31.5 ± 0.4 min (red, Figure 2.19a). This is due to the change in environment of the aromatic side chain of Phe that occurred in parallel to the random coil to β-sheet transition. However, the ellipticity values at 257 nm remained unchanged (red, Figure 2.19b) as no cotton effect is expected at that wavelength. The enhancement of UV absorbance at 257 nm due to the conformational transition was related to the aromatic stacking interactions related to β-sheet stacking[111] and through-space intermolecular interactions among the newly formed β-sheets.[112] Thus, the increase in absorbance may directly be associated to the amyloid formation initiated by aromatic stacking of Phe.

With variable concentration of the peptide **2B**, we observed similar result in UV absorption at 257 nm (10 μM, Figure 2.20a and 5 μM, Figure 2.20c) and the change in ellipticity at 220 nm (10 μM, Figure 2.20b and 5 μM, Figure 2.20d). The increment of $t_{1/2}$ due to aromatic stacking from 31.5 ± 0.4 min (20 μM) to 41.6 ± 0.5 min (10 μM) and further increment to 61.7 ± 0.9 min (5 μM) as observed by monitoring the UV absorption at 257 nm (Figure 2.19a and 2.20a,

c). Again, the $t_{1/2}$ for the onset of β-sheet formation as obtained by the change in ellipticity at 220 nm from 41.4 ± 0.6 min (20 μM) to 58.4 ± 0.7 min (10 μM) and further to 84.6 ± 1.0 min (5 μM) when concentration of peptide **2B** was decreased (Figure 2.19b and 2.20b, d). Slower transitions at lower concentration are reasonable as decreasing concentration usually delays nucleation or amyloid formation. Importantly, at each concentration (5, 10 and 20 μM) tested the $t_{1/2}$ of aromatic stacking became smaller than the corresponding $t_{1/2}$ for the onset of β-sheet formation (backbone H-bonding interactions). These results imply that the aromatic stacking takes place prior to β-sheet formation in the process of aggregation. That implies, aromatic stacking occurs at an earlier stage of β-sheet formation.

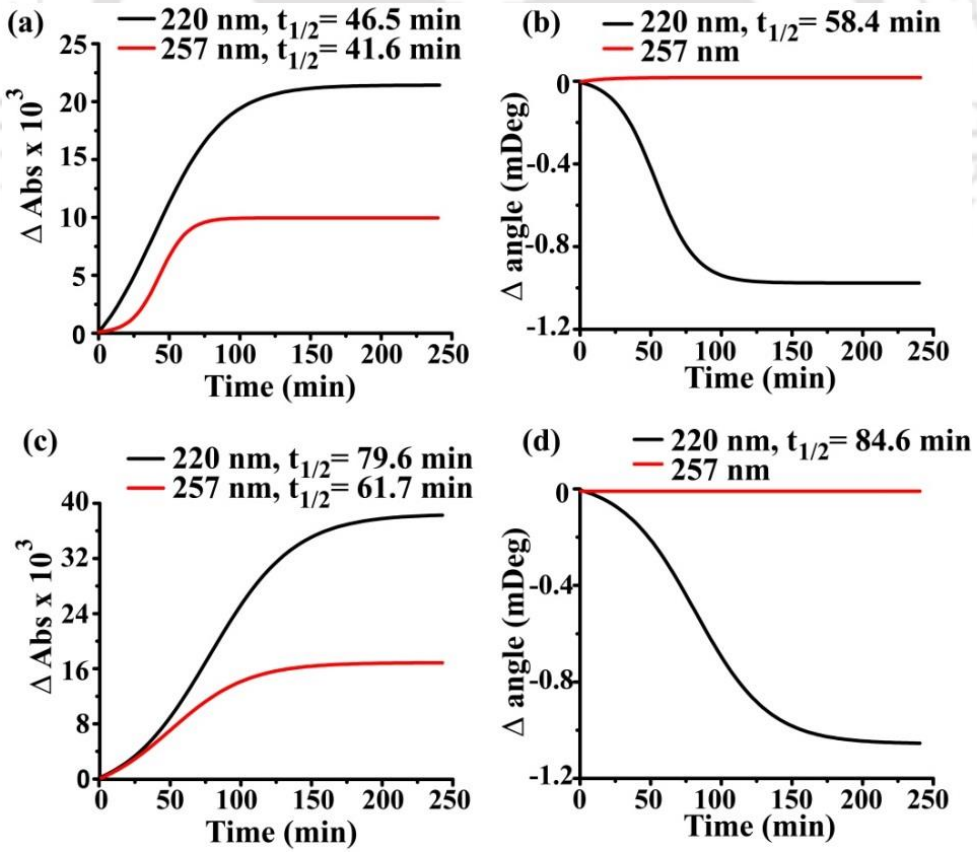

Figure 2.20: Normalized sigmoid fit of the change in (a & c) absorbance and (b &d) ellipticity, at 220 nm & 257 nm of peptide **2B** (10 μM (a, b) and 5 μM (c, d) in PBS pH 7.4).

2.6.3. Monitoring conformational transition of peptide 2B using Raman spectroscopy:

We have already observed from UV and CD analyses that aromatic stacking occurred prior to β-sheet formation. We wanted to verify the same phenomena using Raman spectroscopy. The changes in amide I vibration due to random coil to β-sheet transition of peptide **2B** was monitored by Raman spectroscopy. At t = 0, we observed the amide I band at 1665 cm^{-1}, corresponds to random coil or α-helical conformation and a strong band at ~1020 cm^{-1}, corresponding to the characteristic band for Phe (Figure 2.21).[90]

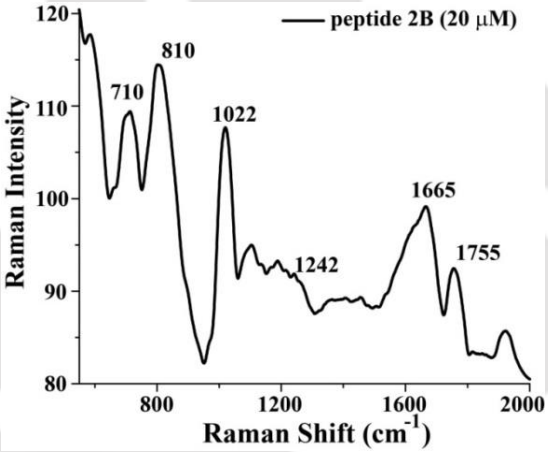

Figure 2.21: Raman spectrum of peptide 2B (20 μM) in PBS pH 7.4.

We performed a kinetic study for the random coil to β-sheet transition of peptide **2B** and observed that the peak at 1665 cm^{-1} was suppressed significantly with time and a new band at 1633 cm^{-1} appeared that corresponds to β-sheet conformation (at 90 min). However, the characteristic band for Phe at ~1020 cm^{-1} did not shift during the random coil to β-sheet conversion but we observed chronological increment of the Raman intensity with time (Figure 2.22).[90,113] The enhancement of intensity may be due to the aromatic stacking. We

observed the rate of increment of intensity at 1020 cm^{-1} was faster than reduction of intensity at 1665 cm^{-1}, indicating the aromatic stacking was faster than the conformational transformation. We could not perform Raman spectroscopic analysis at lower concentrations (< 20 μM) because of high noise and the amide I band was not distinguished well.

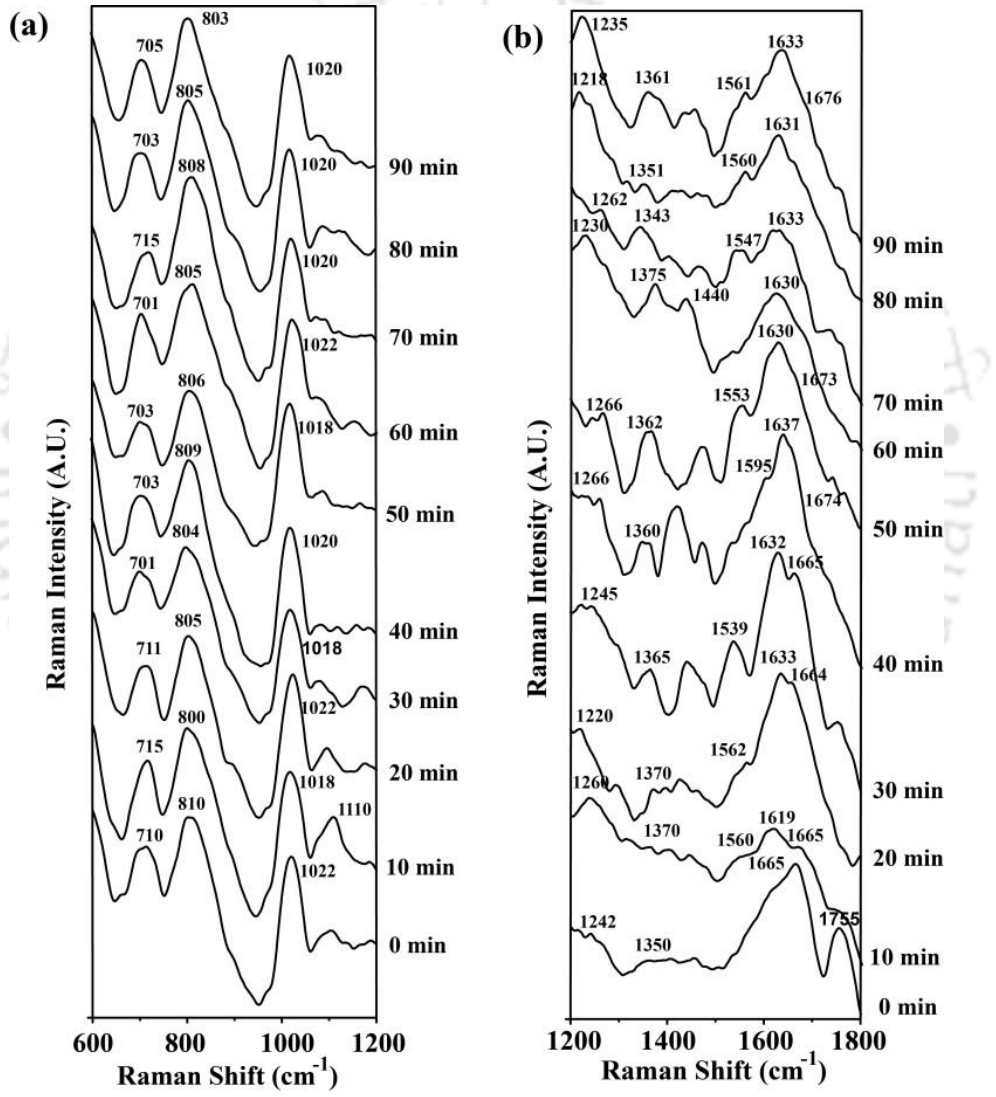

Figure 2.22: Change in Raman bands at different time interval of peptide **2B** (20μM in PBS pH 7.4) at (a) 1200-1800 cm^{-1} and (b) 600-1200 cm^{-1}.

2.6.4. Monitoring of amyloid formation and its inhibition of peptide 2B using UV and CD:

To validate our hypothesis of aromatic stacking occurred prior to the β-sheet formation and fibrillogenesis, further, a comparative UV and CD studies have been performed with peptide **2B** in presence of Phe containing inhibitors (β-sheet breaker peptides, BSBps). For that purpose we have used two reported BSBps, **2C** and **2D**.[50,70] The change in UV and CD due to the β-sheet formation of peptide **2B** (5 μM) in presence of 2 equivalents of peptide **2C** and **2D** have shown in Figure 2.23 (red and green curve). At 5 μM of peptide **2B**, mixing with the inhibitors resulting enhancement of absorbance (red and green, Figure 2.22a) than the absorbance noted in the absence of the inhibitor (black, Figure 2.22a). The increment of absorbance resembles to the situation where the concentration of peptide **2B** was increased (Figure 2.20). But the concentration of peptide **2B** was constant, and 2 equivalents of Phe containing inhibitors were added instead. Hence, it was inferred that the increment in absorbance resulted from the interaction between the inhibitor and the switch-peptide due to aromatic stacking. Parallel CD studies (at 220 nm) exhibited a decrease of β-sheet formation in the presence of the inhibitors (Figure 2.23b) indicating a significant inhibition of β-sheet formation. Therefore it was inferred that, the recognition of the inhibitors by the switch-peptide occurred due to the intermolecular aromatic interaction, which finally resulted in an inhibition of β-sheet formation.

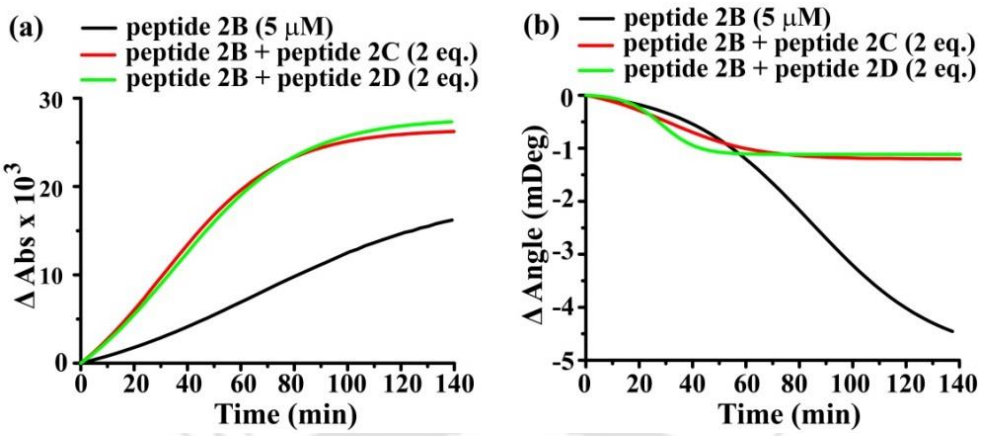

Figure 2.23: Effect of the inhibitors on (a) the aromatic stacking monitored by change in UV at 257 nm and (b) the onset of β-sheet formation monitored by change in CD at 220 nm of peptide **2B** (5 μM) in PBS of pH 7.4 at 37 °C.

2.7. Conclusion:

Our results suggest that the kinetics of the aromatic stacking and the same of the β-sheet formation of a properly designed switch-peptide were two discrete processes that lead to amyloid formation. In our experiments, the kinetics of the aromatic stacking was faster than the same of the β-sheet formation. Therefore, we concluded that the aromatic interaction occurs prior to the conformational conversion, and similarly recognition of the aggregating switch-peptide and the inhibitor takes place prior inhibition. All these evidences on the early events of aggregation may be useful for interpreting the mechanism of aggregation and finding out novel therapeutic strategies against amyloid associated diseases.

Chapter 3: Introduction of β-sheet breaker hybrid peptide and its application for the inhibition of aggregation of model aggregating peptide

3.1. β-sheet breaker hybrid peptide:

Tjernberg and coworkers identified important regions (recognition motifs) in Amyloid-β sequence which is responsible for amyloid formation in Alzheimer's disease (AD).[50] This was a landmark for peptide based drug design against AD. On the other hand, introduction of β-sheet breaker peptides (BSBps) by Soto and coworkers was a great invention in the field of amyloid disruption.[70] They prepared one of the BSBp, termed as iAβ5,[70] by inserting a proline residue as breaker element along with a recognition motif and demonstrated its efficacy to disrupt the amyloid fibrils of Aβ. Due to its inherent rigidity, the proline unit generates a kink in the peptide which helps to disrupt the aggregation. Later, more promising BSBps were reported containing various breaker elements including *N*-methylated amino acids,[71] α-Aminoisobutyric acid (Aib)[114] and Dehydrophenylalanine[115] which potentially disrupted amyloid aggregates. Most of these reported BSB peptides contain either an α-

amino acid or a modified α-amino acid as the β-breaker element. These are not stable against proteolytic degradation when present in proteins or peptides.[116] Since β-amino acids are non-proteinogenic and thus stable against proteolytic degradation, they can be benign candidates for drug design against protein aggregation diseases and other diseases.[117,118]

In this chapter we introduced a new class of BSBps containing an anthranilic acid (Ant, an aromatic β-amino acid) as the β-breaker element and the usual recognition motif of the amyloidgenic peptide. We collectively termed them as β-sheet breaker α/β hybrid peptides (BSBHps). Ant is a non-coded rigid β-amino acid found in many biologically active molecules and also the precursor for the biosynthesis of tryptophan.[119-121] Unlike coded amino acids, Ant and its homologs are structurally rigid and strongly favour helix or turn conformation when formed hybrid peptides with the α-amino acids.[122-124] Also they are stable towards proteolytic degradation. Therefore, we acquired Ant as a β-breaker element and incorporated in a BSBp to design our BSBHp. Finally, we wanted to demonstrate its efficiency to inhibit as well as reverse the self-aggregation of a model aggregating peptide *in vitro*. The general structure of a BSBHp is shown in Figure 3.1, where one of the peptides attached to the Ant unit may act as the recognition sequence.

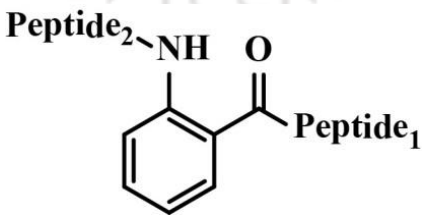

Figure 3.1: General structure of an anthranilic acid containing β-sheet breaker hybrid peptide.

3.2. Proposed hypothesis:

There are various strategies available for the disruption of amyloid and reduce toxicity of Aβ, but no suitable drug is available for complete cure of AD.[65] Since, peptides are selective to the targets, efficacious and relatively safe, peptides have gained increased interest as therapeutics.[76] Therefore, we wanted to develop peptide based molecules for the disaggregation of amyloid, which further can be used as drugs against AD and other amyloid associated diseases. With this motivation we developed Ant containing BSBHps (described in section 3.1) and anticipated that such BSBHps may disrupt amyloid aggregates of Aβ *in vitro*.

Our main target was to disrupt the amyloid aggregates of $A\beta_{1-40}$ *in vitro*. But, at the initial stages of optimization of the concept, direct dealing with $A\beta_{1-40}$ would be difficult and troublesome because of its complex amyloidogenic nature and synthetic complexity. Therefore, we first tested the efficacy of a specially designed BSBHp for the inhibition of a model aggregating switch-peptide (Figure 3.2).[104] In this chapter we mainly focused on the design, synthesis, non-amyloidogenic property of BSBHp and finally its inhibitory activity on aggregation of a model switch-peptide.

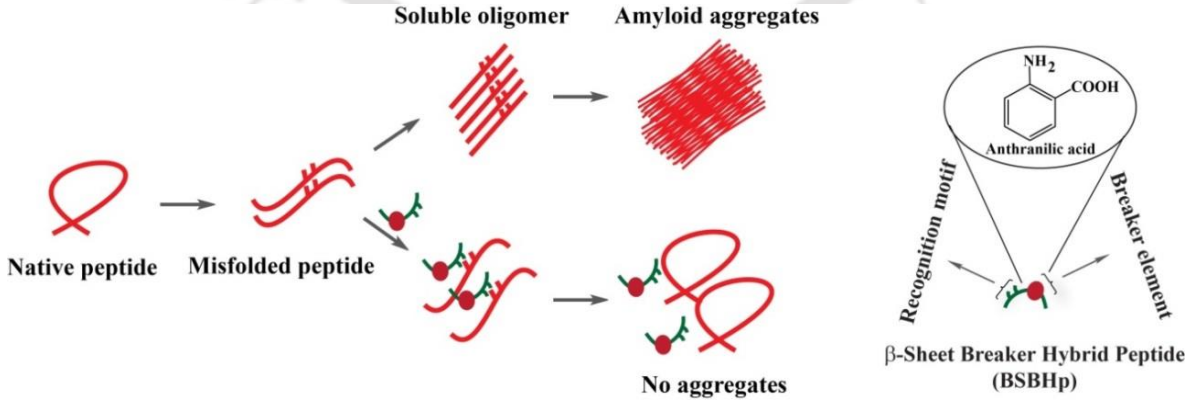

Figure 3.2: Hypothesis for the inhibition of amyloid formation of model aggregating peptide by a β-sheet breaker hybrid peptide.

3.3. Design of peptides:

To test our hypothesis of inhibition of aggregation of a switch-peptide by BSBHps *in vitro*, we first designed a model aggregating switch-peptide which showed similar amyloidogenicity to that of the Aβ and designed two BSBHps each comprised of an oliogopeptide (recognition motif) and an anthranilic acid (Ant) as the breaker element (Table 3.1). The amyloidogenic property of the switch-peptide has been described in chapter 2 (Section 2.3).

Peptide No.	**Peptide Sequence (X = anthranilic acid/Ant)**	**Function**
3A	LSL-**(H^+)S**-LSLG-NH_2	Aggregating peptide
3B	LSL**X**LSLG-NH_2	Inhibitor
3C	Ac-**X**LSLG-NH_2	Inhibitor

Table 3.1: Sequences of designed peptides for the present investigation.

For the ease of the synthesis and experiment, we have selected a simple model -(Ser-Leu)$_n$- based aggregating switch-peptide **3A**. The BSBHps **3B** and **3C** were designed keeping the sequence homology with the corresponding aggregating peptide **3A** for proper recognition. Precisely, -L-S-L- part of the peptides **3B** and **3C** were anticipated to recognize the peptide **3A**.

3.4. Synthesis and characterization of the designed peptides:

We have synthesized all the designed peptides in a similar way as peptide **2B** (Chapter 2, section 2.4) by solid phase peptide synthesis (SPPS) technique using standard Fmoc/^{t}Bu protection strategy on Rink amide MBHA resin.[106-108] The synthetic scheme of a BSBHp (peptide **3B**) have been depicted in scheme 3.1.

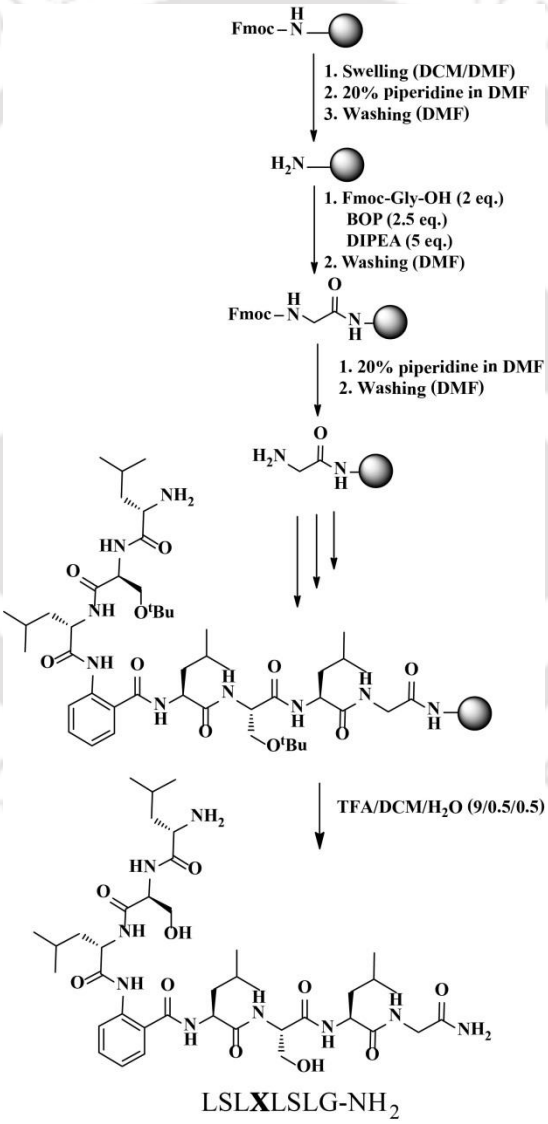

Scheme 3.1: Synthetic scheme of peptide **3B** using Fmoc/^{t}Bu protection based SPPS.

All the designed peptides were purified using semi preparative HPLC and purity was confirmed by HPLC and mass spectrometry. The characterization data for all the designed peptides have been shown below,

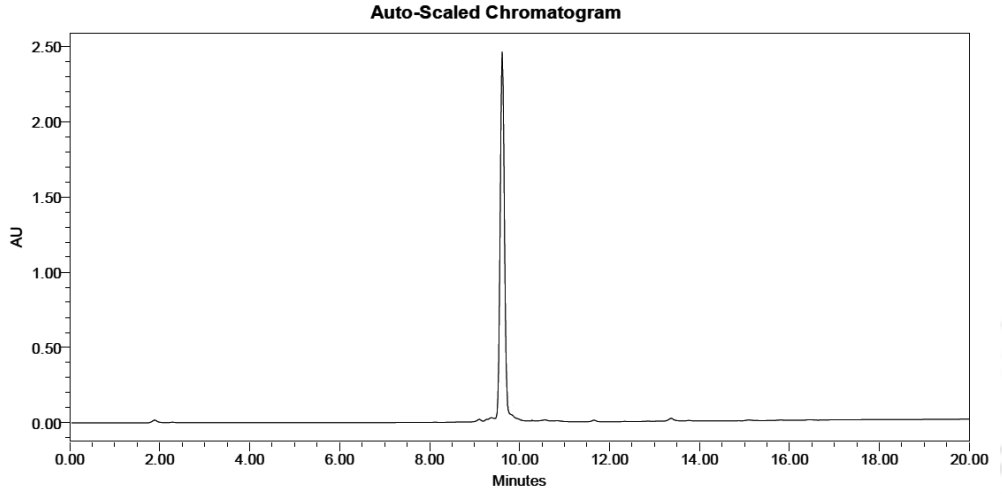

Figure 3.3: HPLC profile of the purified peptide **3A**.

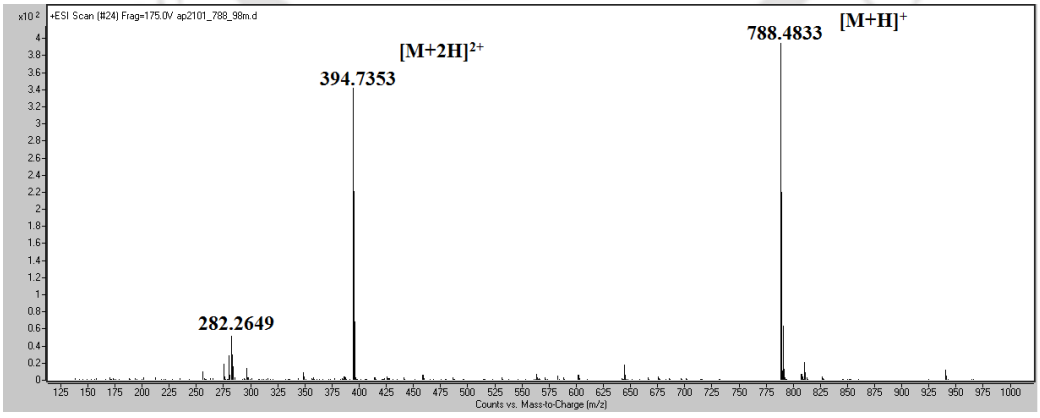

Figure 3.4: Mass spectrum of peptide **3A**. Calculated mass for $C_{35}H_{66}N_9O_{11}$ is 788.49 $[M+H]^+$, observed 788.48 $[M+H]^+$ and 394.73 $[M+2H]^{2+}$.

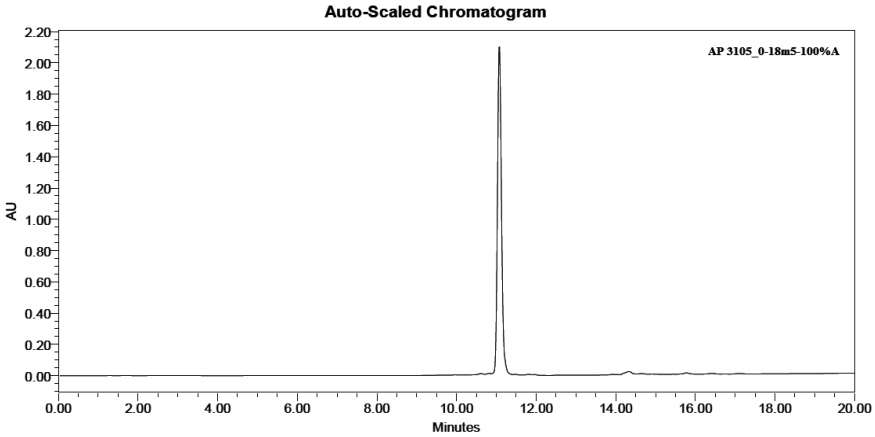

Figure 3.5: HPLC profile of the purified peptide **3B**.

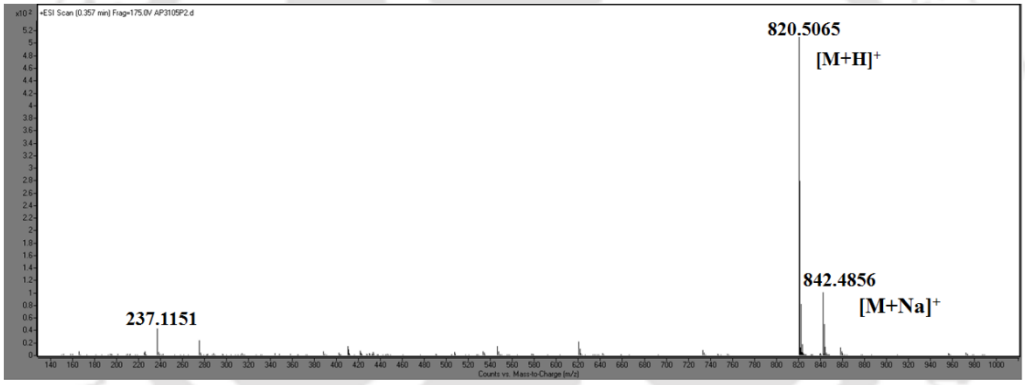

Figure 3.6: Mass spectrum of peptide **3B**. Calculated mass for $C_{39}H_{66}N_9O_{10}$ is 820. 49 $[M+H]^+$, observed 820.50 $[M+H]^+$ and calculated mass for $C_{39}H_{65}N_9O_{10}Na$ is 842. 47 $[M+Na]^+$, observed 842.48 $[M+Na]^+$.

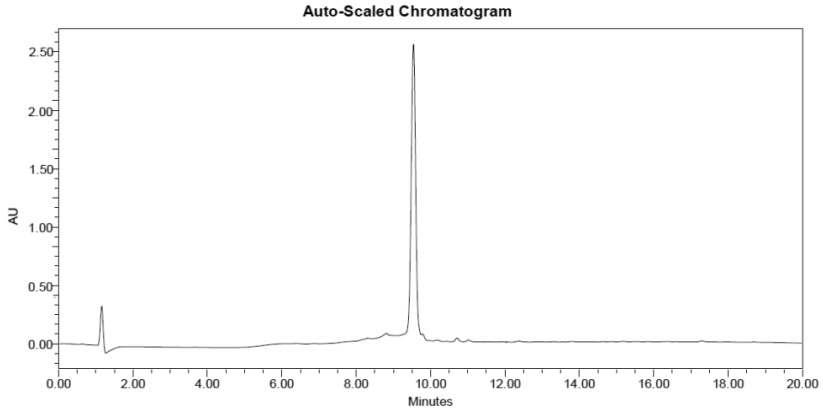

Figure 3.7: HPLC profile of the purified peptide **3C**.

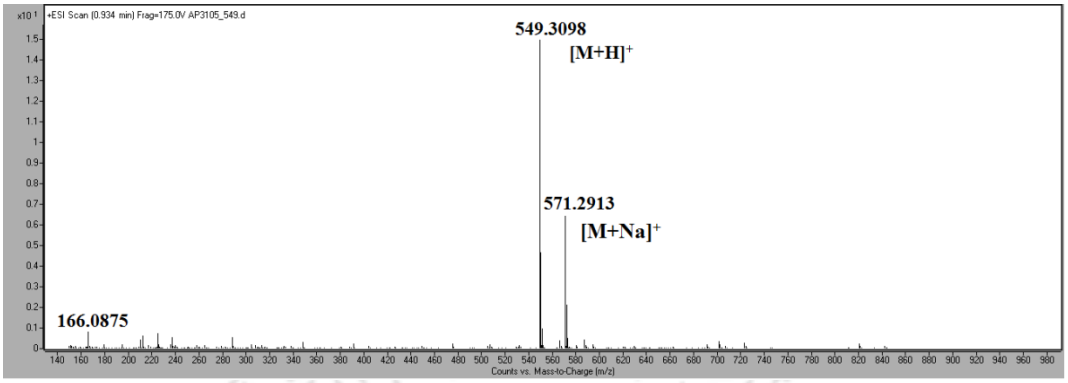

Figure 3.8: Mass spectrum of peptide **3C**. Calculated mass for $C_{26}H_{41}N_6O_7$ is 549.30 $[M+H]^+$, observed 549.31$[M+H]^+$ and calculated mass for $C_{26}H_{41}N_6O_7Na$ is 571.28 $[M+Na]^+$, observed 571.29 $[M+Na]^+$.

3.5. Non-amyloidogenicity of the BSBHps:

It was essential to check the non-amyloidogenicity of the designed BSBHps before its application for the inhibition of aggregation on model aggregating peptides. We studied the non-amyloidogenic nature of the BSBHps using various biophysical tools.

3.5.1. Conformational characterization of BSBHps by CD and FTIR studies:

The conformations of the BSBHps were monitored by the circular dichroism (CD) and the fouriour transformation infra-red (FTIR) spectroscopic analyses. To check the conformational analyses, the BSBHps were dissolved in phosphate buffer solution (PBS, 50 mM, pH 7.4) to make the concentration of the stock solution ~0.5 mM. Then the stock solutions of the BSBHps were incubated on water bath at 37 °C for 5 days. After 5 days the conformational studies were performed using CD and FTIR (Figure 3.9). In CD spectrum of peptide **3B** (black, Figure 3.19a), we observed a negative band centered at ~208 nm and a positive band centered at ~190 nm (percentage of helix content 47.6, β-sheet content 0, turn

content 48.8 and random coil content 3.5: deconvoluted from the CD instrument), indicating non β-sheet conformation of the peptide. Similarly, in the CD spectrum of peptide **3C** (red, Figure 3.9a), we observed a negative band centered at ~222 nm and a positive band centered at ~205 nm (percentage of helix content 30.5, β-sheet content 34.9, turn content 0 and random coil content 34.6: deconvoluted from the CD instrument), indicating presence of mixture of various conformations of the peptide.

Similarly, in FTIR spectra we observed the amide I band at 1659 cm^{-1} for peptide **3B** (black, Figure 3.9b) and a strong band at 1656 cm^{-1} for peptide **3C** (red, Figure 3.9b). These results clearly indicated non-β-sheet conformations of the peptides.

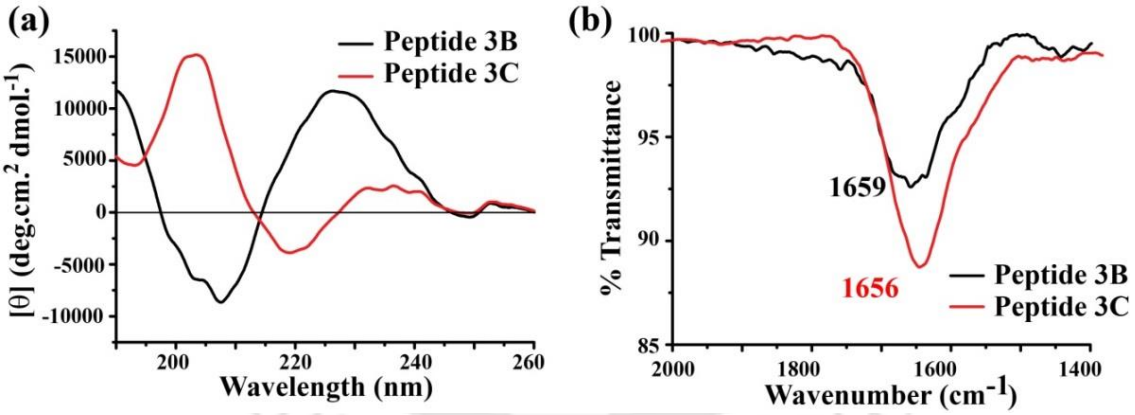

Figure 3.9: (a) CD and (b) FTIR spectra of peptide **3B** (black) and **3C** (red). Spectra were taken after 5 days of incubation of the peptides in PBS pH 7.4 (50 mM) at 37 °C.

3.5.2. Amyloidogenic characterization of BSBHps by TEM and Congo red birefringence studies:

The self-aggregation propensity or amyloidogenicity of the BSBHps were characterized by TEM and Congo red stained birefringence studies (Figure 3.10). From the stock solution (described in section 3.5.1) 10 μL of the peptide sample was added over a carbon coated copper grid, followed by addition of 10 μL of 2% uranyl acetate over it. The droplet was allowed to adsorb for 2 min and excess solution was removed by blotting paper. Then the grid was allowed to dry in open air and examined by TEM at 200 kV. We did not observe any fibrillar assembly from both the BSBHps in TEM (Figure 3.10a), indicating non-amyloidogenic nature of the BSBHps. Also, we did not observe any green gold birefringence for both the BSBHps when stained with Congo red dye and viewed under cross polarized light (Figure 3.10b). Therefore, from the above results, it was confirmed that the Ant containing BSBHps were non-amyloidogenic in nature.

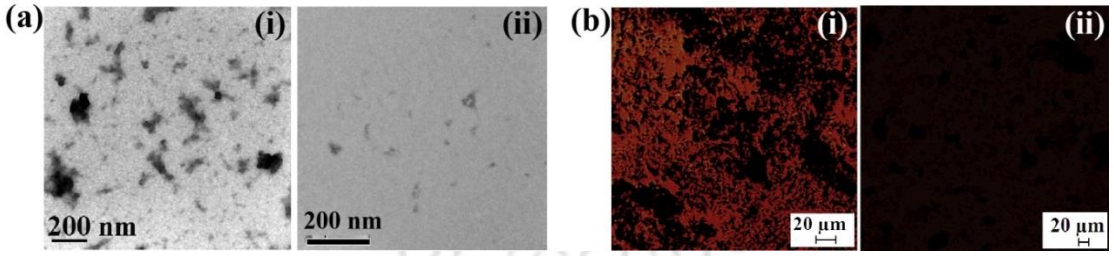

Figure 3.10: (a) TEM and (b) Congo red birefringence images of peptide **3B** (i) and **3C** (ii). Images were taken after 5 days of incubation of the peptides in PBS pH 7.4 (50 mM) at 37 °C.

3.6. Amyloidogenicity of the switch-peptide 3A:

We have already discussed in chapter 2, section 2.5 that the switch-peptides were amyloidogenic in nature at physiological condition (pH 7.4 and 37 °C). In this chapter we have used switch-peptide **3A** which was expected to be amyloidogenic at the same condition. For verification purpose, we checked its amyloidogenicity.

3.6.1. Kinetics of *O* to *N* acyl migration of peptide 3A:

The kinetics of *O* to *N* acyl transfer at pH 7.0 and 37 °C was monitored by LC-MS (Scheme 3.2 and Figure 3.11) in a similar fashion as mentioned earlier (Chapter 2, section 2.5.1).

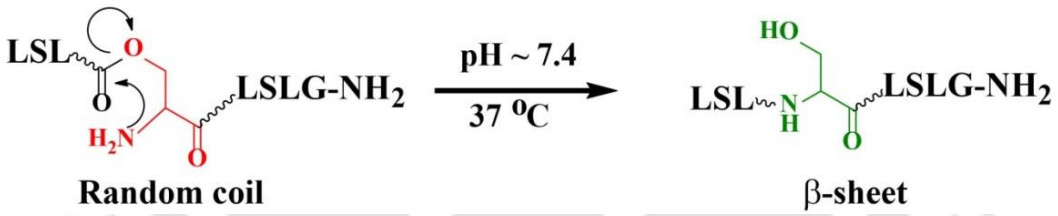

Scheme 3.2: pH triggered *O* to *N* acyl migration of peptide **3A**.

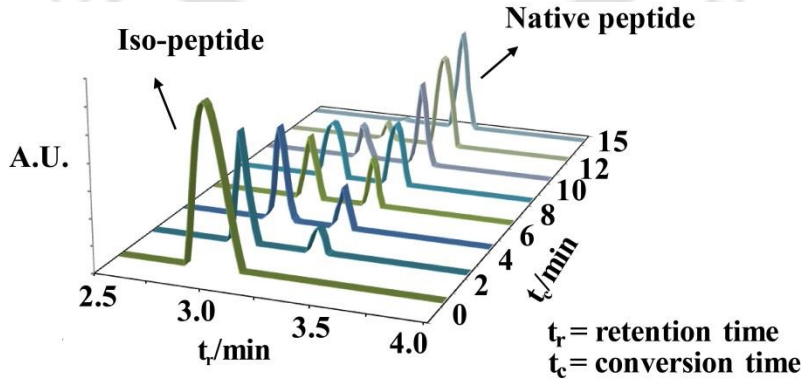

Figure 3.11: The kinetics of *O* to *N* acyl migration of the peptide **3A** at pH 7.4 and 37 °C.

Since, at pH 7.4 the *O* to *N* acyl migration was too fast to detect, the pH of the medium was reduced to pH 7.0 and the kinetics were monitored by LC-MS. A stock solution of ~0.5 mM was prepared in PBS (50 mM, pH 7.0) and incubated at 37 °C on water bath and at different time intervals, 200 µL of sample was taken out from the stock solution in LC-MS vials, quenched with 1N HCl (final pH ~1.0) and injected in LC-MS. The conversion of iso-peptide to native peptide is shown in figure 3.11. A linear gradient of 60% acetonitrile for 6 min, 100% till 7 min, in a total run time of 8 min was used. At zero time, one major peak at t_r 3.0 min (Figure 3.11) corresponding to the pure iso-peptide peptide **3A** was noted. A new peak emerged with time at t_r 3.3 min (Figure 3.11) having the same mass value (Figure 3.12) that increased with time at the cost of decrease of the peak at t_r 3.0 min. We have chosen pH 7.0 only for this experiment to detect properly the two distinct isomeric peaks for the peptide **3A** and measure the kinetics of conversion. Other biophysical studies were performed at pH 7.4 and 37 °C to maintain a similarity with the physiological condition.

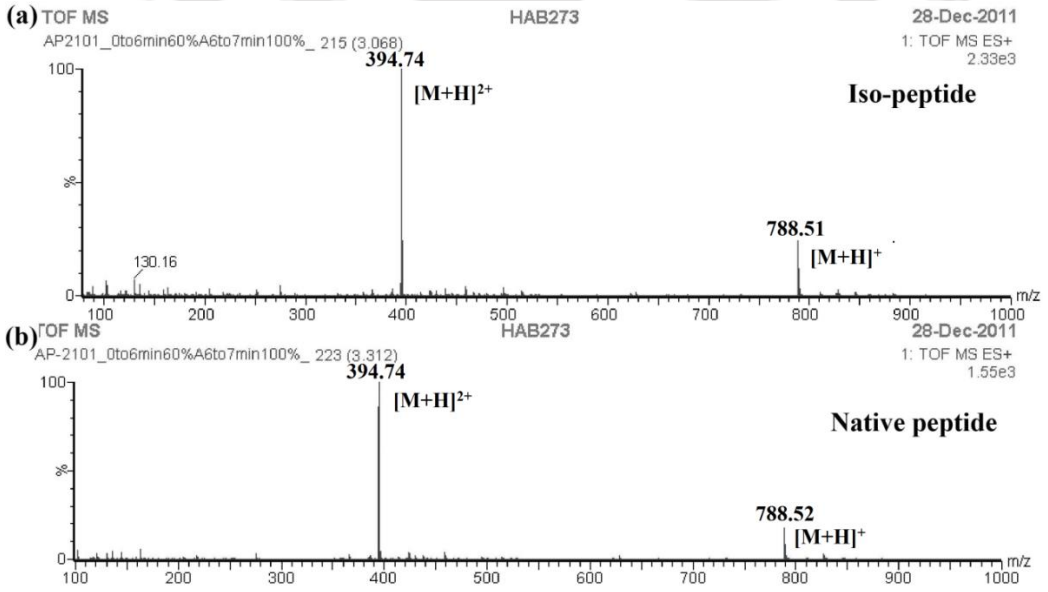

Figure 3.12: ESI-MS spectra of the peptide **3A** in, (a) iso form and (b) native form.

3.6.2. Monitoring conformational transition of peptide 3A by CD and FTIR studies:

For the conformational analysis of the peptide **3A** in iso-peptide form, we dissolve it in sodium acetate buffer (50 mM, pH 4.0) to prepare a concentration ~0.5 mM and performed CD and FTIR studies (Figure 3.13). We observed a negative band at ~207 nm in CD (black, Figure 3.13a) and a strong band at 1673 cm^{-1} in FTIR (black, Figure 3.13b) studies; these correspond to the mixture of random coil and β-turn conformation of the peptide.[23,88]

To check the conformation of the native peptide in amyloidogenic state, we dissolved the pure peptide in PBS (50 mM, pH 7.4) and incubated the solution at 37 °C for 5 days and conformational analysis was performed using CD and FTIR studies. We observed a positive band at ~199 nm, with a negative band at ~232 nm in CD (red, Figure 3.13a) and a strong band at 1633 cm^{-1} in FTIR (red, Figure 3.13b); these correspond to the β-sheet rich conformation of the peptide.

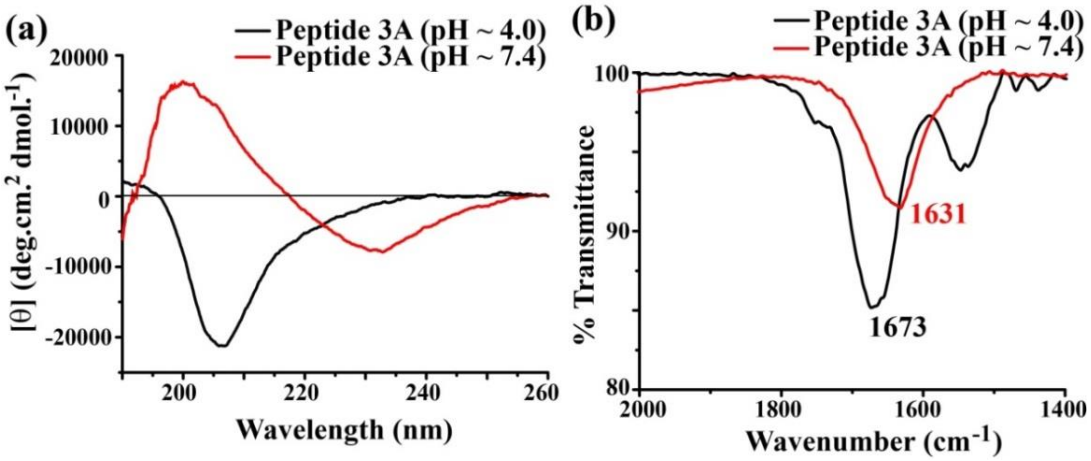

Figure 3.13: (a) CD and (b) FTIR spectra of peptide **2B** at pH 4.0 (black) and pH 7.4 (red).

3.6.3. Monitoring amyloidogenicity of peptide 3A by TEM and Congo red birefringence studies:

We have already observed that at physiological condition peptide **3A** exist in β-sheet rich conformational state. To investigate whether those β-sheet rich contents were part of amyloid or not, we performed TEM and Congo red stained birefringence studies (Figure 3.14).

After, 5 days of incubation in PBS pH 7.4 at 37 °C, 10 μL of the peptide sample from the stock was added over a carbon coated copper grid followed by addition of 10 μL of 2% uranyl acetate over it and allowed to stand for 2 min. The excess solution was removed carefully by blotting paper and allowed to dry in open air, then examined under TEM at 200 kV. We observed a clear fibrillar assembly of the peptide in TEM (Figure 3.14a), indicating the amyloidogenic nature of the peptide.[23]

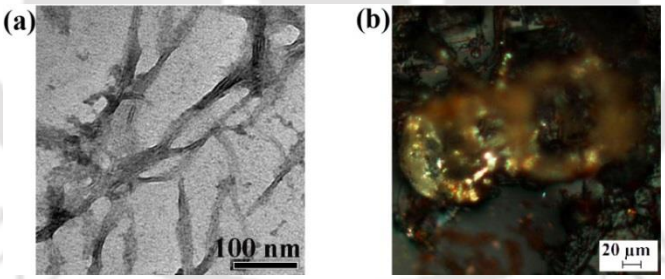

Figure 3.14: (a) TEM and (b) Congo red stained birefringence images of peptide **3A**. The images were taken after 5 days of incubation in PBS of pH 7.4 at 37 °C.

For birefringence study, the sample was prepared in a similar way as described in the previous chapter (Chapter 2, section 2.5.4). Under cross polarized light, we noticed a clear appearance of green gold birefringence (Figure 2.145), indicating the amyloidogenic nature of the switch-peptide **3A**.

3.7: Inhibition of amyloid formation of peptide 3A by BSBHps 3B and 3C:

We have already observed that the BSBHps **3B** and **3C** were non-amyloidogenic in nature and the switch-peptide **3A** forms amyloid fibrils like Aβ. Next, our target was to investigate the inhibitory efficacy of the BSBHps against the amyloid formation of peptide **3A**. To check whether the BSBHps can inhibit the aggregation of peptide **3A** or not, we have added two equivalents of each BSBHp separately with the peptide **3A**, co-incubated for 5 days in PBS pH 7.4 at 37 °C and performed various biophysical studies. We first checked for the change in conformation of aggregating peptide **3A** in absence and presence of BSBHps.

3.7.1. Monitoring conformational transition by CD and FTIR studies:

We have prepared three different sets of solutions where concentrations of peptide **3A** remain same in each case. In the first set, 0.5 mM of peptide **3A** alone was dissolved in PBS, pH 7.4 (50 mM); in the second set, peptide **3A** was mixed with peptide **3B** in a molar ratio of 1:2, and in the third set peptide **3A** was mixed with peptide **3C** in molar ratio of 1:2. Each set contains three replicate solutions. All the three different sets of solutions (stock solutions) were prepared in PBS pH 7.4 and incubated at 37 °C on water bath for 5 days. After 5 days of incubation, we checked the conformation of the peptide solutions using CD and FTIR studies (Figure 3.15). For CD measurement, 200 µL of peptide solution from each stock was taken out separately and placed into a quartz cuvette of 1 mm path length and analyzed using Jasco J-1500 instrument. For FTIR analysis, 20 µL of peptide solution from each stock solution was taken out separately, mixed with separate KBr and pellets were prepared which were analyzed with background subtraction to obtain final spectra.

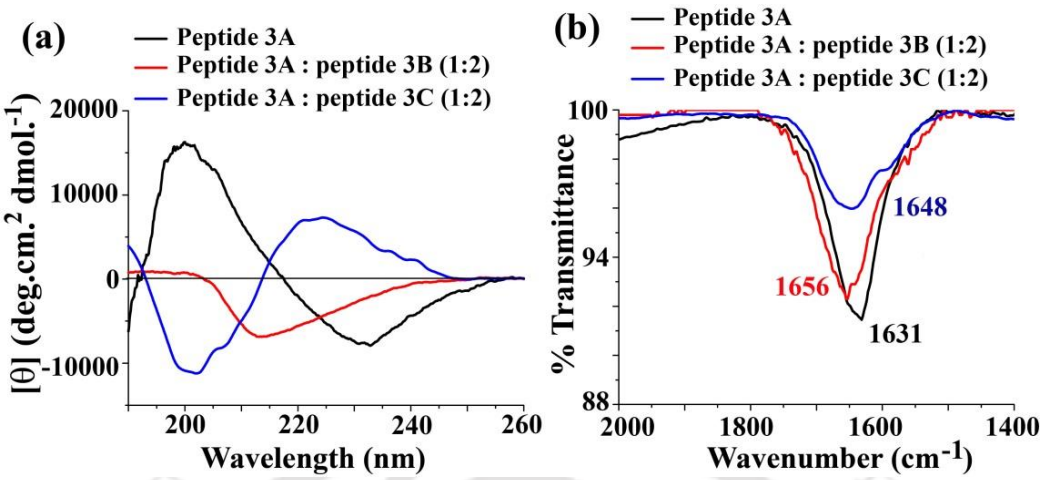

Figure 3.15: (a) CD and (b) FTIR spectra of peptide **3A** in absence (black) and presence of 2 fold molar excess of peptide **3B** (red) or peptide **3C** (blue). Spectra were recorded after 5 days of incubation of the peptide solutions in PBS pH 7.4 at 37 °C.

The peptide **3A** alone showed a positive band at ~199 nm with a negative band at ~232 nm in CD profile (black, Figure 3.15a; percentage of helix content 0, β-sheet content 100, turn content 0 and random coil content 0, deconvoluted from the CD instrument) and a strong band at 1631 cm^{-1} in FTIR spectra (black, Figure 3.15b) indicated the characteristic β-sheet conformation of the peptide **3A**. But when breaker peptides **3B** or **3C** were incubated with peptide **3A** (in 2 fold molar excess), no such characteristic peak for β-sheet was observed. In presence of peptide **3B**, we observed a negative band at ~211 nm in CD profile (red, Figure 3.15a; percentage of helix content 26, β-sheet content 7.4, turn content 30.6 and random coil content 36, deconvoluted from the CD instrument) and a strong band at 1656 cm^{-1} in FTIR, indicating non β-sheet conformation or reduction of β-sheet content. While in presence of peptide **3C**, we observed a negative band at ~202 nm and a positive band at ~224 nm (blue, Figure 3.15a; percentage of helix content 0, β-sheet content 28.9, turn content 20 and random coil content 51.1, deconvoluted from the CD instrument) and a strong band at 1648 cm^{-1} in

FTIR, indicating non β-sheet conformation or reduction of β-sheet content. Therefore, the presence of BSBHps reduced the β-sheet content of the aggregating peptide.

3.7.2. Monitoring the kinetics of amyloid formation by Thioflavin T fluorescence assay:

The increase in fluorescence intensity of a peptide upon binding with thioflavin T (ThT) is a characteristic property of the presence of the amyloid in a solution and the fluorescence intensity is directly proportional to the amount of fibril present in that solution.[23] The kinetics of amyloid formation of peptide **3A** and its inhibition by BSBHps were monitored by a time dependent Thioflavin T (ThT) fluorescence assay. For ThT assay, samples were prepared in a similar fashion as described for CD and FTIR studies in section 3.7.1 and incubated in PBS of pH 7.4 at 37 °C for 5 days. At different time intervals, 40 μL of peptide sample from the stock was mixed with 200 μL of ThT solution (50 μM), total volume was made up to 400 μL with PBS (50 mM, pH 7.4) and fluorescence was measured (λ_{ex} = 440 nm, λ_{em} = 485 nm and band width 3 nm). As described earlier (section 3.7.1), each set contain three replicate peptide solutions and data were plotted as the average of the results from three replicate solutions.

From the ThT assay (Figure 3.16), we observed that in absence of BSBHps peptide **3A** aggregated with time as indicated by the time dependent increase of the fluorescence intensity (black, Figure 3.16). On the other hand, in presence of BSBHps **3B** (red, Figure 3.16) and **3C** (blue, Figure 3.16**)**, the fluorescence intensity was suppressed significantly with time, indicating reduction of amyloid in the system. Above mentioned results indicate that

the BSBHps significantly inhibited the amyloid formation of the model aggregating peptide as anticipated.

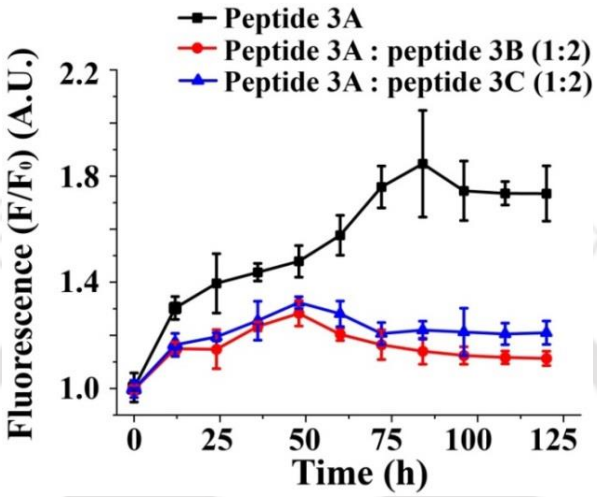

Figure 3.16: Time dependent Thioflavin T-fluorescence assay of peptide **3A** in absence (black) and presence of 2 fold excess peptide **3B** (red) or peptide **3C** (blue). Peptides were incubated in PBS pH 7.4 at 37 °C.

3.7.3. Monitoring the amyloid formation by TEM and Congo red birefringence studies:

The presence of fiber in TEM and the appearance of green gold birefringence under cross polarized light when a peptide stained with Congo red dye are direct evidences for amyloid aggregates.[23] From the stock solutions (described in section 3.7.1) 10 µL of different peptide solutions were taken out and TEM samples were prepared (sample preparation was described in section 3.5.2). Peptide **3A** alone showed clear fibrillar structure when viewed under TEM (Figure 3.17a). But in presence of BSBHp **3B** (Figure 3.17b) no such fibrillar structure was observed indicating absence of amyloid. In presence of BSBHp **3C** (Figure 3.17c) also no fibrillar structure was observed indicating absence of the amyloid in the mixture.

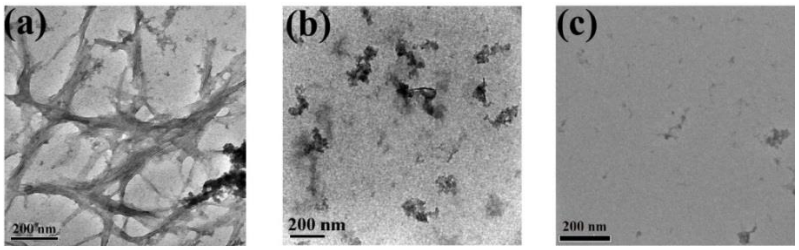

Figure 3.17: TEM images of peptide **3A** in absence (a) and presence of 2 fold molar excess of peptide **3B** or **3C**. Images were taken after 5 days of incubation of the peptide solution in PBS pH 7.4 at 37 °C.

For obtaining a complementary proof of presence or absence of amyloid in the sample, from the stock solution (described in section 3.7.1) 20 µL of sample was placed over a glass slide and dried in air followed by addition of 20 µL of saturated Congo red solution (in 80% aqueous ethanol) over it and dried it. The dried spot was analyzed under optical microscope using cross polarized light (Figure 3.18). We noticed a clear appearance of green gold birefringence when peptide **3A** was alone (Figure 3.18a), indicating presence of amyloid. But, when peptide **3A** was co-incubated with BSBHp **3B** (Figure 3.18b) and **3C** (Figure 3.18c) separately for 5 days in PBS of pH 7.4 at 37 °C, no such characteristic green gold birefringence was observed, indicating absence of amyloid. These results indicated that peptide 3A alone formed amyloid but amyloid formation was suppressed in presence of BSBHps.

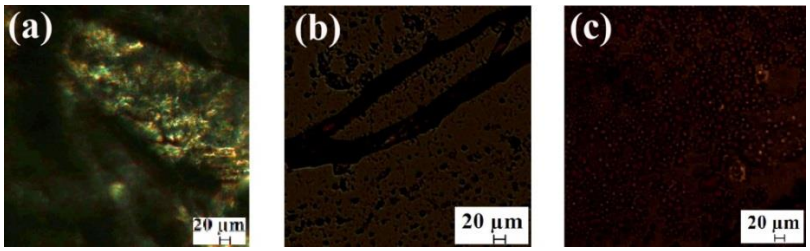

Figure 3.18: Congo red stained birefringence images of peptide **3A** in absence (a) and presence of 2 fold molar excess of peptide **3B** or **3C**. Images were taken after 5 days of incubation of the peptide in PBS pH 7.4 at 37 °C.

3.8. Conclusion:

In this chapter, we have introduced the anthranilic acid containing β-sheet breaker α/β hybrid peptides (BSBHps). We have demonstrated that BSBHps (Peptide **3B** and **3C**) were non-amyloidogenic at physiological condition (pH 7.4 and 37 °C). We also have demonstrated that the switch-peptide **3A** formed amyloid like fibrils, and therefore one could use it as a model aggregating peptide. Finally, we have investigated the β-breaking potential of BSBHps **3B** and **3C** against the amyloid formation of peptide **3A**. Our results suggest that BSBHps **3B** and **3C** inhibited the aggregation of peptide **3A** significantly. Therefore it can be concluded that anthranilic acid containing BSBHps can be used to inhibit the aggregation of amyloidogenic peptides.

Chapter 4: Disruption of Amyloid-β aggregates into non-toxic species by β-sheet breaker hybrid peptide

4.1. Proposed hypothesis:

We have already noted in chapter 3 that the β-sheet breaker hybrid peptides (BSBHps) were non-amyloidogenic in nature and were potentially efficient to inhibit the aggregation of model aggreagating peptides at physiological condition (pH 7.4 and 37 °C). In this chapter, we have jotted down the results of our studies to examine the inhibitory efficacy of specially designed BSBHp on the aggregation of $A\beta_{1\text{-}40}$ peptide as well as the amyloid disruptive capability of the BSBHp.

$A\beta_{1\text{-}40}$ peptide is known as one of the major culprit peptide for progression of the Alzheimer's disease (AD) in human brain along with its other congener $A\beta_{1\text{-}42}$.[70,125,126]

^{1}DAEFRHDSGYEVHHQKLVFFAEDVGSNKGAIIGLMVGGV^{40}V ($A\beta_{1\text{-}40}$)

The aggregation of Aβ ($A\beta_{1–40}$ and $A\beta_{1–42}$) forms neurotoxic oligomers and amyloid fibrils in the brain known to be the major pathogenic factor for AD.[30,55] Therefore, a strategy that disrupt the Aβ aggregates into non-toxic monomers would be very interesting as well as

challenging for drug design against AD. In this chapter, we have demonstrated the disruption of amyloid $A\beta_{1\text{-}40}$ aggregates into non-toxic species *in vitro* by a suitably designed BSBHp at physiological condition (Figure 4.1). We have also compared the β-breaking efficacy of the designed BSBHp with an existing β-sheet breaker peptide (BSBp).

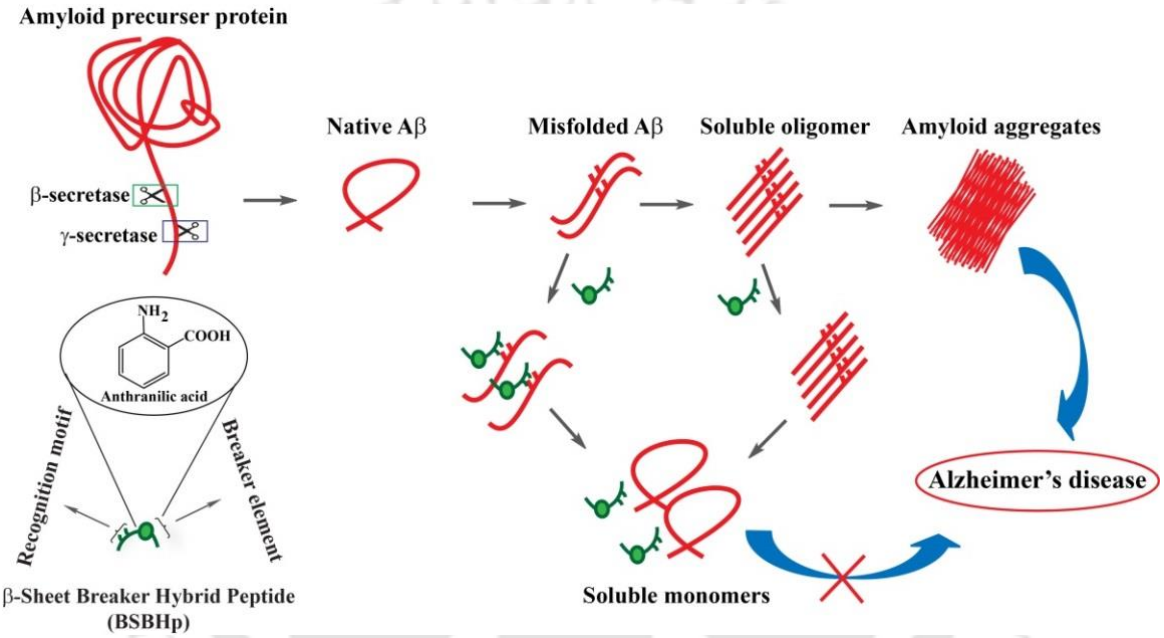

Figure 4.1: Hypothesis for the disruption of Aβ aggregates by a β-sheet breaker hybrid peptide

4.2. Design of peptides:

To test our hypothesis for the disruption of Aβ aggregates into non-toxic monomeric species, we have designed and synthesized a β-sheet breaker hybrid peptide (**4A**). The BSBHp **4A** was designed with an anthranilic acid (Ant) as breaker element and -F-F- partial sequence homology with $A\beta_{19\text{-}20}$ (-F-F) for proper recognition. *N*-terminus was acetylated to make it stable against enzymatic degradation and at the C-terminus aspartic acid was added to

increase solubility of the peptide. We have also designed and synthesized a known control BSBp (peptide **2C**) which is already used in chapter 2 (Table 2.2),[70] for comparing the efficacy with the BSBHp. The $A\beta_{1-40}$ was used as the target amyloidogenic peptide. The synthesized peptides that have been used in this chapter are shown below,

Peptide No.	Peptide Sequence (X = anthranilic acid/Ant)	Function
4A	Ac-L**X**FFD-NH_2	Inhibitor
2C	Ac-LPFFD-NH_2	Inhibitor/ Control

Table 4.1: Sequences of designed peptides for the present investigation.

4.3. Synthesis and characterization of the designed peptides:

We have synthesized all the designed peptides by solid phase peptide synthesis (SPPS) technique using standard Fmoc/^{t}Bu protection strategy on Rink amide MBHA resin in a similar way described in chapter 2, section 2.4.[106-108] The synthetic scheme for synthesis of the BSBHp **4A** is shown in scheme 4.1. The designed peptides were purified using semi preparative HPLC and purity was confirmed by HPLC and mass spectrometry. The characterization data for the synthesized peptides are shown below.

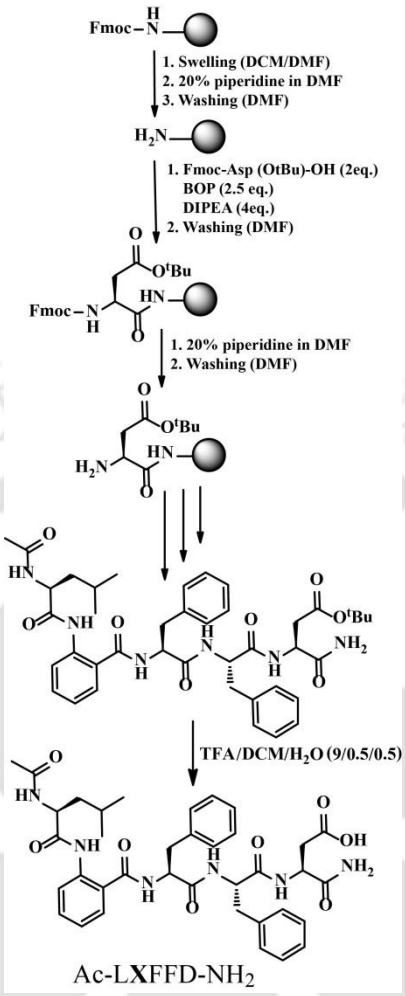

Scheme 4.1: Synthetic scheme of peptide **4A** using Fmoc/^{t}Bu protection based SPPS.

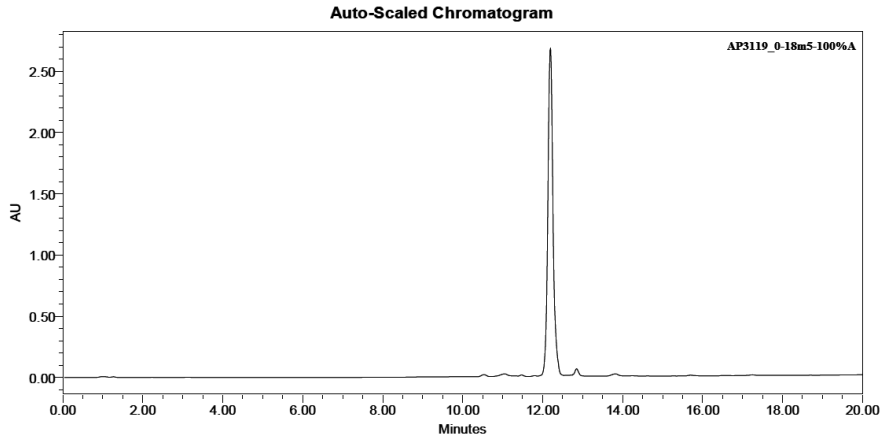

Figure 4.2: HPLC profile of the purified peptide **4A**.

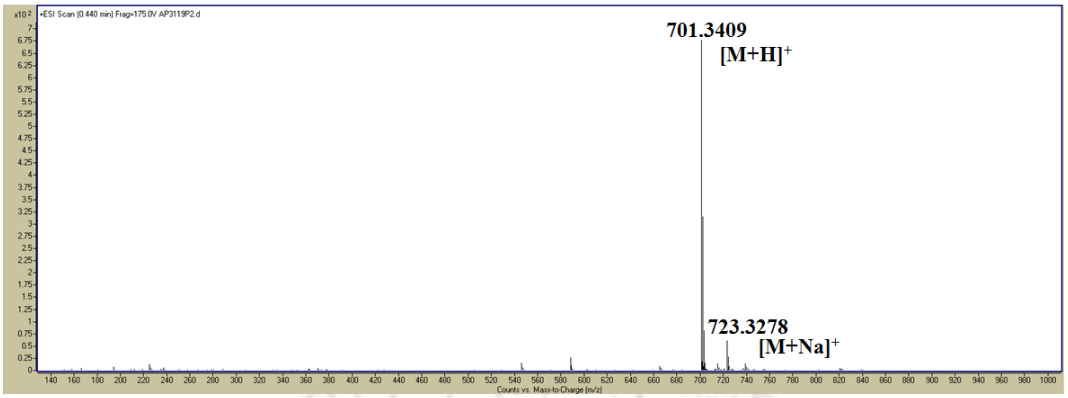

Figure 4.3: Mass spectrum of peptide **4A**. Calculated mass for $C_{37}H_{45}N_6O_8$ is 701.32 $[M+H]^+$, observed 701.34 $[M+H]^+$ and calculated mass for $C_{37}H_{44}N_6O_8Na$ is 723.31 $[M+Na]^+$, observed 723.32 $[M+Na]^+$.

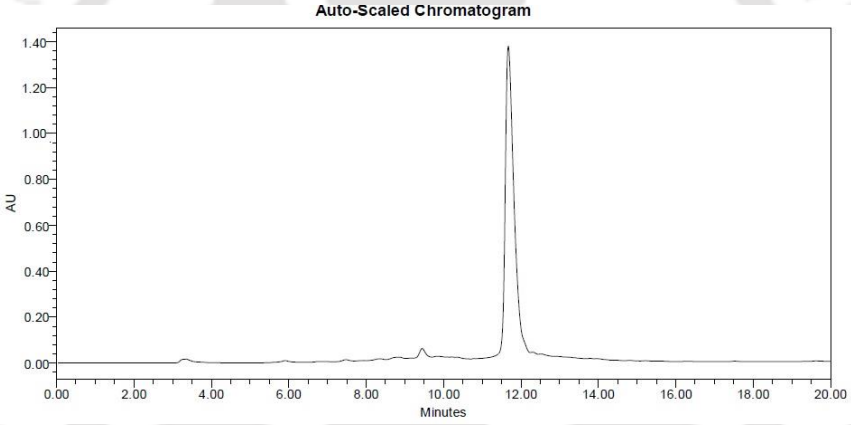

Figure 4.4: HPLC profile of the purified peptide **2C**.

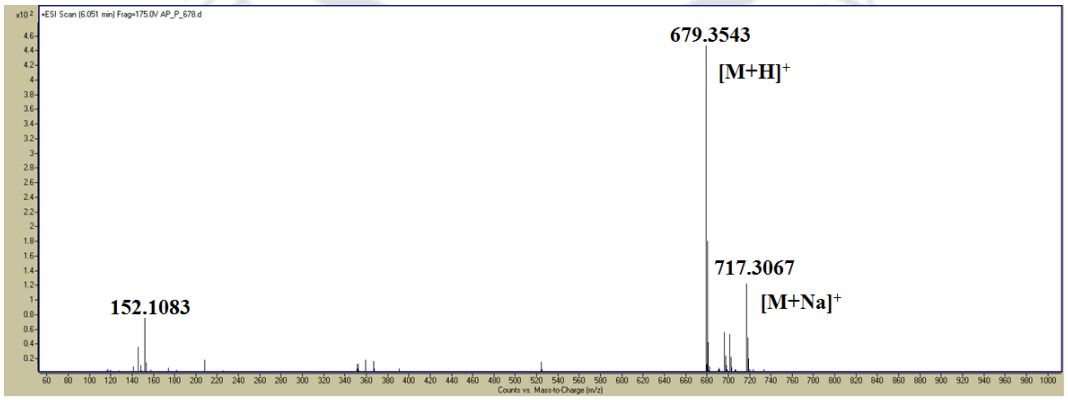

Figure 4.5: Mass spectrum of peptide **2C**. Calculated mass for $C_{35}H_{47}N_6O_8$ is 679.34 $[M+H]^+$, observed 679.35 $[M+H]^+$ and calculated mass for $C_{35}H_{46}N_6O_8K$ is 717.30 $[M+K]^+$, observed 717.30 $[M+K]^+$.

4.4. Non-amyloidogenicity of the BSBHp 4A:

We have already seen in chapter 3, section 3.5, that Ant containing BSBHps were non-amyloidogenic in nature at physiological condition (pH 7.4 and 37 °C). Therefore, BSBHp **4A** is expected to be non-amyloidogenic. However, to confirm that, we checked the non-amyloidogenicity of peptide **4A** using various biophysical tools.

4.4.1. Conformational characterization of peptide 4A by CD and FTIR studies:

To check the conformational state of the peptide **4A**, we dissolved it in PBS (50 mM, pH 7.4) to make the concentration of the stock solution ~0.5 mM and incubated the solution on water bath at 37 °C for 5 days. After 5 days, the conformational studies were performed using CD and FTIR (Figure 4.6). In CD spectrum of peptide **4A** Figure 4.6a, we observed two negative bands centered at ~208 nm and ~222 nm, with a positive band at ~190 nm clearly indicating the α-helix rich conformation of the peptide **4A** (percentage of helix content 48.7, β-sheet content 24.1, turn content 0 and random coil content 27.1; deconvoluted from the CD instrument). Similarly, in FTIR spectrum we observed the amide I band at 1657 cm^{-1} (Figure 4.6b) clearly indicated again α-helix rich conformation of the peptide.[23] These results clearly indicated the non-β-sheet conformation of peptide **4A**.

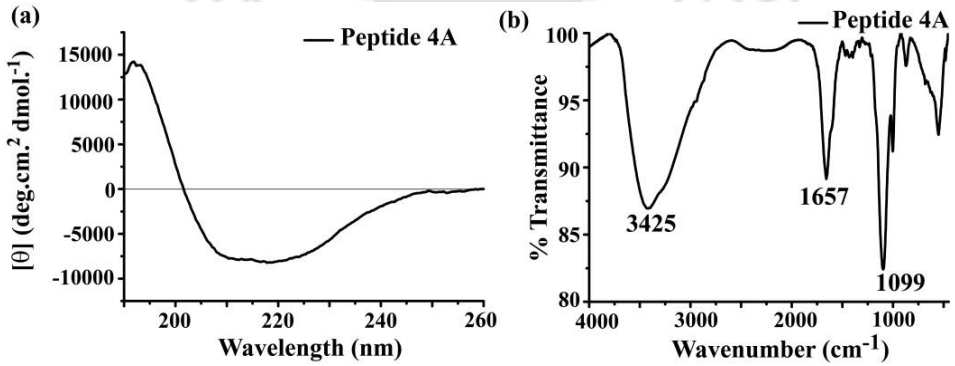

Figure 4.6: (a) CD and (b) FTIR spectra of peptide **4A**. Spectra were taken after 5 days of incubation of the peptide in PBS pH 7.4 (50 mM) at 37 °C.

4.4.2. Characterization of the amyloidogenic nature of peptide 4A by TEM and Congo red birefringence studies:

The amyloidogenicity of the BSBHp was characterized by TEM and Congo red stained birefringence studies. After 5 days of incubation of the peptide solution in PBS (50 mM, pH 7.4) at 37 °C, 10 μL of peptide sample was taken out from the stock solution (described in section 4.4.1) for TEM analysis (sample preparation was already described in chapter 2, section 2.5.4). We did not observe any fibrillar assembly of the peptide **4A** in TEM (Figure 4.7a). Similarly, we did not observed any green gold birefringence of the peptide **4A** when stained with Congo red dye and viewed under cross polarized light (Figure 4.7b). Therefore, from the above results, it was confirmed that the Ant containing BSBHp **4A** was non-amyloidogenic in nature.

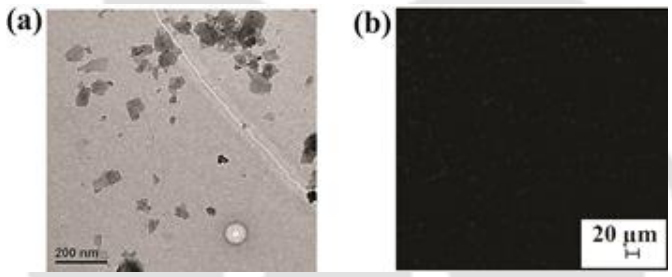

Figure 4.7: (a) TEM and (b) Congo red birefringence images of peptide **4A**. Images were taken after 5 days of incubation of the peptide in PBS pH 7.4 (50 mM) at 37 °C.

4.5: Inhibition of amyloid formation of $A\beta_{1-40}$ by BSBHp 4A:

The BSBHp **4A** was found to be a non-amyloidogenic peptide at pH 7.4 at 37 °C. Therefore, we proceeded further to investigate the inhibitory efficiency of aggregation of $A\beta_{1-40}$ by the BSBHp **4A**. For that we performed various qualitative and quantitative analyses in absence and presence of varied amount of BSBHp **4A** and compared its efficacy with the control BSBp **2C**. The BSBHp **4A** and the control peptide **2C** were co-incubated with $A\beta_{1-40}$ in PBS pH 7.4 at 37 °C up to 7 days in separate vessels and the kinetics of the amyloid formation were monitored using

different biophysical tools. To investigate dose dependence on the inhibitory activity of the peptide **4A** and **2C**; 2, 5 and 10 fold molar excess of breaker peptides (**4A** and **2C**) were co-incubated with 50 μM of $A\beta_{1-40}$ in PBS (50 mM, pH 7.4) at 37 °C.

1.2 mg of commercially available $A\beta_{1-40}$ was dissolved in 20 μL of TFA to obtain disaggregated $A\beta_{1-40}$. TFA was evaporated using nitrogen gas. To remove TFA completely, 20 μL of HFIP was added and evaporated using nitrogen gas to obtain disaggregated $A\beta_{1-40}$.[127] This process was repeated twice. Into the disaggregated material 1.4 mL of PBS (50 mM, pH 7.4) was added followed by sonication and vortex to obtain transparent solution and the whole solution was divided into 7 equal portions followed by addition of 600 μL of PBS to each portion to obtain a final $A\beta_{1-40}$ concentration of 50 μM. For the inhibition study, 2, 5 and 10 fold molar excess of breaker peptides (**4A** and **2C**) were mixed with each portion (800 μL) of $A\beta_{1-40}$ and kept for incubation over water bath for 7 days at 37 °C. For precise result two more replicate solutions of each portion were prepared and fibrillization were monitored by various biophysical tools.

4.5.1. Monitoring conformational transition by CD:

After 7 days, when CD spectra were taken, we observed $A\beta_{1-40}$ peptide alone exhibited a positive band centered at ~200 nm and a negative band centered at ~225 nm, indicating β-sheet rich conformation of $A\beta_{1-40}$ (black, Figure 4.8a,b). But when different doses of peptide **4A** (2-, 5- and 10-fold molar excess) were present with $A\beta_{1-40}$, the β-sheet content were reduced slowly as the doses increased as evident from the figure 4.8a. These results indicated the breaking of β-sheet occured which is also an indication of the inhibiton of aggregation of $A\beta_{1-40}$ occured by the BSBHp **4A**. On the other hand, in presence of different doses of peptide **2C** (2-, 5- and 10-fold molar excess) with $A\beta_{1-40}$ (Figure 4.8b), the β-sheet content were also reduced slowly as the doses increased (Figure 4.8b). These results indicated that the control peptide **2C** also inhibited the aggregation of the $A\beta_{1-40}$.

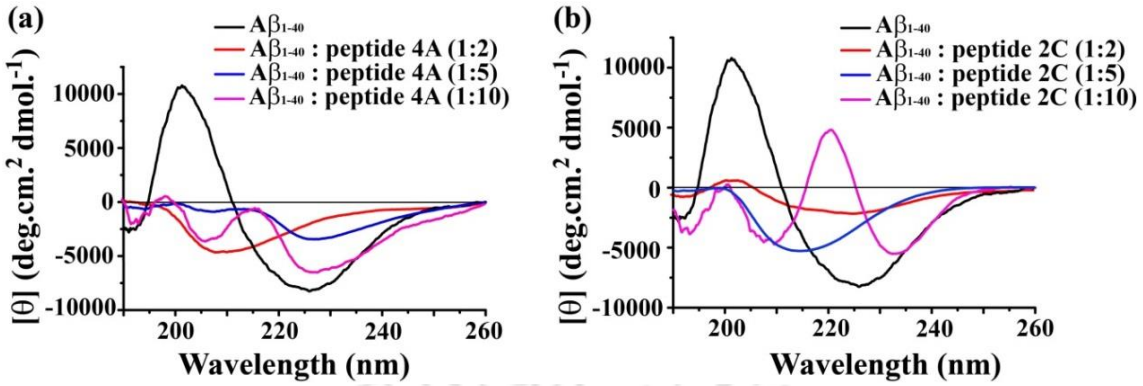

Figure 4.8: CD spectra of $A\beta_{1-40}$ in absence (black) and presence of 2-fold (red), 5-fold (blue) and 10-fold (magenta) molar excess of (a) peptide **4A** and (b) peptide **2C**. Spectra were recorded after 7days incubation of the peptide solutions in PBS pH 7.4 at 37 °C.

4.5.2. Monitoring conformational transition by FTIR:

An intense band at 1623 cm^{-1} was observed in FTIR spectra when $A\beta_{1-40}$ was alone in the solution, which is the characteristic band of a β-sheet[23] conformation (black, Figure 4.9a,b). But, in presence of different doses (2-, 5- and 10-fold molar excess) of peptide **4A** (Figure 4.9a) and **2C** (Figure 4.9b) no such β-sheet conformations were observed as indicated in Figure 4.9.

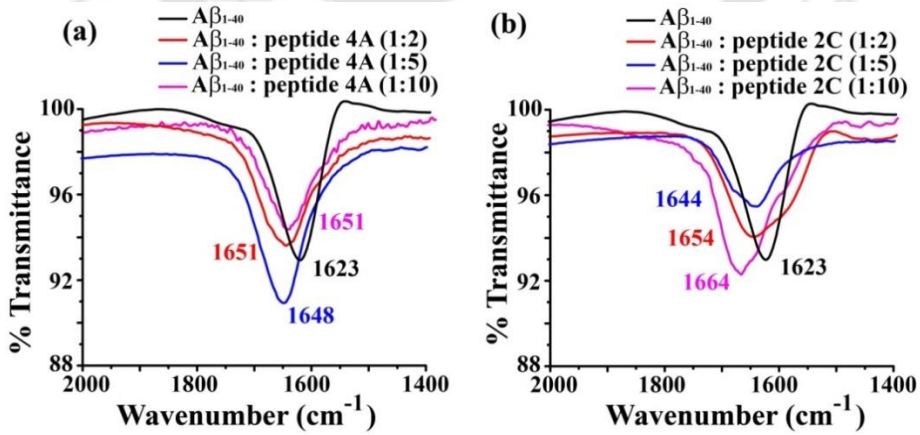

Figure 4.9: FTIR spectra of $A\beta_{1-40}$ in absence (black) and presence of 2-fold (red), 5-fold (blue) and 10-fold (magenta) molar excess of (a) peptide **4A** and (b) peptide **2C**. Spectra were recorded after 7days incubation of the peptide solutions in PBS pH 7.4 at 37 °C.

4.5.3. Monitoring the kinetics of amyloid formation by Thioflavin T fluorescence assay:

For Thioflavin T fluorescence assay, the samples were prepared in a similar manner as described above (Section 4.5). At different time intervals, 40 μL of peptide samples from the stock were mixed with 200 μL of ThT solution (50 μM), total volume was made up to 400 μL with PBS (50 mM, pH 7.4) and fluorescence was measured (λ_{ex} = 440 nm, λ_{em} = 485 nm and band width 3 nm). Normalized spectra were plotted as the average of the three replicate solutions.

From the ThT assay (Figure 4.10), we observed that the fluorescence intensity increased with time when only $A\beta_{1-40}$ was present in the solution. But, in presence of different doses (2-, 5- and 10-fold molar excess) of BSBHp **4A**, the intensity of fluorescence of the $A\beta_{1-40}$ solution decreased as the doses were increased, indicating the reduction of fibrillar mass. This implied that the inhibition of aggregation of $A\beta_{1-40}$ occurred (Figure 4.10a) on presence of BSBHp **4A**. It was clear from the experimental result that 2 fold molar excess (red, Figure 4.10a) of peptide **4A** was not sufficient to inhibit the amyloid formation of $A\beta_{1-40}$, but when **4A** was present in 5 fold molar excess (blue, Figure 4.10a), the inhibition was more pronounced which was further evident when 10 fold molar excess (magenta, Figure 4.10a) of peptide **4A** was co-incubated with $A\beta_{1-40}$ peptide. In presence of peptide **2C** also similar results were obtained (Figure 4.10b).

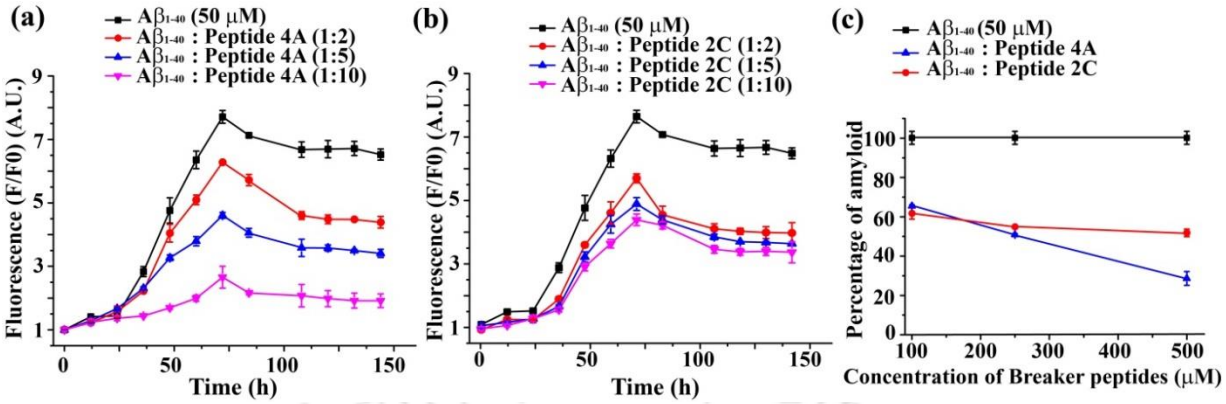

Figure 4.10: Time dependent ThT assay of $A\beta_{1-40}$ in absence (black) and presence of 2 fold (red), 5 fold (blue) and 10 fold (magenta) molar excess of peptide (a) **4A** and (b) **2C**. (c) % of amyloid formation of $A\beta_{1-40}$ in absence (black) and presence of peptide **4A** (blue) and **2C** (red). Peptides were incubated in PBS pH 7.4 at 37 °C.

The amount of amyloid fibril was inhibited significantly up to 71-72 % (blue, Figure 4.10c) when BSBHp **4A** was co-incubated with $A\beta_{1-40}$ in 10 fold molar excess until seven days, but in presence of similar excess of the control peptide **2C**, the amyloid fibril was suppressed by 47-48 % (red, Figure 4.10c) at the same condition. That may indicate that BSBHp **4A** is better amyloid inhibitor than the existing BSBp **2C**. From the above results it was concluded that, the BSBHp significantly inhibited the amyloid formation of the $A\beta_{1-40}$ peptide in a dose dependent manner as anticipated.

4.5.4. Monitoring amyloidogenicity by TEM:

The presence of fiber when observed under electron microscope is a characteristic property of amyloid.[23] The $A\beta_{1-40}$ alone showed clear fibrillar aggregates under TEM (Figure 4.11a). In presence of 2-fold molar excess of BSBHp **4A**, some fiber was noted, indicating 2-fold molar excess of peptide **4A** was not sufficient to inhibit the aggregation (Figure 4.11b). When, the doses of peptide **4A** were increase to 5-fold (Figure 4.11c) and 10-fold (Figure

4.11d) molar excess, no such fiber was observed, indicating absence of amyloid. Similarly, in presence of different doses of peptide **2C** similar results were obtained (Figure 4.12).

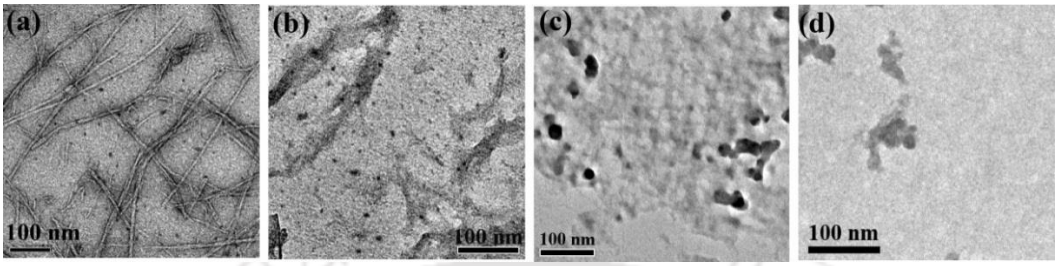

Figure 4.11: TEM images of (a) $A\beta_{1-40}$ alone and in presence of (b) 2-fold, (c) 5-fold or (d) 10-fold molar excess of peptide **4A**. Images were taken after 7 days incubation of the peptide solutions in PBS of pH 7.4 at 37 °C.

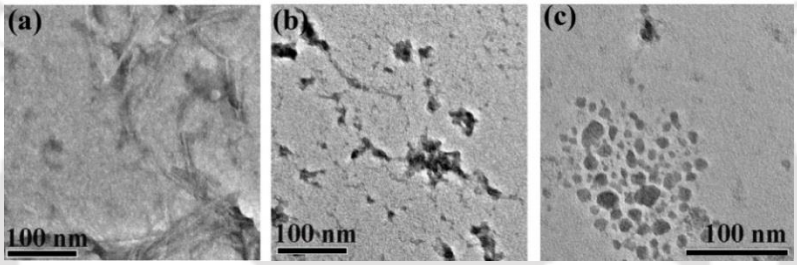

Figure 4.12: TEM images of $A\beta_{1-40}$ in presence of (a) 2-fold, (b) 5-fold or (c) 10-fold molar excess of peptide **2C**. Images were taken after 7 days incubation of the peptide solutions in PBS of pH 7.4 at 37 °C.

4.5.5. Monitoring amyloidogenicity by Congo red birefringence:

The appearance of green gold birefringence of a peptide sample under cross polarized light after staining with Congo red dye indicated the presence of amyloid in the sample.[23] In this experiment, the $A\beta_{1-40}$ alone showed clear green gold birefringence under cross polarized light (Figure 4.13a). But in presence of different doses (2-fold, 5-fold and 10-fold molar excess) of BSBHp **4A** such green gold birefringence were not observed. Although in case of 2-fold (Figure 4.13b) molar excess some green gold birefringence was observed, in presence of 5-fold (Figure 4.13c) and 10-fold (Figure 4.13d) molar excess of peptide **4A** no such

characteristic birefringence were observed. Similar results were obtained in case of peptide **2C** (Figure 4.14). These results support that the BSBHp **4A** significantly inhibited the aggregation of $A\beta_{1-40}$ *in vitro* at physiological condition.

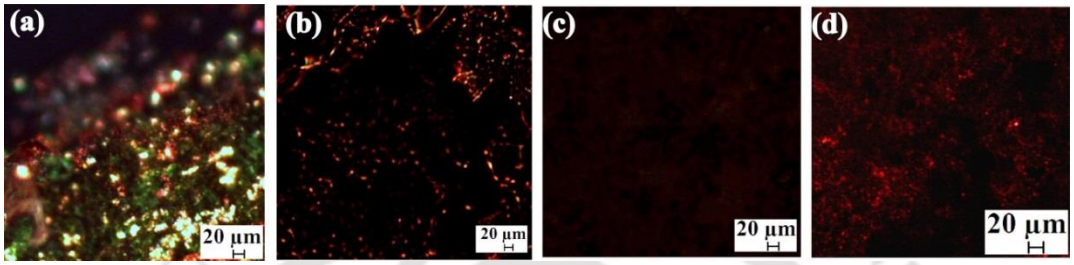

Figure 4.13: Congo red birefringence images of (a) $A\beta_{1-40}$ alone and in presence of (b) 2-fold, (c) 5-fold or (d) 10-fold molar excess of peptide **4A**. Images were taken after 7 days incubation in PBS of pH 7.4 at 37 °C.

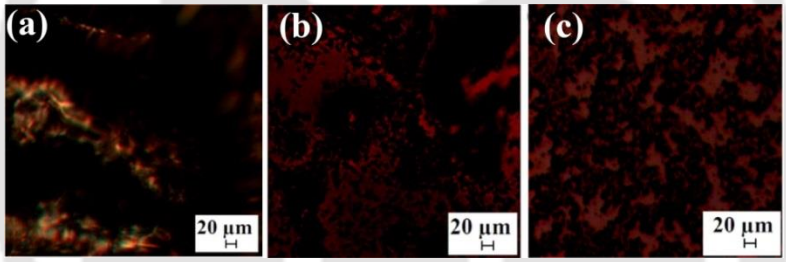

Figure 4.14: Congo red birefringence images of $A\beta_{1-40}$ in presence of (a) 2-fold, (b) 5-fold and (c) 10-fold molar excess of peptide **2C**. Images were taken after 7 days incubation in PBS of pH 7.4 at 37 °C.

4.6. Disruption of preformed Aβ aggregates by BSBHp:

We already observed that when BSBHp **4A** was co-incubated with $A\beta_{1-40}$, it inhibited amyloid formation of $A\beta_{1-40}$ in a dose dependent manner. The Alzheimer's disease affected brain is rich in toxic oligomers and amyloids due to the presence of preformed fibrils at the diseases condition.[38,44] If we want to use our peptide as a drug then it must be able to disrupt preformed fibrils. Therefore, our next target was to check whether the BSBHp can disrupt the

preformed fibrillar aggregates of $A\beta_{1-40}$ or not, *in vitro*. From the ThT assay (black, Figure 4.14), we observed that the growth phase for fibril formation of $A\beta_{1-40}$ at mentioned condition was in the range of 24 h to 72 h. So, we designed an experiment where the peptide **4A** was added into the fibrillar assembly at the time range of fibrillar growth phase. Therefore, $A\beta_{1-40}$ (50 μM) was incubated alone in PBS pH 7.4 at 37 °C for 60 h to form amyloid fibrils and then different doses (2-fold, 5-fold and 10-fold) of peptide **4A** and **2C** were separately added to $A\beta_{1-40}$ aggregates (60 h old) and incubated them till 10 days (240 h = 60 h + 180 h). Further, the amyloid formation of $A\beta_{1-40}$ in absence and presence of peptide **4A** and **2C** were monitored by different biophysical tools, and compared with the previous results.

4.6.1. Monitoring conformational transition by CD:

After 10 days, when CD were analyzed, we observed $A\beta_{1-40}$ peptide alone showed a positive band centered at ~195 nm and a negative band centered at ~213 nm, clearly indicating the characteristic bands for β-sheet rich conformation of $A\beta_{1-40}$ (black, Figure 4.15a,b). But in presence of different doses of peptide **4A** (2-, 5- and 10-fold molar excess), such β-sheet content were reduced slowly as the doses increased (Figure 4.15a), rather some mixture of conformations were observed, indicated the breaking of β-sheet by the BSBHp **4A**. These results clearly supported the occurrence of the disruption of preformed fibrillar aggregates of $A\beta_{1-40}$ by the BSBHp **4A**. Similar results were obtained in presence of different doses of peptide **2C** (2-, 5- and 10-fold molar excess) with $A\beta_{1-40}$ (Figure 4.15b), which also indicated the breaking of β-sheet, subsequently the disruption of preformed fibrillar aggregates of $A\beta_{1-40}$ by the control peptide **2C**.

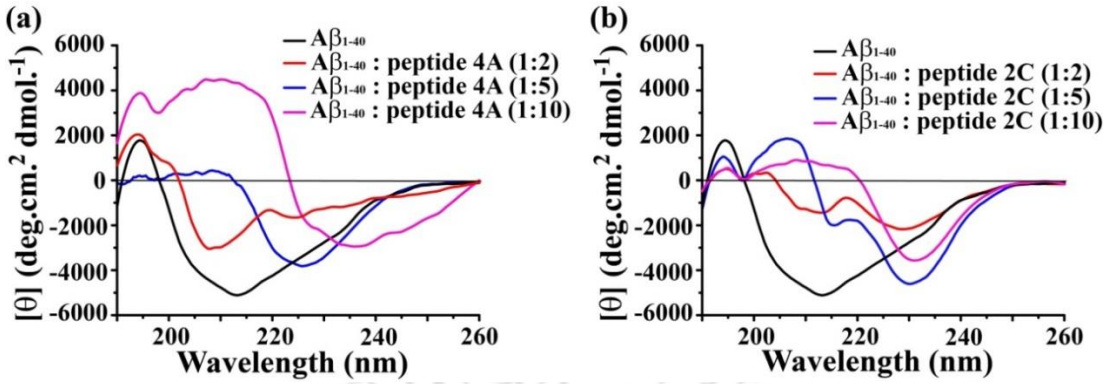

Figure 4.15: CD spectra of $A\beta_{1-40}$ in absence (black) and presence of 2-fold (red), 5-fold (blue) and 10-fold (magenta) molar excess of (a) peptide **4A** and (b) peptide **2C**. Spectra were recorded after 10 days incubation in PBS pH 7.4 at 37 °C.

4.6.2. Monitoring conformational transition by FTIR:

We observed an intense band at 1623 cm^{-1} in FTIR spectra when only $A\beta_{1-40}$ was present in the solution; that confirmed the characteristic β-sheet conformation (black, Figure 4.16a,b). But, in presence of different doses (2-, 5- and 10-fold molar excess) of peptide **4A** (Figure 4.16a) and **2C** (Figure 4.16b) no such characteristic band of β-sheet conformation were observed. These results indicated significant β-breaking effect by the BSBHp **4A** and the control BSBp **2C**.

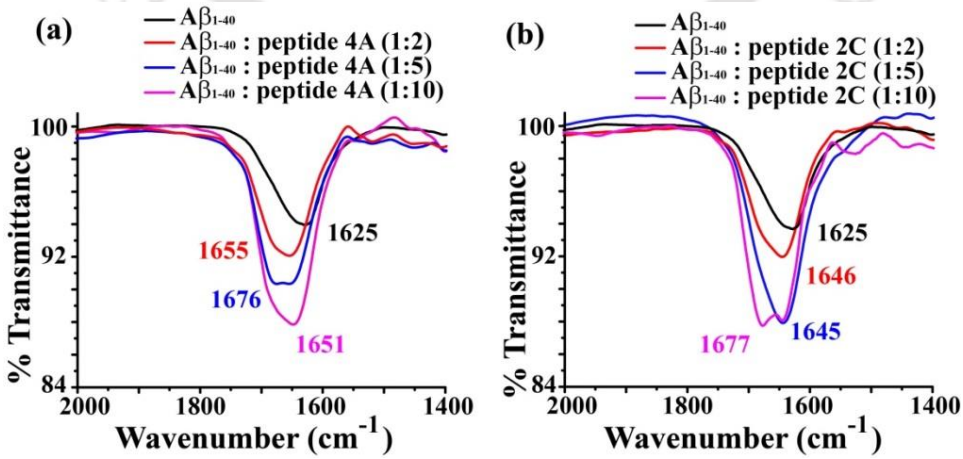

Figure 4.16: FTIR spectra of $A\beta_{1-40}$ in absence (black) and presence of 2-fold (red), 5-fold (blue) and 10-fold (magenta) molar excess of peptide (a) **4A** and (b) **2C**. Spectra were recorded after 10 days incubation in PBS pH 7.4 at 37 °C.

4.6.3. Monitoring the kinetics of amyloid disruption by Thioflavin T assay:

The kinetics of amyloid disruption was monitored by ThT assay. We observed an increment of fluorescence for $A\beta_{1-40}$ peptide when incubated alone (black, Figure 4.17a) but when varied molar excess (2-, 5- and 10-fold molar excess) of peptide **4A** were added to the existing fibrillar assembly of $A\beta_{1-40}$ after 60 h, the fluorescence was suppressed noticeably with time (Figure 4.17a) as the doses increased. Similar results were obtained for peptide **2C** (Figure 4.17b). The amount of fibril of $A\beta_{1-40}$ formed at 60 h was found to be reduced by peptide **4A** (blue, Figure 4.17c) more significantly than peptide **2C** (red, Figure 4.17c). After 10 days, the preformed fibril was reduced up to 51-52% when the peptide **4A** was present in 10 fold molar excess whereas the peptide **2C** could suppress only 32-33 %.

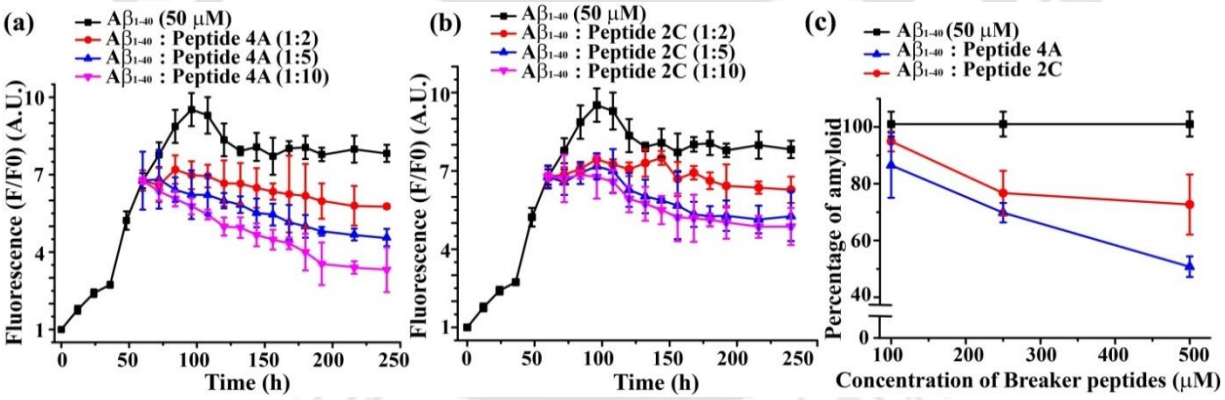

Figure 4.17: Time dependent ThT assay of $A\beta_{1-40}$ in absence (black) and presence of 2 fold (red), 5 fold (blue) and 10 fold (magenta) molar excess of peptide (a) **4A** and (b) **2C**. (c) % of amyloid disruption of $A\beta_{1-40}$ aggregates in absence (black) and presence of peptide **4A** (blue) and **2C** (red). Peptides were incubated in PBS pH 7.4 at 37 °C.

4.6.4. Monitoring amyloidogenicity by TEM:

After 10 days of incubation in PBS pH 7.4 at 37 °C, we observed that the $A\beta_{1-40}$ alone showed clear fibrillar aggregates (Figure 4.18a) under TEM, whereas in presence of 5-fold (Figure 4.18c) or 10-fold (Figure 4.18d) molar excess of BSBHp **4A** no such fibers were observed. But some fibers were noticed when 2-fold molar excess of peptide **4A** was present with $A\beta_{1-40}$, indicating 2-fold molar excess of peptide **4A** was not sufficient to disrupt the preformed aggregates of $A\beta_{1-40}$ (Figure 4.18b). On the other hand, in presence of different doses of peptide **2C** (Figure 4.19), similar results were obtained as for peptide **4A**.

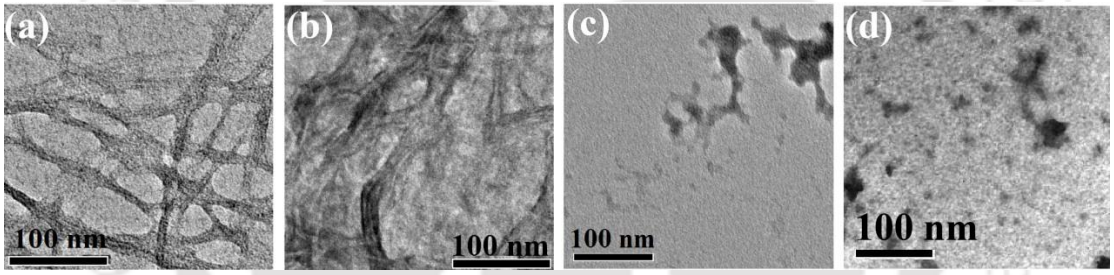

Figure 4.18: TEM images of (a) $A\beta_{1-40}$ alone and in presence of (b) 2-fold, (c) 5-fold or (d) 10-fold molar excess of peptide **4A**. Images were taken after 10 days incubation of the peptide solutions in PBS of pH 7.4 at 37 °C.

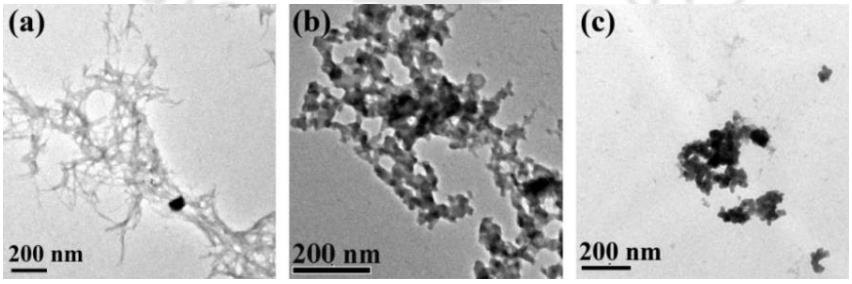

Figure 4.19: TEM images of $A\beta_{1-40}$ in presence of (a) 2-fold, (b) 5-fold or (c) 10-fold molar excess of peptide **2C**. Images were taken after 10 days incubation of the peptide solutions in PBS of pH 7.4 at 37 °C.

4.6.5. Monitoring amyloidogenicity by Congo red birefringence:

Again the disruption of amyloid was further confirmed by Congo red stained birefringence study (Figure 4.20 and 4.21).

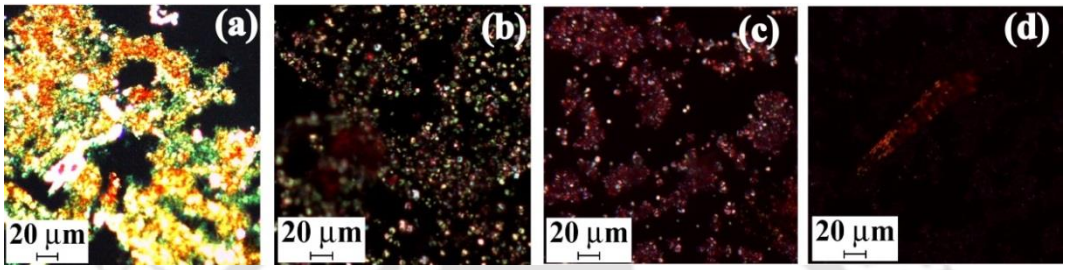

Figure 4.20: Congo red birefringence images of (a) $A\beta_{1-40}$ alone and in presence of (b) 2-fold, (c) 5-fold or (d) 10-fold molar excess of peptide **4A**. Images were taken after 10 days incubation in PBS of pH 7.4 at 37 °C.

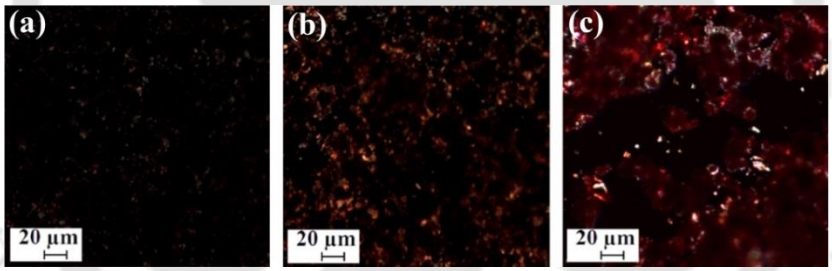

Figure 4.21: Congo red birefringence images of (a) $A\beta_{1-40}$ alone and in presence of (b) 2-fold, (c) 5-fold or (d) 10-fold molar excess of peptide **2C**. Images were taken after 10 days incubation in PBS of pH 7.4 at 37 °C.

When $A\beta_{1-40}$ peptide was analyzed under polarizable microscope, we observed clear appearance of green gold birefringence under cross polarized light when $A\beta_{1-40}$ was alone (Figure 4.20a) in the solution, but in presence of different doses (2-fold, 5-fold and 10-fold molar excess) of BSBHp **4A** such green gold birefringence were not observed. Although, in case of 2-fold (Figure 4.20b) molar excess some birefringence was observed but in presence of 5-fold (Figure 4.20c) and 10-fold (Figure 4.20d) molar excess of peptide **4A** no such

characteristic birefringence were observed. Similar results were obtained in case of peptide **2C** (Figure 4.21) as in case of peptide **4A**. Our results support that the BSBHp **4A** significantly disrupted the preformed fibrillar aggregates of $A\beta_{1-40}$ *in vitro* at physiological condition.

4.7. In vitro toxicity study using dye loaded Large Unilamellar Vesicle (LUV) leakage study

The soluble oligomers of Aβ are known to be more toxic than the mature fibrils due to their ability of pore formation on the cell membrane that causes neuronal dysfunction.[55] Therefore, it was important to know the exact state of the $A\beta_{1-40}$ aggregates after disruption by peptide **4A**. For this purpose we performed *in vitro* toxicity studies of disrupted $A\beta_{1-40}$ aggregates using carboxyfluorescein dye loaded vesicle (LUV) leakage assay. LUV leakage study is a proof of presence of toxic oligomeric species[55,96] in a solution. Amount of dye leakage is proportional to the amount of the toxic soluble oligomeric species present in the solution, as toxicity is originated by pore formation in cell membrane or vesicle. The large unilamellar vesicles (LUVs) were prepared using three different lipids, DPPC, Cholesterol and GM1 with 68:30:2 molar ratios in HEPES buffer (50 mM, pH 7.4) following the reported protocols.[96,128-130] The details of the LUVs preparation and dye entrapment were mentioned in Chapter 7, experimental section. The formation of LUVs was confirmed by TEM (Figure 4.22) and we observed the presence of lipid vesicles of ~200 nm diameter.

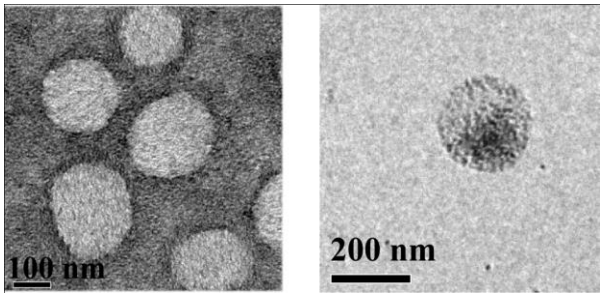

Figure 4.22: TEM images of negatively stained LUVs at concentration of 100 µM of lipid in 50 mM HEPES buffer of pH 7.4. The concentration of the stock solution of lipid was 2 mM.

Before performing the LUVs leakage study, all peptide solutions were prepared in HEPES (50 mM) pH 7.4 and incubated for desired time period (similar to section 4.6). We added the breaker peptides (peptide **4A** and **2C**) to the pre aggregated (60 h old) $A\beta_{1-40}$ solution and incubated them for a total of 10 days (240 h = 60 h + 180 h). Then, dye entrapped LUVs (lipid concentration ~2 mM) were prepared. For the LUV leakage study, we prepared four sets of peptide solutions (3 replicates for each set of solutions),

Solution 1 *$A\beta_{1-40}$ (incubated for 24 h),*

Solution 2 *$A\beta_{1-40}$ (incubated for 10 days),*

Solution 3 *$A\beta_{1-40}$ **:** peptide **4A** (1:10) (peptide **4A** was added to the preformed fibrillar aggregates after 60 h and incubated for total 10 days (60 h + 180 h).*

Solution 4 *$A\beta_{1-40}$: peptide **2C** (1:10) (peptide **2C** was added to the preformed fibrillar aggregates after 60 h and incubated for total 10 days(60 h + 180 h).*

12.5 µL of dye loaded LUVs (2 mM) and 25 µL of peptide solution (50 µM of $A\beta_{1-40}$) were taken and diluted to 500 µL to obtain final concentration of lipid solution 50 µM and $A\beta_{1-40}$ 2.5 µM. In the final solution, peptide and lipid were present in 1:20 molar ratios.[130] To

monitor the dye (carboxyfluorescein) release, we used fluorescence study (λ_{ex} = 485 nm, λ_{em} = 516 nm and band width 3 nm). The emission was recorded for each 5 min interval up to 20 min, then 10 min interval up to 100 min, further 12 h interval up to 72 h. At the end of the experiment 10 µL of Triton X-100 was added to obtain complete dye release from the vesicle and the final fluorescence was measured. In addition to those, the untreated LUVs (natural dye leakage) were also studied and used as control. The % of leakage was calculated as,[130]

$$\% \text{ Leakage} = \frac{(\text{observed fluorescence} - \text{initial fluorescence})}{(\text{total fluorescence} - \text{initial fluorescence})} \times 100\ \%$$

The pore formation on LUVs followed by dye release was monitored by time dependent fluorescence assay (Figure 4.23). We observed that the 24 h old $A\beta_{1-40}$ (red, Figure 4.23a,b) caused more dye leakage (~43% in 72 h) which confirmed the presence of toxic oligomeric species (solution 1). Again, 10 days old $A\beta_{1-40}$ sample (blue, Figure 4.23a,b; solution 2) caused less LUV leakage in comparison with 24 h old Aβ fibril. The results confirmed that soluble oligomers caused more toxic effect on LUVs by pore formation and dye leakage in comparison to the mature fibrils. We observed lesser extent of dye leakage when BSBHp **4A** (magenta, Figure 4.23a,b) was present with $A\beta_{1-40}$ (solution 3) and that leakage was almost comparable with that from the untreated LUVs. The $A\beta_{1-40}$ treated with BSBp **2C** (solution 4) caused more dye leakage (olive, Figure 4.23b,c) in comparison to BSBHp **4A** treated $A\beta_{1-40}$. Therefore, it can be concluded that presence of BSBHp disaggregates the amyloid fibrils of $A\beta_{1-40}$ into non-toxic species.

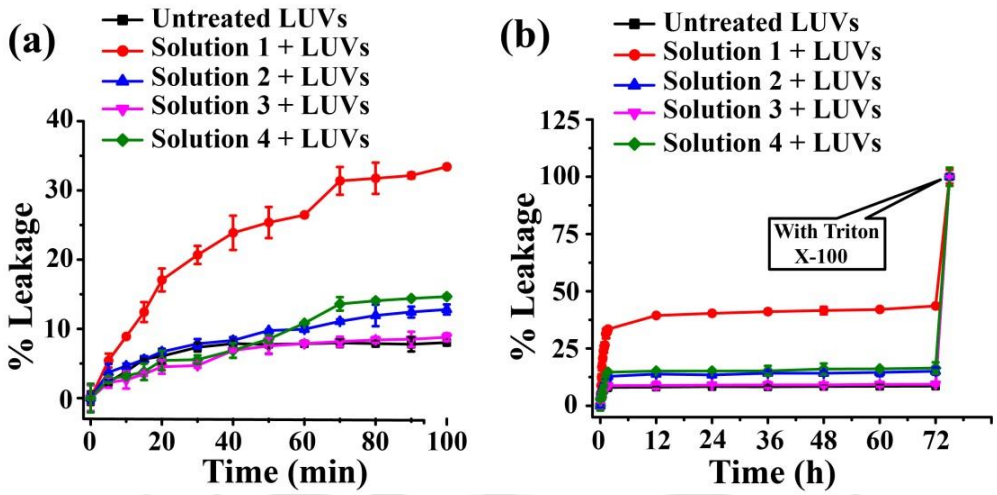

Figure 4.23: (a) and (b) Carboxyfluorescein dye emission showing the effect of $A\beta_{1-40}$ on LUVs with time and % of dye leakage. The spectra showing % of dye leakage by untreated LUVs (black); LUVs treated with solution 1 (red), solution 2 (blue), solution 3 (magenta) and solution 4 (olive). The 100 % dye release was obtained by treating the LUVs with triton X-100. The composition of solution 1, 2, 3 and 4 was mentioned above in the discussion section. For each data point 3 different sets of replicate solutions were scanned separately and average was taken with observed standard deviation.

4.8. Disruption of Aβ aggregates present in human cerebrospinal fluid by BSBHp:

In Alzheimer's disease, Aβ aggregates as plaques in the extracellular spaces in brain and the cerebrospinal fluid (CSF) is directly in contact.[131] Therefore, aggregated Aβ was identified by histo-pathological investigations in CSF. Herein, we investigated the efficacy of BSBHp **4A** to disrupt the amyloid present in human CSF.

4.8.1: Quantification of Aβ present in diseased human cerebrospinal fluid sample:

In the present study, human CSF samples were obtained from a diseased brain and the presence of amyloid in it was confirmed by ThT fluorescence study (Figure 4.24a,b).[131,132]

We prepared a 50 µM solution of $A\beta_{1-40}$ in PBS of pH 7.4 and incubated at 37 °C for 10 days. After 10 days, ThT induced fluorescence was measured in presence of varied amount (20, 50 and 100 µL) of $A\beta_{1-40}$ (Figure 4.24a), for all sets ThT concentration was same. During fluorescence study, volume of the solution in the cuvette was also kept fixed, 400 µL, in which 200 µL of ThT (50 µM) and varied volume of analyte (20, 50 and 100 µL) was present and the remaining volume was made up to the fixed volume using PBS.

From the ThT fluorescence, we noticed that with increasing amount of $A\beta_{1-40}$, fluorescence intensity increased which indicated the amount of amyloid present. Next, we performed ThT fluorescence study of the human CSF sample from the AD patients and observed that the fluorescence intensity was increased with increasing concentration of human CSF (Figure 4.24b). Therefore, the presence of amyloid aggregates in h-CSF was confirmed, and from the normalized spectra, the concentration of Aβ in the CSF sample was found to be ~23 µM.

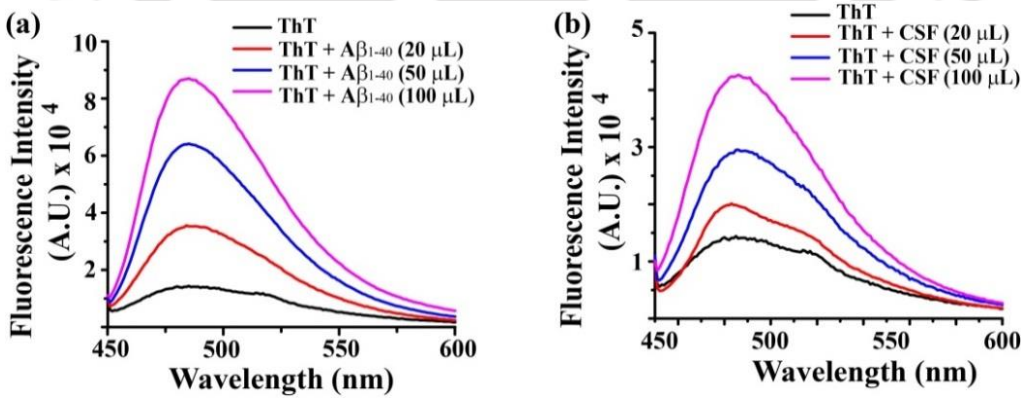

Figure 4.24: Fluorescence spectra of ThT in absence (black) and presence of 20 µL (red), 50 µL (blue) and 100 µL (magenta) of $A\beta_{1-40}$ (a) and human CSF (b).The stock concentration of ThT was 50 µM in PBS (50 mM) pH 7.4.

4.8.2: Monitoring the disruption of Aβ aggregates present in the CSF sample by ThT assay:

From the above study, it was confirmed that the concentration of Aβ in the human CSF sample was ~23 μM. Then, 10 fold molar excess of peptide **4A** and **2C** were added separately with the CSF samples and incubated them at 37 °C for 10 days. The kinetics of disaggregation of amyloid aggregates was monitored by ThT assay (Figure 4.25). In a ThT assay, we observed that fluorescence intensity of CSF was suppressed excessively in presence of peptide **4A** (blue, Figure 4.25) while the CSF alone (black, Figure 4.25) showed increased fluorescence. There was also a suppression of fluorescence observed in case of CSF sample with peptide **2C** (red, Figure 4.25).

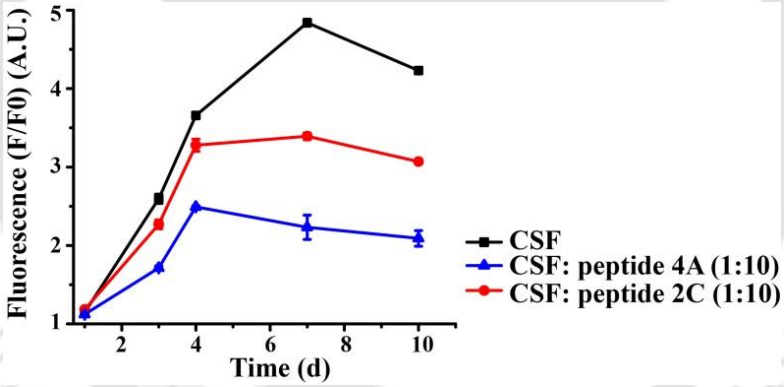

Figure 4.25: Time dependent ThT assay for the disruption of the amyloid present in human cerebrospinal fluid (CSF) in absence (black) and presence of peptide **4A** (blue) & **2C** (red) respectively.

4.8.3: Monitoring the disruption of Aβ aggregates present in the CSF sample by TEM and Congo red birefringence study:

After 10 days incubation of the CSF sample in presence of 10 fold molar excess of peptide **4A** and **2C**, when TEM was analyzed we observed clear fibrillar assembly in case of untreated CSF sample (Figure 4.26a). But such fibrillar assembly was not observed when

peptide **4A** was present in 10 fold molar excess with the CSF (Figure 4.26b). Although some aggregates was noticed in the CSF sample when incubated with peptide **2C** (Figure 4.26c).

On the other hand, the CSF sample alone showed a clear appearance of green gold birefringence (Figure 4.27a). But, no such birefringence was observed in presence of 10 fold molar excess of peptide **4A** (Figure 4.27b), indicating the absence of amyloid. Some shiny birefringence was observed in the CSF sample treated with peptide **2C** (Figure 4.27c).

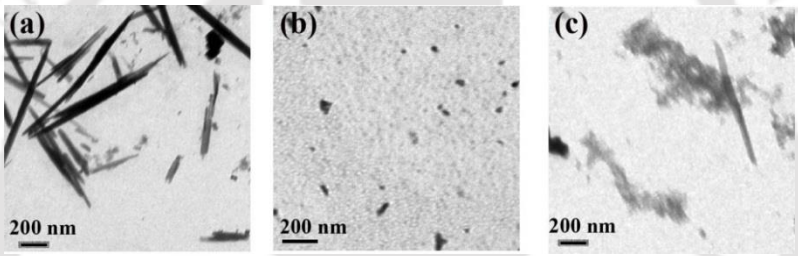

Figure 4.26: TEM images human CSF in absence (a) and presence of 10 fold molar excess of peptide **4A** (b) & peptide **2C** (c).Images were taken after 10 days incubation at 37 °C.

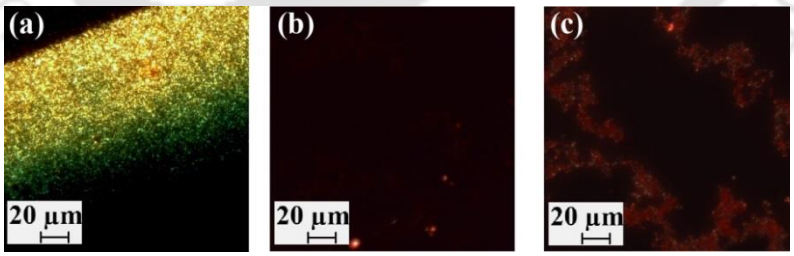

Figure 4.27: Congo red birefringence images human CSF in absence (a) and presence of 10 fold molar excess of peptide **4A** (b) & peptide **2C** (c). Images were taken after 10 days incubation at 37 °C.

4.9. Conclusion:

Based on our experimental results we can conclude that the BSBHp **4A** inhibits the aggregation of $A\beta_{1-40}$ peptide and also disrupts the fibrillar aggregates of $A\beta_{1-40}$ into non-toxic species *in vitro* at pH 7.4 and 37 °C. The BSBHp also disrupted the Aβ aggregates present in the diseased human cerebrospinal fluid sample *in vitro*. Therefore, we can conclude that the anthranilic acid containing β-sheet breaker hybrid peptide can be used to prepare lead molecules which can be used against Alzheimer's disease.

Chapter 5: Disruption of Amyloid-β (Aβ) aggregates into non-toxic species by a β-breaker di-peptide containing Pro-Drug peptide

5.1. Pro-Drug peptide:

We have discussed earlier (Chapter 3, section 3.1) that most of the reported β-sheet breaker peptides (BSBps) contained pre-installed breaker element which includes proline,[70] *N*-methylated amino acids,[71] α-aminoisobutyric acid (Aib),[114] dehydrophenylalanine, etc.[115] The common problem with these pre-installed breaker element containing BSBps is that, they already have acquired a β-breaker element (e.g., a kink) which may prevent proper recognition with existing β-sheet rich amyloidogenic peptide (Aβ) due to conformational mismatch (Figure 5.1a). If recognition is not proper, the breaking activity would be expectedly poor. The recognition or binding affinity of peptides depends on the number of H-bonds, hydrophobic interaction and the planar structure of β-sheet; whereas the breaking effect is govern by the reduction of H-bonds and/or introducing a group that cannot fit in the planner topology of β-sheet commonly known as β-breaker element. Thus, the recognition and the disruption are contradictory to each other. BSBps are known to disrupt amyloid. But,

the mechanism of amyloid disruption is not explained clearly. However, the growing evidences suggest that there are three probable mechanisms exist for such fibril disruption: (a) fibril disintegration from the surface, (b) lateral insertion and disintegration and (c) longitudinal insertion and disintegration. If the breaking element is pre-installed, it already induces a kink in the BSBp and cannot interact with the aggregated Aβ (β-sheet rich) effectively due to conformational mismatch. If the binding of the BSBp to the target Aβ does not occur effectively, disruption of amyloid is least expected. Thus, a pro-drug type construct (Pro-Drug peptide), which is devoid of the breaker element initially and able to interact with the fibril or amyloid easily, but generates the breaker element *in situ* at a later stage and able to disrupt the amyloid would be important for drug design (Figure 5.1b).

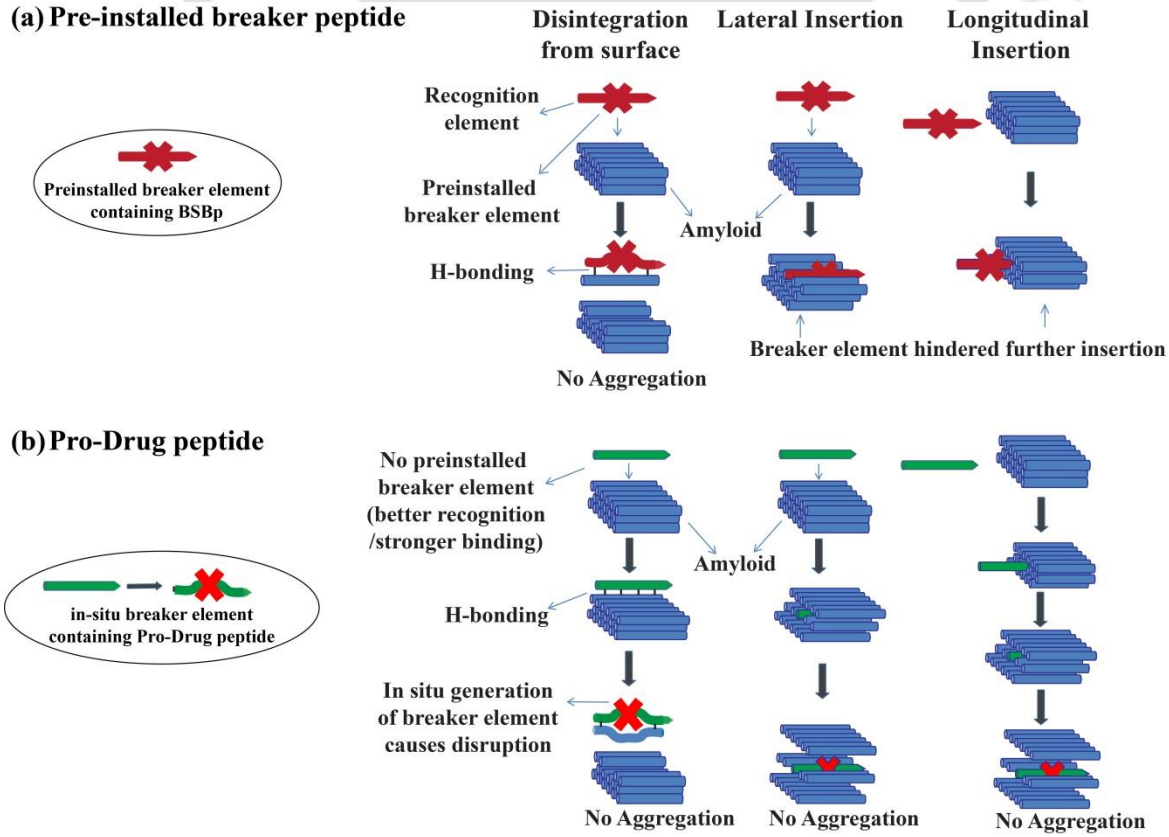

Figure 5.1: Plausible mode of interactions (a) between pre-installed breaker element containing BSBp & amyloid; (b) between Pro-Drug peptide & amyloid.

In this chapter, we have demonstrated a new design strategy of Pro-Drug peptide (PDp) for the disruption of Aβ aggregates into non-toxic species. The PDp contains a di-peptide moiety (Asp(OBzl)-Axx; Axx can be any amino acid) which we called as β-breaker di-peptide (BBDP). The BBDP initially adopts a β-sheet conformation when incorporated in the self-recognizing sequences of aggregating peptides, but generates a kink (a β-sheet breaker element) in its backbone at physiological condition (pH 7.4 and 37 °C) *in situ*, that forces to change its conformation from β-sheet to random coil later and expected to inhibit fibrillization and aggregation of Aβ peptide. The side chain ester linkage of the BBDP unit helps in aspartimide[133] formation easily by O to N acyl migration at 37 °C and pH 7.4. The aspartimide generates a type II' β turn[134] conformation (*in situ*) of the peptide that does not fit in the planer β-sheet topology of the fibril and therefore it should disrupt the preformed fibrillar assembly of Aβ more efficiently (Scheme 5.1, Figure 5.1b). Moreover, aspartimide gets racemized and converted to α-aspartyl and β-aspartyl residues in 1:3 ratios. The generated aspatimide, α- and β-aspartyl derivatives inserted between two amino acids (-Asp(OBzl)-Phe-) act as *in situ* β-breaker elements. Thus these two amino acids are collectively called as β-sheet breaker di-peptide (BBDP) unit.

Therefore, such a PDp peptide is expected to get aligned properly with and get recognized by the amyloidogenic peptides at the initial stage and may get inside the β-sheet network of the amyloidogenic peptides. Such incorporated PDp is supposed to get converted first to the aspartimide derivative of the peptide which again converts to α- and β-aspartyl derivatives at physiological pH. The *in situ* generated aspartimide, α- and β-aspartyl derivatives of the PDp should destabilize the H-bonding network of the β-sheet architecture (Figure 5.1b) and subsequently disrupt the aggregation of the amyloidogenic peptide.

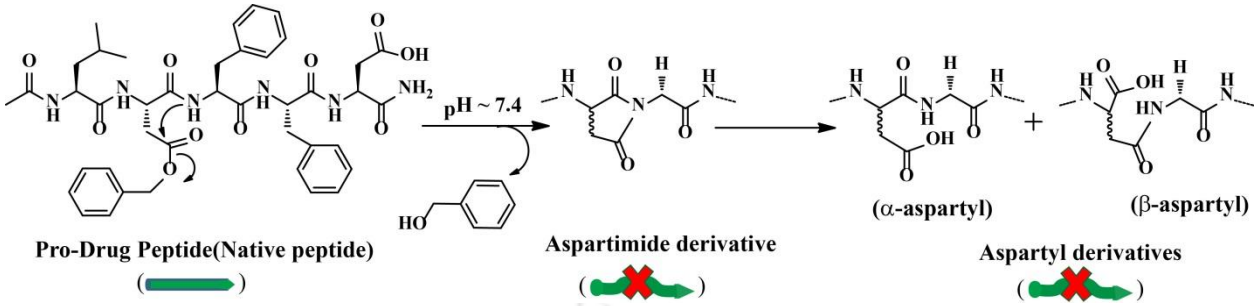

Scheme 5.1: The chemical conversions of PDp and *in situ* generation of breaker element at pH 7.4 and 37 °C.

5.2. Proposed hypothesis:

The aggregation of Aβ ($A\beta_{1–40}$ and $A\beta_{1–42}$) into neurotoxic oligomers and amyloid fibrils in the brain is the major hallmark of Alzheimer's disease (AD).[30,55] A strategy that disrupt the Aβ aggregates into non-toxic monomers would be always interesting for drug design against AD. In this chapter we wanted to show a peptide based molecule, namely, Pro-Drug peptide (PDp) and anticipated that the PDp will effectively disrupt the preformed fibrillar aggregates of $A\beta_{1-40}$ at pH 7.4 and 37 °C (Figure 5.2). We also anticipated that the PDp would align with the $A\beta_{1-40}$ aggregates initially then disrupt it through *in situ* generation of the breaker element.

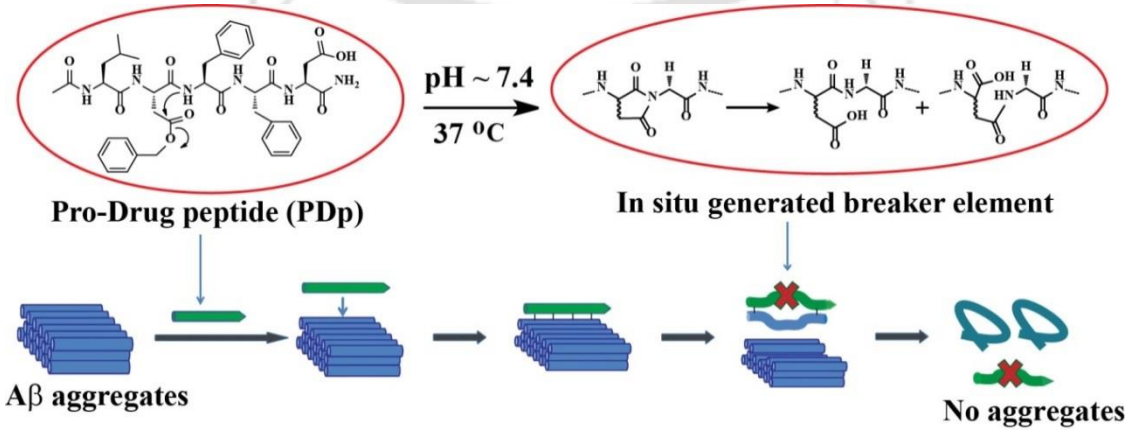

Figure 5.2: Hypothesis for the disruption of Aβ aggregates by the Pro-Drug peptide.

5.3. Design of peptides:

To test our hypothesis, we have designed a Pro-Drug peptide (**5A**), which would inhibit the aggregation of $A\beta_{1-40}$ peptide when co-incubated. The PDp **5A** was designed in a way that initially it was devoid of pre-installed breaker element, but at physiological condition (pH 7.4 and 37 °C) it would undergo a series of chemical conversions, first to aspartimide formation, then the formation of α- and β-aspartyl derivatives, which were expected to disrupt the aggregation of $A\beta_{1-40}$ peptide. The PDp also contain a recognition sequence (-F-F-) homologous with $A\beta_{19-20}$ (-F-F) for proper recognition. We also designed a pre-installed breaker element containing BSBp, commonly known as Soto's peptide (peptide **2C**)[70] which was already used in chapter 2 (Table 2.2) and here it was used as a control breaker. We used the peptide **2C** to compare efficacy of pre-installed breaker element (**2C**) versus the *in situ* breaker element (**5A**) against $A\beta_{1-40}$ aggregation. The $A\beta_{1-40}$ was used as the targeted amyloidogenic peptide.

Peptide No.	Peptide Sequence	Function
5A	Ac-L**D(OBzl)F**FD-NH_2	Inhibitor
2C	Ac-LPFFD-NH_2	Inhibitor/ control

Table 5.1: Sequences of designed peptides for the present investigation.

5.4. Synthesis and characterization of the designed peptides:

The designed peptides were synthesized by solid phase peptide synthesis (SPPS) technique using standard Fmoc/^{t}Bu protection strategy on Rink amide MBHA resin in a similar way described in chapter 2, section 2.4.[106-108] The synthetic scheme of the PDp **5A** has shown in

scheme 5.2. The designed peptides were purified using semi preparative HPLC and purity was confirmed by HPLC and mass spectrometry.

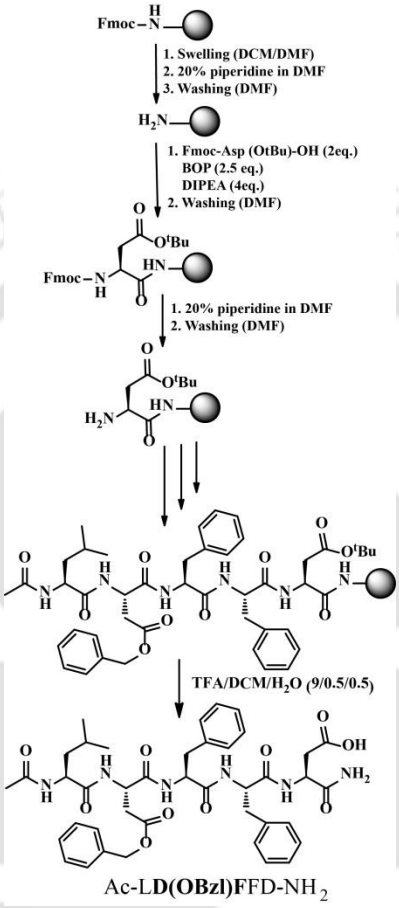

Scheme 5.2: Synthetic scheme of peptide **5A** using Fmoc/^{t}Bu protection based SPPS.

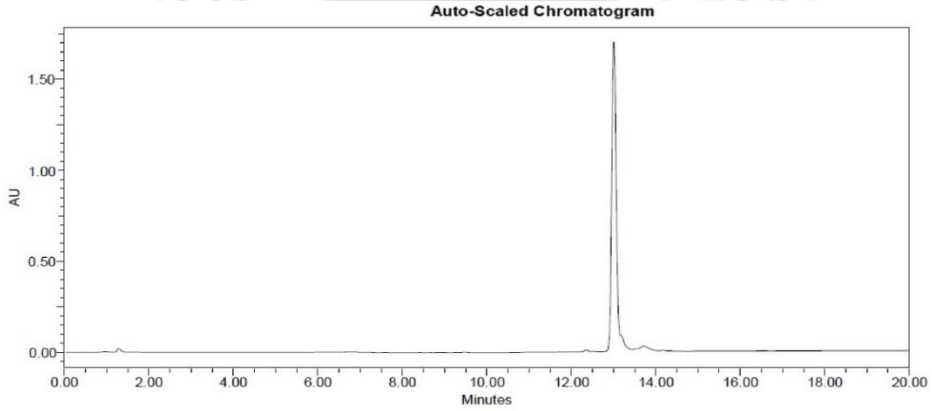

Figure 5.3: HPLC profile of the purified peptide **5A**.

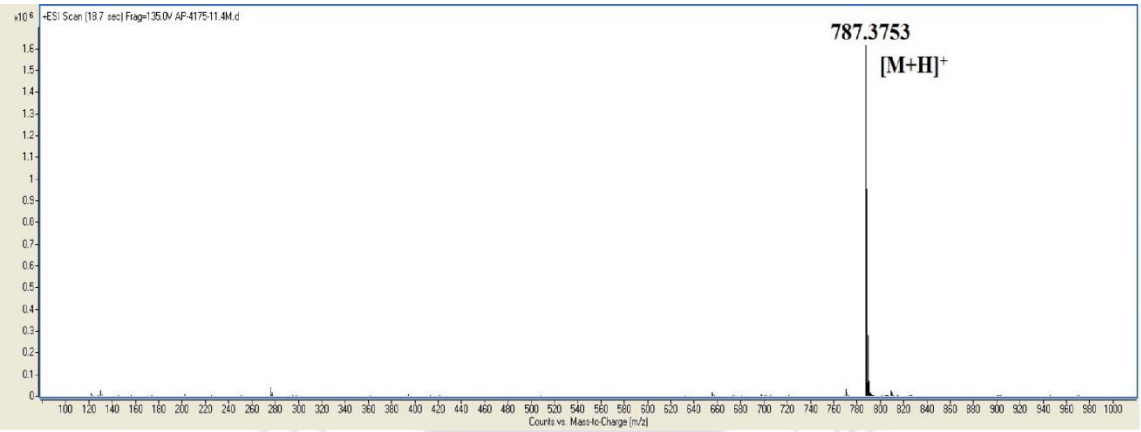

Figure 5.4: Mass spectrum of peptide **5A**. Calculated mass for $C_{41}H_{51}N_6O_{10}$ is 787.3667 and observed mass 787.3753 $[M+H]^+$.

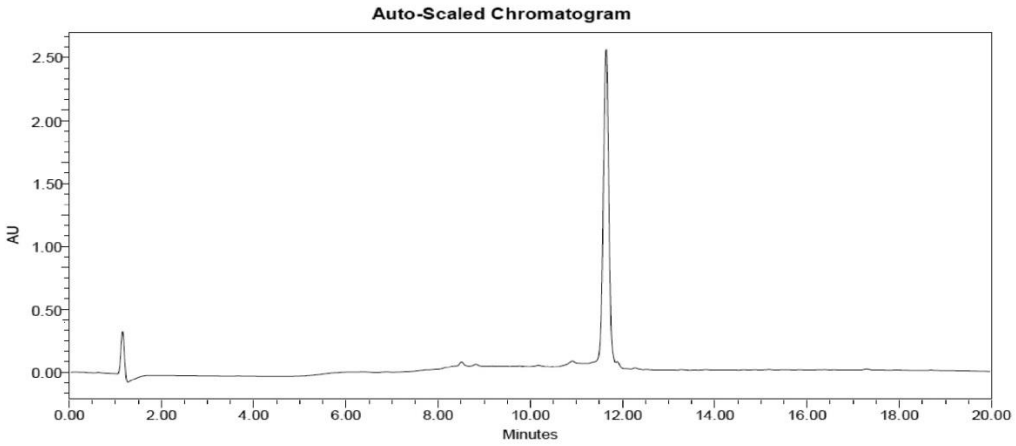

Figure 5.5: HPLC profile of the purified peptide **2C**.

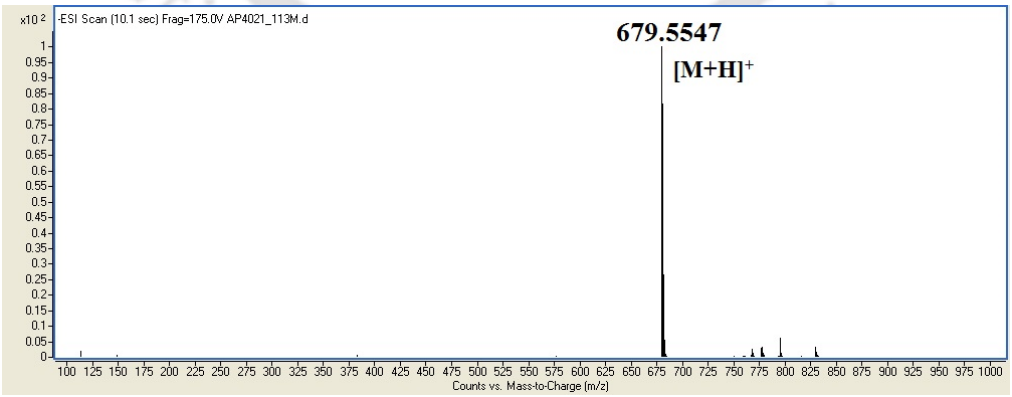

Figure 5.6: Mass spectrum of peptide **2C**. Calculated mass for $C_{35}H_{47}N_6O_8$ is 679.3455 and observed mass is 679.5547 as $[M+H]^+$.

5.5. Non-amyloidogenicity of the PDp 5A at physiological condition:

The PDp was designed in way that initially (pH ~4) it will form β-sheet which was expected to convert to the random coil conformation by changing the pH to 7.4. Therefore, in acidic pH it might form amyloid but at pH 7.4 it was expected to be non-amyloidogenic. Before monitoring the amyloidogenicity of the peptide **5A**, it was important to check the chemical conversion, *O* to *N* acyl migration (first aspartimide, then α- and β- aspartyl derivatives formation) of the peptide at pH 7.4. The chemical transition and amyloidogenicity of peptide **5A** was monitored by appropriate biophysical tools.

5.5.1. Chemical transition of peptide 5A monitored by LC-MS:

The kinetics of the O to N acyl migration or the rate of conversion of BBDP unit (-D(OBzl)-F- unit of the PDp) into aspartimide, α- and β-aspartyl residues was monitored using LC-MS. A stock solution of ~0.5 mM of PDp in PBS (50 mM, pH 7.4) was prepared and incubated at 37 °C on water bath. At different time intervals the stock solution was sonicated and vortexed for 1 min each before taking the sample for injection in LC-MS. A linear gradient of 0 to 100% CH_3CN for 7 min in a total run time of 8 min was selected.

The conversion of benzyl ester of aspartic acid (-D(OBzl)-) to aspartimide followed by α- and β-aspartyl derivatives was monitored by LC-MS (Figure 5.7) till the peaks corresponding to the aspartimide and the aspartyl residues emerged. After ~30 h we noticed that pure peptide completely disappeared and the peaks for α- and β- aspartyl residues emerged (Figure 5.7a). We noticed clear and distinct peaks for all different forms of the peptide and benzyl alcohol. All the intermediates were confirmed from the ESI MS data as shown in the Figure 5.7b-d.

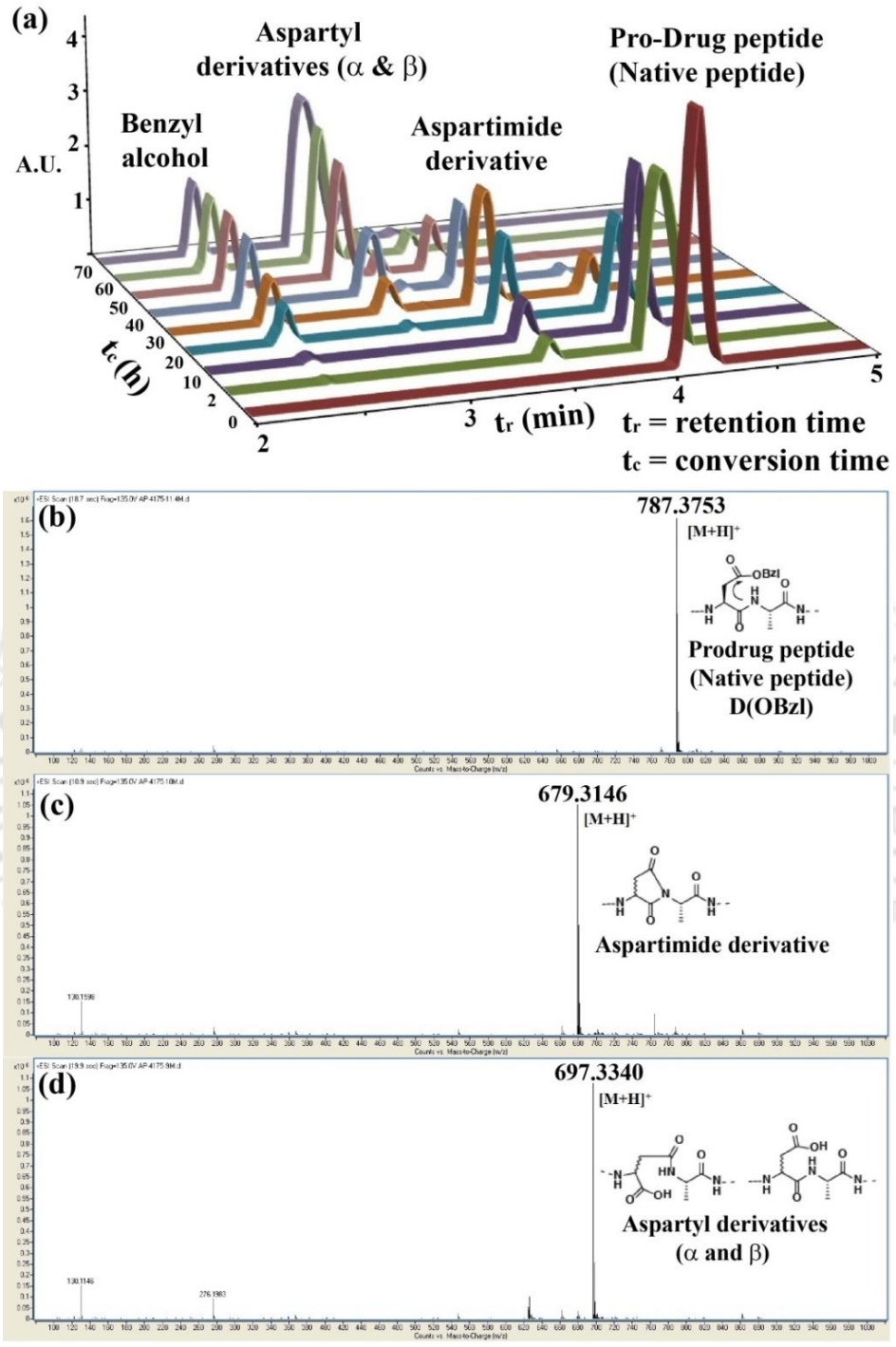

Figure 5.7: Time dependent kinetics of O to N acyl migration (aspartimide formation) and subsequent hydrolysis of the PDp **5A** by LC-MS. (a) LC profile with (b), (c) and (d) ESI-MS of the native PDp, its aspartimide derivative and aspartyl derivatives, respectively.

5.5.2. Conformational characterization of peptide 5A by CD and FTIR studies:

After observing the evidence for the desired chemical conversion, we wanted to check the conformational state of the PDp **5A** in acidic and basic pH by CD and FTIR studies. We were more interested to see the conformational state of PDp in basic pH, since in basic pH we expect chemistry of aspartimide formation would come into play and peptide no longer stays in β-sheet conformation. For the conformational analysis we prepared ~500 μM of solutions of the peptide **5A**, both at acidic pH (sodium acetate buffer of pH 4.0) and basic pH (PBS pH 7.4), and incubated them at 37 °C over water bath for 5 days. After 5 days, conformation of the peptide was monitored by CD and FTIR analyses (Figure 5.8). 0.5 mg of peptide **5A** was dissolved in 1.1 mL of (PBS, 50 mM, pH 7.4) to obtain a final concentration of 500 μM and incubated at 37 °C for 5 days and its conformation was studied.

After 5 days of incubation, in CD spectra of peptide **5A**, we observed a positive band centered at ~195 nm and a negative band centered at ~226 nm, clearly indicating the β-sheet rich conformation of the peptide **5A** (percentage of helix content 0, β sheet content 81.3, turn content 7.9 and random coil content 10.8; deconvoluted from the CD instrument) in acidic pH (black, Figure 5.8a). Again at pH 7.4, we observed a negative band centered at ~199 nm in CD, indicative of a random coil rich conformation (percentage of helix content 0, β sheet content 12, turn content 22.7 and random structure content 65.3; deconvoluted from the CD instrument) of peptide **5A** (red, Figure 5.8a).

Similarly, in FTIR spectra we observed a strong amide I band at 1631 cm^{-1} (black, Figure 5.8b) clearly indicating the β-sheet rich conformations of the PDp **5A** in sodium acetate buffer (pH 4.0). In line with the results of the CD experiments, at basic pH (PBS pH 7.4) we

observed a strong amide I band at 1649 cm^{-1} (Figure 5.8b). These results clearly indicated the random coil conformations of peptide **5A** at pH 7.4.[23,88]

From the conformational analysis it was clear that the PDp initially form β-sheet conformation which later transformed to random coil conformation when the pH jumped from acid to basic pH. This change in conformation probably indicated *in situ* generation of breaker element (aspartimide and aspartyl derivatives**)** which later expected to disturb the amyloid formation of the amyloidogenic peptide.

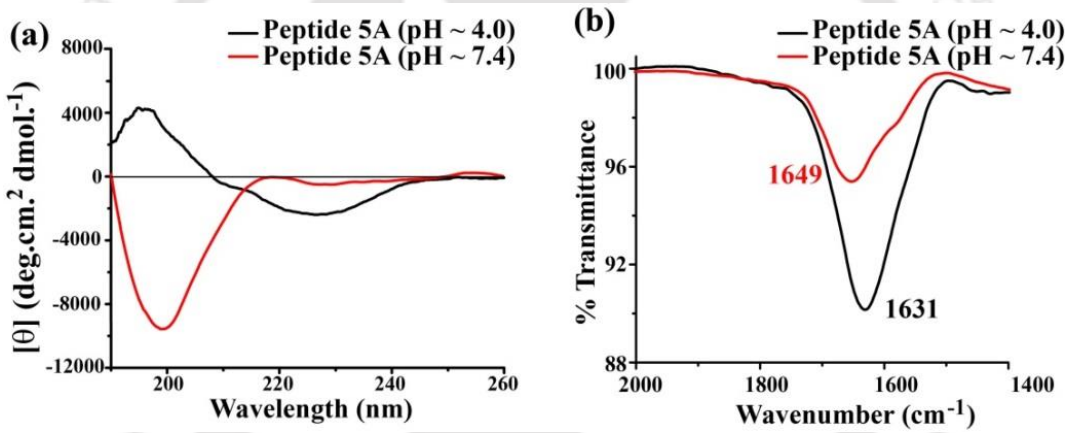

Figure 5.8: (a) CD and (b) FTIR spectra of peptide **5A**. Spectra were taken after 5 days of incubation of the peptide in sodium acetate buffer pH 4.0 (black) and PBS pH 7.4 (red) at 37 °C.

5.5.3. Characterization of amyloidogenic nature of peptide 5A by TEM and Congo red birefringence studies:

After, getting the conformation of the peptide **5A** at different pH, we wanted to check the amyloidogenicity of the PDp **5A** using TEM and Congo red stained birefringence studies.

After 5 days of incubation of the peptide **5A** in sodium acetate buffer, we observed fibrillar aggregates under TEM (Figure 5.9a) and characteristic green gold birefringence under polarizable microscope after stained with Congo red dye (Figure 5.9b). Again, in PBS pH 7.4, we observed no such fibrillar assembly under TEM (Figure 5.9c) and also no characteristic green gold birefringence under polarizable microscope (Figure 5.9d). These results were indicative of the non-amyloidogenic nature of the peptide **5A** in basic pH while the peptide found to be amyloidogenic in acidic pH.

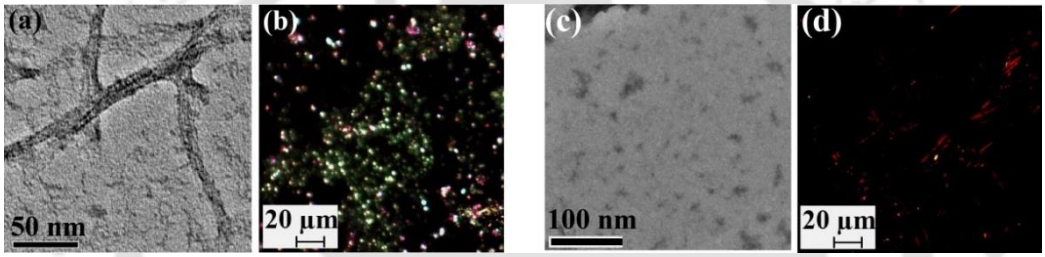

Figure 5.9: TEM images of the peptide **5A** in (a) sodium acetate buffer pH 4.0 and (c) PBS pH 7.4. Congo red birefringence images of the peptide **5A** in (b) sodium acetate buffer pH 4.0 and (d) PBS pH 7.4. Images were taken after 5 days incubation at 37 °C.

5.6: Inhibition of amyloid formation of Aβ by PDp 5A:

The PDp **5A** was found to be a non-amyloidogenic peptide at physiological condition (pH 7.4 and 37 °C). Therefore, we proceeded further to study the inhibition of aggregation of Aβ by the PDp **5A**. As decribed in the previous chapter (Chapter 4, section 4.5), we investigated inhibitory efficacy of PDp **5A** on $A\beta_{1\text{-}40}$ fibrillization in presence of varied amount (2-, 5- and 10- fold molar excess) of the PDp and compared its efficacy with the pre-installed breaker element containing control BSBp **2C**. Varied amount (2-, 5- and 10- fold molar excess) of the peptide **5A** and **2C** were co-incubated with $A\beta_{1\text{-}40}$ 50 µM in PBS pH 7.4 at 37 °C for 7 days and the kinetics of the amyloid formation was monitored using different biophysical tools.

1.2 mg of commercially available $A\beta_{1-40}$ peptide was taken and disaggregated it by TFA and HFIP treatment following the same procedure as discussed in last chapter (Chapter 4, section 4.5.1).[127] The disaggregated material dissolved in 1.4 mL of PBS (50 mM, pH 7.4) by sonication and vortex to obtain transparent solution and the whole solution was divided into 7 equal portions followed by addition of 600 μL of PBS to each portion to obtain a final $A\beta_{1-40}$ concentration of 50 μM. For the inhibition study, 2, 5 and 10 fold molar excess of the breaker peptides (**5A** and **2C**) were mixed with each portion (800 μL) of $A\beta_{1-40}$ solution and kept for incubation over water bath for 7days at 37 °C. For accurate result two more replicate solutions of each portion were prepared and fibrillzation were monitored by various biophysical tools.

5.6.1. Monitoring conformational transition by CD:

After 7 days of incubation at 37 °C, when CD spectra were taken, we observed $A\beta_{1-40}$ peptide alone exhibited a positive band centered at ~198 nm and a negative band centered at ~212 nm, clearly indicating a β-sheet rich conformation of $A\beta_{1-40}$ (black, Figure 5.10a,b). But in presence of different doses of peptide **5A** (2-, 5- and 10-fold molar excess), the β-sheet content of $A\beta_{1-40}$ reduced noticibly with the increment of doses of the PDp (Figure 5.10a), that indicated the breaking of β-sheet occured, which also was an indication of the inhibiton of aggregation of $A\beta_{1-40}$ occured by the PDp **5A**. Again, in presence of different doses of peptide **2C** (2-, 5- and 10-fold molar excess), the β-sheet content of $A\beta_{1-40}$ also reduced slowly as the doses increased (Figure 5.10b), which was an indication that the control peptide **2C** also inhibited the aggregation of the $A\beta_{1-40}$.

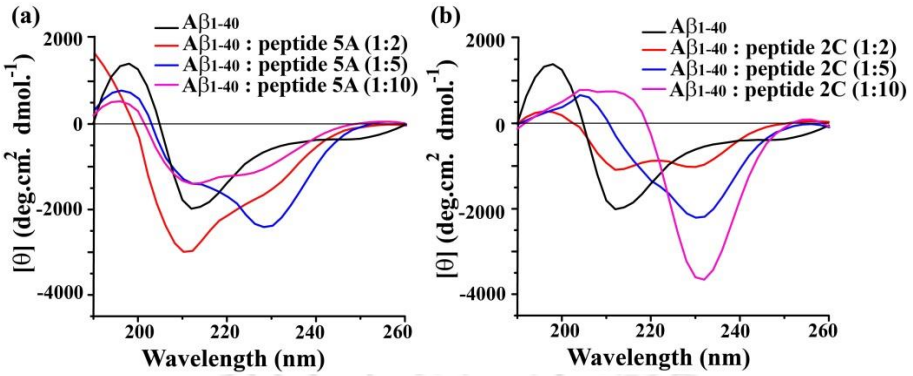

Figure 5.10: CD spectra of $A\beta_{1-40}$ in absence (black) and presence of 2-fold (red), 5-fold (blue) and 10-fold (magenta) molar excess of peptide (a) **5A** and (b) **2C**. Spectra were recorded after 7days of incubation of the peptide solutions in PBS pH 7.4 at 37 °C.

5.6.2. Monitoring conformational transition by FTIR:

Next, the conformational transition was monitored by FTIR analyses (Figure 5.11). We observed an intense band at 1627 cm^{-1} in FTIR spectra when $A\beta_{1-40}$ was alone in the solution, confirmed the characteristic β-sheet[23] conformation (black, Figure 5.11a,b). But, in presence of different doses (2-, 5- and 10-fold molar excess) of peptide **5A** (Figure 5.11a) and **2C** (Figure 5.11b) no such characteristic β-sheet conformations were observed as indicated in the Figure 5.11. These results clearly indicate the β-sheet inhibiting ability of the PDp **5A** at pH 7.4 and 37 °C.

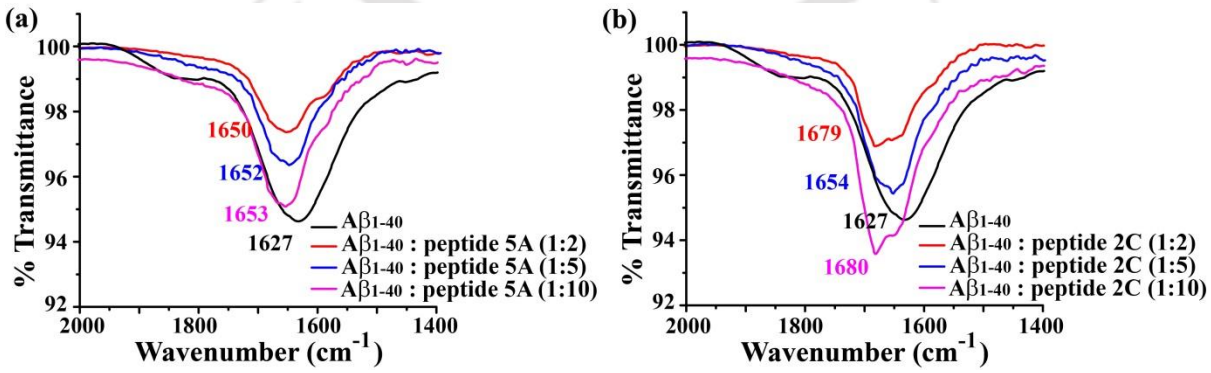

Figure 5.11: FTIR spectra of $A\beta_{1-40}$ in absence (black) and presence of 2-fold (red), 5-fold (blue) and 10-fold (magenta) molar excess of peptide (a) **5A** and (b) **2C**. Spectra were recorded after 7days incubation of the peptide solutions in PBS pH 7.4 at 37 °C.

5.6.3. Monitoring the kinetics of amyloid formation by Thioflavin T fluorescence assay:

For Thioflavin T (ThT) fluorescence assay, at different time intervals, 40 μL of peptide samples from the stock (the preparation of sample was mentioned in section 5.6) were mixed with 200 μL of ThT solution (50 μM), total volume was made up to 400 μL with PBS (50 mM, pH 7.4) and fluorescence was measured (λ_{ex} = 440 nm, λ_{em} = 485 nm and band width 3 nm). Normalized spectra were plotted as the average of the three replicate solutions.

From the ThT assay (Figure 5.12), we observed an increment of fluorescence intensity with time, when $A\beta_{1-40}$ peptide was alone in the solution. But, in presence of different doses (2-, 5- and 10-fold molar excess) of PDp **5A**, the fluorescence intensity decreased significantly as the doses of PDp increased, indicating the reduction of amount of amyloid in the sample, that in turn indicated the inhibition of aggregation of $A\beta_{1-40}$ by PDp (Figure 5.12a). We noticed that 2 fold molar excess (red, Figure 5.12a) of peptide **5A** was not sufficient to inhibit the amyloid formation of $A\beta_{1-40}$, but when the dose of **5A** was increased to 5 fold molar excess (blue, Figure 5.12a), the inhibition was more pronounced which was further evident when 10 fold molar excess (magenta, Figure 5.12a) of peptide **5A** was co-incubated with $A\beta_{1-40}$ peptide. We observed similar results in presence of different doses (2-, 5- and 10-fold molar excess) of peptide **2C** (Figure 5.12b), but less significant than the effect of peptide **5A** (Figure 5.12c).

From figure 5.12c, we observed that the amount of amyloid fibril was inhibited significantly up to 64-65% (blue, Figure 5.12c) when PDp **5A** was co-incubated with $A\beta_{1-40}$ in 10 fold molar excess until seven days, but in presence of similar molar excess of the control peptide **2C**, the amyloid fibril was suppressed by 46-47% (red, Figure 5.12c) at same condition.

These results probably indicated that the superiority of *in situ* generated breaker element (PDp **5A**) over the pre-installed breaker element (peptide **2C**) at the same condition.

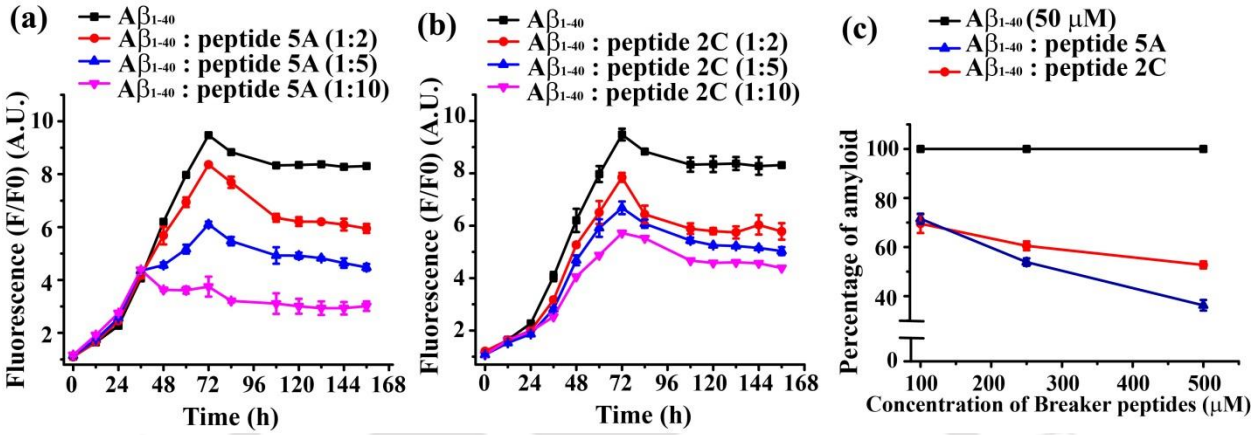

Figure 5.12: Time dependent ThT assay of $A\beta_{1-40}$ in absence (black) and presence of 2 fold (red), 5 fold (blue) and 10 fold (magenta) molar excess of peptide (a) **5A** and (b) **2C**. (c) % of amyloid formation of $A\beta_{1-40}$ in absence (black) and presence of peptide **5A** (blue) and **2C** (red). Peptides were incubated in PBS pH 7.4 at 37 °C.

5.6.4. Monitoring amyloidogenicity by TEM:

We already observed the inhibitory effect of PDp **5A** on the amyloid formation of $A\beta_{1-40}$ in the previous section. The same was further confirmed by TEM analysis. The $A\beta_{1-40}$ alone showed clear fibrillar aggregates under TEM (Figure 5.13a), but in presence of 10-fold molar excess of PDp **5A** (Figure 5.13b) no such aggregates were observed, indicating absence of amyloid. Again, in presence of 10-fold molar excess of peptide **2C**, we did not observe any fibrillar aggregates (Figure 5.13c). Therefore, it was again clear that the presence of PDp **5A** the amyloid formation of $A\beta_{1-40}$ was inhibited significantly at physiological condition *in vitro*.

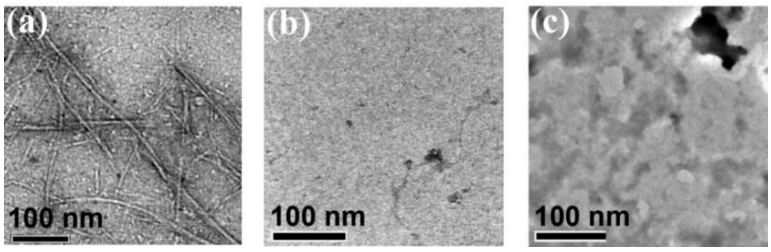

Figure 5.13: TEM images of of $A\beta_{1-40}$ in absence (a) and presence of 10-fold molar excess of peptide **5A** (b) & peptide **2C** (c). Images were taken after 7 days incubation in PBS of pH 7.4 at 37 °C.

5.6.5. Monitoring amyloidogenicity by Congo red birefringence:

The $A\beta_{1-40}$ peptide alone showed clear green gold birefringence under crossed polarized light (Figure 5.14a). But in presence of 10-fold molar excess of peptide **5A** (Figure 5.14b) and **2C** (Figure 5.14c), such green gold birefringence were not observed.

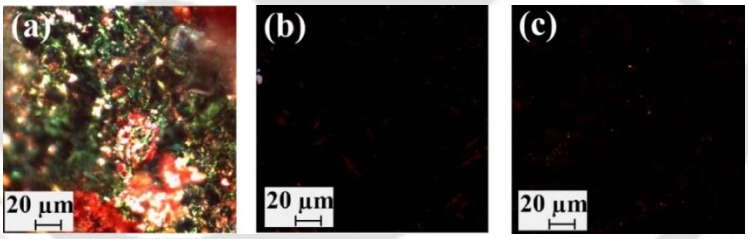

Figure 5.14: Congo red birefringence images of $A\beta_{1-40}$ in absence (a) and presence of 10-fold molar excess of peptide **5A** (b) & peptide **2C** (c). Images were taken after 7 days incubation in PBS of pH 7.4 at 37 °C.

5.7. Disruption of preformed Aβ aggregates by the PDp:

From the above experimental results (section 5.6) it was confirmed that the PDp **5A** significantly inhibited the aggregation of $A\beta_{1-40}$ peptide when co-incubated with it *in vitro* at pH 7.4 and 37 °C. Next, we wanted to check the efficacy of PDp for the disruption of preformed fibrillar aggregates of $A\beta_{1-40}$ *in vitro*. From the ThT assay (black, Figure 5.12a),

we observed that the growth phase for fibril formation of $A\beta_{1-40}$ at mentioned condition was in the range 24 h to 72 h. Therefore, we designed an experiment where the peptide **5A** was added into the fibrillar assembly at the time range of fibrillar growth phase.

Similar to the last chapter (Section 4.6) we designed an experiment, where $A\beta_{1-40}$ (50 μM) was incubated alone in PBS pH 7.4 at 37 °C for 60 h and then different doses (2-fold, 5-fold and 10-fold) of peptide **5A** and **2C** were separately added to $A\beta_{1-40}$ peptide solution and incubated till 10 days (240 h = 60 h + 180 h). Then, the amyloid formation of $A\beta_{1-40}$ in absence and presence of peptide **5A** and **2C** were monitored by different biophysical tools.

5.7.1. Monitoring conformational transition by CD:

When CD was performed after 10 days, we observed that $A\beta_{1-40}$ peptide alone showed a positive band centered at ~202 nm and a negative band centered at ~219 nm, clearly indicating the characteristic bands for β-sheet rich conformation of $A\beta_{1-40}$ (black, Figure 5.15a,b). But in presence of different doses (2-, 5- and 10-fold molar excess) of peptide **5A**, β-sheet contents were reduced slowly as the doses increased (Figure 5.15a). These results clearly indicated the breaking of β-sheet, which was also supportive of the disruption of preformed fibrillar aggregates of $A\beta_{1-40}$ by the PDp **5A**. Similarly, in presence of different doses (2-, 5- and 10-fold molar excess) of peptide **2C** with $A\beta_{1-40}$, the β-sheet content also reduced with the increase of doses (Figure 5.15b), which was an indication that the control peptide **2C** also disrupted the preformed fibrillar aggregates of $A\beta_{1-40}$.

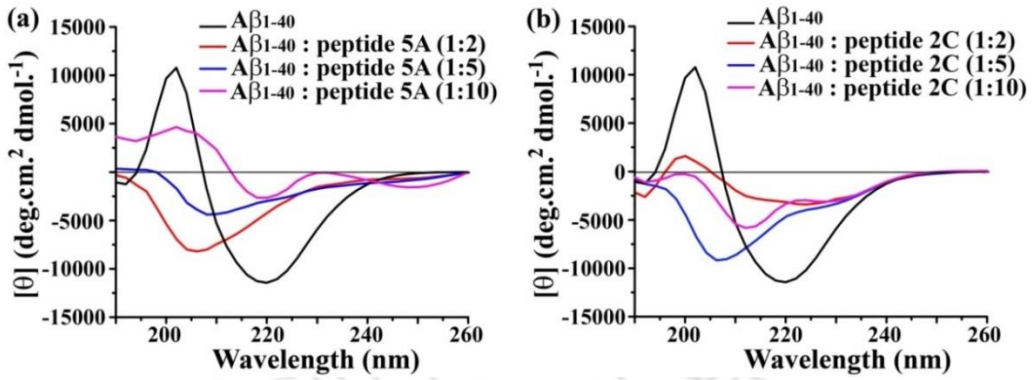

Figure 5.15: CD spectra of $A\beta_{1-40}$ in absence (black) and presence of 2-fold (red), 5-fold (blue) and 10-fold (magenta) molar excess of peptide (a) **5A** and (b) **2C**. Spectra were recorded after 10 days incubation in PBS pH 7.4 at 37 °C.

5.7.2. Monitoring conformational transition by FTIR:

We observed a strong band at 1630 cm^{-1} in FTIR spectra when only $A\beta_{1-40}$ was present in the solution, characteristic band of β-sheet conformation (black, Figure 5.16a,b). But, in presence of different doses (2-, 5- and 10-fold molar excess) of peptide **5A** (Figure 5.16a) and **2C** (Figure 5.16b) no such characteristic band for β-sheet conformations were observed. These results indicated significant β-breaking effect by the PDp **5A**.

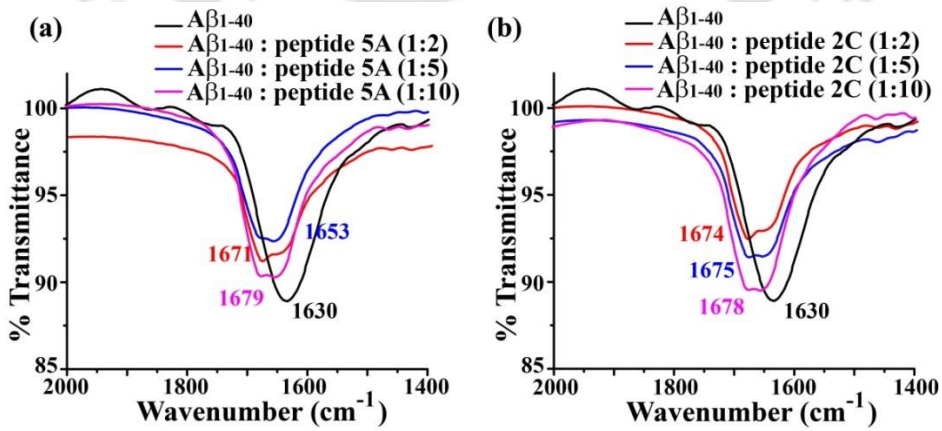

Figure 5.16: FTIR spectra of $A\beta_{1-40}$ in absence (black) and presence of 2-fold (red), 5-fold (blue) and 10-fold (magenta) molar excess of peptide (a) **5A** and (b) **2C**. Spectra were recorded after 10 days incubation in PBS pH 7.4 at 37 °C.

5.7.3. Monitoring the kinetics of amyloid formation by Thioflavin T fluorescence assay:

The kinetics of amyloid formation and its inhibition was monitored by ThT assay. We observed an increment of fluorescence with time for $A\beta_{1-40}$ peptide when incubated alone (black, Figure 5.17a) but when varied molar excess (2-, 5- and 10-fold molar excess) of peptide **5A** were added to the fibrillar assembly of $A\beta_{1-40}$ after 60 h, the fluorescence was suppressed significantly with time (Figure 5.17a). We also observed the dose dependent effect of peptide **5A** on the preformed fibrillar assembly of $A\beta_{1-40}$. Similar results were obtained for peptide **2C** (Figure 5.17b). The amount of fibril of $A\beta_{1-40}$ formed at 60 h was found to be reduced by peptide **5A** (blue, Figure 5.17c) more effectively than peptide **2C** (red, Figure 5.17c). After 10 days the preformed fibril was reduced up to 54-55% when the peptide **5A** was present in 10 fold molar excess whereas the peptide **2C** could suppress only 32-33%.

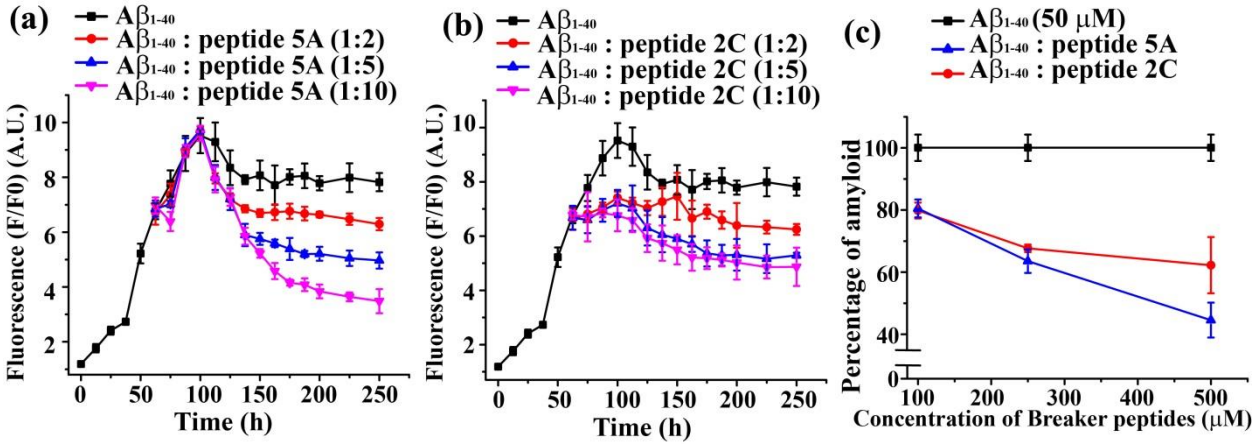

Figure 5.17: Time dependent ThT assay of $A\beta_{1-40}$ in absence (black) and presence of 2 fold (red), 5 fold (blue) and 10 fold (magenta) molar excess of peptide (a) **5A** and (b) **2C**. (c) % of amyloid disruption of preformed $A\beta_{1-40}$ aggregates in absence (black) and presence of peptide **5A** (blue) and **2C** (red). Peptides were incubated in PBS pH 7.4 at 37 °C.

5.7.4. Monitoring amyloidogenicity by TEM:

The formation of amyloid aggregates and its disruption was monitored by TEM (Figure 5.17). After 10 days of incubation in PBS pH 7.4 at 37 °C, we observed that the $A\beta_{1-40}$ alone exhibited clear fibrillar aggregates (Figure 5.18a) under TEM, whereas in presence of 10-fold (Figure 5.18b) molar excess of PDp **5A** no such fibers were observed. Again, in presence of 10-fold molar excess of peptide **2C** (Figure 5.18c) we did not observe any fibrillar assembly.

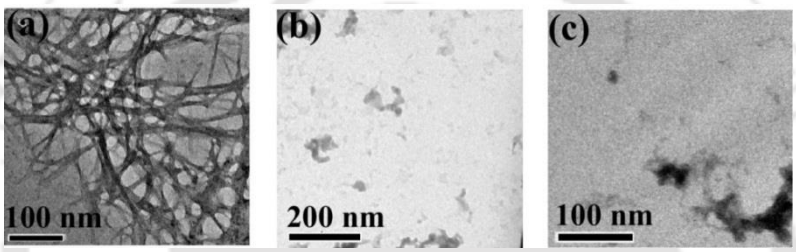

Figure 5.18: TEM images of $A\beta_{1-40}$ in absence (a) and presence of 10-fold molar excess of peptide **5A** (b) & peptide **2C** (c). Images were taken after 10 days incubation of the peptide solutions in PBS of pH 7.4 at 37 °C.

5.7.5. Monitoring amyloidogenicity by Congo red birefringence:

The presence of amyloid aggregates of $A\beta_{1-40}$ and its disruption was also monitored by Congo red stained birefringence study (Figure 5.19). We observed clear appearance of characteristic green gold birefringence under cross polarized light when $A\beta_{1-40}$ was alone (Figure 5.19a) in the solution, but in presence of 10-fold molar excess of peptide **5A** (Figure 5.19b) such green gold birefringence was not observed. Similarly, in presence of 10-fold molar excess of peptide **2C** (Figure 5.19c) we did not observe any birefringence. The above results clearly support that the PDp **5A** significantly disrupted the preformed fibrillar aggregates of $A\beta_{1-40}$ *in vitro* at physiological condition in a better manner than the BSBp **2C**.

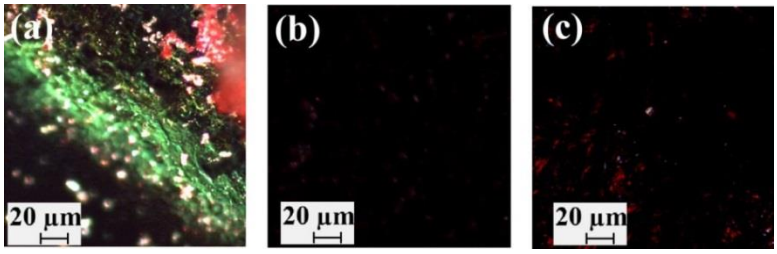

Figure 5.19: Congo red birefringence images of $A\beta_{1-40}$ in absence (a) and presence of 10-fold molar excess of peptide **5A** (b) & **2C** (c). Images were captured after 10 days incubation of the peptide solutions in PBS of pH 7.4 at 37 °C.

5.8. In vitro toxicity study using dye loaded Large Unilamellar vesicle (LUV) leakage study

Since, the soluble oligomers of Aβ are known to be more toxic than the mature fibrils for their ability of pore formation to the cell membrane and cause neuronal dysfunction,[55] it was important to know the exact state of the $A\beta_{1-40}$ aggregates disrupted by peptide **5A**. To check the fate of disrupted $A\beta_{1-40}$ by peptide **5A**, we performed *in vitro* toxicity studies using carboxyfluorescein dye loaded vesicles (LUVs) leakage assay. LUVs leakage study is a proof of presence of toxic oligomeric species in a solution.[55,96] The LUVs were prepared in a similar manner as described in chapter 4, section 4.7 (for detail, see Chapter 7, experimental section). The formation of LUVs was confirmed by FESEM images (Figure 5.22) and we observed the presence of lipid vesicles with ~200 nm diameter.

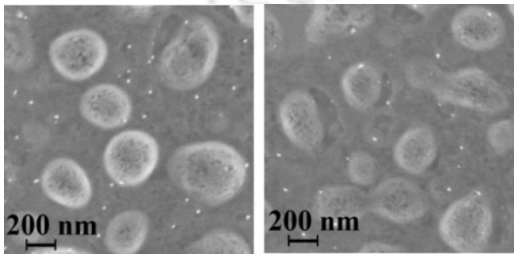

Figure 5.20: FESEM images of LUVs at concentration of 100 µM of lipid in 50 mM HEPES buffer of pH 7.4. The stock concentration of lipid was 2 mM.

To perform the LUVs leakage study, all peptide solutions were prepared in HEPES (50 mM, pH 7.4) and incubated for desired time period (similar to section 5.7). We added the breaker peptides (peptide **5A** and **2C**) to the pre-aggregated (60 h old) $A\beta_{1\text{-}40}$ solution and incubated them for a total of 10 days (240 h = 60 h + 180 h). In parallel, the dye entrapped LUVs (lipid concentration ~2 mM) were also prepared. For the LUV leakage study we prepared four sets of peptide solutions (3 replicates for each set of solutions):

Solution 1 *$A\beta_{1\text{-}40}$ (incubated for 24 h); expected to be oligomers,*

Solution 2 *$A\beta_{1\text{-}40}$ (incubated for 10 days), expected to be mature fibrils,*

Solution 3 *$A\beta_{1\text{-}40}$ **:** peptide **5A** (1:10) (peptide **5A** was added to the preformed fibrillar aggregates after 60 h and incubated for total 10 days (60 h + 180 h).*

Solution 4 *$A\beta_{1\text{-}40}$: peptide **2C** (1:10) (peptide **2C** was added to the preformed fibrillar aggregates after 60 h and incubated for total 10 days(60 h + 180 h).*

The lipids and peptides were mixed in a ratio of 1:20 (as mentioned in Chapter 4, Section 4.7), monitored the dye (carboxyfluorescein) release assay by fluorescence study (λ_{ex} = 485 nm, λ_{em} = 516 nm and band width 3 nm). The emission was recorded for each 10 min interval up to 100 min, further 12 h interval up to 72 h. At the end of the experiment 10 µL of Triton X-100 was added to obtain complete dye release from the vesicle and the final fluorescence was measured. The untreated LUVs (natural dye leakage) were also studied and used as control. The % leakage was calculated as,[130]

$$\%\ \text{Leakage} = \frac{(\text{observed fluorescence} - \text{initial fluorescence})}{(\text{total fluorescence} - \text{initial fluorescence})} \times 100\ \%$$

From LUV leakage study, we observed that the 24 h old $A\beta_{1-40}$ (red, Figure 5.21a,b) caused more dye leakage (~45% in 72 h) which confirmed the presence of toxic oligomers (solution 1). Again, 10 days old $A\beta_{1-40}$ sample (blue, Figure 5.21a,b; solution 2) caused less LUV leakage in comparison with 24 h old Aβ fibril, indicating the mature fibrils were less toxic than the soluble oligomers. We observed lesser extent of dye leakage when PDp **5A** (olive, Figure 5.21a,b) was present with $A\beta_{1-40}$ (solution 3) and that leakage was almost comparable with that from the untreated LUVs, indicating the PDp disrupted the $A\beta_{1-40}$ aggregates into non-toxic species. The $A\beta_{1-40}$ treated with peptide **2C** (solution 4) caused more dye leakage (magenta, Figure 5.21b,c) in comparison to peptide **5A** treated $A\beta_{1-40}$. Therefore, it can be concluded that the presence of PDp disaggregates the amyloid fibrils of $A\beta_{1-40}$ into non-toxic species *in vitro* at pH 7.4 and 37 °C.

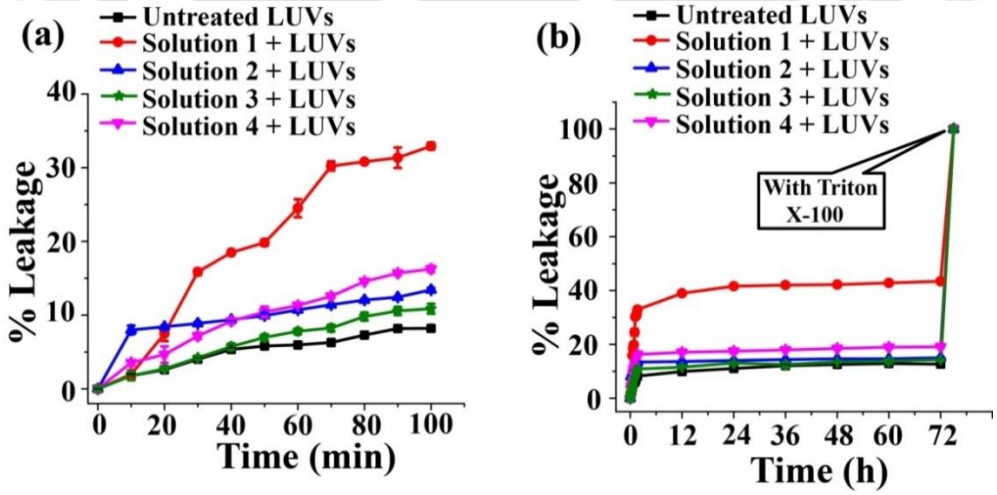

Figure 5.21: (a) and (b) Carboxyfluorescein dye emission showing the effect of $A\beta_{1-40}$ on LUVs with time and % of dye leakage. The spectra showing % of dye leakage by untreated LUVs (black); LUVs treated with solution 1 (red), solution 2 (blue), solution 3 (olive) and solution 4 (magenta). The 100% dye release was obtained by treating the LUVs with Triton X-100. The composition of solution 1, 2, 3 and 4 was mentioned above in the discussion section. For each data point, 3 different sets of replicate solutions were scanned separately and average was taken with observed standard deviation.

5.9. Disruption of Aβ aggregates present in human cerebrospinal fluid by PDp:

We also performed the efficacy of PDp **5A** for the disruption of Aβ aggregates present in human cerebrospinal fluid (CSF) in vitro at pH 7.4 and 37 °C.

5.9.1: Quantification of Aβ present in diseased human cerebrospinal fluid sample:

The human CSF samples were obtained from an AD affected brain and the presence of amyloid was confirmed by ThT fluorescence study (Figure 5.22a,b) in similar manner as described in chapter 4, section 4.8.[131,132] To get the probable concentration of the obtained CSF, we prepared a 50 μM solution of $A\beta_{1-40}$ in PBS of pH 7.4 and incubated at 37 °C for 10 days. After 10 days, ThT induced fluorescence was measured with varied amount (20, 50 and 100 μL) of $A\beta_{1-40}$ (Figure 5.22a) and CSF (Figure 5.22b), keeping the ThT concentration same.

From the ThT assay, we observed that with increasing amount of $A\beta_{1-40}$, fluorescence intensity was also increasing which indicated amyloid was present. Similarly, we performed ThT fluorescence study of the human CSF sample from the AD affected brain and observed that the fluorescence intensity increased with increasing concentration of human CSF (Figure 5.22b). Therefore, the presence of amyloid aggregates in human CSF was confirmed. Also, from the normalized spectra, the concentration of Aβ in the CSF sample was determined to be ~20 μM by comparison of the fluorescence intensity with the authentic $A\beta_{1-40}$ sample.

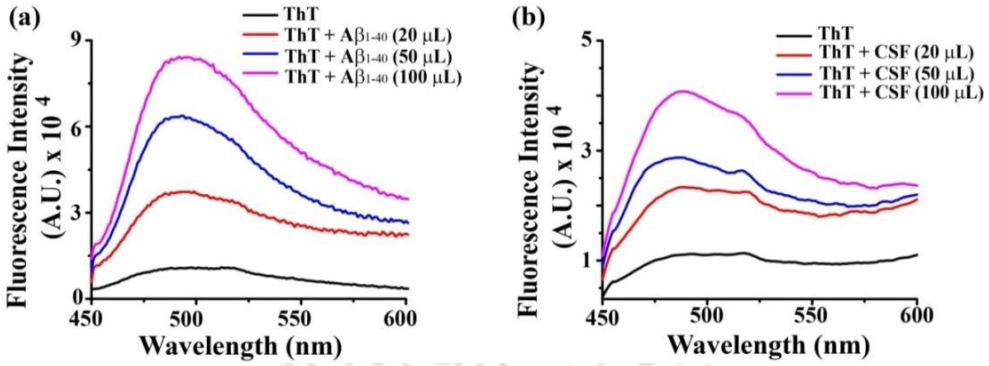

Figure 5.22: Fluorescence spectra of ThT in absence (black) and presence of 20 µL (red), 50 µL (blue) and 100 µL (magenta) of $A\beta_{1\text{-}40}$ (a) and human CSF (b). The stock concentration of ThT was 50 µM in PBS (50 mM) pH 7.4.

5.9.2: Monitoring the disruption of Aβ aggregates present in the CSF sample by ThT assay:

It was confirmed from the above study that the concentration of Aβ in the human CSF sample was ~20 µM. Then, 10 fold molar excess of peptide **5A** and **2C** were added separately with the CSF samples and incubated them at 37 °C for 10 days. The kinetics of disaggregation of amyloid aggregates was monitored by ThT assay (Figure 5.23).

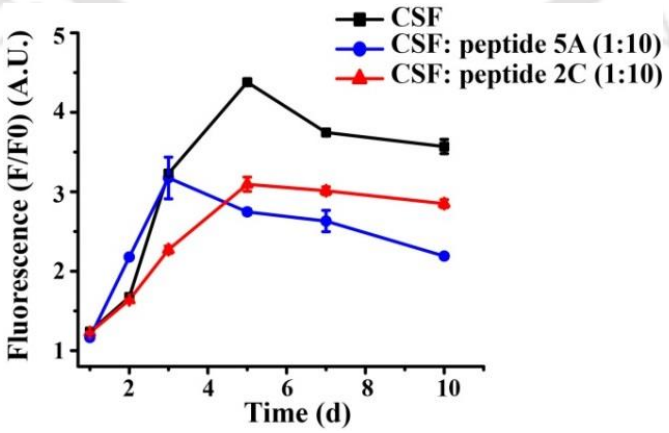

Figure 5.23: Time dependent ThT assay for the disruption of the amyloid present in human cerebrospinal fluid (CSF) in absence (black) and presence of peptide **5A** (blue) & **2C** (red) respectively.

In a ThT assay, we observed that fluorescence intensity of CSF was suppressed excessively in presence of peptide **5A** (blue, Figure 5.23) while the CSF alone (black, Figure 5.23) showed increased fluorescence. There was also a suppression of fluorescence observed in case of CSF sample with peptide **2C** (red, Figure 5.23).

5.9.3: Monitoring the disruption of Aβ aggregates present in the CSF sample by TEM and Congo red birefringence study:

After 10 days incubation of the CSF sample in presence of 10 fold molar excess of peptide **5A** and **2C**, when TEM was analyzed we observed clear fibrillar assembly in case of untreated CSF sample (Figure 5.24a). But we did not observe such fibrillar assembly when peptide **5A** was present in 10 fold molar excess with the CSF (Figure 5.24b). Although some aggregates were noticed in the CSF sample when incubated with peptide **2C** (Figure 5.24c).

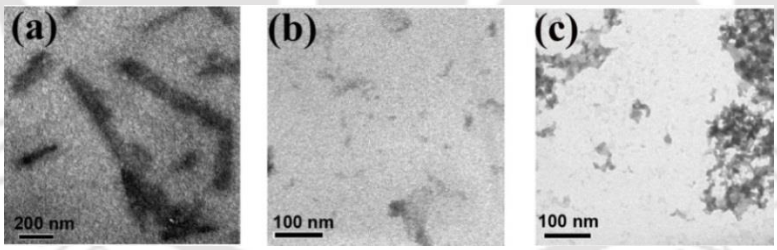

Figure 5.24: TEM images human CSF in absence (a) and presence of 10 fold molar excess of peptide **5A** (b) & peptide **2C** (c). Images were taken after 10 days incubation at 37 °C.

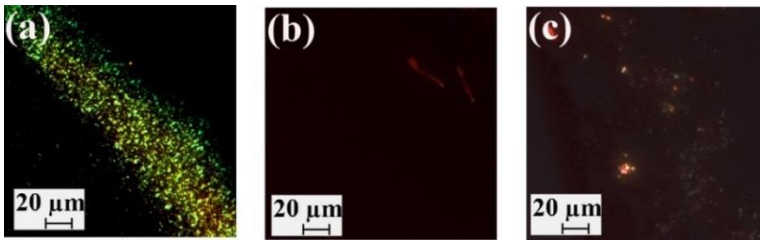

Figure 5.25: Congo red birefringence images human CSF in absence (a) and presence of 10 fold molar excess of peptide **5A** (b) & peptide **2C** (c). Images were taken after 10 days incubation at 37 °C.

The CSF sample alone exhibited a clear appearance of green gold birefringence (Figure 5.25a). But, no such birefringence was observed in presence of 10 fold molar excess of peptide **5A** (Figure 5.25b), indicating the absence of amyloid. Some shiny birefringence was observed in the CSF sample treated with peptide **2C** (Figure 5.25c).

5.10. Conclusion:

Based on our experimental results we can conclude that the PDp **5A** inhibits the aggregation of $A\beta_{1-40}$ peptide and also disrupts the fibrillar aggregates of $A\beta_{1-40}$ into non-toxic species *in vitro* in a better manner than the peptide **2C**. The results also justified that the *in situ* generated breaker element containing pro-drug peptide was superior over the pre-installed breaker element containing β-sheet breaker peptide. The PDp also disrupted the Aβ aggregates present in human cerebrospinal fluid sample. Therefore, we can conclude that the *in situ* generated breaker element containing pro-drug peptide can act as a lead molecule which can be used for drug design against Alzheimer's disease. Also, similar idea can be used for drug design against other amyloid associated diseases.

Chapter 6: Disruption of Amyloid-β aggregates into non-toxic species by synthetic zipper peptide

6.1. The synthetic zipper peptide:

In this chapter, we have demonstrated a new strategy for the disruption of $A\beta_{1-40}$ aggregates into non-toxic species *in vitro* at pH 7.4 and 37 °C. For the drug design against Alzheimer's disease (AD), the recognition factor is very important along with a strategy for reducing *H*-bonding between the Aβ molecules.[50,59,65] Keeping those points in mind, we have designed a peptide based molecule in a way that it will recognize and bind with the aggregated Aβ, wrap it, and inhibit further aggregation by *H*-bond elimination due to presence of *N*-methylation[71,135,136] on alternate amino acids of the peptide sequence, named it as synthetic zipper peptide (Figure 6.1). We have designed the zipper peptide inspired by the β-hairpin structure of Aβ.[137,138] But unlike β-hairpin structure, the zipper peptide contains two parallel β-strands (zipper strands) along with a flexible polyethylene glycol (PEG) unit. The zipper peptide was made up of three different units, a recognition motif containing two parallel β-strands (for proper recognition with Aβ peptide),[50] *H*-bond eliminator using *N*-methylation[135] (breaker element) and a flexible unit comprised of a hydrocarbon chain and PEG.[139,140] This

flexible unit (PEG) is expected to generate a turn in the zipper peptide, enhance stability, solubility, and reduce toxicity of the zipper peptide. We have incorporated the PEG unit in between two zipper strands. We anticipated that the zipper peptide will generate β-sheet conformation in aqueous solution of pH 7.4, but it will not aggregate to form fibrillar assembly due to presence of *N*-methylation on alternate amino acids. We also anticipated, when the zipper peptide would be added to the fibrillar assembly of Aβ, it would easily recognize the Aβ sequence and the two β-strands of the zipper peptide would form a packed zipper like structure and the presence of *N*-methylation would disaggregate the amyloid through *H*-bond elimination.

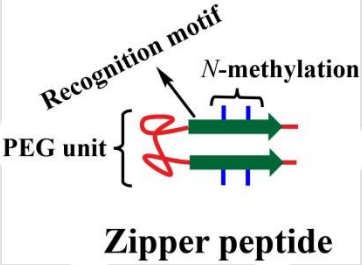

Figure 6.1: The general structure of the zipper peptide.

6.2. Proposed hypothesis:

Since, AD is associated mainly with the aggregation of Aβ peptide which is rich in β-sheet structure; a molecule which easily binds with the Aβ aggregates and disrupts its aggregation will be very interesting for drug design against AD. Therefore, in this chapter we wanted to show a peptide based molecule, namely, the zipper peptide and anticipated that the zipper peptide will bind strongly by recognizing the target (Aβ) and effectively disrupt the preformed fibrillar aggregates of $A\beta_{1\text{-}40}$ at pH 7.4 and 37 °C *in vitro* (Figure 6.2).

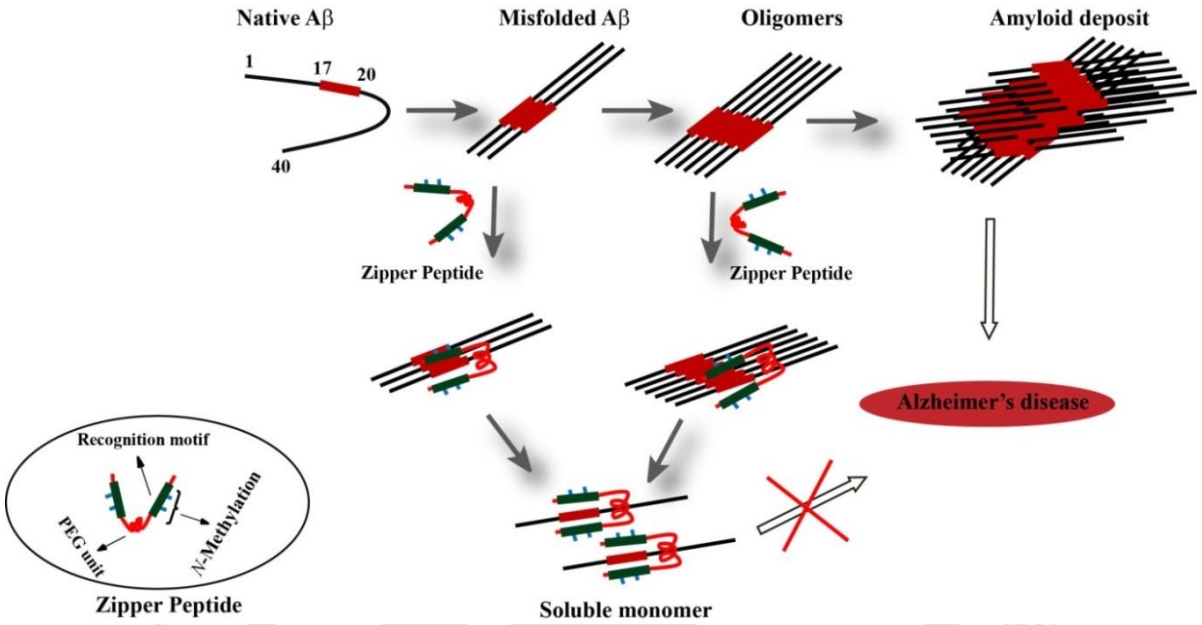

Figure 6.2: Hypothesis for the disruption of Aβ aggregates by a synthetic zipper peptide.

6.3. Design of peptides:

To test our hypothesis (Figure 6.2) for the disruption of Aβ aggregates into non-toxic monomeric species, we have designed a synthetic zipper peptide **6A** (Table 6.1). The design of the zipper peptide was inspired by the action of the epitope binding part of an antibody. The zipper peptide **6A** was designed in a way that it contains two zipper strands with a sequence homology with $A\beta_{17\text{-}21}$ (-L-V-F-F-A-) for proper recognition, *N*-methylation on alternate amino acids in the zipper strands and a PEG unit for flexibility and turn generation in the zipper peptide. We also designed a control peptide **6B** which contains one of the single strands of the zipper peptide along with *N*-methylation on alternate amino acids, for comparing the efficacy with the zipper peptide.

Peptide No.	Peptide Sequence (X= dansyl attached diamino propaonic acid *i.e.*, 2-amino-3-(5-(dimethylamino)naphthalene-2-sulfonamido)propanoic acid)	Function
6A	H_2N-A**(*N*-Me)**FF**(*N*-Me)**VLG-Succinyl-PEG_3-Adipoyl-G**(*N*-Me)**LV**(*N*-Me)**FFA-NH_2	Inhibitor
6B	Ac-G**(*N*-Me)**LV**(*N*-Me)**FFA-NH_2	Control inhibitor
6C	H_2N-A**(*N*-Me)**FF**(*N*-Me)**VLG-Succinyl-PEG_3-Adipoyl-G**(*N*-Me)**LV**(*N*-Me)**FFA**W**-NH_2	Inhibitor/ FRET donor
6D	H_2N-**X**A**(*N*-Me)**FF**(*N*-Me)**VLG-Succinyl-PEG_3-Adipoyl-G**(*N*-Me)**LV**(*N*-Me)**FFA-NH_2	Inhibitor/ FRET acceptor
6E	H_2N-**X**A**(*N*-Me)**FF**(*N*-Me)**VLG-Succinyl-PEG_3-Adipoyl-G**(*N*-Me)**LV**(*N*-Me)**FFA**W**-NH_2	Inhibitor/ FRET donor-acceptor

Table 6.1: Sequences of designed peptides for the present investigation

To prove the structural orientation and the mechanistic investigation of the zipper peptide for the inhibition of aggregation, we have designed three more peptides which were used for Förster resonance energy transfer (FRET) study.[140-144] We have designed peptide **6C** where a tryptophan (FRET donor) was attached at one terminal of peptide **6A** and the other terminal was remaining free from fluorophore. We also designed peptide **6D** where a dansyl group (FRET acceptor) was attached at one terminal of the peptide **6A** and the other terminal was remaining free from fluorophore. Finally, we have designed a peptide **6E**, which contains both the donor and acceptor at the two different terminals of the peptide **6A**. The $A\beta_{1-40}$ was used as the targeted amyloidogenic peptide. The peptides that have been used in this chapter are shown in Table 6.1.

6.4. Synthesis and characterization of the designed peptides:

We have synthesized all the designed peptides by solid phase peptide synthesis (SPPS) technique using standard Fmoc/^{t}Bu protection strategy on Rink amide MBHA resin.[108] To synthesize the zipper peptide, at first, one strand (HO-Adi-Gly-(*N*-Me)Leu-Val-(*N*-Me)Phe-Phe-Ala-NH_2) was prepared separately, cleaved from the resin and then attached to the other resin bound strand (H_2N-PEG_3-Suc-Gly-Leu-(*N*-Me)Val-Phe-(*N*-Me)Phe-Ala-Resin) using coupling reagent and DIPEA (detail synthetic method described in SPPS section, Chapter 7). Both strands were retro-inverso peptide sequence to one another which were linked together by a di-caboxylic acid (HO-Succinyl-PEG_3-Adipoyl-OH). The synthetic scheme of the zipper peptide **6A** is shown in scheme 6.1.

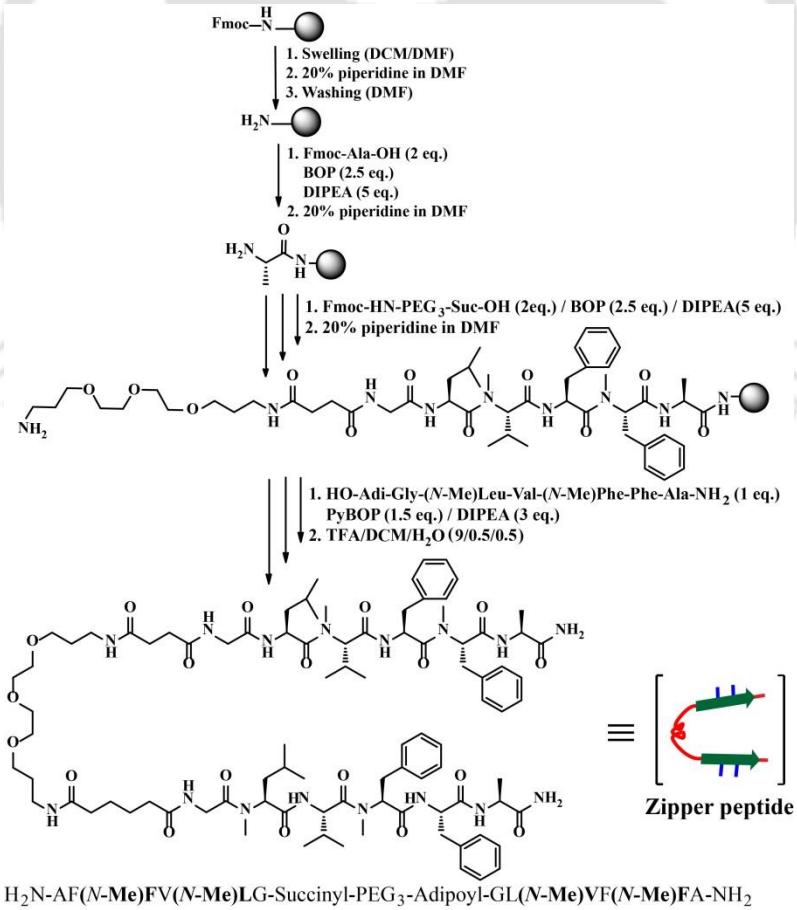

Scheme 6.1: The synthetic scheme of peptide **6A** using Fmoc/^{t}Bu protection based SPPS.

The designed peptides were purified using semi preparative HPLC and purity was confirmed by HPLC and mass spectrometry. The characterization data for the designed peptides are also depicted below.

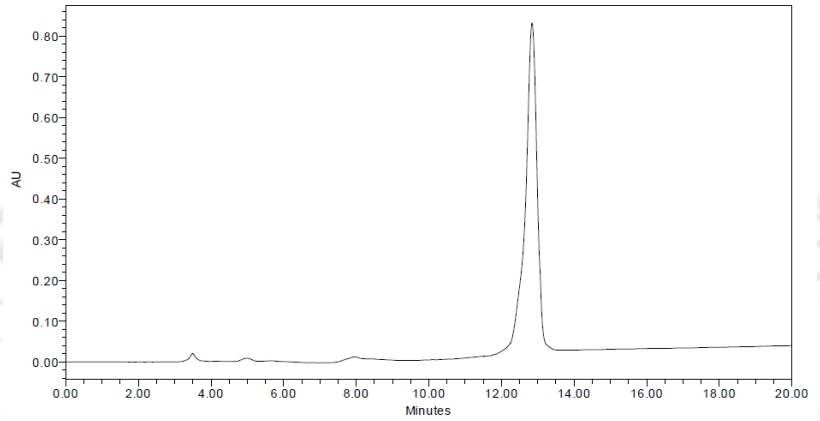

Figure 6.3: HPLC profile of the purified peptide **6A**.

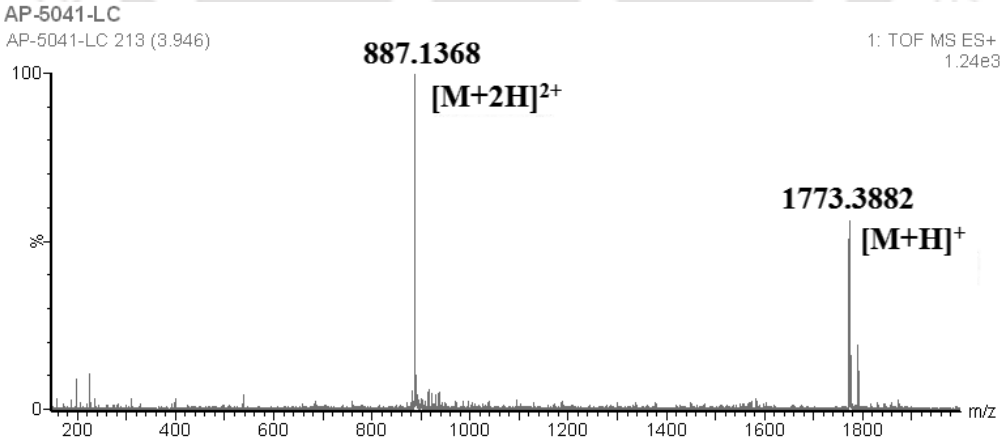

Figure 6.4: Mass spectrum of peptide **6A**. Calculated mass for $C_{92}H_{139}N_{16}O_{19}$ is 1773.04 $[M+H]^+$, observed 1773.38 $[M+H]^+$ and 887.1368 $[M+2H]^{2+}$.

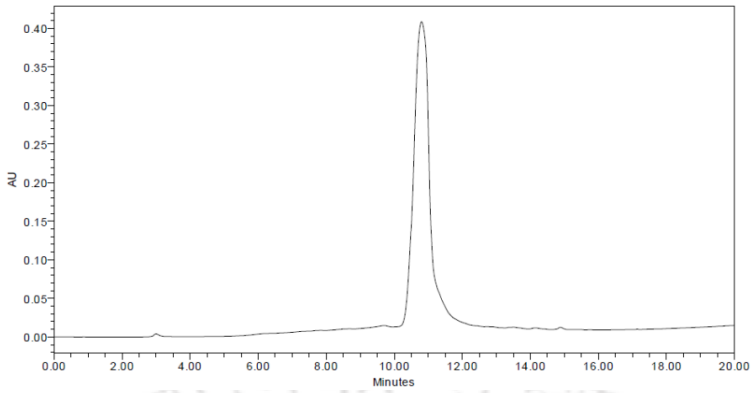

Figure 6.5: HPLC profile of the purified peptide **6B**.

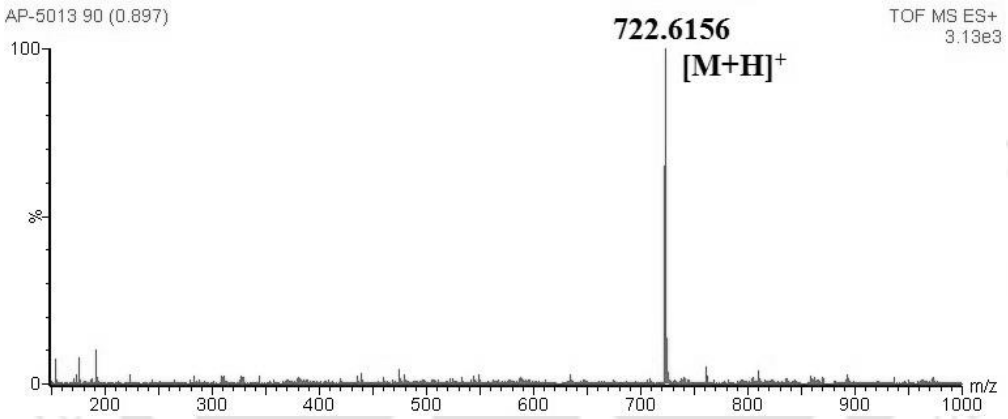

Figure 6.6: Mass spectrum of peptide **6B**. Calculated mass for $C_{38}H_{56}N_7O_7$ is 722.42 $[M+H]^+$, observed 722.61$[M+H]^+$.

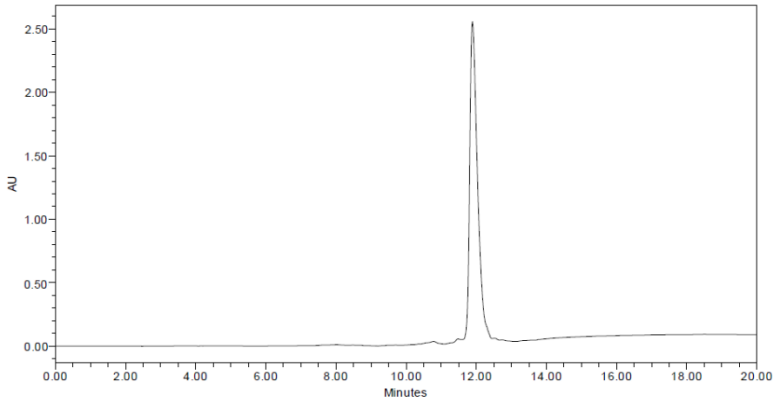

Figure 6.7: HPLC profile of the purified peptide **6C.**

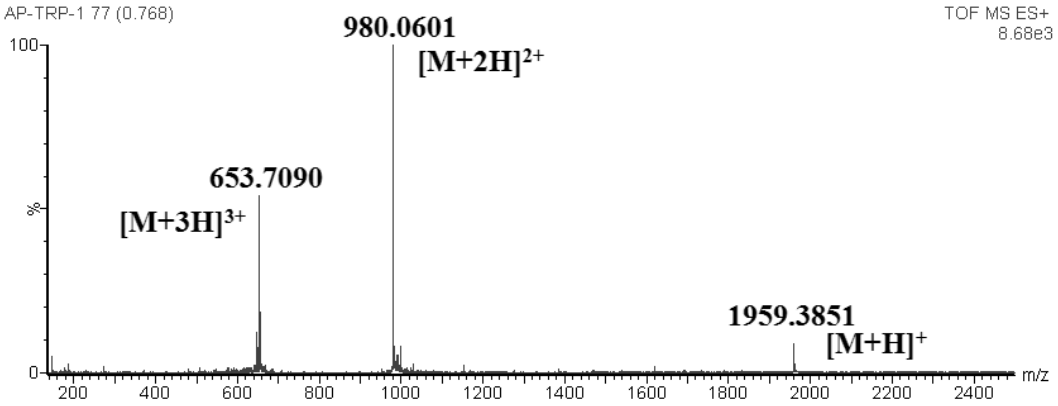

Figure 6.8: Mass spectrum of peptide **6C**. Calculated mass for $C_{103}H_{149}N_{18}O_{20}$ is 1959.12 $[M+H]^+$, observed 1259.38 $[M+H]^+$, 980.06 $[M+ 2H]^{2+}$ and 653.71 $[M+3H]^{3+}$.

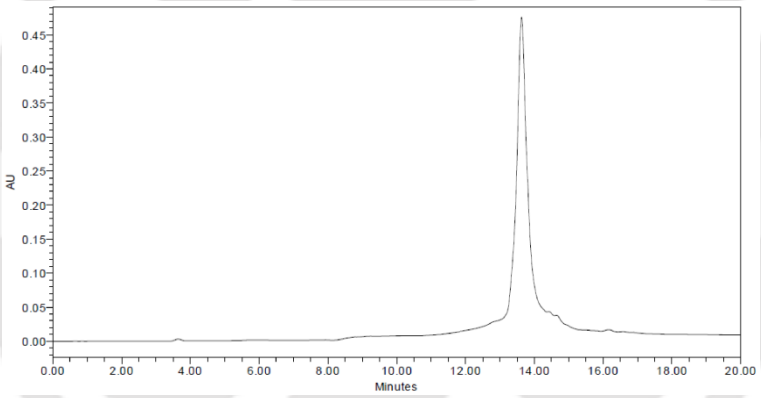

Figure 6.9: HPLC profile of the purified peptide **6D**.

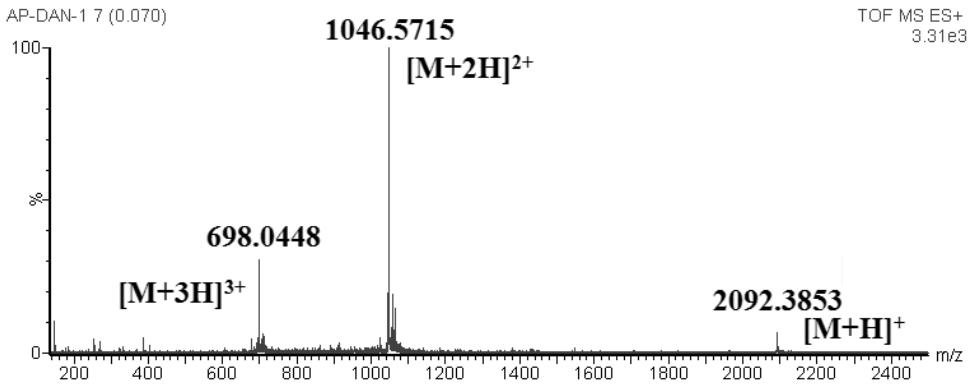

Figure 6.10: Mass spectrum of peptide **6D**. Calculated mass for $C_{107}H_{156}N_{19}O_{22}S$ is 2092.14 $[M+H]^+$, observed 2092.38 $[M+H]^+$, 1046.57 $[M+2H]^{2+}$ and 698.04$[M+3H]^{3+}$.

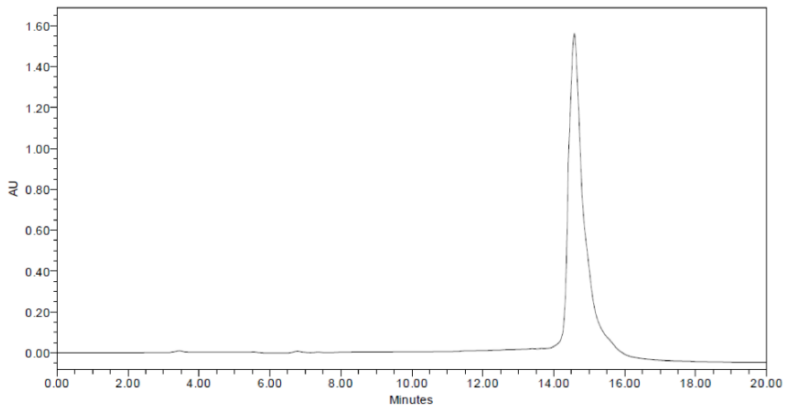

Figure 6.11: HPLC profile of the purified peptide **6E**.

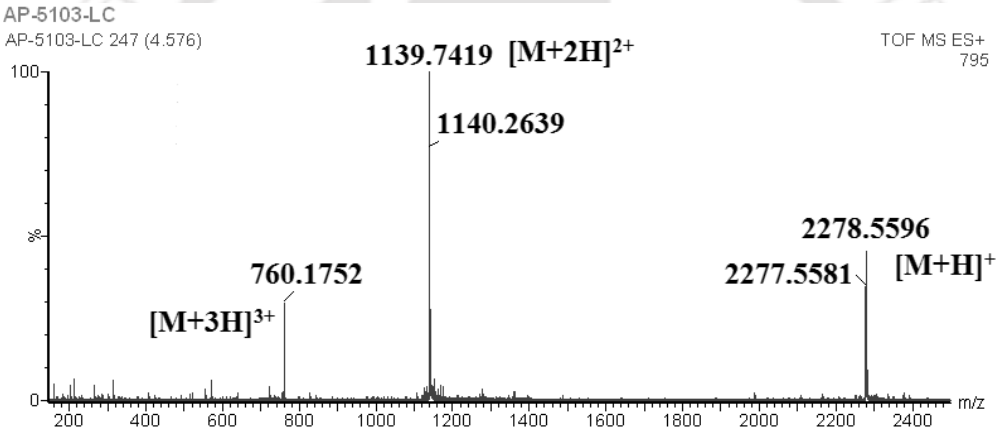

Figure 6.12: Mass spectrum of peptide **6E**. Calculated mass for $C_{118}H_{166}N_{21}O_{23}S$ is 2278.22 $[M+H]^+$, observed 2278.55 $[M+H]^+$, 1139.74 $[M+2H]^{2+}$ and 760.17 $[M+3H]^{3+}$.

6.5. Non-amyloidogenicity of the zipper peptide 6A:

The *N*-methylated amino acids containing peptides were non-amyloidogenic in nature at physiological condition (pH 7.4 and 37 °C) and were used as β-sheet breaker peptides before.[135,136] Therefore, the zipper peptide **6A** was expected to be non-amyloidogenic. To confirm the anticipation, we checked the non-amyloidogenicity of peptide **6A** using various biophysical tools.

6.5.1. Conformational characterization of peptide 6A by CD and FTIR studies:

To check the conformational state of the peptide **6A**, we dissolved it in PBS (50 mM, pH 7.4) to make the concentration of the stock solution (~100 μM) and incubated the solution over water bath at 37 °C for 5 days. Similarly, we prepared a stock solution (~100 μM) for the control peptide **6B** and incubated in a similar fashion for 5 days. After 5 days the conformational studies were perform using CD and FTIR (Figure 6.13). In CD spectrum of peptide **6A** (black, Figure 6.13a), we observed a positive band centered at ~198 nm and a negative band centered at ~226 nm, indicated the presence of β-sheet rich conformation of the peptide **6A** (percentage of helix content 25.1, β content 54.9, turn content 0 and random content 20; deconvoluted from the CD instrument). Similarly, in FTIR spectrum we observed a strong amide I band at 1638 cm^{-1} (black, Figure 6.13b) clearly indicated again β-sheet rich conformations of the peptide **6A**. We also observed a β-sheet conformation for the peptide **6B** as evident from both in CD (red, Figure 6.13a) and FTIR (red, Figure 6.13b) spectra.

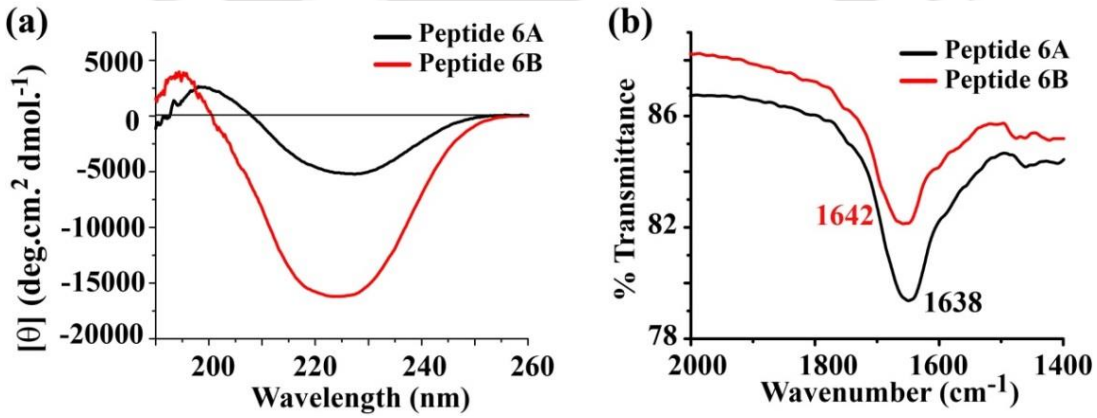

Figure 6.13: (a) CD and (b) FTIR spectra of peptide **6A** (black) and **6B** (red). Spectra were taken after 5 days of incubation of the peptide in PBS pH 7.4 (50 mM) at 37 °C.

6.5.2. Amyloidogenic characterization of peptide 6A by TEM and Congo red birefringence studies:

The amyloidogenicity of the zipper peptide **6A** and the control peptide **6B** were characterized by TEM and Congo red stained birefringence studies. We did not observe any fibrillar assembly for the peptide **6A** in TEM (Figure 6.14a). We also did not notice any green gold birefringence of the peptide **6A** when stained with Congo red dye and viewed under cross polarized light (Figure 6.14b). Therefore, it was confirmed that the zipper peptide **6A** was non-amyloidogenic in nature at pH 7.4 and 37 °C, although it forms soluble beta sheet as evidenced by the results from the CD studies. Similarly, the control peptide **6B** also was found to be non amyloidogenic as evident from TEM (Figure 6.14c) and Congo red birefringence (Figure 6.14d) images.

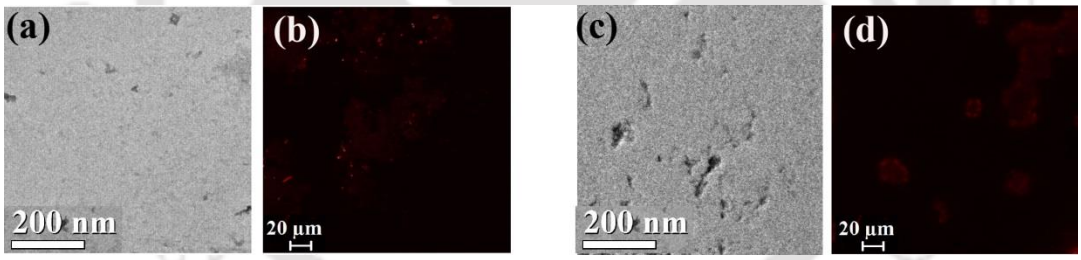

Figure 6.14: (a) TEM & (b) Congo red birefringence images of peptide **6A**. (c) TEM & (d) Congo red birefringence images of peptide **6A**. Images were taken after 5 days of incubation of the peptide in PBS pH 7.4 (50 mM) at 37 °C.

The β-sheet rich conformation of peptide **6A** is probably due to the formation of monomeric β-sheet between the two β-strands of the zipper peptide, which remained soluble but did not aggregate to form amyloid due to presence of *N*-methylation on alternate amino acids in the sequence.

6.6. Inhibition of amyloid formation of $A\beta_{1-40}$ by the zipper peptide 6A:

The zipper peptide **6A** was found to be a non-amyloidogenic peptide at physiological condition (pH 7.4 and 37 °C). Next, we proceeded further to our target, the inhibition of aggregation of $A\beta_{1-40}$ by the zipper peptide **6A**. To investigate the inhibitory efficacy of the zipper peptide **6A** on $A\beta_{1-40}$ fibrillization, we performed various qualitative and quantitative analyses in presence of varied amount (0.5-, 1-, 2- and 5- fold molar excess) of the zipper peptide **6A** and compared its efficacy with the control peptide **6B** in a similar fashion as described in chapter 4, section 4.5. Varied amount (0.5-, 1-, 2- and 5- fold molar excess) of the peptide **6A** and **6B** were co-incubated with $A\beta_{1-40}$ (50 μM) in PBS pH 7.4 at 37 °C for 7 days and the kinetics of the amyloid formation was monitored using different biophysical tools.

1.5 mg of commercially available $A\beta_{1-40}$ peptide was taken and disaggregated it by TFA and HFIP treatment following the same procedure as discussed earlier (Chapter 4, section 4.5.1).[128] The disaggregated material dissolved in 1.8 ml of PBS (50 mM, pH 7.4) by sonication and vortex to obtain transparent solution and the whole solution was divided into 9 equal portions followed by addition of 600 μL of PBS to each portion to obtain a final $A\beta_{1-40}$ concentration of 50 μM. For the inhibition study, 0.5-, 1-, 2- and 5- fold molar excess of the inhibitors (**6A** and **6B**) were mixed with each portion (800 μL) of $A\beta_{1-40}$ solution in presence of 3% DMSO and kept for incubation over water bath for 7 days at 37 °C. To obtain precise results two more replicate solutions of each portion were prepared (total number of samples for this experiment was 27) and fibrillzation was monitored by various biophysical tools.

6.6.1. Monitoring conformational transition by CD:

After 7 days of incubation at pH 7.4 and 37 °C, when CD spectra were taken, we observed $A\beta_{1-40}$ peptide alone exhibited a positive band centered at ~196 nm and a negative band centered at ~217 nm, indicating a β-sheet rich conformation of $A\beta_{1-40}$ (black, Figure 6.15a,b). But in presence of different doses of peptide **6A** (0.5-, 1-, 2- and 5-fold molar excess), the β-sheet content was increased with increment of the dose of the zipper peptide **6A**, which was probably due to the enhanced soluble β-sheet content of either the zipper peptide or the $A\beta_{1-40}$ wrapped by the zipper peptide (Figure 6.15a). The $A\beta_{1-40}$ peptide wrapped by zipper peptide remained in soluble monomeric form which did not aggregate further due to the presence of *N*-methylation, in the zipper peptide, that reduced the *H*-bonding between the $A\beta_{1-40}$ peptides.

Similarly, in presence of different doses of **6B** (0.5-, 1-, 2- and 5-fold molar excess), the β-sheet content of $A\beta_{1-40}$ also increased slowly as the doses increased (Figure 6.15b).

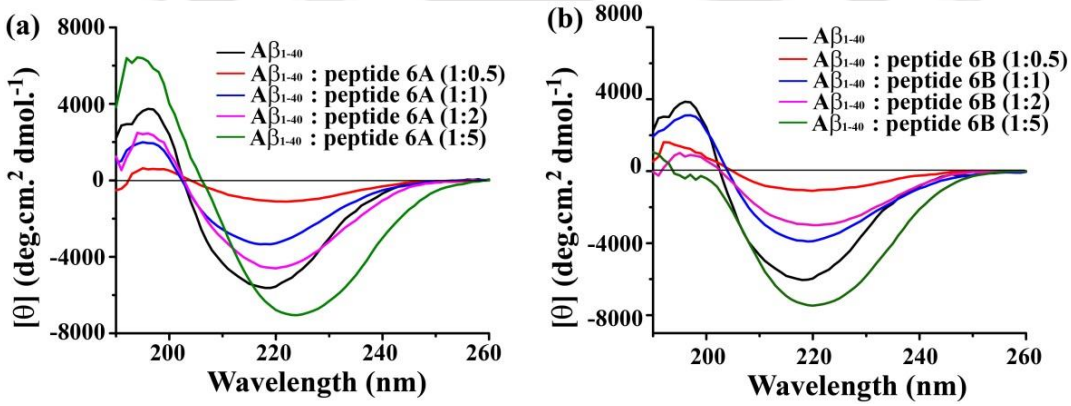

Figure 6.15: CD spectra of $A\beta_{1-40}$ in absence (black) and presence of 0.5-fold (red), 1-fold (blue), 2-fold (magenta) and 5-fold (olive) molar excess of (a) peptide **6A** and (b) peptide **6B**. Spectra were recorded after 7 days incubation of the peptide solutions in PBS in presence of (3% DMSO) pH 7.4 at 37 °C.

6.6.2. Monitoring conformational transition by FTIR:

The conformational transitions were also monitored by FTIR analysis (Figure 6.16). In FTIR spectra, we observed an intense band at 1631 cm^{-1} when $A\beta_{1-40}$ was alone in the solution, confirmed the characteristic β-sheet rich conformation (black, Figure 6.16a,b). However, in presence of different doses (0.5-, 1-, 2- and 5-fold molar excess) of peptide **6A** (Figure 6.16a) we observed again β-sheet rich conformation along with some other mixture of conformations. These β-sheet rich conformations were probably due to the β-strands of $A\beta_{1-40}$ wrapped by the zipper peptide and the added zipper peptides which remained as intramolecular β-sheet form. Again, in presence of different doses of (0.5-, 1-, 2- and 5-fold molar excess) of peptide **6B**, we observed β-sheet conformation of $A\beta_{1-40}$ reduced as the doses increased as evident in the Figure 6.16b.

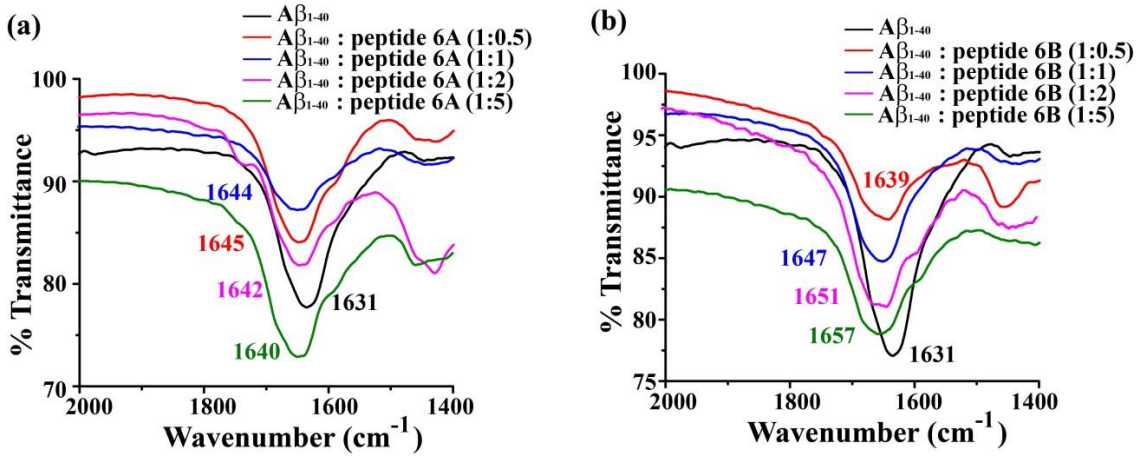

Figure 6.16: FTIR spectra of $A\beta_{1-40}$ in absence (black) and presence of 0.5-fold (red), 1-fold (blue), 2-fold (magenta) and 5-fold (olive) molar excess of (a) peptide **6A** and (b) peptide **6B**. Spectra were recorded after 7 days incubation of the peptide solutions in PBS of pH 7.4 at 37 °C (in presence of 3% DMSO).

6.6.3. Monitoring the kinetics of amyloid formation by Thioflavin T fluorescence assay:

The amyloid formation of $A\beta_{1-40}$ and its inhibition was monitored by Thioflavin T (ThT) fluorescence assay. For ThT assay, at different time intervals, 40 μL of peptide samples from the stock were mixed with 200 μL of ThT solution (50 μM), total volume was made up to 400 μL with PBS (50 mM, pH 7.4) and fluorescence was measured (λ_{ex} = 440 nm, λ_{em} = 485 nm and band width 3 nm). Normalized spectra were plotted as the average of the three replicate experiments. From the ThT assay (Figure 6.17), we observed an increment of fluorescence intensity with time, when $A\beta_{1-40}$ peptide was alone in the solution. But, in presence of different doses (0.5-, 1-, 2- and 5-fold molar excess) of zipper peptide **6A**, the fluorescence intensity decreased significantly as the doses increased, indicating the reduction of amount of amyloid in the sample, which indicated the inhibition of aggregation of $A\beta_{1-40}$ by the zipper peptide **6A** (Figure 6.17a). We observed similar results in presence of different doses (0.5-, 1-, 2- and 5-fold molar excess) of peptide **6B** (Figure 6.17b), but less significant inhibition than the effect of peptide **6A** (Figure 6.17c).

The amount of amyloid fibril was inhibited significantly up to 60-61% (blue, Figure 6.17c) when the zipper peptide **6A** was co-incubated with $A\beta_{1-40}$ in just 2-fold molar excess until seven days and the inhibition was increased up to 64-65% in presence of 5-fold molar excess of zipper peptide **6A**, whereas in presence of 5-fold molar excess of the control peptide **6B**, the amyloid fibril was suppressed by only 44-45 % (red, Figure 6.17c) at same condition. These results clearly indicated that 2-fold molar excess of the zipper peptide **6A** was much effective for the inhibition of amyloid formation of $A\beta_{1-40}$ than the 5-fold molar excess of the control peptide **6B**.

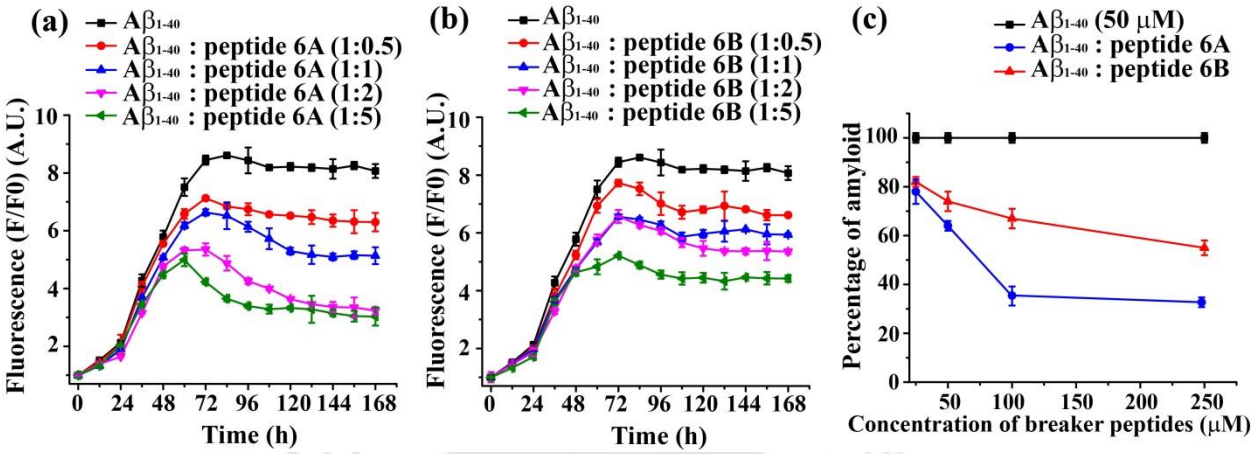

Figure 6.17: Time dependent ThT assay of $A\beta_{1-40}$ in absence (black) and presence of 0.5-fold (red), 1-fold (blue), 2-fold (magenta) and 5-fold (olive) molar excess of peptide (a) **6A** and (b) **6B**. (c) Dose dependent ThT assay for the inhibition of amyloid formation of $A\beta_{1-40}$ in absence (black) and presence of peptide **6A** (blue) and **6B** (red). Peptides were incubated in PBS of pH 7.4 at 37 °C (in presence of 3% DMSO).

6.6.4. Monitoring amyloidogenicity by TEM:

The presence of fiber under electron microscope is a characteristic property of amyloid.[23] The $A\beta_{1-40}$ alone showed clear fibrillar aggregates under TEM (Figure 6.18a). In presence of 0.5-fold molar excess of the zipper peptide **6A**, some fibers were noticed, indicating 0.5-fold molar excess of peptide **6A** was not sufficient to inhibit the aggregation of $A\beta_{1-40}$ (Figure 6.18b). When, the doses of peptide **6A** were increase to 1-fold (Figure 6.18c), 2-fold (Figure 6.18d), and 5-fold (Figure 6.18e) molar excess, no such fiber was observed, indicating absence of amyloid. However, we observed clear appearance of fibrils in presence of 0.5-fold (Figure 6.19a), 1-fold (Figure 6.19b) and 2-fold (Figure 6.19c) molar excess of the control peptide **6B**, but when the doses increased to 5-fold molar excess such fibrils were not observed (Figure 6.19d).

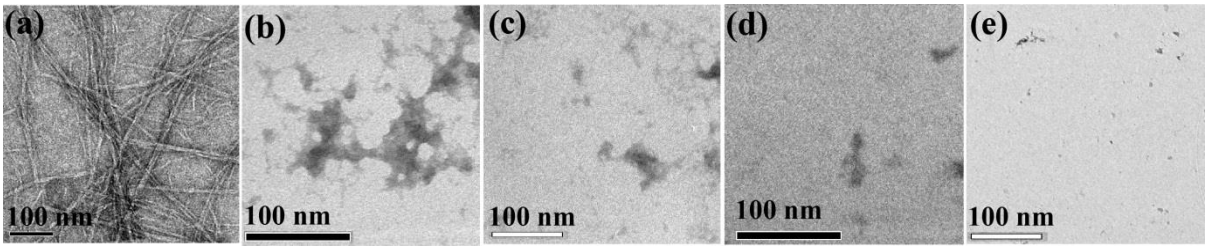

Figure 6.18: TEM images of (a) $A\beta_{1-40}$ alone and in presence of (b) 0.5-fold, (c) 1-fold, (d) 2-fold or (e) 5-fold molar excess of peptide **6A**. Images were taken after 7 days incubation of the peptide solutions in PBS of pH 7.4 at 37 °C (in presence of 3% DMSO).

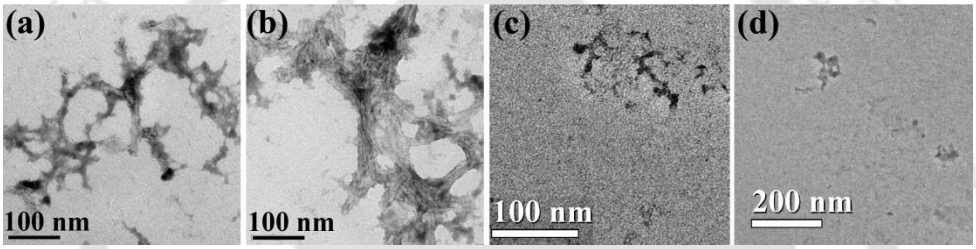

Figure 6.19: TEM images of $A\beta_{1-40}$ in presence of (a) 0.5-fold, (b) 1-fold, (c) 2-fold or (d) 5-fold molar excess of peptide **6B**. Images were taken after 7 days incubation of the peptide solutions in PBS of pH 7.4 at 37 °C (in presence of 3% DMSO).

These results again indicated that the 0.5-fold, 1-fold and 2-fold molar excess of the peptide **6B** were not sufficient to inhibit the aggregation of $A\beta_{1-40}$ *in vitro*, while 1-fold or more excess of zipper peptide **6A** was sufficient to inhibit the aggregation of $A\beta_{1-40}$ *in vitro*.

6.6.5. Monitoring amyloidogenicity by Congo red birefringence:

The appearance of green gold birefringence of a peptide sample under crossed polarized light after staining with Congo red dye indicated the presence of amyloid in the sample.[23] The $A\beta_{1-40}$ peptide alone showed clear green gold birefringence under crossed polarized light (Figure

6.20a). In presence of 0.5-fold (Figure 6.20b) molar excess of peptide **6A**, some green gold birefringence was observed while 1-fold or more molar excess of peptide **6A** (Figure 6.20c-e) no birefringence were observed. Again, in presence of 0.5-fold (Figure 6.21a) and 1-fold (Figure 6.21b) molar excess of peptide **6B** some green gold birefringence were observed while in presence of 2-fold or more molar excess of 6**B** (Figure 6.22), such green gold birefringence were not observed. These results again supported that 1-fold or more molar excess of the zipper peptide was sufficient for the significant inhibition of aggregation of $A\beta_{1\text{-}40}$.

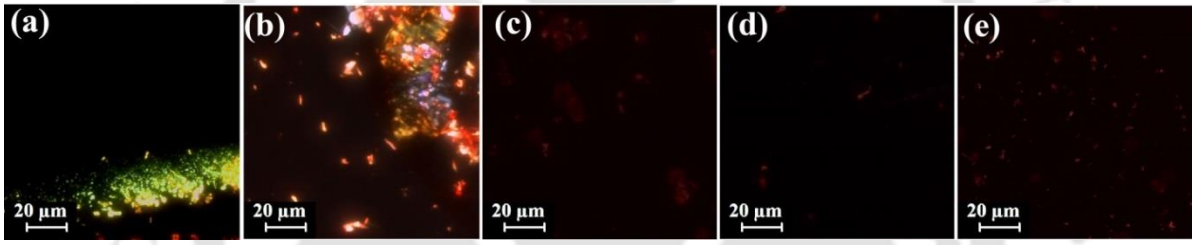

Figure 6.20: Congo red birefringence images of (a) $A\beta_{1\text{-}40}$ alone and in presence of (b) 0.5-fold, (c) 1-fold, (d) 2-fold or (e) 5-fold molar excess of peptide **6A**. Images were taken after 7 days incubation of the peptide solutions in PBS of pH 7.4 at 37 °C (in presence of 3% DMSO).

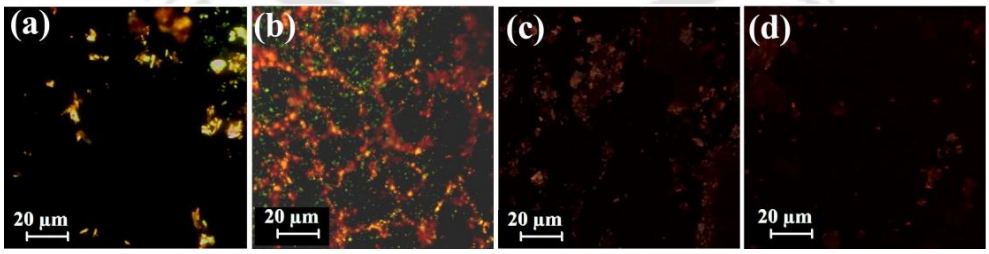

Figure 6.21: Congo red birefringence images of $A\beta_{1\text{-}40}$ in presence of (a) 0.5-fold, (b) 1-fold, (c) 2-fold or (d) 5-fold molar excess of peptide **6B**. Images were taken after 7 days incubation of the peptide solutions in PBS of pH 7.4 at 37 °C (in presence of 3% DMSO).

6.7. Disruption of preformed $A\beta_{1-40}$ aggregates by the zipper peptide 6A:

We already observed in the previous section that the zipper peptide **6A** when was co-incubated with $A\beta_{1-40}$ in a dose dependent manner, it inhibited amyloid formation of $A\beta_{1-40}$ increasingly with the rise of doses. Next, we wanted to check the efficacy of the zipper peptide **6A** for the disruption of preformed fibrillar aggregates of $A\beta_{1-40}$ *in vitro*. From the ThT assay (black, Figure 6.17a), we observed that the growth phase for fibril formation of $A\beta_{1-40}$ at mentioned condition was in the range of 24 h to 60 h. Therefore, we designed an experiment where the zipper peptide **6A** was added into the preformed fibrillar assembly at the time range of fibrillar growth phase. Similar to Chapter 4, Section 4.6; we designed an experiment, where $A\beta_{1-40}$ (50μM) was incubated alone in PBS pH 7.4 at 37 °C for 60 h and then different doses (0.5-fold, 1-fold, 2-fold and 5-fold) of peptide **6A** and **6B** were separately added (in presence of 3% DMSO) to $A\beta_{1-40}$ peptide (60 h old) solution and incubated over water bath at 37 °C till 10 days (240 h = 60 h + 180 h). Then, the amyloid formation of $A\beta_{1-40}$ in absence and presence of peptide **6A** and **6B** were monitored by different biophysical tools.

6.7.1. Monitoring conformational transition by CD:

After 10 days, when CD were analyzed, $A\beta_{1-40}$ peptide alone exhibited a positive band centered at ~195 nm and a negative band centered at ~213 nm, clearly indicating the characteristic bands for β-sheet rich conformation of $A\beta_{1-40}$ (black, Figure 6.22a,b). However, in presence of different doses of peptide **6A** (0.5-, 1-, 2- and 5-fold molar excess), the β-sheet conformations of $A\beta_{1-40}$ did not disappear rather appeared along with some mixture of conformations (Figure 6.22a). The presence of β-sheet probably indicated the presence of

soluble of $A\beta_{1-40}$ wrapped by the zipper peptide. Similarly, in presence of different doses of **6B** (0.5-, 1-, 2- and 5-fold molar excess), the β-sheet of $A\beta_{1-40}$ was observed along with some mixture of conformations (Figure 6.22b).

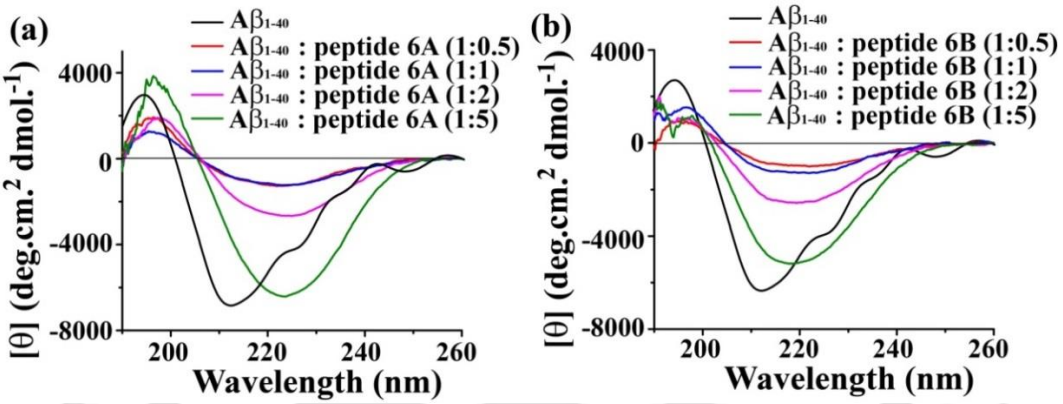

Figure 6.22: CD spectra of $A\beta_{1-40}$ in absence (black) and presence of 0.5-fold (red), 1-fold (blue), 2-fold (magenta) and 5-fold (olive) molar excess of (a) peptide **6A** and (b) peptide **6B**. Spectra were recorded after 10 days of incubation of the peptide solutions in PBS pH 7.4 at 37 °C (in presence of 3% DMSO).

6.7.2. Monitoring conformational transition by FTIR:

The conformational transitions were also monitored by FTIR analysis (Figure 6.23).

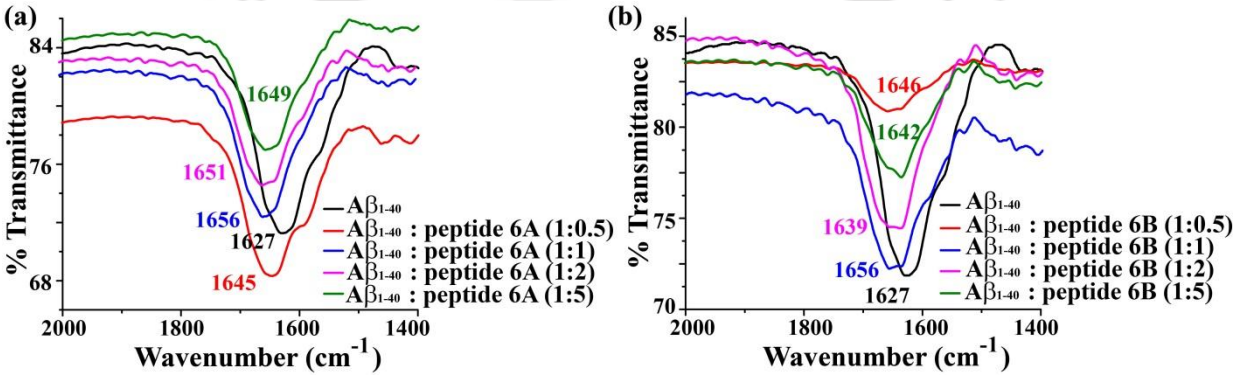

Figure 6.23: FTIR spectra of $A\beta_{1-40}$ in absence (black) and presence of 0.5-fold (red), 1-fold (blue), 2-fold (magenta) and 5-fold (olive) molar excess of (a) peptide **6A** and (b) peptide **6B**. Spectra were recorded after 10 days of incubation of the peptide solutions in PBS pH 7.4 at 37 °C (in presence of 3% DMSO).

We observed a strong band at 1627 cm^{-1} in FTIR spectra when $A\beta_{1-40}$ was alone in the solution, confirmed the characteristic β-sheet rich conformation (black, Figure 6.23a,b). However, in presence of different doses (0.5-, 1-, 2- and 5-fold molar excess) of peptide **6A** (Figure 6.23a) we observed again β-sheet rich conformation along with some other mixture of conformations. These β-sheet rich conformations were probably due to the soluble β-sheet content of $A\beta_{1-40}$ wrapped by the zipper peptide **6A**. On the other hand, in presence of different doses of (0.5-, 1-, 2- and 5-fold molar excess) of peptide **6B,** we observed β-sheet conformation of $A\beta_{1-40}$ was present along with some mixture of conformations (Figure 6.23b).

6.7.3. Monitoring the kinetics of amyloid disruption by Thioflavin T fluorescence assay:

Next, the kinetics of amyloid disruption was monitored by ThT assay. We observed an increment of fluorescence for $A\beta_{1-40}$ peptide when incubated alone (black, Figure 6.24a) but when varied molar excess (0.5-, 1-, 2- and 5-fold molar excess) of peptide **6A** were added to the fibrillar assembly of $A\beta_{1-40}$ after 60 h, the fluorescence intensity decreased significantly with time as the doses increased, indicating the reduction of amount of amyloid in the sample. This result clearly indicated the disruption of preformed fibrillar aggregates of $A\beta_{1-40}$ by the zipper peptide **6A** (Figure 6.24a). We observed similar results in presence of different doses (0.5-, 1-, 2- and 5-fold molar excess) of peptide **6B** (Figure 6.24b), but less significant than the effect of peptide **6A** (Figure 6.24c).

The amount of fibril of $A\beta_{1-40}$ formed at 60 h was found to be reduced by the zipper peptide **6A** (blue, Figure 6.24c) more significantly than peptide **6B** (red, Figure 6.24c). After 10 days, the preformed fibril was reduced up to 56-57% in presence of 5-fold molar excess of the zipper peptide **6A** whereas the peptide **6B** (in 5-fold molar excess) could suppress only 38-39 % of the preformed fibrillar aggregates of $A\beta_{1-40}$.

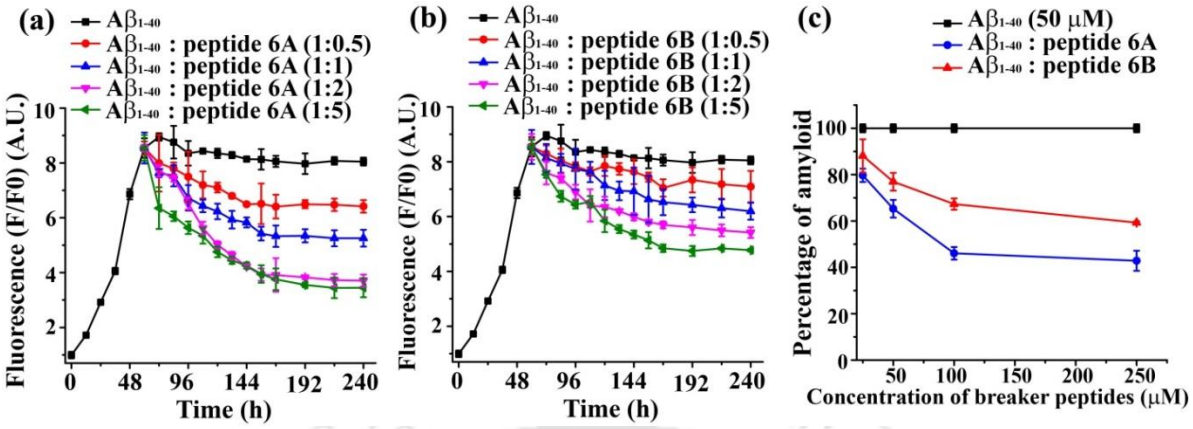

Figure 6.24: Time dependent ThT assay of $A\beta_{1-40}$ in absence (black) and presence of 0.5-fold (red), 1-fold (blue), 2-fold (magenta) and 5-fold (olive) molar excess of peptide (a) **6A** and (b) **6B**. (c) % of amyloid disruption of preformed $A\beta_{1-40}$ aggregates in absence (black) and presence of peptide **6A** (blue) and **6B** (red). Peptides were incubated in PBS of pH 7.4 at 37 °C (in presence of 3% DMSO).

6.7.4. Monitoring of amyloid disruption by TEM:

The formation of amyloid aggregates and its disruption was monitored by TEM (Figure 6.25 and 6.26). After 10 days of incubation in PBS pH 7.4 at 37 °C, we observed that the $A\beta_{1-40}$ alone showed clear fibrillar aggregates (Figure 6.25a) under TEM, whereas in presence of 1-fold (Figure 6.25c), 2-fold (Figure 6.25d) or 5-fold (Figure 6.25e) molar excess of the zipper peptide **6A** no such fibers were observed. But some fibers were noticed when 0.5-fold (Figure 6.25b) molar excess of peptide **6A** was present with $A\beta_{1-40}$, indicating 0.5-fold molar excess of the zipper peptide **6A** was not sufficient to disrupt the preformed aggregates of $A\beta_{1-40}$. When the control breaker peptide **6B** was present in 5-fold (Figure 6.26d) molar excess we did not observe any fibrillar assembly, however in presence of 0.5-fold (Figure 6.26a), 1-fold (Figure 6.26b) and 2-fold (Figure 6.26c) molar excess of the peptide **6B** the fibrillar assembly was clearly visible. These results clearly indicated that to disrupt the preformed fibrillar

aggregates of $A\beta_{1-40}$, 5-fold molar excess of the control peptide **6B** was required, whereas 1-fold to 2-fold molar excess of the zipper peptide **6A** was enough to disrupt the aggregates.

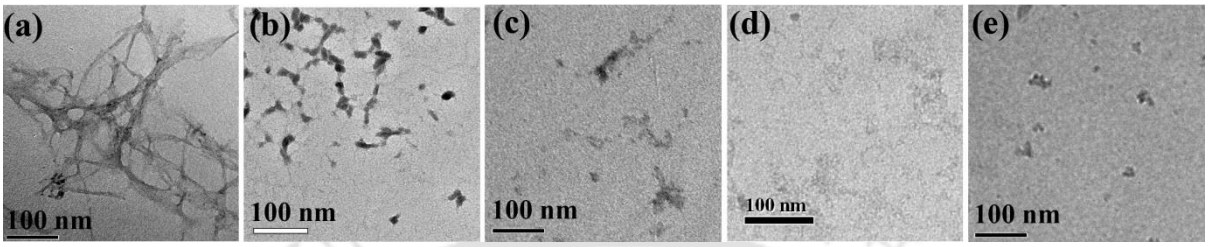

Figure 6.25: TEM images of (a) $A\beta_{1-40}$ alone and in presence of (b) 0.5-fold, (c) 1-fold, (d) 2-fold or (e) 5-fold molar excess of peptide **6A**. Images were taken after 7 days incubation of the peptide solutions in PBS of pH 7.4 at 37 °C (in presence of 3% DMSO).

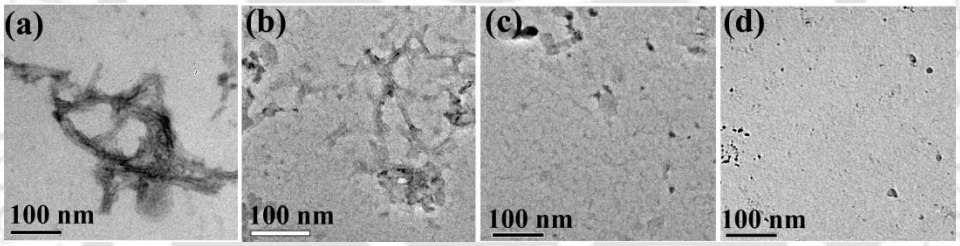

Figure 6.26: TEM images of $A\beta_{1-40}$ alone and in presence of (a) 0.5-fold, (b) 1-fold, (c) 2-fold or (d) 5-fold molar excess of peptide **6B**. Images were taken after 7 days incubation of the peptide solutions in PBS of pH 7.4 at 37 °C (in presence of 3% DMSO).

6.7.5. Monitoring of amyloid disruption by Congo red birefringence:

We observed clear appearance of green gold birefringence under cross polarized light when $A\beta_{1-40}$ was alone (Figure 6.27a) in the solution, but in presence of 1-fold (Figure 6.27c), 2-fold (Figure 6.27d) or 5-fold (Figure 6.27e) molar excess of the zipper peptide **6A** no birefringence was observed. Whereas some birefringence was notice when 0.5-fold molar excess of peptide **6A** was present with $A\beta_{1-40}$, indicating 0.5-fold molar excess of the zipper peptide **6A** was not sufficient to disrupt the preformed aggregates of $A\beta_{1-40}$ (Figure 6.27b).

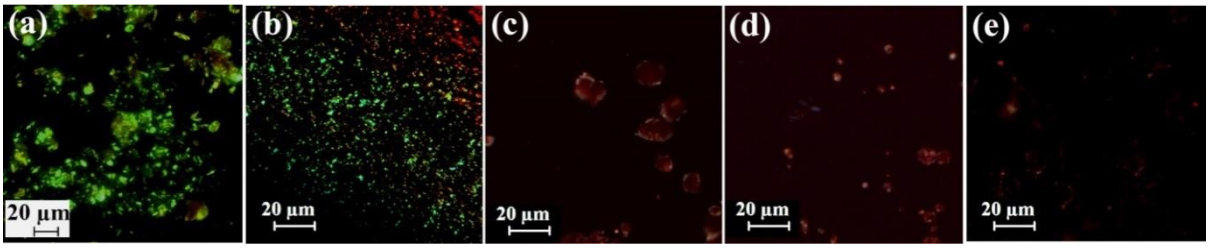

Figure 6.27: Congo red birefringence images of (a) $A\beta_{1-40}$ alone and in presence of (b) 0.5-fold, (c) 1-fold, (d) 2-fold or (e) 5-fold molar excess of peptide **6A**. Images were taken after 7 days incubation of the peptide solutions in PBS of pH 7.4 at 37 °C (in presence of 3% DMSO).

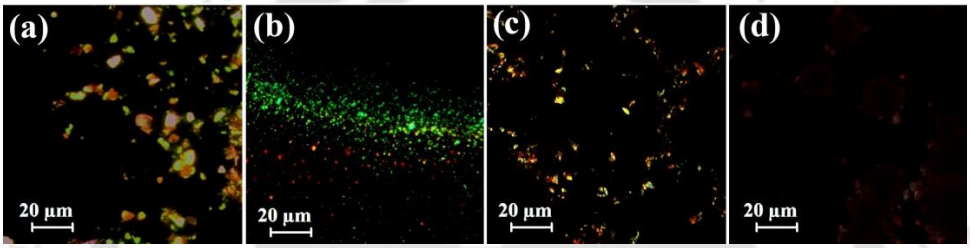

Figure 6.28: Congo red birefringence images of $A\beta_{1-40}$ alone and in presence of (a) 0.5-fold, (b) 1-fold, (c) 2-fold or (d) 5-fold molar excess of peptide **6B**. Images were taken after 7 days incubation of the peptide solutions in PBS of pH 7.4 at 37 °C (in presence of 3% DMSO).

When the control peptide **6B** was present in 5-fold (Figure 6.28d) molar excess, we did not notice any birefringence, however in presence of 0.5-fold (Figure 6.28a), 1-fold (Figure 6.28b) and 2-fold (Figure 6.28c) molar excess of the peptide **6B**, some green gold birefringence were visible. These results clearly indicated that 1-fold to 2-fold molar excess of the zipper peptide **6A** was enough to disrupt the preformed fibrillar aggregates of $A\beta_{1-40}$, whereas 5-fold molar excess of the control peptide **6B** was required to disrupt the same.

6.8. *In vitro* toxicity study using dye loaded Large Unilamellar vesicle (LUV) leakage study

Since, the soluble oligomers of Aβ are known to be more toxic than the mature fibrils for their ability of pore formation to the cell membrane and cause neuronal dysfunction,[55] we next checked the state (oligomers or monomers) of $A\beta_{1-40}$ aggregates disrupted by the zipper peptide **6A** using carboxyfluorescein dye loaded vesicles (LUVs) leakage assay. LUVs leakage study is a proof of presence of toxic oligomeric species in a solution.[55,96] The LUVs were prepared in a similar manner as described in chapter 4, section 4.7 (for detail, see Chapter 7, experimental section). The formation of LUVs was confirmed by TEM images (Figure 6.29) and we noticed the presence of lipid vesicles of ~200 nm diameter.

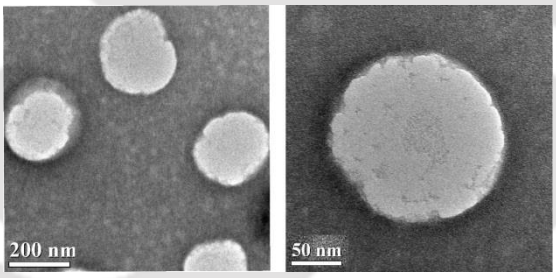

Figure 6.29: TEM images of negatively stained LUVs at concentration of 100 μM of lipid in 50 mM HEPES buffer of pH 7.4. The stock concentration of lipid was 2 mM.

To perform the LUVs leakage study, we prepared first peptide solutions in HEPES (50 mM) pH 7.4 and incubated at 37 °C for desired time period (similar to section 6.7). We added the breaker peptides (peptide **6A** and **6B**) to the pre-aggregated (60 h old) $A\beta_{1-40}$ solution and incubated them for a total of 10 days (240 h = 60 h + 180 h). In parallel, the dye entrapped LUVs (lipid concentration ~2 mM) were prepared. For the LUV leakage study we prepared four different sets of peptide solutions (3 replicates of each set),

Solution 1 *$A\beta_{1-40}$ (incubated for 12 h),*

Solution 2 *$A\beta_{1-40}$ (incubated for 10 days),*

Solution 3 *$A\beta_{1-40}$ **:** peptide **6A** (1:5) (peptide **6A** was added to the preformed fibrillar aggregates after 60 h and incubated for total 10 days (60 h + 180 h).*

Solution 4 *$A\beta_{1-40}$: peptide **6B** (1:5) (peptide **6B** was added to the preformed fibrillar aggregates after 60 h and incubated for total 10 days(60 h + 180 h).*

The lipids and peptides were mixed in a ratio of 1:20 (as mentioned in Chapter 4, Section 4.7) and monitored the dye (carboxyfluorescein) leakage assay by fluorescence study (λ_{ex} = 485 nm, λ_{em} = 516 nm and band width 3 nm). The emission was recorded for each 10 min interval up to 100 min, further 12 h interval up to 72 h. At the end of the experiment, 10 µL of Triton X-100 was added to obtain complete dye release from the vesicle and the final fluorescence was measured. The untreated LUVs (natural dye leakage) were also studied and used as control. The % of leakage was calculated as,[130]

$$\% \text{ Leakage} = \frac{(\text{observed fluorescence} - \text{initial fluorescence})}{(\text{total fluorescence} - \text{initial fluorescence})} \times 100\ \%$$

From LUV leakage study, we observed that the 12 h old $A\beta_{1-40}$ (red, Figure 6.30a,b) caused more dye leakage (~49-50% in 72 h) which confirmed the presence of toxic species probably oligomers of $A\beta_{1-40}$ (solution 1). However, the 10 days old $A\beta_{1-40}$ sample (blue, Figure 6.30a,b; solution 2) caused less LUV leakage in comparison with 12 h old Aβ fibril, indicating the mature fibrils were less toxic than the soluble oligomers. We observed lesser extent of dye leakage when the zipper peptide 6**A** (olive, Figure 6.30a,b) was present with $A\beta_{1-40}$ (solution 3) and that leakage was almost comparable with that from the untreated

LUVs (black, Figure 6.30a,b), indicating the zipper peptide disrupted the $A\beta_{1-40}$ aggregates into non-toxic species. The $A\beta_{1-40}$ treated with the control peptide **6B** (solution 4) caused more dye leakage (magenta, Figure 6.30b,c) in comparison to the zipper peptide **6A** treated $A\beta_{1-40}$. Therefore, it can be concluded that presence of zipper peptide disaggregates the amyloid fibrils of $A\beta_{1-40}$ into non-toxic species *in vitro* at pH 7.4 and 37 °C.

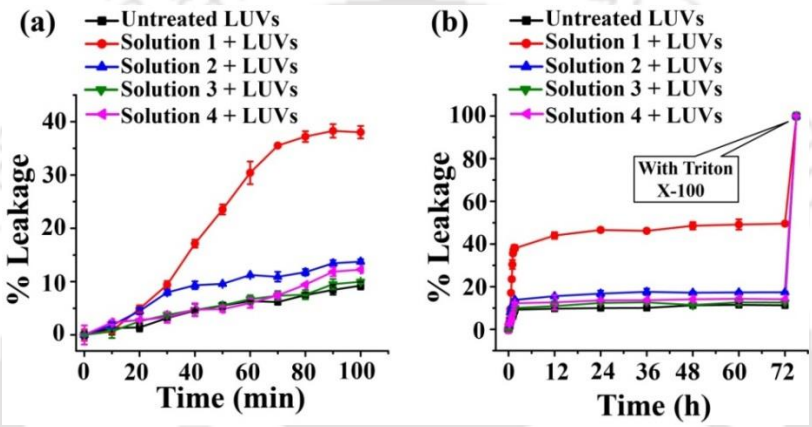

Figure 6.30: (a) and (b) Carboxyfluorescein dye emission showing the effect of $A\beta_{1-40}$ on LUVs with time and % of dye leakage. The spectra showing % of dye leakage by untreated LUVs (black); LUVs treated with solution 1 (red), solution 2 (blue), solution 3 (olive) and solution 4 (magenta). The 100 % dye release was obtained by treating the LUVs with triton X-100. The composition of solution 1, 2, 3 and 4 was mentioned above in the discussion section. For each data point 3 different sets of replicate solutions were scanned separately and average was taken with observed standard deviation.

6.9. Disruption of Aβ aggregates present in human cerebrospinal fluid by the zipper peptide:

It was clear from all the above experimental results that the zipper peptide disrupted the $A\beta_{1-40}$ aggregates into non-toxic species *in vitro* at pH 7.4 and 37 °C. Next, we examined the efficacy of the zipper peptide 6**A** for the disruption of Aβ aggregates present in human cerebrospinal fluid (CSF) *in vitro* at pH 7.4 and 37 °C.

6.9.1: Quantification of Aβ present in diseased human cerebrospinal fluid sample:

The human CSF samples were obtained from an AD affected brain and the presence of amyloid was confirmed by ThT fluorescence study (Figure 6.31) in similar manner as described in chapter 4, section 4.8.[131,132] To determine the approximate concentration of Aβ aggregates present in the CSF, we prepared a 50 μM solution of $A\beta_{1\text{-}40}$ in PBS of pH 7.4 and incubated at 37 °C for 10 days.

After 10 days, ThT induced fluorescence was measured with varied amount (20, 50 and 100μL) of $A\beta_{1\text{-}40}$ (Figure 6.31a) and CSF (Figure 6.31b), keeping the ThT concentration same. From the ThT assay (similar to Chapter 4, section 4.8.1), the concentration of Aβ in the CSF sample was determined to be ~23 μM by comparison of the fluorescence intensity with the authentic 50 μM of $A\beta_{1\text{-}40}$ sample.

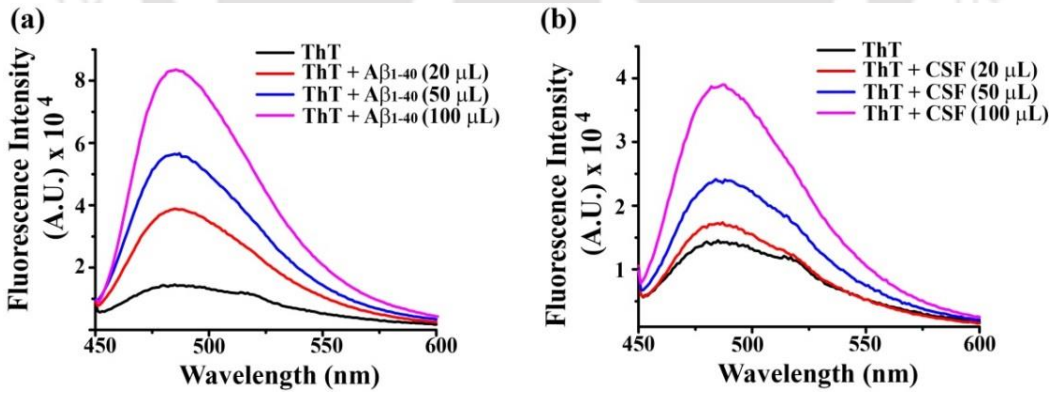

Figure 6.31: Fluorescence spectra of ThT in absence (black) and presence of 20 μL (red), 50 μL (blue) and 100 μL (magenta) of $A\beta_{1\text{-}40}$ (a) and human CSF (b).The stock concentration of ThT was 50 μM in PBS (50 mM) pH 7.4.

6.9.2: Monitoring the disruption of Aβ aggregates present in the CSF sample by ThT assay:

It was confirmed from the above study that the concentration of Aβ in the human CSF sample was ~23 µM. Next, 5 fold molar excess of peptide **6A** and **6B** were added separately with the CSF samples and incubated them at 37 °C for 10 days. The kinetics of disaggregation of amyloid aggregates was monitored by ThT assay (Figure 6.32). In ThT assay, we observed that fluorescence intensity of CSF was suppressed significantly in presence of peptide **6A** (blue, Figure 6.32) while the CSF alone (black, Figure 6.32) showed increased fluorescence. There was also a suppression of fluorescence observed in case of CSF sample with peptide **6B** (red, Figure 6.32) but in lesser extent in comparison to the zipper peptide **6A**.

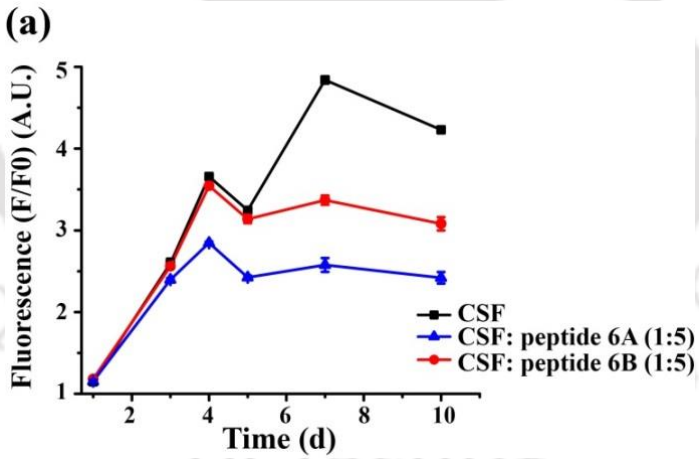

Figure 6.32: Time dependent ThT assay for the disruption of the amyloid present in human cerebrospinal fluid (CSF) in absence (black) and presence of peptide **6A** (blue) & **6B** (red) respectively.

6.9.3: Monitoring the disruption of Aβ aggregates present in the CSF sample by TEM and Congo red birefringence study:

After 10 days of incubation of the CSF sample in presence of 5-fold molar excess of peptide **6A** and **6B**, when TEM was analyzed we noticed clear fibrillar assembly in case of untreated CSF sample (Figure 6.33a). But we did not notice such fibrillar assembly when the zipper peptide **6A** was present in 5-fold molar excess with the CSF (Figure 6.33b). Although some aggregates was noticed in the CSF sample when co-incubated with peptide **6B** (Figure 6.33c). Again, the CSF sample alone showed a clear appearance of green gold birefringence (Figure 6.34a). But, no such birefringence was observed in presence of 5-fold molar excess of the zipper peptide **6A** (Figure 6.34b), indicating the absence of amyloid. We did not notice any birefringence in the CSF sample treated with peptide **6B** also (Figure 6.34c).

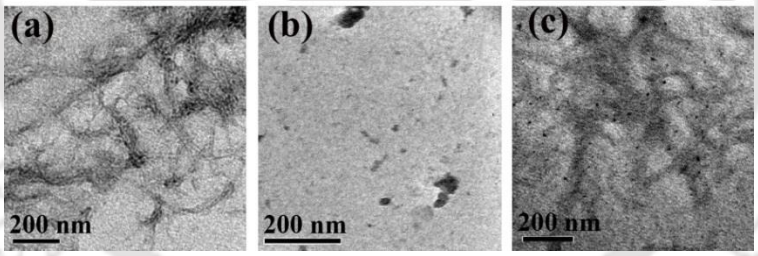

Figure 6.33: TEM images human CSF in absence (a) and presence of 10 fold molar excess of peptide **6A** (b) & peptide 6**B** (c).Images were taken after 10 days incubation at 37 °C.

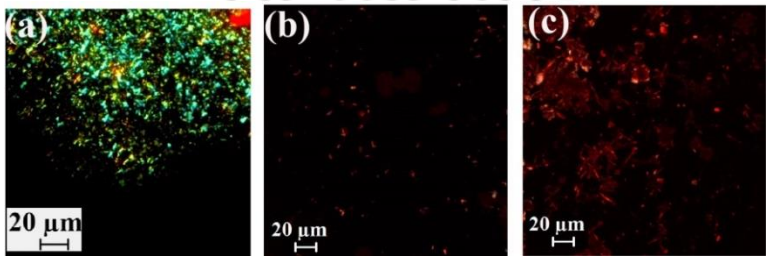

Figure 6.34: Congo red birefringence images human CSF in absence (a) and presence of 10 fold molar excess of peptide **6A** (b) & peptide **6B** (c).Images were taken after 10 days incubation at 37 °C.

6.10. Mechanistic investigation on the action of the zipper peptide on $A\beta_{1-40}$ peptide:

We have observed the efficacy of the zipper peptide **6A** for the disruption of amyloid aggregates of $A\beta_{1-40}$ and inhibition of its formation *in vitro* at physiological condition (pH 7.4 and 37 °C). Now, it is very important to understand the mechanism of such action of the zipper peptide.

Before verifying the exact pathway of interaction between the zipper peptide and the $A\beta_{1-40}$, it was important to check the structural orientation of the zipper peptide in the solution. To identify the structural orientation of the zipper peptide **6A**, we designed and synthesized three derivatives of the zipper peptide **6A**, namely, **6C**, **6D** and **6E** (Table 6.1) and performed fluorescence resonance energy transfer (FRET) assay. Peptide **6C** contained a tryptophan (FRET donor) at one terminal of peptide **6A** and other terminal was kept free from fluorophore. Peptide **6D** contained a dansyl group (FRET acceptor) at one terminal (opposite to the tryptophan in peptide **6C**) of the peptide **6A** and the other terminal was kept free from fluorophore. We also synthesized peptide **6E**, which contains both the donor and acceptor at the two different terminals of the peptide **6A**.

6.10.1. FRET study to elucidate the structural orientation of the zipper peptide:

To identify the structural orientation of the zipper peptide we expected three possibilities of the structural orientation (Figure 6.35), where the zipper peptide might exist either in bent (Figure 6.35a,b) orientation or straight chain orientation (Figure 6.35c).

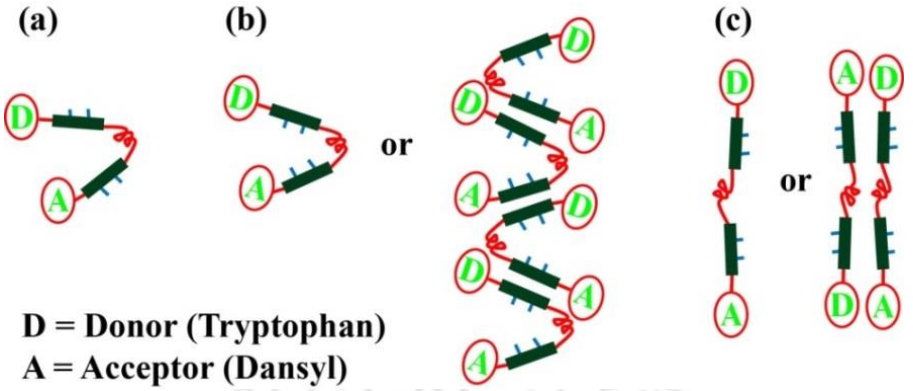

Figure 6.35: Different structural possibilities of the zipper peptide.

Since the zipper peptide was identified as non-amyloidogenic in nature (Section 6.5), one possibility (Figure 6.35b) might be excluded, as neither *N*-methylations will allow that kind of arrangement nor depicted polymeric arrangement can stay in solution without aggregation in the experimental concentration. Therefore, we expected two possibilities of the structural orientation of the zipper peptide **6A** (Figure 6.35a,c).

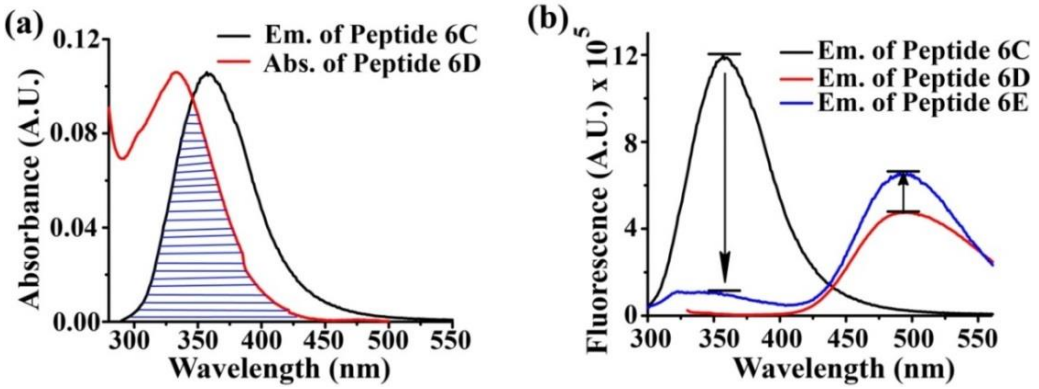

Figure 6.36: (a) Overlap of the emission spectrum of donor-peptide **6C** (black) and the absorbance spectrum of acceptor-peptide **6D** (red). (b) Fluorescence emission spectra of peptide **6C** (black), **6D** (red) and **6E** (blue). Spectra were recorded with 20 μM solutions of the peptides in PBS (50 mM) pH 7.4 in presence of 3% DMSO. Peptide **6C** and **6E** were excited at 290 nm whereas peptide **6D** was excited at 320 nm.

To elucidate the structural orientation of the zipper peptide **6A**, we performed fluorescence resonance energy transfer (FRET) study. If the zipper peptide would acquire hairpin like structure (Figure 6.35a) it must show intra-molecular FRET, whereas if the zipper peptide exist in straight chain orientation (Figure 6.35c) it would show FRET trough intermolecular interaction.

For FRET study, we prepared ~20 μM solutions of all fluorophoric peptides (**6C**, **6D** and **6E**) in PBS pH 7.4 (50 mM, in presence of 3% DMSO) and performed various photo-physical studies. The UV-visible and fluorescence spectra of the individual donor and acceptor revealed that the fluorescence spectrum of dansyl in peptide **6D** (acceptor) overlapped significantly with the absorption spectrum of tryptophan in peptide **6C** (donor, Figure 6.36a). Importantly, peptide **6E** contained both the donor (tryptophan) and acceptor (dansyl), which can be selectively excited at 290 nm (the absorbance maximum of donor, peptide **6C**) where there is very low absorbance of the acceptor (dansyl, peptide **6D**). Therefore, these two fluorophores (tryptophan and dansyl) should form a FRET pair in the designed peptide **6E** where the conceptual donor (tryptophan) and the acceptor (dansyl) acted as a FRET donor and acceptor, respectively.[142,145] This observation encouraged us to proceed for the FRET analysis.

For a proper FRET observation some criteria must be fulfilled, which include the energy transfer from the donor to the acceptor and the decrease of the fluorescence of the donor (both intensity and lifetime), whereas the fluorescence of the acceptor is expected to be increased.[97,142] We observed from the figure 6.36b that the fluorescence intensity of the donor (tryptophan in peptide **6E**, λ_{max}^{Em} = 355 nm) in presence of acceptor decreased almost 10 to 11

times from that of the emission of donor alone (peptide **6C**, λ_{max}^{Em} = 355 nm) when it was excited at the maximum absorbance of the donor (λ_{max}^{Abs} = 290 nm). Simultaneously, the fluorescence intensity of the acceptor (in presence of donor) in the peptide **6E** increased almost 1.5 times that of the fluorescence of the acceptor (peptide **6D**, λ_{max}^{Em} = 495 nm). This clear change in fluorescence intensity provided visual evidence of the FRET process from donor (tryptophan) to acceptor (dansyl). This result suggests that the probable orientation of the zipper peptide is either as depicted in Figure 6.35a or in Figure 6.35c.

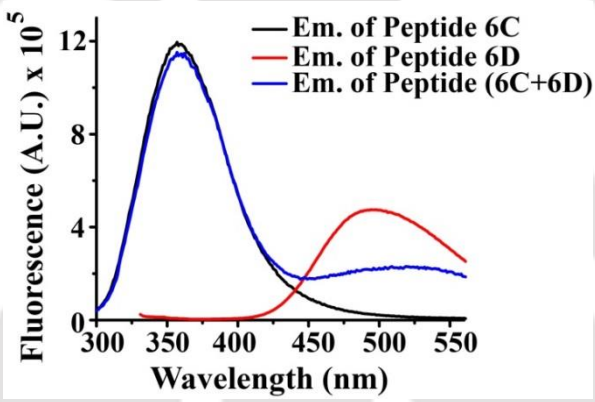

Figure 6.37: Fluorescence emission spectra of peptide **6C** (black), **6D** (red) and the mixture of peptides (**6C**+**6D**, blue). Spectra were recorded with 20 μM solutions of the peptides in PBS (50 mM) pH 7.4 in presence of 3% DMSO. Peptide **6C** and the mixture peptides were excited at 290 nm whereas peptide **6D** was excited at 320 nm.

Now, it was important to know whether the occurrence of FRET was intra-molecular (Figure 6.35a) or inter-molecular (Figure 6.35c). To prove that we mixed peptide **6C** and **6D** (donor and acceptor both were present in same solution but in different molecules) at same concentration (~20 μM) as discussed above and performed FRET study. If the observation of FRET appeared through inter-molecular interaction (Figure 6.35c) that is anti-parallel straight chain interaction, we would expect FRET from the mixture of peptides (peptide

6C+**6D**, donor and acceptor both present in same solution but in different molecules). But, we did not observe such occurrence (Figure 6.37). Rather we observed the fluorescence intensity of the donor (tryptophan in peptide **6C+6D**) in the mixture was almost unchanged in comparison to the emission of donor alone (peptide **6C**, λ_{max}^{Em} = 355 nm) when it was excited at the maximum absorbance of the donor (λ_{max}^{Abs} = 290 nm). Also, the fluorescence intensity of the acceptor (dansyl, in peptide **6C+6D**) in the mixture did not increase in comparison to the fluorescence of the acceptor (dansyl in peptide **6D**, λ_{max}^{Em} = 495 nm). This visual observation clearly indicated no occurrence of FRET (Figure 6.37). Absence of notable FRET through inter-molecular interaction of the zipper peptide clearly did not satisfy the straight chain orientation of the zipper peptide (Figure 6.35c) but satisfied the zipper or hairpin like structural orientation (Figure 6.35a).

We observed FRET from peptide **6E** (donor and acceptor both were present in the same molecule) as indicated in figure 6.36b but did not observe the same from the mixture of peptides **6C** and **6D** (donor and acceptor were present in same solution but in different molecules) as indicated in figure 6.37. These results supported the hairpin like (Figure 6.35a) structural orientation of the zipper peptide. The Förster radius (R_0)[97,141] of tryptophan/dansyl system in peptide **6E** was calculated using equation 1 and found to be 27.9 Å.

$$\boldsymbol{R_0 = 0.2108 \left[\kappa^2\, \Phi_D n^{-4} \int_0^{\infty} F_D(\lambda)\varepsilon_A(\lambda)\lambda^4 d\lambda\right]^{1/6}} \quad \ldots\ldots\ldots\ldots\ldots\ldots\ldots\ldots\ldots (1)$$

Where, κ^2 (= 2/3) is the orientation factor, n is the refractive index of the medium (= 1.33), Φ_D (= 0.06) is the quantum yield of the donor (peptide **6C**) in the absence of acceptor and $\int_0^{\infty} F_D(\lambda)\varepsilon_A(\lambda)\lambda^4 d\lambda$ is the overlap integral (= 4.206 x 10^{14}) of the fluorescence emission spectrum of the donor (peptide **6C**) and the absorption spectrum of the acceptor (peptide **6D**). R_0 (= 27.9 Å) is the critical distance when the energy transfer efficiency is 50%.

The fluorescence quantum yields (Φ_f) were determined using the equation 2 where quinine sulphate was used as a reference with the known Φ_f (0.546)[141] in 0.1 molar solution in sulphuric acid.

$$\Phi_S = \Phi_R \frac{Fl_S^{Area}.\ Abs_R\ .n_S^2}{Fl_R^{Area}\ .\ Abs_S\ .\ n_R^2} \ldots\ldots\ldots\ldots\ldots\ldots\ldots\ldots\ldots\ldots (2)$$

Where, Φ_R is the quantum yield of standard reference, Fl_S^{Area} (sample) and Fl_R^{Area} (reference) are the integrated emission peak areas, Abs_S (sample) and Abs_R (reference) are the absorbance at the excitation wavelength, and n_S (sample) and n_R (reference) are the refractive indices of the solutions.

Again, the efficiency of energy transfer (E)[97] was calculated using the equation 3 and found to be 91.7 %. And, the donor-acceptor distance (r) in the zipper peptide **6E** was found to be 18.7 Å, which is far less than their theoretical distance when the peptide was in fully stretched conformation.

$$\mathbf{E}=\frac{\mathbf{R_0^6}}{\mathbf{R_0^6 + r^6}} = \mathbf{1} - \frac{\mathbf{F}}{\mathbf{F_0}} \qquad \ldots\ldots\ldots\ldots\ldots\ldots\ldots\ldots\ldots (3)$$

Where, F and F_0 are the fluorescence intensity of donor in the presence (peptide **6E**) and absence (peptide **6C**) of acceptor, r is the distance between donor and the acceptor and R_0 (= 27.9 Å) is the Förster radius.

From the time-resolved fluorescence study we observed that the donor lifetime (tryptophan in peptide **6C**, λ_{ex} = 290 nm, λ_{em} = 355 nm) was decreased from 2.9 ns to 1.8 ns in peptide **6E**, indicating the occurrence of the FRET process. Moreover, the life time of the acceptor (dansyl in peptide **6D**, λ_{ex} = 290 nm, λ_{em} = 495 nm) was increased in peptide **6E** from 6 ns to 15 ns (Table 6.2 and Figure 6.38) which was also an indication of FRET.

But in the mixture peptide (**6C**+**6D**), the life time of the donor (2.9 ns) did not change from that of the donor in peptide **6C** (2.9 ns). Similarly, the life time of the acceptor in the mixture peptide (**6C**+**6D**) found 5.5 ns in comparison with the life time of the acceptor alone 6 ns (Table 6.2 and Figure 6.38). The life time data also indicated no occurrence of FRET.

We already observed that the zipper peptide comprised of the β-sheet rich conformation (Section 6.5.1) and later the FRET study revealed that the two ends of the zipper peptide was close to each other (18.7 Å apart). These evidences were highly supportive of the hairpin like (Figure 6.35a) structural orientation of the zipper peptide, but not the straight chain like orientation (Figure 6.35c).

peptide	Φ_f	λ_{em} (nm)	τ_1 (ns)	τ_2 (ns)	$<\tau>$ (ns)	k_f (10^8 s^{-1})	k_{nr} (10^8 s^{-1})	χ^2
Peptide **6C**	0.06	355	1.352 (27%)	3.559 (73%)	2.951	0.202	3.186	0.98
Peptide **6D**	0.051	495	3.124 (48%)	8.741 (52%)	6.033	0.085	1.573	1.02
Peptide **6E**	0.058	355	1.069 (70%)	3.345 (30%)	1.772	0.328	5.315	0.98
	0.058	495	6.260 (15 %)	16.728 (85 %)	15.145	0.038	0.622	1.03
Mixture peptide (**6C**+**6D**)	0.65	355	1.350 (28%)	3.500 (72%)	2.902	0.222	0.3224	1.03
	0.65	495	3.857 (43%)	6.750 (57%)	5.486	0.118	1.705	0.98

Table 6.2: Summary of the fluorescence lifetimes of the peptide **6C**, **6D**, **6E** and the mixture (**6C**+**6D**). All the peptides were excited at λ_{ex} = 290 nm; Concentration of all the peptides were same = 20μM; $<\tau>$, k_f and k_{nr} are weighted means from the biexponential fits: $<\tau> = 1/ (\alpha_1/\tau_1 + \alpha_2/\tau_2)$, $k_f = \Phi/<\tau>$, and $k_{nr} = (1-\Phi_f)/<\tau>$.[145]

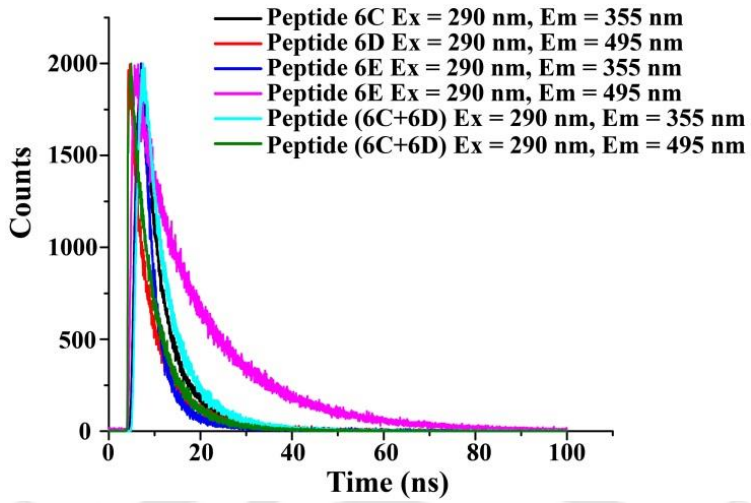

Figure 6.38: Time resolved fluorescence spectra of the peptide **6C** (black, λ_{ex} = 290 nm, λ_{em} = 355 nm), **6D** (red, λ_{ex} = 290 nm, λ_{em} = 495 nm), **6E** (for blue, λ_{ex} = 290 nm, λ_{em} = 355 nm and for magenta, λ_{ex} = 290 nm, λ_{em} = 495 nm) and mixture peptide **6C**+**6D** (for cyan, λ_{ex} = 290 nm, λ_{em} = 355 nm and for olive, λ_{ex} = 290 nm, λ_{em} = 495 nm). Spectra were recorded in 20μM of peptide solutions in PBS pH 7.4 (in presence of 3% DMSO).

6.10.2. FRET analysis of the zipper peptide in presence of $A\beta_{1-40}$:

It was clear from the above experimental evidences that the zipper peptide have actually zipper or hairpin like structural orientation. But, how the zipper peptide effectively interacted with $A\beta_{1-40}$ aggregates; that is, the mechanistic pathway of interaction between the zipper peptide and $A\beta_{1-40}$ during disruption process need more evidences. For the mechanistic elucidation, we can expect four possible pathways (Figure 6.39) of interaction between the zipper peptide and the $A\beta_{1-40}$ peptide. Since, the zipper peptide effectively inhibited the aggregation of $A\beta_{1-40}$ and also disrupted the $A\beta_{1-40}$ aggregates *in vitro* at pH 7.4 and 37 °C (Section 6.6 to 6.9), indicated the $A\beta_{1-40}$ evidently interacted or bound with the zipper peptide. These evidences eventually excluded the possibilities of path A and path B (Figure 6.39). Therefore, the interactions might be by either path C or path D (Figure 6.39). If, the interactions followed the path C or D (Figure 6.39), we would expect the appearance of

FRET where the zipper peptide might bind with the $A\beta_{1-40}$ and the presence of *N*-methylation would inhibit $A\beta_{1-40}$ aggregation. The difference between these two pathways was the zipper peptide exhibited intra-molecular FRET in path D (Figure 6.39) whereas the zipper peptide show FRET through inter-molecular interaction in path C (Figure 6.39).

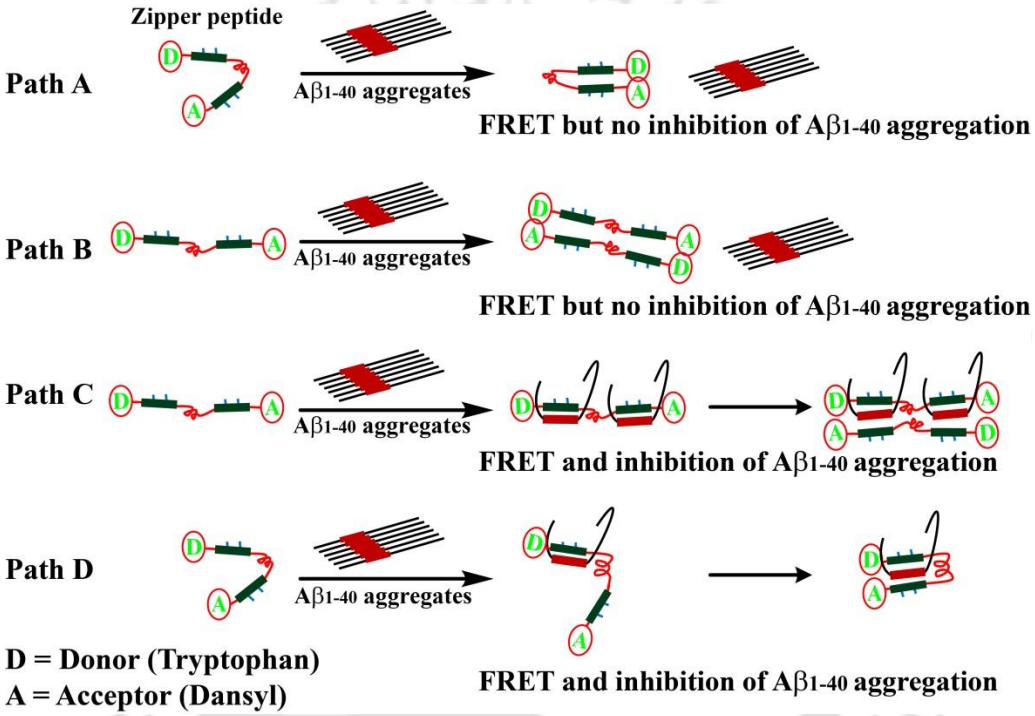

Figure 6.39: Different possibilities of interaction between the zipper peptide and the $A\beta_{1-40}$.

To prove the mechanistic pathway of the zipper peptide against $A\beta_{1-40}$ aggregates (path C or path D in Figure 6.39) we designed an experiment where the fluorophore attached zipper peptides (**6C**, **6D**, **6E** and mixture peptides (**60C**+**6D**)) were added to the 50 μM of $A\beta_{1-40}$ aggregates (60 h old sample, $A\beta_{1-40}$ peptide was alone incubated at 37 °C for 60 h to form fibrillar aggregates in a similar manner as described in section 6.7) with a ratio of 1:2 ($A\beta_{1-40}$ **:** zipper peptide) and incubated them for a total 150 h (60 h + 90 h) at 37 °C under dark

environment to avoid quenching from the light. After 150 h of incubation all peptide samples were diluted to 20 μM with respect to the fluorophore attached zipper peptides and FRET study was performed in a similar manner as described in previous section (Section 6.10.1).

The UV-visible and fluorescence spectra of the peptide **6C** and **6D** in presence of $A\beta_{1-40}$ aggregates again revealed that the fluorescence spectrum of peptide **6D** (acceptor) overlapped significantly with the absorption spectrum of peptide **6C** (donor, Figure 6.40a). Moreover, the peptide **6E** when selectively excited at 290 nm (the absorbance maximum of donor, tryptophan in peptide **6C**), there was very low absorbance of the acceptor (dansyl, peptide **6D**). Therefore, these two fluorophores (tryptophan and dansyl) form a FRET pair in the designed peptide **6E** as discussed earlier.

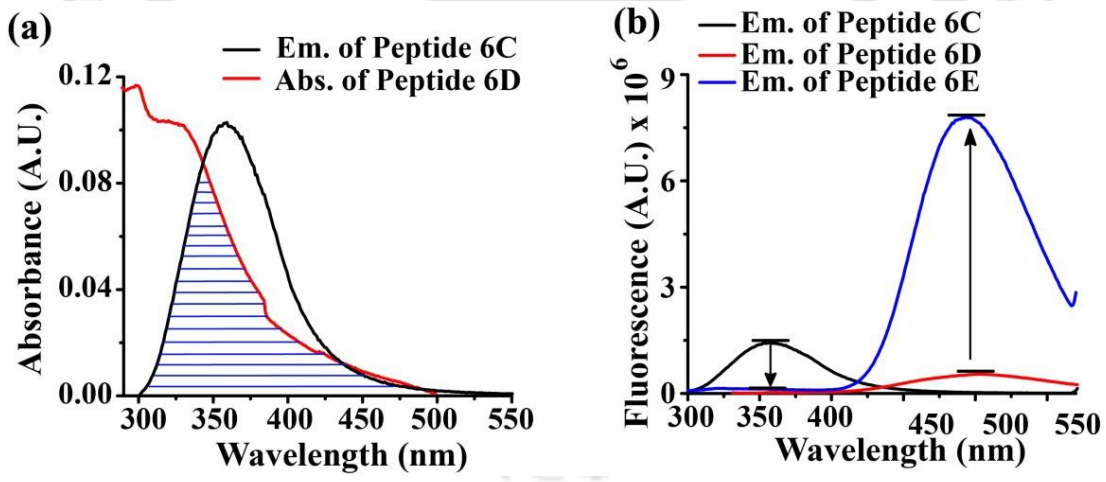

Figure 6.40: (a) Overlap of the emission spectrum of donor-peptide **6C** (black) and the absorbance spectrum of acceptor-peptide **6D** (red) in presence of $A\beta_{1-40}$ aggregates. (b) Fluorescence emission spectra of peptide **6C** (black), **6D** (red) and **6E** (blue) in presence of $A\beta_{1-40}$ aggregates. Spectra were recorded with 20 μM solutions of the peptides in PBS (50 mM) pH 7.4 in presence of 3% DMSO. Peptide **6C** and **6E** were excited at 290 nm whereas peptide **6D** was excited at 320 nm.

From the fluorescence measurement (Figure 6.40b), we observed that the fluorescence intensity of donor (tryptophan in peptide **6E**) in presence of acceptor was decreased almost 12 times from that of the emission of donor alone (peptide **6C**, λ_{max}^{Em} = 355 nm), when it was excited at the maximum absorbance of the donor (λ_{max}^{Abs} = 290 nm). On the other hand, the fluorescence intensity of the acceptor (in presence of donor) in the peptide **6E** was increased almost 13 times that of the fluorescence of the acceptor alone (peptide **6D**, λ_{max}^{Em} = 495 nm). These observations clearly justified the occurrence of FRET process from donor (tryptophan) to acceptor (dansyl) (Figure 6.40b). This result indicated that the mechanism of inhibition must be followed either path C or path D as depicted in Figure 6.39.

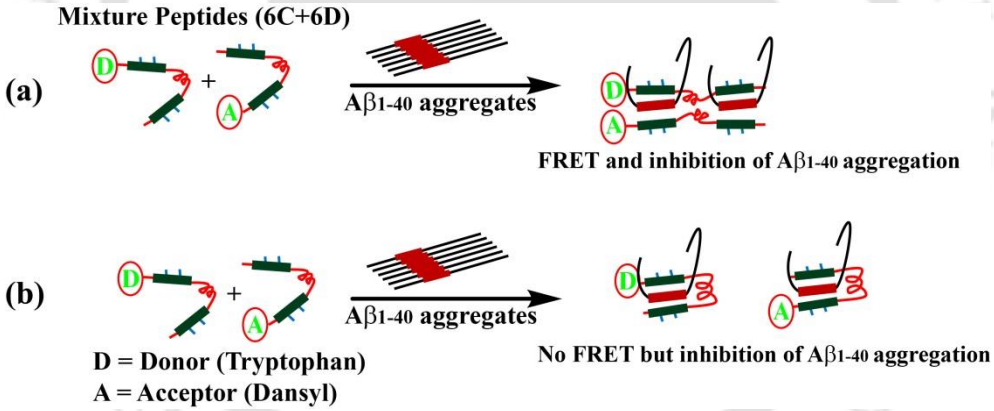

Figure 6.41: Possible way of interaction between the zipper peptide and the $A\beta_{1\text{-}40}$.

Next, it was important to understand the appearance of FRET whether followed inter-molecular zipping in path C (Figure 6.39) or intra-molecular zipping in path D (Figure 6.39). To prove that we performed FRET study with the mixture peptides **6C**+**6D** (donor and acceptor were present in same solution but in different molecules) at same concentration (~20 μM) as discussed above. If the observation of FRET appeared through inter-molecular

interaction (Figure 6.41a and path C in Figure 6.39) that is anti-parallel straight chain interaction, we would expect FRET from the mixture of peptides (peptide **6C**+**6D**, donor and acceptor were present in same solution but in different molecules). But, if the interaction occurred through zipping intra-molecular pathway (Figure 6.41b and path D in Figure 6.39), we might not expect FRET from the mixture of peptides (peptide **6C**+**6D**, donor and acceptor were present in same solution but in different molecules).

When the mixture of peptides (**6C**+**6D**) was present with $A\beta_{1\text{-}40}$, we did not observe any FRET (Figure 6.42). Rather, we observed that the fluorescence intensity of the donor in the mixture (tryptophan in peptide **6C+6D**) was almost unchanged in comparison to the emission of donor alone (peptide **6C**, λ_{max}^{Em} = 355 nm) when it was excited at the maximum absorbance of the donor (λ_{max}^{Abs} = 290 nm). Similarly, the fluorescence intensity of the acceptor (dansyl, in peptide **6C+6D**) in the mixture was not increased in comparison to the fluorescence of the acceptor (dansyl in peptide **6D**, λ_{max}^{Em} = 495 nm). This observation clearly indicated no occurrence of FRET (Figure 6.42). These results clearly justified that the zipper peptide interacted with the $A\beta_{1\text{-}40}$ through zipping not through the straight chain orientation (Figure 6.41).

We observed FRET from peptide **6E** (donor and acceptor were present in same molecule but at opposite end) in presence of $A\beta_{1\text{-}40}$ (Figure 6.40b) but did not observe the same from the mixture of peptides **6C** and **6D** (donor and acceptor were present in same solution but in different molecules) in presence of $A\beta_{1\text{-}40}$ (Figure 6.42). That clearly indicated the interaction between the zipper peptide and the $A\beta_{1\text{-}40}$ occurred through path D (Figure 6.39), i.e., through zipping action. The Förster radius (R_0) of the tryptophan/dansyl system in zipper peptide **6E** was calculated using equation 1 and found to be 28.2 Å (the overlap integral value = 3.629 x

10^{14} and the quantum yield of the donor is 0.075). The efficiency of energy transfer (E) was calculated using the equation 3 and found to be 87 %. The donor-acceptor distance (r) in peptide **6E** in presence of $A\beta_{1\text{-}40}$ aggregates was found to be 20.6 Å.

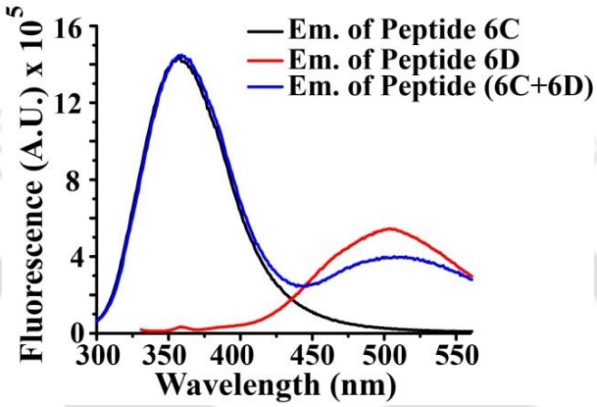

Figure 6.42: Fluorescence emission spectra of peptide **6C** (black), **6D** (red) and the mixture of peptides (**6C**+**6D**, blue) in presence of $A\beta_{1\text{-}40}$. Spectra were recorded with 20 μM solutions of the peptides in PBS (50 mM) pH 7.4 in presence of 3% DMSO. Peptide **6C** and the mixture peptides were excited at 290 nm whereas peptide **6D** was excited at 320 nm.

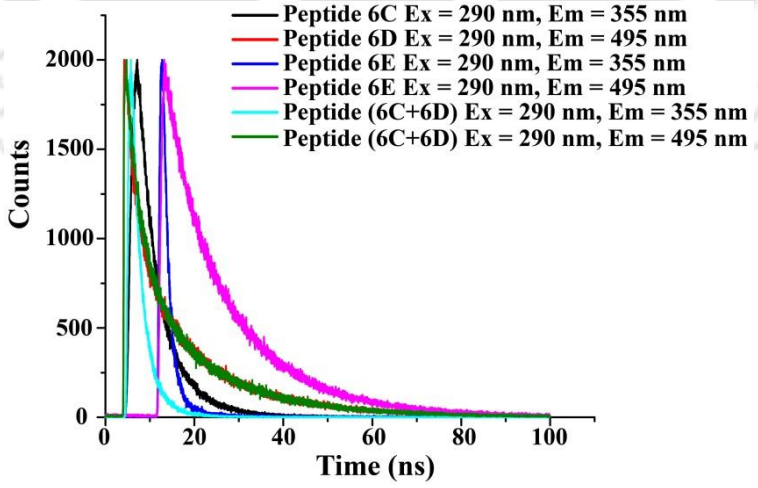

Figure 6.43: Time resolved fluorescence spectra of the peptide **6C** (black, λ_{ex} = 290 nm, λ_{em} = 355 nm), **6D** (red, λ_{ex} = 290 nm, λ_{em} = 495 nm), **6E** (for blue, λ_{ex} = 290 nm, λ_{em} = 355 nm and for magenta, λ_{ex} = 290 nm, λ_{em} = 495 nm) and mixture peptide **6C**+**6D** (for cyan, λ_{ex} = 290 nm, λ_{em} = 355 nm and for olive, λ_{ex} = 290 nm, λ_{em} = 495 nm) in presence of $A\beta_{1\text{-}40}$. Spectra were recorded in 20μM of peptide solutions in PBS pH 7.4 (in presence of 3% DMSO).

Again, from the time-resolved fluorescence study we observed that the donor lifetime (tryptophan in peptide **6C**, λ_{ex} = 290 nm, λ_{em} = 355 nm) decreased from 2.6 ns to 1.6 ns in peptide **6E**, indicating the occurrence of the FRET process. Moreover, the life time of the acceptor (dansyl in peptide **6D**, λ_{ex} = 290 nm, λ_{em} = 495 nm) increased in peptide **6E** from 13.4 ns to 14.9 ns (Figure 6.43 and Table 6.3) which was also an indication of occurrence of FRET. But in the mixture of peptides (**6C**+**6D**), the life time of the donor remained same (2.6 ns) in comparison with donor alone in peptide **6C** (2.6 ns) and also the life time of the acceptor in the mixture peptide (**6C**+**6D**) found similar, 13.1 ns in comparison to the life time of the acceptor alone 13.4 ns (Figure 6.43 and Table 6.3). The life time data also indicated no occurrence of FRET in the mixture of peptides (**6C**+**6D**).

peptide	Φ_f	λ_{em} (nm)	τ_1 (ns)	τ_2 (ns)	$<\tau>$ (ns)	k_f (10^8 s^{-1})	k_{nr} (10^8 s^{-1})	χ^2
Peptide **6C**	0.075	355	1.261 (34%)	3.256 (66%)	2.577	0.29	3.591	0.99
Peptide **6D**	0.039	495	3.223 (26%)	16.985 (74%)	13.367	0.029	0.719	1.05
Peptide **6E**	0.26	355	1.098 (75%)	3.313 (25%)	1.636	1.589	4.522	0.99
	0.26	495	6.090 (15%)	16.519 (85%)	14.968	0.174	0.494	1.02
Mixture peptide (**6C**+**6D**)	0.114	355	1.548 (43%)	3.421 (57%)	2.615	0.434	3.389	1.00
	0.114	495	3.430 (27%)	16.60 (73%)	13.090	0.087	0.677	1.04

Table 6.7: Summary of the fluorescence lifetimes of the peptide **6C**, **6D**, **6E** and mixture peptide (**6C**+**6D**) in presence of $A\beta_{1\text{-}40}$. All the peptides were excited at λ_{ex} = 290 nm; Concentration of all the peptides were same = 20μM; $<\tau>$, k_f and k_{nr} are weighted means from the biexponential fits: $<\tau> = 1/ (\alpha_1/\tau_1 + \alpha_2/\tau_2)$, $k_f = \Phi/<\tau>$, and $k_{nr} = (1-\Phi_f)/<\tau>$.[145]

We already observed in section 6.10.1 that the zipper peptide exists in hairpin like structural orientation which remained unchanged in presence of $A\beta_{1-40}$ aggregates also. Since, the zipper peptide effectively inhibited the aggregation of $A\beta_{1-40}$ and disrupted the existing aggregates into non-toxic species *in vitro*, it was inferred that the interaction between the zipper peptide and the $A\beta_{1-40}$ aggregates occurred. Moreover, we observed a clear evidence of FRET of the zipper peptide in presence of $A\beta_{1-40}$ aggregates. Therefore, the zipper peptide possibly interacted with the $A\beta_{1-40}$ peptide and arrested it through zipping action as anticipated in Figure 6.39, path D.

6.11. Conclusion:

Based on our experimental results we can conclude that the designed synthetic zipper peptide effectively disrupted the $A\beta_{1-40}$ aggregates into non-toxic species *in vitro* at pH 7.4 and 37 °C. We also provided evidences that the zipper peptide exhibited hairpin like structural orientation which probably trapped the $A\beta_{1-40}$ monomers from the aggregates through zipping action. The presence of *N*-methylation on the zipper peptide did not allow further aggregation after entrapment of $A\beta_{1-40}$. The zipper peptide also disrupted the Aβ aggregates present in human cerebrospinal fluid sample. Therefore, we can conclude that the zipper peptide exhibiting the hairpin like orientation can act as a lead molecule which can be used for drug design against Alzheimer's disease.

Chapter 7: Experimental section

7.1 Materials and methods:

Reagents and solvents

Rink amide MBHA resin (Loading 1.1 mmol/g), BOP [(Benzotriazole-1-yloxy) tris (dimethylamino) phosphonium hexafluorophosphate], PyBOP [(Benzotriazole-1-yloxy-tris-pyrolidine-phosphonium hexafluorophosphate], Diisopropyl ethylamine (DIPEA), Diisopropyl azodicarboxylate (DIAD), 1,8-Diazabicyclo[5.4.0]undec-7-ene (DBU), Fmoc-Ant-OH (Fmoc-anthranilic acid), *N*-Fmoc-*N*″-succinyl-4,7,10-trioxa-1,13-tridecanediamine, 1,1,1,3,3,3-hexafluoro-2-propanol (HFIP), Dansyl chloride and 5(6)-Carboxyfluorescein were purchased from Sigma-Aldrich. 1,2-Dipalmitoyl-sn-glycero-3-phosphocholine (DPPC), 1,2-Dimyristoyl-sn-glycero-3-phosphocholine (DMPC), Ganglioside GM1 were purchased from Avanti Polar Lipid, Inc. Dimethylformamide (DMF), dichloromethane (DCM) and acetonitrile of HPLC grade were obtained from Merck (India). Cholesterol (99%), acetic anhydride, *N*-methyl imidazole, *N*-2-hydroxyethyl piperazine-*N*-2-ethane sulphonic acid (HEPES) and Trifluoroacetic acid (TFA) of highest grade were purchased from SRL (India). Milli-Q water at 18.2 Ω was used. All Fmoc amino acids, Fmoc-*N*-methylated amino acids and human Alzheimer's β-

amyloid ($A\beta_{1-40}$) acid were purchased from GL Biochem (Shanghai). Human Cerebrospinal fluid (h-CSF) samples (late-stage) were obtained from Guwahati Neurological Research Center (GNRC) and Hospital, Guwahati, India, for performing biophysical studies acceding to the bioethics policy of the hospital.

Aβ Sample Preparation

The commercially available $A\beta_{1-40}$ (*e.g.* 1.2 mg) was dissolved in small volume (20 µL) of TFA to obtain disaggregated $A\beta_{1-40}$. TFA was evaporated using nitrogen gas. To remove TFA completely, HFIP was added and evaporated using nitrogen gas. This process was repeated twice. Then, required volume of PBS (~5.6 mL) was added to it followed by sonication and vortexed to obtain soluble $A\beta_{1-40}$ (50 µM).[127]

CSF sample preparation

Human cerebrospinal fluid (CSF) samples (colorless) of the diseased brain were obtained from the Guwahati Neurological Research Center (GNRC) and Hospital, Guwahati, India and used without further dilution. Before any biophysical study, the CSF samples were first sonicated and vortexed properly to obtained clear solution. The approximate concentration of a CSF sample was obtained by a comparative study with the authentic 50 µM pre-aggregated $A\beta_{1-40}$ peptide (before use, the $A\beta_{1-40}$ peptide was incubate in PBS pH 7.4 at 37 °C for 10 days) solution using Thioflavin T fluorescence assay.[132]

Large Unilamellar Vesicles (LUVs) Preparation and Carboxyfluorescein Entrapment

The large unilamellar vesicles (LUVs) were prepared using three different lipids; DMPC (or DPPC), Cholesterol and GM1 with 68:30:2 molar ratios following a reported protocol.[127] Prior to the vesicle preparation, the required lipids were taken in clean glass

vessel and solubilize them in chloroform and methanol (2:1) to make 2 mM stock solution. Then the solvents were evaporated completely using nitrogen gas to make thin lipid film. The glass vessel containing the lipid film was placed in a vacuum desiccator for overnight to remove solvents completely. The lipid film was hydrated with 500 µL of carboxyfluorescein solution (200 µM) in 50 mM HEPES buffer of pH 7.4. Then, the solution was vortexed vigorously for 30 min to emulsify the lipid mixtures. Further, the glass vessel was dipped into the liquid nitrogen for instant cooling and after 5 min the frozen solution was dipped into water bath at 50-60 °C for thawing.[128] The step was repeated five times. The excess dye was removed by ultracentrifugation at 20000 rpm and the supernatant dye solution was discarded and the lipid pellet was re-hydrated with 50 mM HEPES buffer. This step was repeated 2 more times to remove the excess dye and the final lipid pellet was collected followed by addition of 500 µL of HEPES buffer and vortexed to obtain homogenous suspension of 2 mM stock of lipid vesicles.[129] Finally the lipid solution was filtered through 0.45 µm polycarbonate membrane to obtain the dye loaded LUVs. The formation of LUVs was confirmed by TEM or FESEM images. The dye leakage assay was performed on a Fluoromax-4, Horiba instrument.

Liquid chromatography

All crude peptides were purified by RP-HPLC (reverse phase-high performance liquid chromatography) using C_{18}-µ Bondapak semi preparative column on Waters 600E at a flow rate of 5 mL/min. Binary solvent system were used, solvent A (0.1% TFA in H_2O) and solvent B (0.1% TFA in CH_3CN). A Waters 2489 UV detector was used with an option of dual detection at 214 and 254 nm (in some cases 280 nm and 330 nm were used). A total run time of 20 min was used and gradient used for purification was 5−100% CH_3CN for 18 min followed by 100% CH_3CN till 20 min.

Purity of the peptides was confirmed from Waters UPLC-MS system (ESI +ve mode), Micromass Q-TOF equipped with Masslynx software was used. Mobile phase comprised of solvent A (0.1% TFA in H_2O) and solvent B (0.1% TFA in CH_3CN) on C_{18} column with a flow rate of 0.25 mL/min. dual wavelength were selected at 214 nm and 254 nm (in some cases 280 nm and 330 nm were used). Linear gradient of 5 to 100% CH_3CN was used in a total run time of 8 min.

Purity was also confirmed using Waters 600E Analytical HPLC system, Waters C_{18} analytical column at a flow rate of 1 mL/min, linear gradient of 5-100% CH_3CN over 18 minutes in a total run time of 20 min. Dual wavelength was selected at 214 nm and 254 nm (in some cases 280 nm and 330 nm were used).

Mass spectrometry

Mass of the synthesized peptides were analyzed using two different instruments on Waters UPLC-MS (ESI +ve mode) Micromass Q-TOF equipped with Masslynx software and Agilent-Q-TOF 6500 instrument (ESI +ve mode) was used equipped with Mass hunter work station software.

Ultraviolet (UV) absorption

The purified peptide samples were dissolved in PBS (50 mM, pH 7.4) to obtain the desire concentration (5, 10 or 20 μM for peptide **2A** and **2B**). The stock solution was used directly used for UV study using an UV cuvette of path length 1 cm. Spectra were recorded from 200 nm to 500 nm on Lamda 750 PerkinElmer instrument.

Circular dichroism (CD)

The purified peptide samples alone and in some cases mixed with other peptides (in case of inhibition study) were dissolved in PBS (50 mM, pH 7.4) and sodium acetate buffer

(50 mM, pH 4.0) as required to obtain desired concentration (50 μM in case of $A\beta_{1-40}$). 400 μL of the sample was taken in a cuvette of 1 mm path length and CD study was performed. The spectra were recorded as an average of three measurements, from 190 nm to 260 nm on JASCO J-815 instrument.

Fourier Transformation Infra-Red Spectroscopy (FTIR)

The purified peptide samples alone and in some cases mixed with other peptides (in case of inhibition study) were dissolved in PBS (50 mM, pH 7.4) and sodium acetate buffer (50 mM, pH 4.0) as required to obtain desired concentration (50 μM in case of $A\beta_{1-40}$). 20 μL of the peptide sample from the stock was mixed with activated KBr and a pellet was prepared. At first, background was obtained followed by sample with total 20 scans using Thermo Scientific instrument.

Raman Spectroscopy

The purified peptide samples were dissolved in PBS (50 mM, pH 7.4) to obtain the desire concentration (20 μM for peptide **2B**). 600 μL of peptide solution was placed in a fluorescence cuvette with path length of 1 cm. The samples were excited at 488 nm with an Ar+ ion laser and spectra were recorded from 500 to 2000 cm^{-1}on HORIBA Jobin Yvon, Model LabRAM HR Raman spectroscope. The spectra were recorded after 20 accumulations and plotted using OriginPro 8 software.

Thioflavin T (ThT) fluorescence assay

ThT stock solution was prepared at a concentration of 3.14 mM, stored at 4 °C with proper protection from light to prevent quenching.[92] Before fluorescence study the ThT was diluted to 50 μM. Purified peptide samples (amyloidogenic peptide alone and in some cases mixed with breaker peptide) were dissolved in PBS (50 mM, pH 7.4) to obtain a stock solution of 100 μM to 500 μM (50 μM in the case of $A\beta_{1-40}$ peptide) and incubated

at 37 °C on a water bath. Then, for ThT assay at different time intervals the required peptide samples (40 μL) was mixed with 200 μL of ThT (50 μM) solution and total volume was made up to 400 μL (final cuvette concentration: 2 to 5 μM and thioflavin T: 25 μM). Fluorescence emission was measured at 485 nm and excitation of 435 nm, slit of 3 nm on Fluoromax-4, Horiba instrument.

Time resolved photoluminescence (TRPL)

For measurement of life time of a fluorophore we have used TRPL study. The peptide samples (peptide **6C**, **6D** and **6E**)) were dissolved in PBS (in presence of 3% DMSO) to make a solution of concentration ~20 μM. Then, 600 μL of peptide sample was placed in a 1 mL fluorescence cuvette and measure the excited state life time on Eddinburg FSP920 Instrument.

Transmission electron microscopy (TEM)

10 μL aliquot from the stock peptide solution (50 μM in case of $A\beta_{1-40}$) after incubation of 5 days (7 days in case of $A\beta_{1-40}$) was added over the dark side of carbon coated copper grid and allowed to float for 1 min. Then 2% uranyl acetate solution (10 μL) was added on the same grid and was allowed to float for another 1 min. The excess solution was removed using blotting paper. The sample was dried at room temperature and was kept in desiccator before taking TEM analysis on JEOL (Model: JEM 2100) instrument at 200 kV.

Congo-red birefringence

Commercially available Congo red was dissolved in 80% aqueous ethanol to prepare a saturated solution. Then saturated solution of sodium chloride was added into the saturated Congo red solution and filtered to obtain required Congo red solution for analysis.[23] After 5 days of incubation (7 days in case of $A\beta_{1-40}$) of the peptide solution, a 20 μL aliquot of the required peptide solution was placed over a glass slide followed by

20 µL of the saturated Congo red solution and the sample was dried at room temperature, and was kept in desiccator before birefringence analysis under a Leica ICC50 HD polarizable microscope.

Field Emission Scanning Electron Microscope (FESEM)

The formation of LUVs was confirmed by FESEM. 10µL lipid vesicle solution from the stock of 100 µM was added over the clean glass slide covered with aluminum foil, allowed to dry at room temperature, and kept in desiccators before taking FESEM analysis on Ziess, Sigma VP instrument.

7.2 Solid Phase Peptide Synthesis (SPPS) protocol:

The syntheses were performed manually on a Stuart blood tube rotator (20 rpm) using reported protocols.[107,108] The rink amide MBHA resin (loading of 1.1 mmol/g) was taken into a 5 mL frit-fitted plastic syringe and swollen in DCM for 2 h followed by DMF for 1h. Distilled DCM and N_2 purged DMF were used for the syntheses.

Coupling reaction

For a standard coupling, 2 equivalents of Fmoc amino acid was dissolved in DMF and added to the resin. 2.5 equivalents of BOP or PyBOP and 5 equivalents of DIPEA were added to that later. Coupling time varied from 45 min to 6 h (depending on amino acids). In case of incomplete coupling, the step was repeated. Resin was washed with DMF and DCM for 5 min each (1 min x 5) after each coupling. All couplings were performed at room temperature.

Fmoc deprotection

For N_{α}-Fmoc deprotection, 20% piperidine in DMF was used for 21 min (7 min x 3). Resin was washed with DMF and DCM for 5 min each (5 x 1 min) after deprotection.

Esterification method (for switch peptides)

3 equivalents of Boc-Ser(OH)-OH was dissolved in DMF and added to the resin followed by 3 equivalents of BOP and 7 equivalents of DIPEA were added to the reaction vessel. The coupling time was kept for 2 h. The next amino acid coupling with the serine side chain formed an iso-peptide linkage (ester).

***N*-methylation on amino acids[108]**

For *N*-methylation, first *o*-NBS protection was performed on Fmoc deprotected resin using 4 equivalents *o*-NBS-Cl and 10 equivalents of *sym*-collidine in DMF for 30 min (2 x 15 min). Then the resin was washed with DMF for 5 min (5 x 1 min). After that the resin was washed with dry THF for 4 min (2 x 2 min) followed by addition of 5 equivalents of triphenylphosphine and 10 equivalents of MeOH in THF. Then, 5 equivalents of DIAD was dissolved in dry THF and slowly added to the resin and kept for 2h (2 x 1h) to get the *N*-methylation. Later the *o*-NBS group was removed using a mixture of 2-Mercaptoethanol (10 equivalents) and DBU (5 equivalents) in DMF for 30 min (3 x 10 min) to get the desired *N*-methylated product.

Kaiser test [146]

Kaiser A: 0.5 g ninhydrin in 10 mL ethanol

Kaiser B: 0.4 mL of 0.001M KCN_{aq} in 20 mL of pyridine.

To monitor the complete coupling Kaiser test was performed. A few beads of resin were placed in a small fusion tube and 50 µL of Kaiser A and 50 µL Kaiser B were added. Tube was heated at 80 °C for 5 min over a sand bath. A positive test is indicated by the presence of blue or purple color.

Acetylation/ capping

After repeating the coupling step when positive Kaiser test was observed, acetylation was performed. 3 equivalents of Ac_2O and 3 equivalents of *N*-methyl imidazole were mixed in DCM and added to the resin and the reaction was carried out for 1h (2 x 30 min).

Cleavage of peptide from the resin

The Rink amide MBHA resin was treated with a solution of TFA/DCM/H_2O (9/0.5/0.5) for 3h. Approximately 1 mL of the cocktail solution was used for 100 mg of the resin. After cleavage the crude peptide was precipitated using cold diethyl ether, centrifuged to obtained solid crude which later purified by semi preparative HPLC.

7.3. Synthetic procedure of the individual designed peptides:

Peptide 2A (*Ac-Ser-Leu-Ser-Leu-(H^+)Ser-Leu-Ser-Leu-Ser-Leu-Gly-NH_2*)

The switch peptide **2A** was synthesized on 300 mg of Rink amide MBHA resin (loading 1.1 mmol/g). Each coupling was performed with 2 equivalents of Fmoc amino acid, 2.5 equivalents of BOP and 5 equivalents of DIPEA. After each coupling resin was washed with DMF and DCM for 5 min each (5 x 1 min) and Kaiser test was performed. Fmoc group was removed using 20% piperidine in DMF mixture for 21 min (3 x 7 min). Finally, the peptide was cleaved from the resin using a mixture of TFA/DCM/H_2O

(9/0.5/0.5) 3 mL for 3 h. The crude peptide was precipitated using cold diethyl ether, centrifuged and washed 3 times with ether. Peptide was purified on semi preparative HPLC (C_{18} μ-Bondapak, a linear gradient was used from 5 to 100% CH_3CN till 18 min in a total run time of 20 min) and lyophilized to obtain pure peptide **2A**.

Texture: Fluffy white powder

Yield: 51 mg; 13.8%, with respect to the resin loading

ESI-MS: (m/z) 1117.67 $[M+H]^+$

HPLC: Retention time (t_R) 9.5 min (C_{18}, a linear gradient from 5 to 100% CH_3CN till 18 min in a total run time of 20 min).

Peptide 2B (*Ac-Ser-Leu-Ser-Leu-His-Gln-Lys-Leu-Val-Phe-Phe-(H^+)Ser-Glu-Asp-Val-Ser-Leu-Gly-NH_2*)

The Aβ derived switch peptide **2B** was synthesized on 300 mg of Rink amide MBHA resin (loading 1.1 mmol/g). Each coupling was performed with 2 equivalents of Fmoc amino acid, 2.5 equivalents of BOP and 5 equivalents of DIPEA. After each coupling resin was washed with DMF and DCM for 5 min each (1 x 5 min) and Kaiser test was performed. Fmoc group was removed using 20% piperidine in DMF mixture for 21 min (3 x 7 min). Finally, the peptide was cleaved from the resin using a mixture of TFA/DCM/H_2O (9/0.5/0.5) 3 mL for 3 h. The crude peptide was precipitated using cold diethyl ether, centrifuged and washed 3 times with ether. Peptide was purified on semi preparative HPLC (C_{18} μ-Bondapak, a linear gradient was used from 5 to 100% CH_3CN till 18 min in a total run time of 20 min) and lyophilized to obtain pure peptide **2B**.

Texture: Fluffy white powder

Yield: 51 mg; 8.4%, with respect to the resin loading

ESI-MS: (m/z) 2048.12 $[M+H]^+$, 1024.55 $[M+2H]^{2+}$, 683.36 $[M+3H]^{3+}$.

HPLC: t_R 11 min (C_{18}, a linear gradient from 5 to 100% CH_3CN till 18 min in a total run time of 20 min).

Peptide 2C *(Ac-Leu-Pro-Phe-Phe-Asp-NH_2)*

The β-sheet breaker peptide (BSBp) **2C** was synthesized on 300 mg of Rink amide MBHA resin (loading 1.1 mmol/g). Each coupling was performed with 2 equivalents of Fmoc amino acid, 2.5 equivalents of BOP and 5 equivalents of DIPEA. After each coupling resin was washed with DMF and DCM for 5 min each (5 x 1 min) and Kaiser test was performed. Fmoc group was removed using 20% piperidine in DMF mixture for 21 min (3 x 7 min). Finally, the peptide was cleaved from the resin using a mixture of TFA/DCM/H_2O (9/0.5/0.5) 3 mL for 3 h. The crude peptide was precipitated using cold diethyl ether, centrifuged and washed 3 times with ether. Peptide was purified on semi preparative HPLC (C_{18} μ-Bondapak, a linear gradient was used from 5 to 100% CH_3CN till 18 min in a total run time of 20 min) and lyophilized to obtain pure peptide **2C**.

Texture: White powder

Yield: 43 mg; 19%, with respect to the resin loading

ESI-MS: (m/z) 679.35 $[M+H]^+$.

HPLC: t_R 11.8 min (C_{18}, a linear gradient from 5 to 100% CH_3CN till 18 min in a total run time of 20 min).

Peptide 2D *(Ac-Leu-Val-Phe-Phe-Asp-NH_2)*

The β-sheet breaker peptide **2D** was synthesized on 300 mg of Rink amide MBHA resin (loading 1.1 mmol/g). Each coupling was performed with 2 equivalents of Fmoc amino acid, 2.5 equivalents of BOP and 5 equivalents of DIPEA. After each coupling resin was

washed with DMF and DCM for 5 min each (5 x 1 min) and Kaiser test was performed. Fmoc group was removed using 20% piperidine in DMF mixture for 21 min (3 x 7 min). Finally, the peptide was cleaved from the resin using a mixture of TFA/DCM/H_2O (9/0.5/0.5) 3 mL for 3 h. The crude peptide was precipitated using cold diethyl ether, centrifuged and washed 3 times with ether. Peptide was purified on semi preparative HPLC (C_{18} μ-Bondapak, a linear gradient was used from 5 to 100% CH_3CN till 18 min in a total run time of 20 min) and lyophilized to obtain pure peptide **2D**.

Texture: White powder

Yield: 47 mg; 21%, with respect to the resin loading

ESI-MS: (m/z) 681.34 $[M+H]^+$.

HPLC: t_R 11.4 min (C_{18}, a linear gradient from 5 to 100% CH_3CN till 18 min in a total run time of 20 min).

Peptide 3A *(H-Leu-Ser-Leu-(H^+)Ser-Leu-Ser-Leu-Gly-NH_2)*

The switch peptide **3A** was synthesized on 300 mg of Rink amide MBHA resin (loading 1.1 mmol/g). Each coupling was performed with 2 equivalents of Fmoc amino acid, 2.5 equivalents of BOP and 5 equivalents of DIPEA. After each coupling resin was washed with DMF and DCM for 5 min each (5 x 1 min) and Kaiser test was performed. Fmoc group was removed using 20% piperidine in DMF mixture for 21 min (3 x 7 min). Finally, the peptide was cleaved from the resin using a mixture of TFA/DCM/H_2O (9/0.5/0.5) 3 mL for 3 h. The crude peptide was precipitated using cold diethyl ether, centrifuged and washed 3 times with ether. Peptide was purified on semi preparative HPLC (C_{18} μ-Bondapak, a linear gradient was used from 5 to 100% CH_3CN till 18 min in a total run time of 20 min) and lyophilized to obtain pure peptide **3A**.

Texture: White powder

Yield: 32 mg; 12.3%, with respect to the resin loading

ESI-MS: (m/z) 788.49 $[M+H]^+$ and 394.73 $[M+2H]^{2+}$.

HPLC: t_R 9.6 min (C_{18}, a linear gradient from 5 to 100% CH_3CN till 18 min in a total run time of 20 min).

Peptide 3B *(H-Leu-Ser-Leu-Ant-Leu-Ser-Leu-Gly-NH_2)*

The anthranilic acid (Ant) containing β-sheet breaker hybrid peptide (BSBHp) **3B** was synthesized on 300 mg of Rink amide MBHA resin (loading 1.1 mmol/g). Each coupling was performed with 2 equivalents of Fmoc amino acid, 2.5 equivalents of BOP and 5 equivalents of DIPEA. After each coupling resin was washed with DMF and DCM for 5 min each (5 x 1 min) and Kaiser test was performed. Fmoc group was removed using 20% piperidine in DMF mixture for 21 min (3 x 7 min). Finally, the peptide was cleaved from the resin using a mixture of TFA/DCM/H_2O (9/0.5/0.5) 3 mL for 3 h. The crude peptide was precipitated using cold diethyl ether, centrifuged and washed 3 times with ether. Peptide was purified on semi preparative HPLC (C_{18} μ-Bondapak, a linear gradient was used from 5 to 100% CH_3CN till 18 min in a total run time of 20 min) and lyophilized to obtain pure peptide **3B**.

Texture: Pale yellow color powder

Yield: 21 mg; 7.7%, with respect to the resin loading

ESI-MS: (m/z) 820.50 $[M+H]^+$.

HPLC: t_R 11.1 min (C_{18}, a linear gradient from 5 to 100% CH_3CN till 18 min in a total run time of 20 min).

Peptide 3C *(Ac-Ant-Leu-Ser-Leu-Gly-NH_2)*

The anthranilic acid (Ant) containing BSBHp **3C** was synthesized on 300 mg of Rink amide MBHA resin (loading 1.1 mmol/g). Each coupling was performed with 2 equivalents of Fmoc amino acid, 2.5 equivalents of BOP and 5 equivalents of DIPEA. After each coupling resin was washed with DMF and DCM for 5 min each (5 x 1 min) and Kaiser test was performed. Fmoc group was removed using 20% piperidine in DMF mixture for 21 min (3 x 7 min). Finally, the peptide was cleaved from the resin using a mixture of TFA/DCM/H_2O (9/0.5/0.5) 3 mL for 3 h. The crude peptide was precipitated using cold diethyl ether, centrifuged and washed 3 times with ether. Peptide was purified on semi preparative HPLC (C_{18} μ-Bondapak, a linear gradient was used from 5 to 100% CH_3CN till 18 min in a total run time of 20 min) and lyophilized to obtain pure peptide **3C**.

Texture: Pale yellowish powder

Yield: 23 mg; 12.7%, with respect to the resin loading

ESI-MS: (m/z) 549.31 $[M+H]^+$.

HPLC: t_R 9.5 min (C_{18}, a linear gradient from 5 to 100% CH_3CN till 18 min in a total run time of 20 min).

Peptide 4A *(Ac-Leu-Ant-Phe-Phe-Asp-NH_2)*

The anthranilic acid (Ant) containing BSBHp **4A** was synthesized on 300 mg of Rink amide MBHA resin (loading 1.1 mmol/g). Each coupling was performed with 2 equivalents of Fmoc amino acid, 2.5 equivalents of BOP and 5 equivalents of DIPEA. After each coupling resin was washed with DMF and DCM for 5 min each (5 x 1 min) and Kaiser test was performed. Fmoc group was removed using 20% piperidine in DMF

mixture for 21 min (3 x 7 min). Finally, the peptide was cleaved from the resin using a mixture of TFA/DCM/H_2O (9/0.5/0.5) 3 mL for 3 h. The crude peptide was precipitated using cold diethyl ether, centrifuged. Peptide was purified on semi preparative HPLC (C_{18} µ-Bondapak, a linear gradient was used from 5 to 100% CH_3CN till 18 min in a total run time of 20 min) and lyophilized to obtain pure peptide **4A**.

Texture: Pale yellowish powder

Yield: 17 mg; 7.6%, with respect to the resin loading

ESI-MS: (m/z) 701.34 $[M+H]^+$.

HPLC: t_R 12.3 min (C_{18}, a linear gradient from 5 to 100% CH_3CN till 18 min in a total run time of 20 min).

Peptide 5A *(Ac-Leu-Asp(OBzl)-Phe-Phe-Asp-NH_2)*

The Pro-Drug peptide (PDp) **5A** was synthesized on 300 mg of Rink amide MBHA resin (loading 1.1 mmol/g). Each coupling was performed with 2 equivalents of Fmoc amino acid, 2.5 equivalents of BOP and 5 equivalents of DIPEA. After each coupling resin was washed with DMF and DCM for 5 min each (5 x 1 min) and Kaiser test was performed. Fmoc group was removed using 20% piperidine in DMF mixture for 21 min (3 x 7 min). Finally, the peptide was cleaved from the resin using a mixture of TFA/DCM/H_2O (9/0.5/0.5) 3 mL for 3 h. The crude peptide was precipitated using cold diethyl ether, centrifuged and washed 3 times with ether. Peptide was purified on semi preparative HPLC (C_{18} µ-Bondapak, a linear gradient was used from 5 to 100% CH_3CN till 18 min in a total run time of 20 min) and lyophilized to obtain pure peptide **5A**.

Texture: White powder

Yield: 24 mg; 9.2%, with respect to the resin loading

ESI-MS: (m/z) 787.37 $[M+H]^+$.

HPLC: t_R 13 min (C_{18}, a linear gradient from 5 to 100% CH_3CN till 18 min in a total run time of 20 min).

Peptide 6A *(H_2N-Ala-(N-Me)Phe-Phe-(N-Me)Val-Leu-Gly-Suc-PEG_3-Adi-Gly-(N-Me)Leu-Val-(N-Me)Phe-Phe-Ala-NH_2)*

The zipper peptide **6A** was synthesized on 300 mg of Rink amide MBHA resin (loading 1.1 mmol/g) using the same protocol mentioned above (Section 7.2). We first synthesized one zipper strand, peptide fragment **6P** (HO-Adi-Gly-(*N*-Me)Leu-Val-(*N*-Me)Phe-Phe-Ala-NH_2, Adi = Adipic acid) separately and attached to other strand, a resin bounded peptide, H-PEG_3-Suc-Gly-Leu-(*N*-Me)Val-Phe-(*N*-Me)Phe-Ala-Resin (Suc = Succinic acid) using PyBOP (3 equivalents) and DIPEA (7 equivalents) to get the desired zipper peptide **6A**, in which the two zipper strands were retro-inverso peptide to one another. Each coupling was performed with 2 equivalents of Fmoc amino acid, 2.5 equivalents of BOP and 5 equivalents of DIPEA. After each coupling resin was washed with DMF and DCM for 5 min each (5 x 1 min) and Kaiser test was performed. Fmoc group was removed using 20% piperidine in DMF mixture for 21 min (7 min x 3). The final zipper peptide was cleaved from the resin using a mixture of TFA/DCM/H_2O (9/0.5/0.5) 3 mL for 3 h. The crude peptide was precipitated using cold diethyl ether. Due to hydrophobicity in the peptide precipitate was very less. Therefore, the excess ether was evaporated and the crude peptide was purified on semi preparative HPLC (C_{18} µ-Bondapak, a linear gradient was used from 5 to 20% CH_3CN till 2 min and 20 to 100% CH_3CN till 18 min in a total run time of 20 min) and lyophilized to obtain pure zipper peptide **6A**.

Texture: Off-white solid

Yield: 14.6 mg; 2.5%, with respect to the resin loading

ESI-MS: (m/z) 1773.38 $[M+H]^+$ and 887.14 $[M+2H]^{2+}$.

HPLC: t_R 12.8 min (C_{18}, a linear gradient from 5 to 20% CH_3CN till 2 min and 20 to 100% CH_3CN till 18 min in a total run time of 20 min).

Peptide 6B *(Ac-Gly-(N-Me)Leu-Val-(N-Me)Phe-Phe-Ala-NH_2)*

The *N*-methylated control peptide **6B** was synthesized on 300 mg of Rink amide MBHA resin (loading 1.1 mmol/g). Each coupling was performed with 2 equivalents of Fmoc amino acid, 2.5 equivalents of BOP and 5 equivalents of DIPEA. After each coupling resin was washed with DMF and DCM for 5 min each (5 x 1 min) and Kaiser test was performed. Fmoc group was removed using 20% piperidine in DMF mixture for 21 min (3 x 7 min). Finally, the peptide was cleaved from the resin using a mixture of TFA/DCM/H_2O (9/0.5/0.5) 3 mL for 3 h. The crude peptide was precipitated using cold diethyl ether, centrifuged and washed 3 times with ether. Peptide was purified on semi preparative HPLC (C_{18} μ-Bondapak, a linear gradient was used from 5 to 100% CH_3CN till 18 min in a total run time of 20 min) and lyophilized to obtain pure peptide **6B**.

Texture: White powder

Yield: 16 mg; 6.7%, with respect to the resin loading

ESI-MS: (m/z) 722.61 $[M+H]^+$.

HPLC: t_R 10.7 min (C_{18}, a linear gradient from 5 to 100% CH_3CN till 18 min in a total run time of 20 min).

Peptide 6C *(H_2N-Ala-(N-Me)Phe-Phe-(N-Me)Val-Leu-Gly-Suc-PEG_3-Adi-Gly-(N-Me)Leu-Val-(N-Me)Phe-Phe-Ala-Trp-NH_2)*

The Tryptophan attached zipper peptide **6C** was synthesized on 300 mg of Rink amide MBHA resin (loading 1.1 mmol/g). Similar to peptide **6A**, we first synthesized one zipper strand, peptide fragment **6Q** (H-PEG_3-Suc-Gly-Leu-(*N*-Me)Val-Phe-(*N*-Me)Phe-Ala-NH_2**,** Suc =succinic acid) separately and attached to another zipper strand, a resin bounded peptide fragment (HO-Adi-Gly-(*N*-Me)Leu-Val-(*N*-Me)Phe-Phe-Ala-Trp-Resin) in presence of PyBOP (3 equivalents) and DIPEA (7 equivalents) to get the desired zipper peptide **6C**, in which the two zipper strands were retro-inverso peptide to one another. Each coupling was performed with 2 equivalents of Fmoc amino acid, 2.5 equivalents of BOP and 5 equivalents of DIPEA. After each coupling resin was washed with DMF and DCM for 5 min each (5 x 1 min) and Kaiser test was performed. Fmoc group was removed using 20% piperidine in DMF mixture for 21 min (3 x 7 min). The final peptide **6C** was cleaved from the resin using a mixture of TFA/DCM/H_2O (9/0.5/0.5) 3 mL for 3 h. The crude peptide was precipitated using cold diethyl ether. Due to hydrophobicity in the peptide precipitate was very less. Therefore, the excess ether was evaporated and the crude peptide was purified on semi preparative HPLC (C_{18} μ-Bondapak, a linear gradient was used from 5 to 20% CH_3CN till 2 min and 20 to 100% CH_3CN till 18 min in a total run time of 20 min) and lyophilized to obtain pure peptide **6C**.

Texture: Off-white solid

Yield: 7 mg; 1.1%, with respect to the resin loading

ESI-MS: (m/z) 1959.38 $[M+H]^+$, 980.06 $[M+ 2H]^{2+}$ and 653.71 $[M+3H]^{3+}$

HPLC: t_R 12 min (C_{18}, a linear gradient from 5 to 20% CH_3CN till 2 min and 20 to 100% CH_3CN till 18 min in a total run time of 20 min).

Peptide 6D *(H_2N-(Dansyl)Dap-Ala-(N-Me)Phe-Phe-(N-Me)Val-Leu-Gly-Suc-PEG_3-Adi-Gly-(N-Me)Leu-Val-(N-Me)Phe-Phe-Ala-NH_2)*

The dansyl attached zipper peptide **6D** was synthesized on 300 mg of Rink amide MBHA resin (loading 1.1 mmol/g). Similar to peptide **6A**, we first synthesized one zipper strand, a peptide fragment **6P** (HO-Adi-Gly-(*N*-Me)Leu-Val-(*N*-Me)Phe-Phe-Ala-NH_2, Adi = Adipic acid) separately and attached to another zipper strand, a resin bounded peptide fragment, H-PEG_3-Suc-Gly-Leu-(*N*-Me)Val-Phe-(*N*-Me)Phe-Ala-(Dansyl)Dap-Resin (Dap = (S)-2,3-diaminopropanoic acid, dansyl was attached at 3-amino position in Dap) in presence of PyBOP (3 equivalents) and DIPEA (7 equivalents) to get the desired zipper peptide **6D**, in which the two zipper strands were retro-inverso peptide to one another. Each coupling was performed with 2 equivalents of Fmoc amino acid, 2.5 equivalents of BOP and 5 equivalents of DIPEA. After each coupling resin was washed with DMF and DCM for 5 min each (5 x 1 min) and Kaiser test was performed. Fmoc group was removed using 20% piperidine in DMF mixture for 21 min (3 x 7 min). The final peptide **6D** was cleaved from the resin using a mixture of TFA/DCM/H_2O (9/0.5/0.5) 3 mL for 3 h. The crude peptide was precipitated using cold diethyl ether. Due to hydrophobicity in the peptide precipitate was very less. Therefore, the excess ether was evaporated and the crude peptide was purified on semi preparative HPLC (C_{18} μ-Bondapak, a linear gradient was used from 5 to 20% CH_3CN till 2 min and 20 to 100% CH_3CN till 18 min in a total run time of 20 min) and lyophilized to obtain pure peptide **6D**.

Texture: Pale yellowish solid

Yield: 5.9 mg; 0.8%, with respect to the resin loading

ESI-MS: (m/z) 2092.38 $[M+H]^+$, 1046.57 $[M+2H]^{2+}$ and 698.04$[M+3H]^{3+}$.

HPLC: t_R 13.7 min (C_{18}, a linear gradient from 5 to 20% CH_3CN till 2 min and 20 to 100% CH_3CN till 18 min in a total run time of 20 min).

Peptide 6E *(H_2N-(Dansyl)Dap-Ala-(N-Me)Phe-Phe-(N-Me)Val-Leu-Gly-Suc-PEG_3-Adi-Gly-(N-Me)Leu-Val-(N-Me)Phe-Phe-Ala-Trp-NH_2)*

The donor and acceptor fluorophore containing zipper peptide **6E** was synthesized on 300 mg of Rink amide MBHA resin (loading 1.1 mmol/g). Similar to peptide **6A**, we first synthesized one zipper strand, a peptide fragment **6R** (H-PEG_3-Suc-Gly-Leu-(*N*-Me)Val-Phe-(*N*-Me)Phe-Ala-(Dansyl)Dap-NH_2; Dap = (*S*)-2,3-diamino propanoic acid, dansyl was attached at 3-amino position in Dap) separately and attached to another zipper strand, a resin bounded peptide fragment (HO-Adi-Gly-(*N*-Me)Leu-Val-(*N*-Me)Phe-Phe-Ala-Trp-Resin) in presence of PyBOP (3equivalents) and DIPEA (7 equivalents) to get the desired zipper peptide **6E,** in which the two zipper strands were retro-inverso peptide to one another. Each coupling was performed with 2 equivalents of Fmoc amino acid, 2.5 equivalents of BOP and 5 equivalents of DIPEA. After each coupling resin was washed with DMF and DCM for 5 min each (5 x 1 min) and Kaiser test was performed. Fmoc group was removed using 20% piperidine in DMF mixture for 21 min (3 x 7 min). The final peptide **6E** was cleaved from the resin using a mixture of TFA/DCM/H_2O (9/0.5/0.5) 3 mL for 3 h. The crude peptide was precipitated using cold diethyl ether. Due to hydrophobicity in the peptide, precipitate was very less. Therefore, the excess ether was evaporated and the crude peptide was purified on semi preparative HPLC (C_{18} μ-Bondapak, a linear gradient was used from 5 to 20% CH_3CN till 2 min and 20 to 100% CH_3CN till 18 min in a total run time of 20 min) and lyophilized to obtain pure peptide **6E**.

Texture: Pale yellowish solid

Yield: 6 mg; 0.8%, with respect to the resin loading

ESI-MS: (m/z) 2278.55 $[M+H]^+$, 1139.74 $[M+2H^{2+}$ and 760.17 $[M+3H]^{3+}$.

HPLC: t_R 14.6 min (C_{18}, a linear gradient from 5 to 20% CH_3CN till 2 min and 20 to 100% CH_3CN till 18 min in a total run time of 20 min).

7.4. Supporting data:

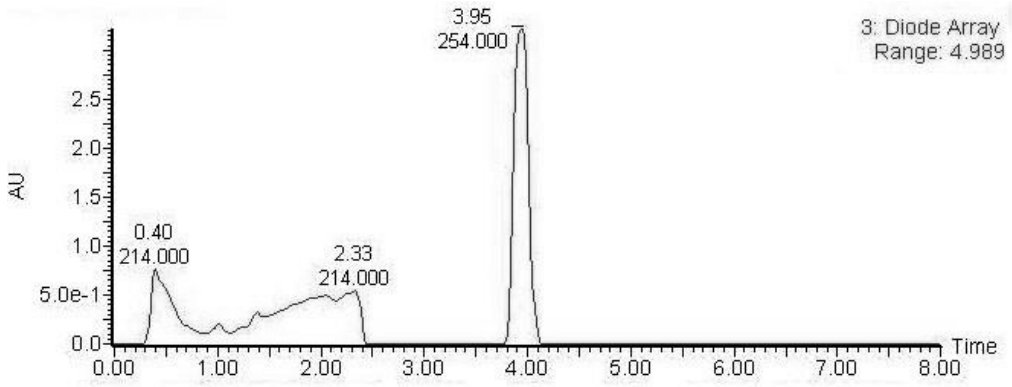

Figure 7.1: LC-MS profile of peptide **6P**. t_R 3.95 min (C_{18}: a linear gradient from 5 to 20% CH_3CN for 2 min; 20 to 100% CH_3CN for 2 to 7 min, in a total run time of 8 min).

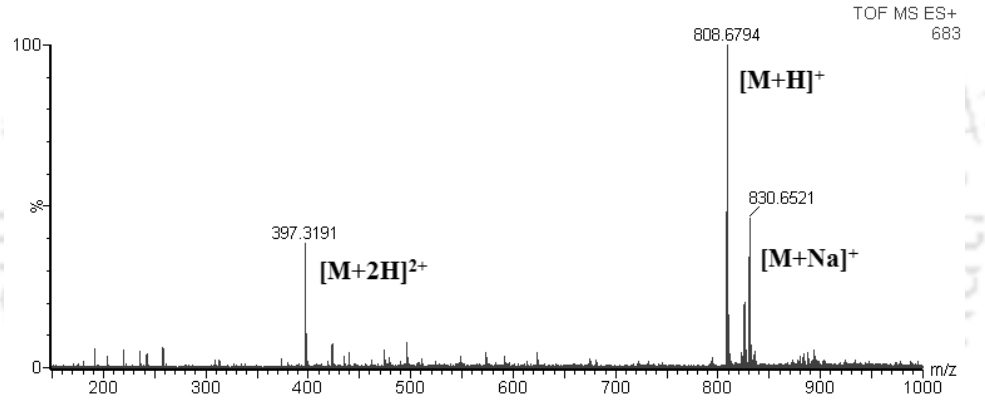

Figure 7.2: Mass spectrum of peptide **6P**. Calculated mass for $C_{42}H_{62}N_7O_9$ is 808.46 $[M+H^+]$, observed 808.67 $[M+H]^+$, 830.65 $[M+Na]^+$ and 397.32 $[M+2H]^+$.

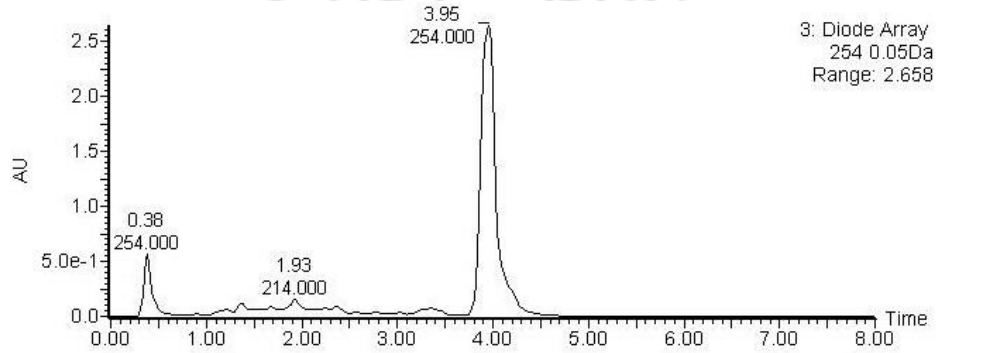

Figure 7.3: LC-MS profile of peptide **6Q**. t_R 3.95 min (C_{18}: a linear gradient from 5 to 25% CH_3CN for 2 min; 25 to 100% CH_3CN for 2 to 7 min, in a total run time of 8 min).

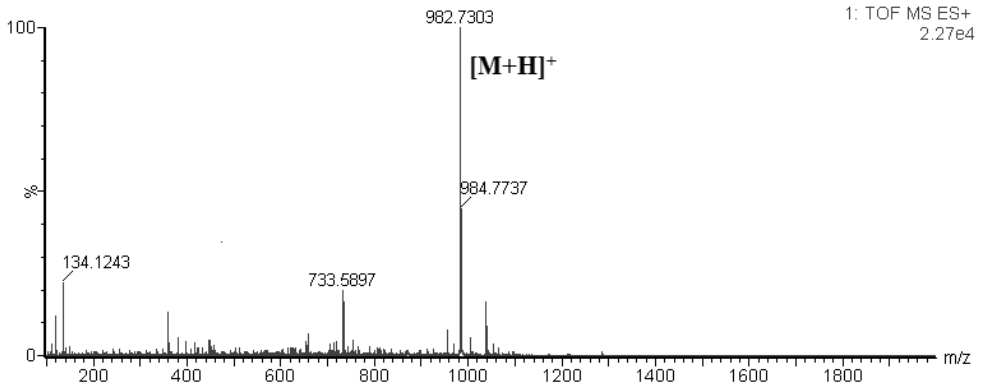

Figure 7.4: Mass spectrum of peptide **6Q**. Calculated mass for $C_{50}H_{80}N_9O_{11}$ is 982.59 $[M+H^+]$, observed 982.73 $[M+H]^+$.

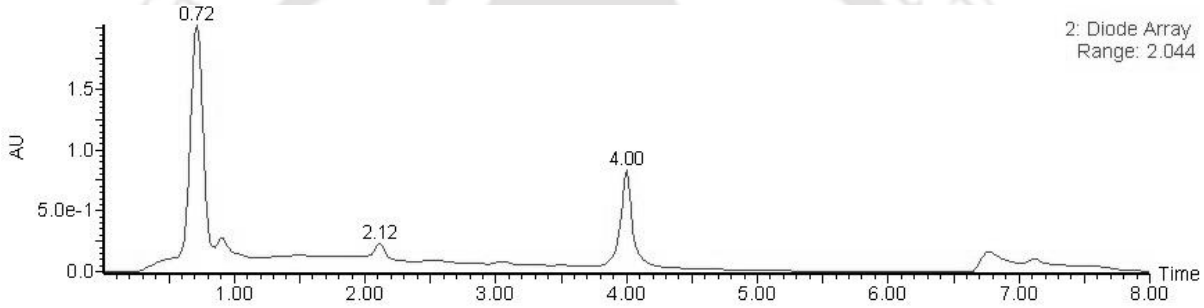

Figure 7.5: LC-MS profile of peptide **6R**. t_R 4.00 min (C_{18}: a linear gradient from 5 to 25% CH_3CN for 2 min; 25 to 100% CH_3CN for 2 to 7 min, in a total run time of 8 min).

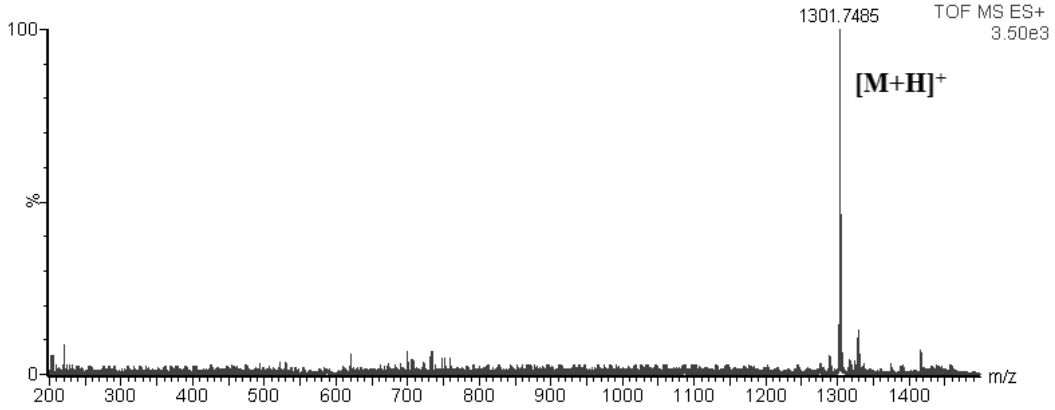

Figure 7.6: Mass spectrum of peptide **6R**. Calculated mass for $C_{65}H_{97}N_{12}O_{14}S$ is 1301.70 $[M+H^+]$, observed 1301.75 $[M+H]^+$.

Conclusions and future directions

Conclusions:

The work presented in this thesis mainly focused on the investigation on the early events of amyloid formation and the development of new strategies for Alzheimer's amyloid disruption.

In chapter 2, we have described an investigation on the early onset of protein aggregation using properly designed Amyloid-β derived switch-peptide (functional mimic of Aβ peptide) and from the experimental results we concluded that during the conformational transition, the aromatic side chains of the amyloidogenic peptide sequences interact prior to conformational transformation (random coil to β-sheet formation).

In chapter 3, we have described the introduction of anthranilic acid (Ant) containing β-sheet breaker hybrid peptides (BSBHps) and showed that the BSBHps were non-amyloidogenic in nature at physiological condition (pH 7.4 and 37 °C). The experimental evidences also support that the BSBHps were very efficient to inhibit the aggregation of model amyloidogenic peptide at the physiological condition.

In chapter 4, we extended the application of BSBHp on the aggregation of $A\beta_{1-40}$ peptide. We have designed and synthesized an Ant containing a BSBHp, keeping a recognition motif and showed that the BSBHp inhibited the aggregation of $A\beta_{1-40}$ peptide *in vitro* at physiological condition. The BSBHp also disrupted the pre-existing amyloid fibrils of $A\beta_{1-40}$ peptide into

non-toxic species. The BSBHp was found to be significantly efficient for the disruption of the Aβ amyloid present in human CSF sample *in vitro* at physiological condition.

In chapter 5, we have described another peptide based strategy, Pro-Drug peptide (PDp), for the disruption of Aβ aggregates into non-toxic species. From the experimental results it was clear that the PDp initially adopts a β-sheet structure which was essential to align with the $A\beta_{1-40}$ peptide in an aggregated assembly. Later the PDp generated a breaker element (aspartimide and aspartyl residues) at physiological condition, which disturbed the alignment with the aggregated $A\beta_{1-40}$ peptide and disrupted the $A\beta_{1-40}$ aggregates into non-toxic species. The PDp also effectively disrupted the Aβ aggregates present in human CSF sample *in vitro* at physiological condition.

In chapter 6, we have described another peptide based strategy of synthetic zipper peptide for the disruption of Aβ aggregates into non-toxic species. From the experimental results we concluded that the designed zipper peptide exists as soluble intra-molecular β-sheet monomer and the two ends of the peptide are close to each other (as evident from FRET study), which is highly supportive of a hairpin or zipper like structural orientation of the peptide. The zipper peptide effectively inhibited the aggregation of $A\beta_{1-40}$ peptide *in vitro* at physiological condition and also disrupted the pre-existing fibrils of $A\beta_{1-40}$ at same condition. The zipper peptide also efficiently disrupted the Aβ aggregates present in human CSF sample *in vitro* at physiological condition.

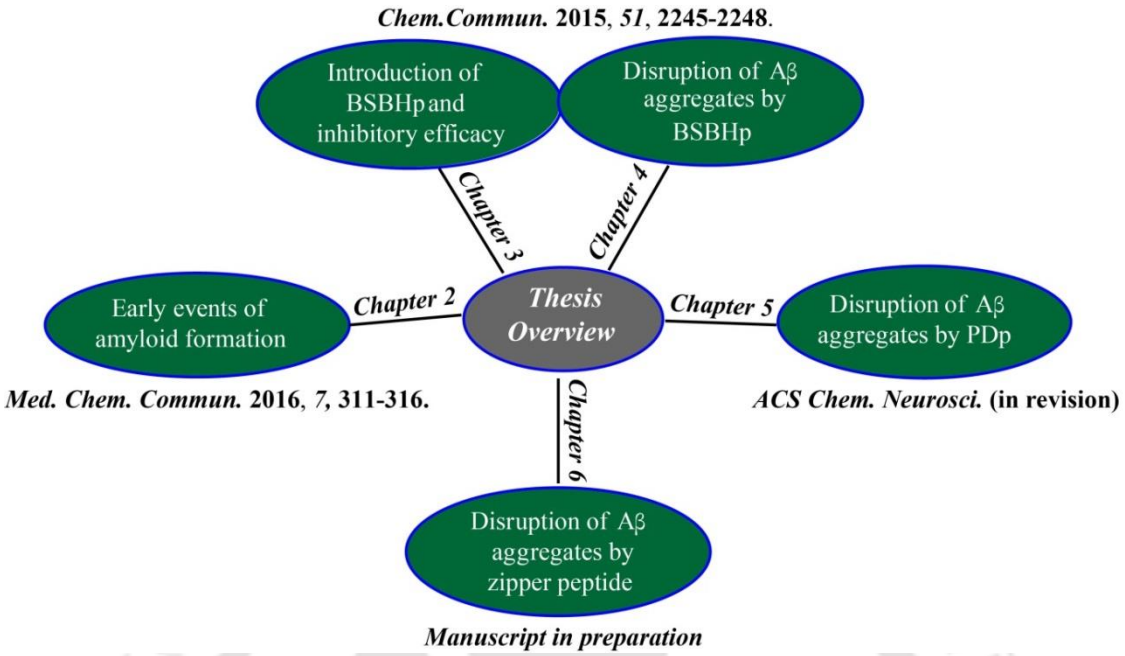

Future directions:

Although, we have demonstrated three new peptide based strategies for the disruption of Aβ aggregates *in vitro* at physiological condition, more wide-ranging investigations are required to make them suitable drug candidates against Alzheimer's disease. Next we would like to explore these strategies with the neuronal cell lines *in vitro* before in vivo experiments. In near future we also would like to explore these strategies on other amyloidogenic proteins like IAPP (responsible for diabetes type-2 disease) and α-Synuclein (responsible for Parkinson's disease) and the work is likely to be performed by my successors. We are also interested to explore the mechanism of the zipping action of zipper peptide in a molecular level, for that some more analogs of the zipper peptide need to be synthesized to check the interactions with Aβ peptide using suitable spectroscopic and biophysical tools including NMR, Fluorescence, CD and ITC, *etc*.

References:

1. Clamp, M., Fry, B., Kamal, M., Xie, X., Cuff, J., Lin, M. F., Kellis, M., Lindblad-Toh, K., and Lander, E. S. (2007) Distinguishing protein coding and noncoding genes in the human genome. *Proc. Natl. Acad. Sci. USA 104*, 19428-19433.
2. Berg, J., Tymoczko, J., and Stryer, L. (2002) *Biochemistry. (5th edition) New York: W H Freeman*.
3. Priller, C., Bauer, T., Mitteregger, G., Krebs, B., Kretzschmar, H. A., and Herms, J. (2006) Synapse formation and function is modulated by the amyloid precursor protein. *J. Neurosci. 26*, 7212–7221.
4. Petsko, G., and Ringe, D. (2004) *Protein structure and function. (1st edition) London: New Age Press*.
5. Nelson, D. L, and Cox, M. M. (2005) *Lehninger's Principles of Biochemistry (4th edition) New York, W. H. Freeman and Company*.
6. Ross, C. A., and Poirier, M. A. (2004) Protein aggregation and neurodegenerative disease. *Nat. Med. 10*, S10–S17.
7. Takalo, M., Salminen, A., Soininen, H., Hiltunen, M., and Haapasalo, A. (2013) Protein aggregation and degradation mechanisms in neurodegenerative diseases. *Am. J. Neurodegener. Dis.* 2, 1–14.
8. Raguse, T. L., Lai, J. R., LePlae, P. R. and Gellman, S. H. (2001) Toward β-peptide tertiary structure: self-association of an amphiphilic 14-helix in aqueous solution. *Org. Lett. 3*, 3963–3966.
9. Das, R., and Baker, D. (2008) Macromolecular modeling with rosetta. *Annu. Rev. Biochem. 77*, 363–382.
10. Rohl, C. A., Strauss, C. E., Misura, K.M., and Baker, D. (2004) Protein structure prediction using Rosetta. *Methods Enzymol. 383*, 66–93.
11. Soto, C. (1999) Alzheimer's and prion disease as disorders of protein conformation: implications for the design of novel therapeutic approaches. *J. Mol. Med.* 77, 412–418.
12. Gazit, E. (2002) The "Correctly Folded" State of Proteins: Is it a Metastable State? *Angew. Chem. Int. Ed. 41*, 257–259.
13. Wang, L., Maji, S.K., Sawaya, M.R., Eisenberg, D., and Riek, R. (2008) Bacterial inclusion bodies contain amyloid-like structure. *PLoS biology 6*, e195.

14. Greenwald, J., and Riek, R. (2010) Biology of Amyloid: Structure, Function, and Regulation. *Structure 18*, 1244–1260.
15. Knowles, T. P., Fitzpatrick, A. W., Meehan, S., Mott, H. R., Vendruscolo, M., Dobson, C. M., and Welland, M. E. (2007) Role of Intermolecular Forces in Defining Material Properties of Protein Nanofibrils. *Science 318*, 1900–1903.
16. Makin, O. S., and Serpell, L. C. (2005) Structures for amyloid fibrils. *FEBS Journal 272*, 5950–5961.
17. Tycko, R., and Wickner, R. B. (2013) Molecular Structures of Amyloid and Prion Fibrils: Consensus versus Controversy. *Acc. Chem. Res. 46*, 1487–1496.
18. Jimenez, J.L., Nettleton, E.J., Bouchard, M., Robinson, C.V., Dobson, C.M., and Saibil, H.R. (2002) The protofilament structure of insulin amyloid fibrils. *Proc. Natl. Acad. Sci. USA* 99, 9196–9201.
19. Jarrett, J. T., and Lansbury, P. T., Jr. (1993) Seeding "one-dimensional crystallization" of amyloid: a pathogenic mechanism in Alzheimer's disease and scrapie? *Cell 73*, 1055–1058.
20. Morris, A. M., Watzky, M. A., and Finke, R. G. (2009) Protein aggregation kinetics, mechanism, and curve-fitting: A review of the literature. *Biochim. Biophys. Acta 1794*, 375–397.
21. Andersen, C. B., Yagi, H., Manno, M., Martorana, V., Ban, T., Christiansen, G., Otzen, D. E., Goto, Y., and Rischel, C. (2009) Branching in Amyloid Fibril Growth. *Biophys. J. 96*, 1529–1536.
22. Knowles, T. P., Waudby, C. A., Devlin, G. L., Cohen, S. I., Aguzzi, A., Vendruscolo, M., Terentjev, E. M., Welland, M. E., and Dobson, C. M. (2009) An analytical solution to the kinetics of breakable filament assembly. *Science 326*, 1533–1537.
23. Nilsson, M. R. (2004) Techniques to study amyloid fibril formation in vitro. *Methods 34*, 151–160.
24. Westermark, P., Benson, M. D., Buxbaum, J. N., Cohen, A. S., Frangione, B., Ikeda, S., Masters, C. L., Merlini, G., Saraiva, M. J., and Sipe, J. D. (2007) A primer of amyloid nomenclature. *Amyloid 14*, 179–183.
25. Chiti, F., and Dobson, C. M. (2006) Protein misfolding, functional amyloid, and human disease. *Annu. Rev. Biochem. 75*, 333–366.
26. Reitz, C., Brayne, C., and Mayeux, R. (2011) Epidemiology of Alzheimer disease. *Nature Reviews Neurology 7*, 137–152.
27. Hebert, L. E., Weuve, J., Scherr, P. A., and Evans, D. A. (2013) Alzheimer disease in the United States (2010–2050) estimated using the 2010 census. *Neurology 80*, 1778–1783.

28. Alzheimer's Association (2015) Alzheimer's disease facts and figures. *Alzheimers Dement 11*, 332–384.
29. Jakob-Roetne, R., and Jacobsen, H. (2009) Alzheimer's disease: From pathology to therapeutic approaches. *Angew. Chem. Int. Ed. 48*, 3030–3059.
30. Querfurth, H. W., and LaFerla, F. M. (2010) Alzheimer's disease. *N. Engl. J. Med. 362*, 329–344.
31. Alzheimer, A., Stelzmann, R. A., Schnitzlein, H. N., and Murtagh, F. R. (1995) An English translation of Alzheimer's 1907 paper, "Uber eine eigenartige Erkankung der Hirnrinde". *Clin. Anat. 8*, 429-431.
32. Hardy, J., and Selkoe, D. J. (2002) The amyloid hypothesis of Alzheimer's disease: progress and problems on the road to therapeutics. *Science 297*, 353−356.
33. Harrison, F. E. (2012) A critical review of vitamin C for the prevention of age-related cognitive decline and Alzheimer's disease. *J. Alzheimer's Dis. 29*, 711-726.
34. Luchsinger, J. A., Cheng, D., Tang, M. X, Schupf, N., and Mayeux, R. (2012) Central obesity in the elderly is related to late-onset Alzheimer disease. *Alzheimer Dis. Assoc. Disord. 26*, 101−105.
35. Kalaria, R. N., Akinyemi, R., and Ihara, M. (2012) Does Vascular Pathology Contribute to Alzheimer Changes? *J. Neurol. Sci. 322*, 141−147.
36. Markesbery, W. R. (1997) Oxidative stress hypothesis in Alzheimer's disease. *Free Radic. Biol. Med. 23*, 134–147.
37. Jeong, H. K., Ji, K. M., Kim, B., Kim, J., Jou, I., and Joe, E. H. (2010) Inflammatory responses are not sufficient to cause delayed neuronal death in ATP-induced acute brain injury. *PLoS One. 5*, e13756.
38. Butterfield, D. A., Swomley, A. M., and Sultana, R. (2013) Amyloid β-peptide 1–42-induced oxidative stress in Alzheimer disease: importance in disease pathogenesis and progression. *Antioxid. Redox Signal. 19*, 823–835.
39. Savelieff, M. G., Lee, S., Liu, Y. and Lim, M. H. (2013) Untangling Amyloid-β, Tau, and Metals in Alzheimer's Disease. *ACS Chem. Biol. 8*, 856–865.
40. Biasutti, M., Dufour, N., Ferroud, C., Dab, W., and Temime, L. (2012) Cost-Effectiveness of Magnetic Resonance Imaging with a New Contrast Agent for the Early Diagnosis of Alzheimer's Disease. *PLoS One. 7(4)*, e35559.
41. Massoud, F., and Gauthier, S. (2010) Update on the pharmacological treatment of Alzheimer's disease. *Curr. Neuropharmacol. 8(1)*, 69–80.

42. Crespo-Biel, N., Theunis, C., and Van Leuven, F. (2012) Protein tau: prime cause of synaptic and neuronal degeneration in Alzheimer's disease. *Int. J. Alzheimers Dis. 2012*, 251426.
43. Chen, W. T., Liao, Y. H., Yu, H. M., Cheng, I. H., and Chen. Y. R. (2011) Distinct Effects of Zn^{2+}, Cu^{2+}, Fe^{3+}, and Al^{3+} on Amyloid-β Stability, Oligomerization, and Aggregation. *J. Biol. Chem. 286*, 9646–9656.
44. LaFerla, F. M., Green, K. N., and Oddo, S. (2007) Intracellular Amyloid-β in Alzheimer's disease. *Nat. Rev. Neurosci. 8*, 499–509.
45. Thinakaran, G. and Koo, E.H. (2008) Amyloid precursor protein trafficking, processing, and function. *J. Biol. Chem. 283*, 29615–29619.
46. Haass, C., and Selkoe, D. J. (2007) Soluble protein oligomers in neurodegeneration: lessons from the Alzheimer's amyloid β-peptide. *Nat. Rev. Mol. Cell Biol. 8*, 101–112.
47. Petkova, A. T., Ishii, Y., Balbach, J. J., Antzutkin, O. N., Leapman, R. D., Delaglio, F., and Tycko, R. (2002) A structural model for Alzheimer's β-amyloid fibrils based on experimental constraints from solid state NMR. *Proc. Natl. Acad. Sci. USA 99*, 16742–16747.
48. Sharoar, M. G., Thapa, A., Shahnawaz, M., Ramasamy, V. S., Woo, E. R., Shin, S. Y., and Park, I. S. (2012) Keampferol-3-O-rhamnoside abrogates amyloid beta toxicity by modulating monomers and remodeling oligomers and fibrils to non-toxic aggregates. *J. Biomed. Sci. 19*, 104.
49. Harper, J. D., and Lansbury, P. T., Jr. (1997) Models of Amyloid seeding in Alzheimer's disease and scrapie: Mechanistic truths and physiological consequences of the time-dependent solubility of amyloid proteins. *Annu. Rev. Biochem. 66*, 385–407.
50. Tjernberg, L. O., Naslund, J., Lindqvist, F., Johansson, J., Karlstromi, A. R., Thyberg, J., Terenius, L., and Nordstedt, C. (1996) Arrest of β-amyloid fibril formation by a pentapeptide ligand. *The J. Biol. Chem. 271*, 8545–8548.
51. Tartaglia, G. G., Cavalli, A., Pellarin, R., and Caflisch, A. (2004) The role of aromaticity, exposed surface, and dipole moment in determining protein aggregation rates. *Protein Science 13*, 1939–1941.
52. Doran, T. M., Kamens, A. J., Byrnes, N. K., and Nilsson, B. L. (2012) Role of amino acid hydrophobicity, aromaticity, and molecular volume on IAPP(20–29) amyloid self-assembly. *Proteins 80*, 1053–1065.
53. Silva, D. F., Esteves, A. R., Arduino, D. M., Oliveira, C. R., and Cardoso, S. M. (2011) Amyloid-β-induced mitochondrial dysfunction impairs the autophagic lysosomal pathway in a tubulin dependent pathway. *J Alzheimers Dis. 26*, 565–81.

54. Butterfield, D. A., Reed, T., Newman, S. F., and Sultana, R. (2007) Roles of amyloid beta-peptide-associated oxidative stress and brain protein modifications in the pathogenesis of Alzheimer's disease and mild cognitive impairment. *Free Radic. Biol. Med. 43*, 658–677.

55. Larson, M. E., and Lesne, S. E. (2012) Soluble Aβ oligomer production and toxicity. *J. Neurochem.120*, 125–139.

56. Luo, Y., Yue, W., Quan, X., Wang, Y., Zhao, B., and Lu, Z. (2015) Asymmetric dimethylarginine exacerbates Aβ-induced toxicity and oxidative stress in human cell and Caenorhabditis elegans models of Alzheimer disease. *Free Radic Biol Med. 79*, 117–126.

57. Kimpe, D. L, Bennis, A., Zwart, R., van Haastert, E. S., Hoozemans, J. J., and Scheper, W. (2012) Disturbed Ca^{2+} homeostasis increases glutaminyl cyclase expression; connecting two early pathogenic events in Alzheimer's disease in vitro. *PLoS One. 7(9)*, e44674.

58. Hampel, H., Frank, R., Broich, K., Teipel, S. J., Katz, R. G., Hardy, J., Herholz, K., Bokde, A. L., Jessen, F., Hoessler, Y. C., Sanhai, W. R., Zetterberg, H., Woodcock, J., and Blennow, K. (2010) Biomarkers for Alzheimer's disease: academic, industry and regulatory perspectives. *Nat. Rev. Drug. Discov. 9*, 560–574.

59. Blennow, K. (2010) Biomarkers in Alzheimer's disease drug development. *Nat. Med. 16*, 1218–1822.

60. Hampel, H., Goernitz, A., and Buerger, K. (2003) Advances in the development of biomarkers for Alzheimer's disease: from CSF total tau and Aβ(1-42) proteins to phosphorylated tau protein. *Brain Res. Bull. 61*, 243–253.

61. Becker, R. E., and Greig, N. H. (2014) A new regulatory road-map for Alzheimer's disease drug development. *Curr Alzheimer Res. 11*, 215-220.

62. Jones, R. W., Kivipelto, M., Feldman, H., Sparks, L., Doody, R., Waters, D. D., Heyhadavi, J., Breazna, A., Schindler, R. J., and Ramos, H. (2008) The Atorvastatin/Donepezil in Alzheimer's Disease Study (LEADe): design and baseline characteristics. *Alzheimers Dement. 4*, 145–153.

63. Imbimbo, B. P. (2009) An update on the efficacy of non-steroidal anti-inflammatory drugs in Alzheimer's disease. *Expert Opin Investig. Drugs 18*, 1147–1168.

64. Yiannopoulou, K. G. and Papageorgiou, S. G. (2013) Current and future treatments for Alzheimer's disease. *Ther. Adv. Neurol. Disord. 6*, 19–33.

65. Citron, M. (2010) Alzheimer's disease: strategies for disease modification. *Nat. Rev. Drug Discov. 9*, 387–398.

66. Ghosh, A. K., Kumaragurubaran, N., Hong, L., Kulkarni, S., Xu, X., Miller, H. B., Reddy, D. S., Weerasena, V., Turner, R., Chang, W., Koelsch, G., and Tang, J. (2008) Potent memapsin 2 (β-secretase) inhibitors: design, synthesis, protein-ligand X-ray structure, and in-vivo evaluation. *Bioorg. Med. Chem. Lett. 18*, 1031–1036.

67. Fleisher, A. S., Raman, R., Siemers, E. R., Becerra, L., Clark, C. M., Dean, R. A., Farlow, M. R., Galvin, J. E., Peskind, E. R., Quinn, J. F., Sherzai, A., Sowell, B. B., Aisen, P. S., and Thal, L. J. (2008) Phase-2 safety trial targeting amyloid β production with a γ-secretase inhibitor in Alzheimer disease. *Arch Neurol 65*, 1031–1038.

68. Fahrenholz, F. and R. Postina (2006) α-Secretase activation an approach to Alzheimer's disease therapy. *Neurodegener Dis. 3*, 255–261.

69. Marcade, M., Bourdin, J., Loiseau, N., Peillon, H., Rayer, A., Drouin, D., Schweighoffer, F., and Desire, L. (2008) Etazolate, a neuroprotective drug linking GABA (A) receptor pharmacology to amyloid precursor protein processing. *J Neurochem. 106*, 392–404.

70. Soto, C., Sigurdsson, E. M., Morelli, L., Kumar, R. A., Castano, E. M., and Frangione, B. (1998) β-sheet breaker peptides inhibit fibrillogenesis in a rat brain model of amyloidosis: Implications for Alzheimer's therapy. *Nature Medicine 4*, 822–826.

71. Hughes, E., Burke, R. M., and Doig, A. J. (2000) Inhibition of toxicity in the β-amyloid peptide fragment β-(25–35) using N-methylated derivatives: a general strategy to prevent amyloid formation. *J. Biol. Chem. 275*, 25109–25115.

72. Lowe, T., Strzelec, A., Kiessling, L. L., and Murphy, R. M. (2001) Structure-Function Relationships for Inhibitors of β-Amyloid Toxicity Containing the Recognition Sequence KLVFF. *Biochemistry 40*, 7882–7889.

73. Takahashi, T., and Mihara, H. (2008) Peptide and protein mimetics inhibiting amyloid β-peptide aggregation. *Acc. Chem. Res. 41*, 1309–1318.

74. Rajasekhar, K., Chakrabarti, M., and Govindaraju, T. (2015) Function and toxicity of amyloid beta and recent therapeutic interventions targeting amyloid beta in Alzheimer's disease. *Chem. Commun. 51*, 13434–13450.

75. Hard, T., and Lendel, C. (2012) Inhibition of Amyloid Formation. *J. Mol. Biol. 421*, 441–465.

76. Fosgerau, K., and Hoffmann, T. (2015) Peptide therapeutics: current status and future directions. *Drug Discovery Today 20*, 122–128.

77. Wu, W. H., Lei, P., Liu, Q., Hu, J., Gunn, A. P., Chen, M. S., Rui, Y. F., Su, X. Y., Xie, Z. P., Zhao, Y. F., Bush, A. I., and Li, Y. M. (2008) Sequestration of Copper from β-Amyloid Promotes Selective Lysis by Cyclen-Hybrid Cleavage Agents. *J. Biol. Chem. 283*, 31657–31664.

78. Doig, A. J. and Derreumaux, P. (2015) Inhibition of protein aggregation and amyloid formation by small molecules. *Curr. Opin. Struct. Biol*. *30*, 50–56.

79. McLaurin, J., Golomb, R., Jurewicz, A., Antel, J. P. and Fraser, P. E. (2000) Inositol stereoisomers stabilize an oligomeric aggregate of Alzheimer amyloid β peptide and inhibit abeta -induced toxicity. *J Biol. Chem. 275*, 18495-502.

80. Nguyen, T., Hamby, A., and Massa, S. M. (2005) Clioquinol down-regulates mutant huntingtin expression in vitro and mitigates pathology in a Huntington's disease mouse model. *Proc. Natl. Acad. Sci. USA 102*, 11840–11845.

81. Solomon, B. (2001) Immunotherapeutic strategies for prevention and treatment of Alzheimer's disease. *DNA Cell Biol. 20*, 697–703.

82. Dodel, R., Hampel, H., Depboylu, C., Lin, S., Gao, F., Schock, S., Jäckel, S., Wei, X., Buerger, K., Höft, C., Hemmer, B., Möller, H. J., Farlow, M., Oertel, W. H., Sommer, N., and Du, Y. (2002) Human antibodies against amyloid β peptide: a potential treatment for Alzheimer's disease. *Ann. Neurol. 52*, 253–256.

83. DeMattos, R. B., Bales, K. R., Cummins, D. J., Dodart, J. C., Paul, S. M., and Holtzman, D. M. (2001) Peripheral anti-Aβ antibody alters CNS and plasma Aβ clearance and decreases brain Aβ burden in a mouse model of Alzheimer's disease. *Proc. Natl Acad. Sci. USA 98*, 8850–8855.

84. Thala, D. R., Holzer, M., Rüb, U., Waldmann, G. Günzel, S., Zedlick, D., and Schober, R. (2000) Alzheimer related tau pathology in the perforant path target zone and in the hippocampal stratum oriens and radiatum Correlates with onset and degree of dementia. *Exp. Neurol. 163*, 98–110.

85. Wischik, C., Bentham, P., Wischik, D., and Seng, K. (2008) O3-04-07: Tau aggregation inhibitor (TAI) therapy with rember™ arrests disease progression in mild and moderate Alzheimer's disease over 50 weeks. *Alzheimers Dement. 4*, T167.

86. Brewster, M. E., Hora, M. S., Simpkins, J. W., Bodor, N. (1991) Use of 2-Hydroxypropyl-β-cyclodextrin as a solubilizing and stabilizing excipient for protein drugs. *Pharm. Res. 8*, 792–795.

87. Colon, W. (1999) Analysis of Protein Structure by Solution Optical Spectroscopy. *Methods Enzymol. 309*, 605–632.

88. Kelly, S. M., Jess, T. J., and Price, N. C. (2005) How to study proteins by circular dichroism. *Biochim. Biophysica. Acta. 1751*, 119–139.

89. Rygula, A., Majzner, K., Marzec, K. M., Kaczor, A., Pilarczyka, M., and Baranskaa, M. (2013) Raman Spectroscopy of Proteins: a Review. *J. Raman Spectrosc. 44*, 1061–1076.

90. Maiti, N. C., Apetri, M. M., Zagorski, M. G., Carey, P. R., and Anderson, V. E. (2004) Raman spectroscopic characterization of secondary structure in natively unfolded proteins: α-synuclein. *J. Am. Chem. Soc. 126*, 2399–2408.
91. Levine, H. (1993) Thioflavine T interaction with synthetic Alzheimer's disease β-amyloid peptides: Detection of amyloid aggregation in solution. *Protein Sci. 2*, 404-410.
92. Khurana, R., Coleman, C., Zanetti-Ionescu, C., Carter, S. A., Krishna, V., Grover, R. K., Roy, R., and Singh, S. (2005) Mechanism of thioflavin T binding to amyloid fibrils. *J. Struc. Bio. 151*, 229–238.
93. Serpell, L. C. (2000) Alzheimer's amyloid fibrils: structure and assembly. *Biochim. Biophys. Acta. 1502*, 16–30.
94. Dobson, C. M. (2001) The structural basis of protein folding and its links with human disease. *Philos. Trans. R. Soc. Land. 356*, 133–145.
95. Dutt, A., Spencer, E. C., Howard, J. A. K., and Pramanik, A. (2010) Studies of Amyloid-Like Fibrillogenesis through β-sheet mediated self-assembly of short synthetic peptides. *Chemistry & Biodiversity 7*, 363–375.
96. Williams, T. L., Day, I. J., and Serpell, L. C. (2010) The effect of Alzheimer's Aβ aggregation state on the permeation of biomimetic lipid vesicles. *Langmuir 26*, 17260–17268.
97. Lakowicz, J. R. (2006) Principles of Fluorescence Spectroscopy, *Springer, New York, 3rd edition*.
98. Kelly, J. W. (2000) Mechanism of Amyloidogenesis. *Nature Structural Biology 7*, 824–826.
99. Bitan, G., Kirkitadze, M. D., Lomakin, A., Vollers, S. S., Benedek, G. B., and Teplow, D. B. (2003) Amyloid β-protein (Aβ) assembly: $A\beta_{40}$ and $A\beta_{42}$ oligomerize through distinct pathways. *Proc. Natl. Acad. Sci. USA 100*, 330–335.
100. Karran, E., Mercken, M., and Strooper, B. D. (2011) The amyloid cascade hypothesis for Alzheimer's disease: an appraisal for the development of therapeutics. *Nat. Rev. Drug. Discov. 10*, 698–712.
101. Tracz, S. M., Abedini, A., Driscoll, M., and Raleigh, D. P. (2004) Role of Aromatic Interactions in Amyloid Formation by Peptides Derived from Human Amylin. *Biochemistry 43*, 15901–15908.
102. Gazit, E. (2002) A possible role for π-stacking in the self-assembly of amyloid fibrils. *FASEB J. 16*, 77–83.
103. Adler-Abramovich, L., Vaks, L., Carny1, O., Trudler, D., Magno, A., Caflisch, A., Frenkel, D., and Gazit, E. (2012) Phenylalanine assembly into toxic fibrils suggests amyloid etiology in phenylketonuria. *Nat. Chem. biol. 8*, 701–706.

104. Mutter, M., Chandravarkar, A., Boyat, C., Lopez, J., Santos, S. D., Mandal, B., Mimna, R., Murat, K., Patiny, L., Saucede, L. and Tuchscherer, G. (2004) Switch peptides in statu nascendi: Induction of conformational transitions relevant to degenerative diseases. *Angew. Chem. Int. Ed. 43*, 4172–4178.
105. Camus, M. S., Santos, S. D., Chandravarkar, A., Mandal, B., Schmid, A. W., Tuchscherer, G., Mutter, M., Lashuel, H. A. (2008) Switch-peptides: Design and characterization of controllable super amyloid forming host guest peptides as tool for identifying anti amyloid agents. *ChemBioChem 9*, 2104-2112.
106. Stewart, J. M., and Young, J. D. (1984) *Solid Phase Peptide Synthesis*. 2nd ed.; Pierce Chemical, Rockford, IL.
107. Coin, I., Beyermann, M., and Bienert, M. (2007) Solid-phase peptide synthesis: from standard procedures to the synthesis of difficult sequences. *Nat. Protoc. 2*, 3247–3256.
108. Chatterjee, J., Laufer, B., and Kessler, H. (2012) Synthesis of N-methylated cyclic peptides. *Nat. Protoc. 7*, 432–444.
109. Rosenheck, K., and Doty, P. (1961) The far ultraviolet absorption spectra of polypeptide and protein solutions and their dependence on conformation. *Proc. Natl. Acad. Sci. USA. 47*, 1775–1785.
110. Rosenheck, K., and Sommer, B. (1967) Theory of the far-ultraviolet spectrum of polypeptides in the β Conformation. *J. Chem. Phys. 46*, 532–536.
111. Kayed, R., Bernhagen, J., Greenfield, N., Sweimeh, K., Brunner, H., Voelter, W., and Kapurniotu, A. (1999) Conformational Transitions of Islet Amyloid Polypeptide (IAPP) in Amyloid Formation in Vitro. *J. Mol. Biol. 287*, 781–796.
112. Woody, R. W., and Dumker, K. (1997) Aromatic and cystine side-chain circular dichroism in proteins. Plenum Press, New York and London 109–158.
113. Bertoluzza, A., Fagnano, C., Caramazza, C., Barbaresi, E., and Mancini, S. (1989) In vivo Raman Spectroscopy of Human, Animal and Artificial Ocular Lenses. *J. Mol. Struct. 214*, 111–117.
114. Gilead, S., and Gazit, E. (2004) Inhibition of amyloid fibril formation by peptide analogues modified with α-Aminoisobutyric acid. *Angew. Chem. Int. Ed. 43*, 4041-4044.
115. Mishra, A., Misra, A., Vaishnavi, T. S., Thota, C., Gupta, M., Ramakumar, S., and Chauhan, V. S. (2013) *Chem. Commun. 49*, 2688–2690.
116. Shen, Y., Hixson, K. K., Tolic, N., Camp, D. G., Purvine, S. O., Moore, R. J., and Smith, R. D. (2008) Mass spectrometry snalysis of proteome-wide proteolytic post-translational degradation of proteins. *Anal. Chem. 80*, 5819–5828.

117. Steer, D. L., Lew, R.A., Perlmutter, P., Smith, A. I., and Aguilar, M. I. (2000) Design and synthesis of inhibitors incorporating beta–amino acids of metalloendopeptidase EC 3.4.24.15. *J. Pept. Sci*. *6*, 470–477.

118. Cheng, R. P., Gellman, S. H., and DeGrado, W. F. (2001) β-Peptides: from structure to function. *Chem. Rev. 101*, 3219–3232.

119. Haynes, S. W., Gao, X., Tang, Y., Walsh, C. T. (2012) Assembly of asperlicin peptidyl alkaloids from anthranilate and tryptophan: a two-enzyme pathway generates heptacyclic scaffold complexity in asperlicin E. *J. Am. Chem. Soc. 134*, 17444–17447.

120. Pavan, M. V., Lassiani, L., Berti, F., Stefancich, G., Ciogli, A., Gasparrini, F., Mennuni, L., Ferrari, F., Escrieut, C., Marco, E., Makovec, F., Fourmy, D., and Varnavas, A. (2011) New Anthranilic Acid Based Antagonists with High Affinity and Selectivity for the Human Cholecystokinin Receptor 1 (hCCK1-R) *J. Med. Chem. 2011, 54*, 5769–5785.

121. Radwanski, E. R., and Last, R. L. (1995) Tryptophan biosynthesis and molecular genetics. *Plant Cell. 7*, 921–934.

122. Kale, S. S., Priya, G., Kotmale, A. S., Gawade, R. L., Puranik, V. G., Rajamohanan, P. R., and Sanjayan, G. J. (2013) Orthanilic acid-promoted reverse turn formation in peptides. *Chem. Commun. 49*, 2222–2224.

123. Maity, S., Jana, P., Maity, S. K., Kumar, P., and Haldar, D. (2012) Conformational heterogeneity, self-assembly, and gas adsorption studies of isometric peptides. *Cryst. Growth. Des. 12*, 422–428.

124. Pravakaran, P., Kale, S. S., Puranik, V. G., Rajamohanan, P. R., Chetina, O., Howard, J .A. K., Hofmann, H. J., and Sanjayan, G. J. (2008) Sequence-specific unusual (1→2) type helical turns in α/β-hybrid peptides. *J. Am. Chem. Soc. 130*, 17743-17754.

125. van Oijen, M., Hofman, A., Soares, H. D., Koudstaal, P. J., and Breteler, M. M. B. (2006) Plasma $A\beta_{1–40}$ and $A\beta_{1–42}$ and the risk of dementia: a prospective case-cohort study. *Lancet Neurol., 5*, 655–660.

126. Hamley, I. W. (2012) The Amyloid Beta peptide: A chemist's perspective. Role in Alzheimer's and fibrillization. *Chem. Rev. 112*, 5147−5192.

127. Chen, S., and Wetzel, R. (2001) Solubilization and disaggregation of polyglutamine peptides. *Protein Sci*. *10*, 887−891.

128. Traikia, M., Warschawski, D. E., Recouvreur, M., Cartaud, J., and Devaux, P. F. (2000) Formation of unilamellar vesicles by repetitive freeze-thaw cycles: characterization by electron microscopy and 31P-nuclear magnetic resonance. *Eur Biophys J., 29*, 184−195.

129. Sheynis, T., Friediger, A., Xue, W. F., Hellewell, A. L., Tipping, K. W., Hewitt, E. W., Radford, S. E., and Jeilinek, R. (2013) Aggregation Modulators Interfere with Membrane Interactions of β_2-Microglobulin Fibrils. *Biophys., J. 105*, 745−755.

130. McLaurin, J., and Chakrabartty, A. (1996) Membrane Disruption by Alzheimer's β-Amyloid Peptides Mediated through Specific Binding to Either Phospholipids or Gangliosides. *J. Biol. Chem., 271*, 26482–26489.

131. Seubert, P., Vigo-Pelfrey, C., Esch, F., Lee, M., Dovey, H., Davis, D., Sinha, S., Schlossmacher, M., Whaley, J., Swindlehurst, C. *et al.* (1992) Isolation and quantification of soluble Aβ-peptide from biological fluids. *Nature 359*, 325−327.

132. Muthuraj, B., Layek, S., Balaji, S.N., Trivedi, V., and Iyer, P. K. (2015) Multiple Function Fluorescein Probe Performs Metal Chelation, Disaggregation, and Modulation of Aggregated Aβ and Aβ-Cu Complex. *ACS Chem. Neurosci. 6*, 1880–1891.

133. Nicolas, E., Pedroso, E., and Giralt., E. (1989) Formation of aspartimide peptides in Asp-Gly sequences. *Tetrahedron Lett. 30*, 497−500.

134. Clarke, S. (1987) Propensity for spontaneous succinimide formation from aspartyl and asparaginyl residues in cellular proteins. *Int. J. Pept. Protein Res. 30*, 808−821.

135. Kapurniotu, A., Schmauder, A., and Tenidis, K. (2002) Structure based design and study of non amyloidogenic, double *N*-methylated IAPP amyloid core sequences as inhibitors of IAPP amyloid formation and cytotoxicity. *J. Mol. Biol. 315*, 339–350.

136. Rijkers, D. T. S., Hoppener, J. W. M., Posthuma, G., Lips, C. J. M., and Liskamp, R. M. J. (2002) Inhibition of amyloid fibril formation of human amylin by N-alkylated amino acid and α-hydroxy acid residue containing peptides. *Chem. Eur. J. 8*, 4285–4291.

137. Hoyer, W., Grönwall, C., Jonsson, A., Stahl, S., and Härd, T. (2008) Stabilization of a beta-hairpin in monomeric Alzheimer's amyloid-beta peptide inhibits amyloid formation. *Proc. Natl. Acad. Sci. U S A. 105*, 5099–5104.

138. Sathaye, S., Zhang, H., Sonmez, C., Schneider, J. P., MacDermaid, C. M., Von Bargen, C. D., Saven, J. G., and Pochan, D. J. (2014) Engineering Complementary Hydrophobic Interactions to Control β‑Hairpin Peptide Self-Assembly, Network Branching, and Hydrogel Properties. *Biomacromolecules 15*, 3891−3900.

139. Nakanishi, M., Patil, R., Ren, Y., Shyam, R., Wong, P., and Mao, H. Q. (2011) Enhanced stability and knockdown efficiency of poly(ethylene glycol)-b-polyphosphoramidate/siRNA micellar nanoparticles by co-condensation with sodium triphosphate. *Pharm. Res. 28*, 1723−1732.

140. Sakurai, T., Iwasaki, T., Okuno, T., Kawataa, Y., and Kisea, N. (2011) Evaluation of Aβ fibrillization inhibitory effect by a PEG–peptide conjugate based on an Aβ peptide fragment with intra-molecular FRET. *Chem. Commun., 47*, 4709–4711.
141. Valeur, B. (2002) Molecular Fluorescence: Principles and Applications *Wiley-VCH Verlag GmbH, 69469, Weinheim (Federal Republic of Germany).*
142. Gustiananda, M., Liggins, J. R., Cummins, P. L., and Gready, J. E. (2004) Conformation of Prion Protein Repeat Peptides Probed by FRET Measurements and Molecular Dynamics Simulations. *Biophys. J. 86*, 2467–2483.
143. Berney, C., and Danuser, G. (2003) FRET or No FRET: A Quantitative Comparison. *Biophys. J. 84*, 3992–4010.
144. Erbse, A. H., Berlinberg, A. J., Cheung, C. Y., Leung, W. Y., and Falke, J. J. (2011) OS-FRET: A New One-Sample Method for Improved FRET Measurements. *Biochemistry 50*, 451–457.
145. Bag, S. S., Jana, S., Yashmeen, A., Senthilkumar, K., and Bag, R. (2014) Triazolyl-donor–acceptor chromophore-decorated unnatural amino acids and peptides: FRET events in a β-turn conformation. *Chem. Commun., 50*, 433–435.
146. Kaiser, E., Colescot, R. L., Bossinge, C. D., and Cook, P. I. (1970) Color test for detection of free terminal amino groups in solid phase synthesis of peptides. *Anal. Biochem. 34*, 595-598.

Product Index

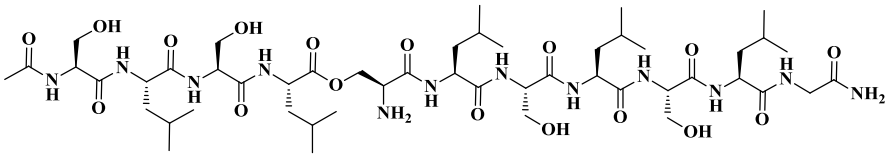

Ac-SLSL-(H$^+$)S-LSLSLG-NH$_2$ (Peptide 2A)

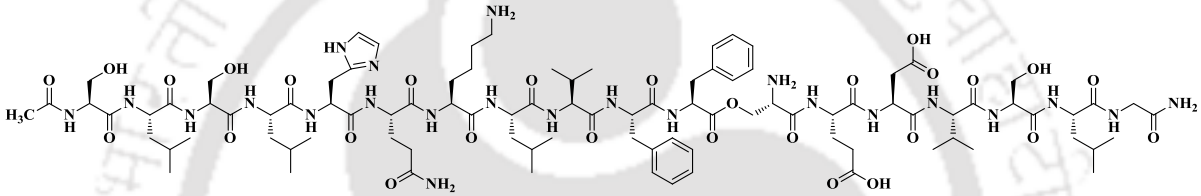

Ac-SLSLHQKLVFF-(H$^+$)S-EDVSLG-NH$_2$ (Peptide 2B)

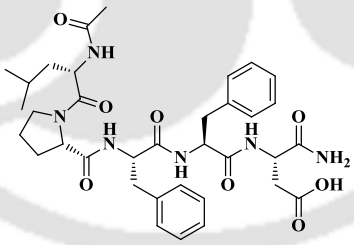

Ac-LPFFD-NH$_2$ (Peptide 2C)

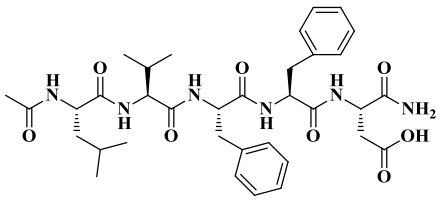

Ac-LVFFD-NH$_2$ Peptide 2D

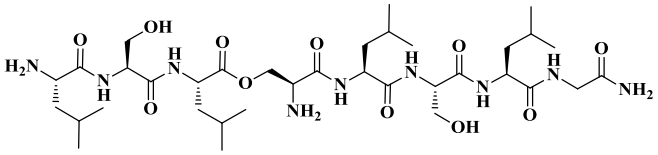

LSL-(H$^+$)S-LSLG-NH$_2$ (Peptide 3A)

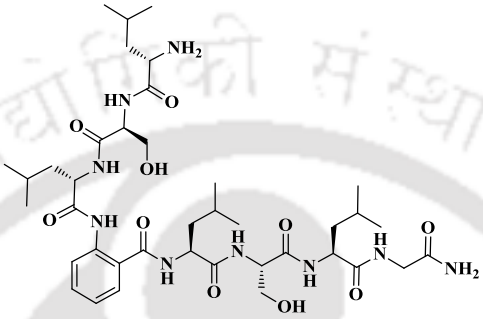

LSLXLSLG-NH$_2$ (Peptide 3B)

(X = Anthranilic acid)

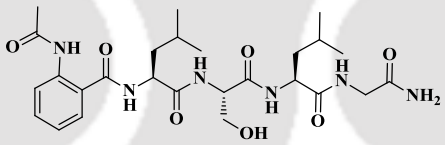

Ac-XLSLG-NH$_2$ (Peptide 3C)

(X = Anthranilic acid)

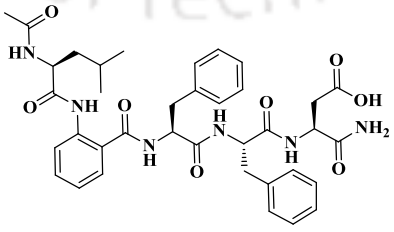

Ac-LXFFD-NH$_2$ (Peptide 4A)

X = Anthranilic acid

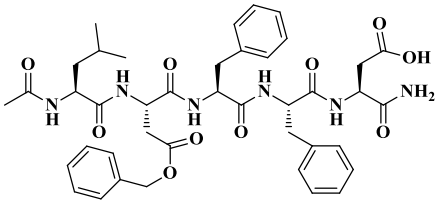

Ac-L<u>D(OBzl)</u>FFD-NH_2 (Peptide 5A)

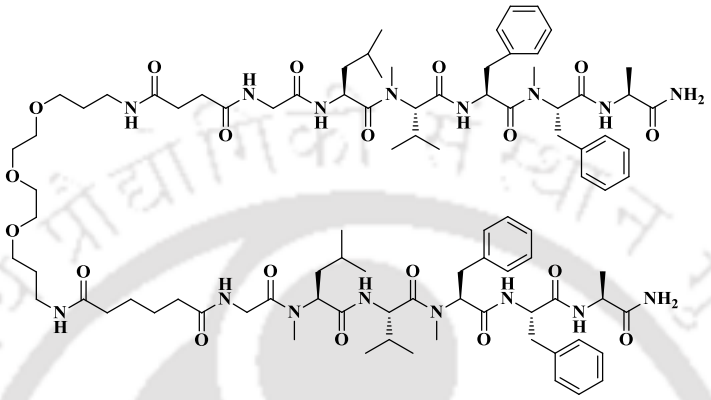

H_2N-A<u>(*N*-Me)</u>F<u>F(*N*-Me)</u>VLG-Succinyl-PEG_3-Adipoyl-G<u>(*N*-Me)</u>L<u>V(*N*-Me)</u>F<u>FA</u>-NH_2 (Peptide 6A)

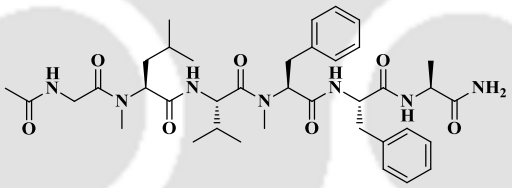

Ac-G<u>(*N*-Me)</u>L<u>V(*N*-Me)</u>F<u>FA</u>-NH_2 (Peptide 6B)

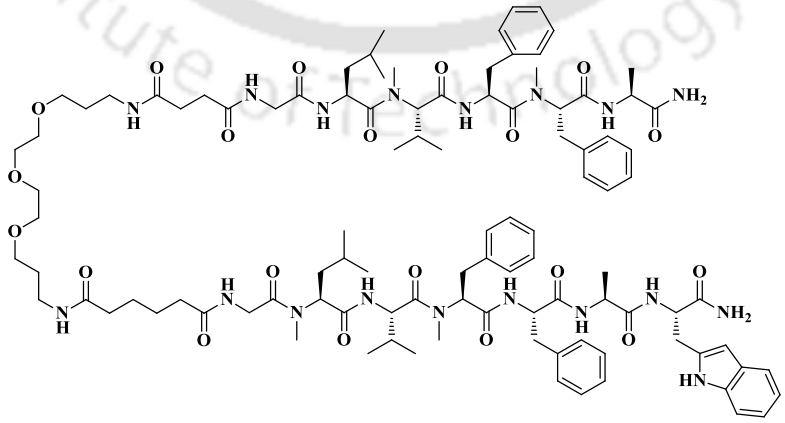

H_2N-A<u>(*N*-Me)</u>F<u>F(*N*-Me)</u>VLG-Succinyl-PEG_3-Adipoyl-G<u>(*N*-Me)</u>L<u>V(*N*-Me)</u>FF<u>AW</u>-NH_2 (Peptide 6C)

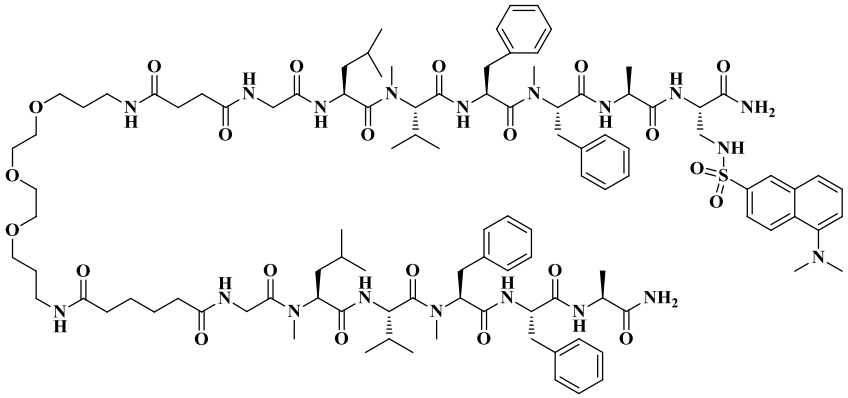

H_2N-XA(*N*-Me)FF(*N*-Me)VLG-Succinyl-PEG_3-Adipoyl-G(*N*-Me)LV(*N*-Me)FFA-NH_2

(Peptide 6D)

(X = 2-amino-3-(5-(dimethylamino)naphthalene-2-sulfonamido)propanoic acid)

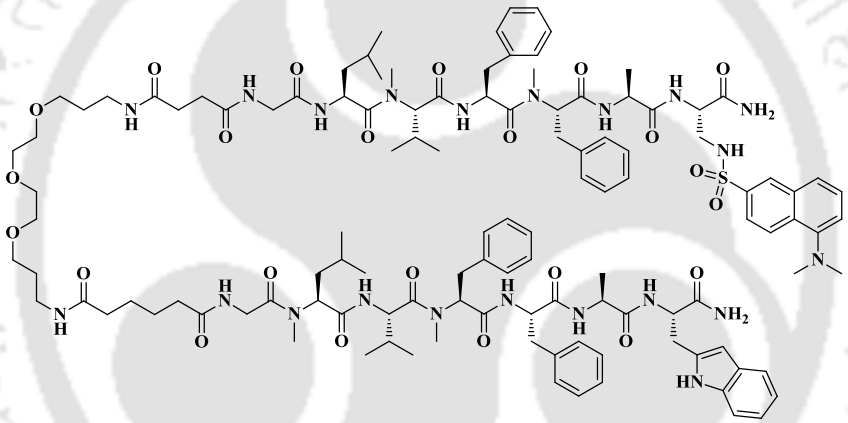

H_2N-XA(*N*-Me)FF(*N*-Me)VLG-Succinyl-PEG_3-Adipoyl-G(*N*-Me)LV(*N*-Me)FFAW-NH_2

(Peptide 6E)

(X = 2-amino-3-(5-(dimethylamino)naphthalene-2-sulfonamido)propanoic acid)

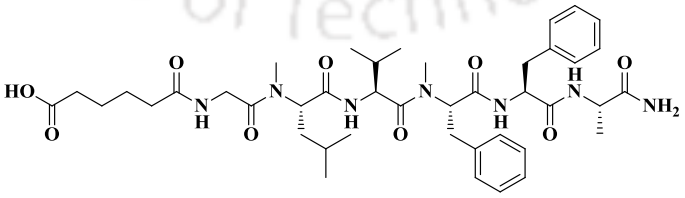

HO-Adi-G(*N*-Me)LV(*N*-Me)FFA-NH_2 (Peptide 6P)

(Adi = adipic acid)

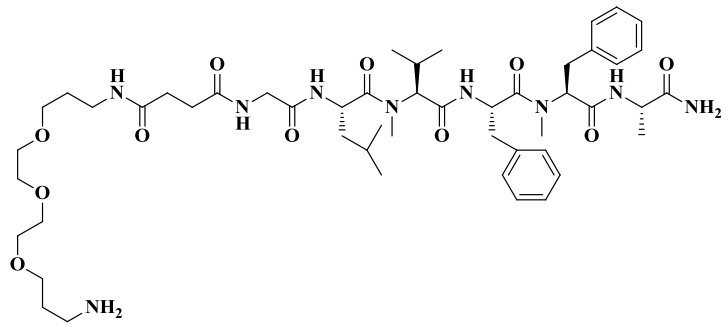

H-PEG$_3$-Suc-Gly-Leu-(N-Me)Val-Phe-(N-Me)Phe-Ala-NH$_2$ (Peptide 6Q)

(Suc = succinic acid)

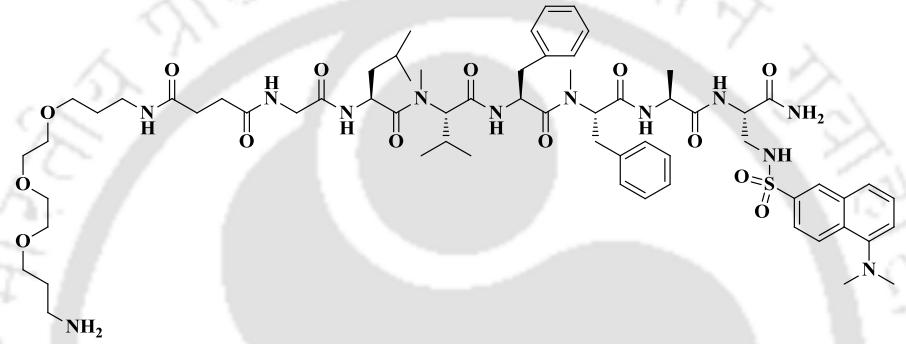

H-PEG$_3$-Suc-Gly-Leu-(N-Me)Val-Phe-(N-Me)Phe-Ala-(Dansyl)Dap-NH$_2$

(Peptide 6R)

(Dap = (*S*)-2,3-diamino propanoic acid, dansyl is attached at 3-amino position in Dap)

Patent and publications

Patent:

Mandal, B., and **Paul, A.** "Beta Sheet Breaker Peptides for Anti-Alzheimer's Drug Design" an Indian patent application, IPA No - E-2/1727/2015/KOL (complete application filed on the 17th September, 2015); provisional IPA No - 997/KOL/2014 (filed on the 26th September, 2014).

Publications:

1. **Paul, A**., kumar, S., Hazra, S., Kalita, S., Ghosh, A. K., Mondal A. C., and Mondal, B., (**2016**) A Peptide Based Pro-Drug Ameliorates $A\beta_{1-40}$ Induced Neuronal Apoptosis in SH-SY5Y cells: An in-vitro Study for Alzheimer's disease. *ACS Chem. Neurosci.* (in revision).
2. **Paul, A.**, Sharma, B., Mondal, T., Thalluri, K., Paul, S., and Mandal, B. (**2016**) Amyloid β Derived Switch-Peptides as a Tool for Investigation of Early Events of Aggregation: A Combined Experimental and Theoretical Approach. *Med. Chem. Commun. 7*, 311-316.
3. Manne, S. R., Thalluri, K., Giri, R. S., **Paul, A**., and Mandal, B. (**2015**) Racemization free longer N-terminal peptide hydroxamate synthesis on solid support using ethyl 2-(tert-butoxycarbonyloxyimino)-2-cyanoacetate. *Tetrahedron Lett. 56*, 6108–6111.
4. **Paul, A**., Nadimpally, K. C., Mondal, T., Thalluri, K., and Mandal, B. (**2015**) Inhibition of Alzheimer's Amyloid-β Peptide Aggregation and its Disruption by a Conformationally Restricted α/β Hybrid Peptide. *Chem. Commun*. *51*, 2245–2248.
5. Thalluri, K., **Paul, A**., Manne, S. R., Dev, D., and Mandal, B. (**2014**) Microwave Assisted Chemoselective Organocatalytic Peptide Alcohol Synthesis from C-terminal Amide. *RSC Adv*., *4*, 47841–47847.

6. Nadimpally, K. C., **Paul, A**., and Mandal, B. (**2014**) Reversal of aggregation using β breaker dipeptide containing peptides: Application to Aβ1-40 self-assembly and its inhibition. *ACS Chem. Neurosci. 5*, 400–408.

7. Saha, A., Nadimpally, K. C., **Paul, A**., Kalita, S., and Mandal, B. (**2014**) Phenolic ester mediated oligopeptide synthesis promoted by HOBt. *Protein Pept. Lett*. *21*, 188–193.

8. Nadimpally, K. C., **Paul, A**., Saha,A., and Mandal, B. (**2013**) Modulation of Aggregation Propensity of Aβ38 by Site Specific Multiple Proline Substitution. *Int. J. Pept. Res. Ther*. *19*, 365–371.

9. Thalluri, K., Nadimpally, K. C., Chakravarty, M. P., **Paul, A**., and Mandal, B. (**2013**) Ethyl 2-(tert-Butoxycarbonyloxyimino)-2-Cyanoacetate (Boc-Oxyma) as Coupling Reagent for Racemization free Esterification, Thioesterification, Amidation and Peptide Synthesis. *Adv. Synth. Catal. 355*, 448–462.

10. Thalluri, K., Nadimpally, K. C., **Paul, A**., and Mandal, B. (**2012**) Waste reduction in amide synthesis by a continuous method based on recycling of the reaction mixture. *RSC Adv*. *2*, 6838–6845.

11. Kumar, S., **Paul, A**., Kalita, S., Mondal A. C., Ghosh, A. K., Mondal, B., and Mondal, A. C. Protective effects of β-sheet breaker α/β hybrid peptide against Amyloid β induced neuronal apoptosis in vitro. (Communicated)

12. **Paul, A**., Kalita, S., and Mondal, B. Aminobenzoic acid containing α/β and α/γ Hybrid Peptides but not α/δ Hybrid Peptide as Potent Inhibitors Against Diabetes Type-2 (Communicated).

13. **Paul, A**., Kalita, S., kumar, S., Hazra, S., Mondal A. C., and Mandal, B. Arresting and Disrupting of Alzheimer's Amyloid aggregates by Synthetic Zipper Peptide (in preparation).

Conference Paper:

Prasad, S., Mandal, I., **Paul, A.**, Mandal, B., Venkatramani, R., Swaminathan, R. (2016) Investigation of Novel Spectroscopic Features in the Near Ultraviolet Region Arising from Non-Aromatic Amino Acids in Peptides and Proteins. *Biophysical Journal, 110, 489a*.

Oral and poster presentation in conferences:

1. **Paul, A.** and Mandal, B. (2015) Peptide Based Drug Development Against Alzheimer's Disease. *Assam Biotechnology Conclave* 20-21st November, 2015, organized by Guwahati Biotech Park, India. (**Oral**)

2. **Paul, A.**, Mondal, T., and Mandal, B. (2015) Disruption of toxic alzheimer's amyloid aggregates into non-toxic species by conformationally restricted α/β hybrid peptide. *10th International Symposium on Bio-Organic Chemistry (ISBOC 10)*, 11th-15th January, 2015, IISER Pune, India with sponsorship of IUPAC, PP 088, page 237. (**Poster**)

3. **Paul, A.**, Thalluri, K., Manne, S. R., Kalita, S., and Mandal, B. Synthesis of biologically active peptide alcohols from C-terminal amide under microwave irradiation. *Frontier in Chemical Sciences (FICS-2014)*, 4th-6th December, 2014, IIT Guwahati, India, P-24, Page 70. (**Poster**)

4. **Paul, A.**, Mondal, T., Dev, D., and Mandal, B. Inhibition of Alzheimer's amyloid β derived peptide aggregation by β-sheet breaker hybrid peptide. *8th Mid-Year chemical research society of India (CRSI), National symposium in chemistry*. 10th-12th July, 2014, CSIR-NEIST, Jorhat, India. P-88429, page-138. (**Poster**)

5. **Paul, A.**, Nadimpally, K. C, Thalluri, K., and Mandal, B. One pot protocol for amide synthesis of unprotected amino acids. *Abstract book National symposium on recent trends in chemical science and technology (RTCST-2012)*, 3rd-4th March, 2012, IIT Patna, P 28, page 80. (**Poster**)

Curriculum vitae

Ashim Paul

Personal details:
Date of Birth: 29th June, 1987
Nationality: Indian
Religion: Hindu
Marital status: Single
Tel no. +91-9678337723
Email: ashim.ismu@gmail.com / p.ashim@iitg.ernet.in

Present Address:
Senior Research Fellow, Laboratory of Peptide & Amyloid Research, Department of Chemistry, IIT Guwahati, Guwahati-781039, Assam, India.

Permanent Address:

H. No.10, Satyajit Pally, Benachity, Duragpur-713213, Burdwan, West Bengal, India.

Qualifications

12/2010–Present
Ph.D. in Chemistry (CPI 8.75 out of 10)
Indian Institute of Technology Guwahati, Assam, India
Thesis: Development of New Strategies for Peptide Based Drug Design against Alzheimer's Disease
Thesis advisor: Dr. Bhubaneswar Mandal

07/2008–05/2010
M.Sc. in Chemistry (First Class with Distinction)
Indian School of Mines Dhanbad, Jharkhand, India
Thesis: Corrosion Inhibition of Mild Steel using Thiosemicabazide Derivatives
Thesis advisor: Dr. Mahendra Yadav

07/2005–05/2008
B.Sc. in Chemistry Honours (First Class) with Physics, Mathematics and English
Burdwan University, West Bengal, India

Honours/Awards

- Received 5th prize in the talent search contest on innovative research ideas leading to the entrepreneurial venture in biotechnology and allied areas on 21st Nov, 2015. (Assam Biotechnology Conclave, 20-21st November, 2015).
- Received Senior Research Fellowship on Jan, 2013 and Junior Research Fellowship on Jan, 2011 from UGC, India.
- Received National Eligibility Test (NET-JRF) June-2011 (UGC-rank 79), Dec-2010 (UGC-rank 476) and June-2010 (UGC-rank 363) in Chemical Science.
- Received Graduate Aptitude Test in Engineering (GATE) 2010 in Chemistry (rank 781).

Research Experiences

- I have worked on peptide self-assembly, Alzheimer's disease, Diabetes type-2 and peptide synthesis including solution phase and solid phase peptide synthesis (SPPS) during my Ph.D. career.
- I have expertise in various instrumental techniques including, HPLC, ESI-MS, Fluorescence, UV-Vis, CD, FTIR, TEM, Optical-polarizable microscope, *etc*.
- During my PhD tenure, I mainly focused on the design and synthesis of different peptide based molecules as inhibitors against Alzheimer's disease and Diabetes type-2. I have developed three different strategies for drug design against Alzheimer's disease, including anthranilic acid (Ant) containing β-sheet breaker α/β-hybrid peptide (BSBHp, Ac-Leu-**Ant**-Phe-Phe-Asp), *in situ* generated breaker element (aspartimide and α/β aspartyl residue) containing Pro-Drug peptide (PDp, Ac-Leu-**Asp(OBzl)**-Phe-Phe-Asp) and N-methyl amino acid/ PEG containing Zipper peptide (Ala-**(*N*-Me)Phe**-Phe-**(*N*-Me) Val**-Leu-Gly-Succinyl-**PEG_3**-Adipoyl-Gly-**(*N*-Me)Leu**-Val-**(*N*-Me)Phe**-Phe-Ala). All these peptide molecules showed excellent anti-Alzheimer's activities which were verified *in-vitro* using various biophysical tools, including TEM, Congo red birefringence studies and Thioflavin T fluorescence assay.
- During my Ph.D. tenure, I have also worked on the mechanism of amyloidosis mainly on the early events of protein misfolding and amyloid formation.
- In parallel, I have also worked on synthetic organic chemistry, native chemoselective ligation and development of coupling reagents for peptide synthesis and other organic transformations. We have developed a novel coupling reagent, ethyl 2-(tert-butoxycarbonyloxyimino)-2-cyanoacetate, namely "Boc-Oxyma" for racemization-free esterification, thio-esterification, hydroxamate, amidation and peptide synthesis.

Academic and Professional Skills

- **Laboratory and Instrumentation:** Familiar with Synthetic Organic Chemistry, peptide synthesis (solution phase and solid phase), NMR Spectroscopy (1D, 2D), HPLC, Mass Spectrometry (ESI, MALDI), UV-Visible spectroscopy, Fluorescence spectroscopy, Circular Dichroism, Optical Polarisable microscope.
- **Software:** Gaussian, Origin, Adobe Illustrator, Adobe Photoshop, MS-Office, Chem Draw, and Spin works.
- **Teaching Experience:** Worked as Teaching Assistant (TA) in B.Tech and M.Sc Laboratory at IIT Guwahati, India.
- **Language:** Bengali, English, Hindi and Assamese.

Research Interests

- Protein and peptide chemistry
- Protein/peptide self-assembly, Alzheimer's disease and other protein aggregation diseases.
- Chemical Biology